Improved techniques for isolation of pure cellular organelles with magnetic ferrofluid

Mathew W. Walker

Ph.D. 2014

Abstract

Lysosomes are essential cellular organelles known to be the main site for the breakdown and recycling of endocytosed macromolecules within cells. However, our knowledge of lysosomal function has changed considerably over the last decade with the lysosome now being a recognized Ca^{2+} signaling organelle with additional roles in plasma membrane repair, clearance of defective organelles and mediating cell death as well as established roles in clearing infection. Our ability to study these unique organelles has however been stymied by a dearth of good techniques for the purification of functional lysosomes not contaminated by other organelles.

Utilising superparamagnetic iron oxide nanoparticles we have devised a technique based on previous studies that incubated cells with iron oxide-dextran particles to purify lysosomes magnetically. Whilst these early studies suffered from cellular toxicity and low yields our nanoparticles have proven to be stable and relatively non-toxic to cells allowing for the first time the rapid purification of high yields of ultra-pure functional lysosomes from normal and lysosomal disease cells.

We have utilized this assay to assist in the characterization of basic lysosomal disease cell biology questions that would otherwise have perhaps remained unanswered. We have confirmed that lysosomal Ca^{2+} uptake is indeed the cause of the lysosomal Ca^{2+} homeostatic defect in Niemann-Pick C disease and have used the assay to characterse the first function for the lysosomal CLN3 protein as a lysosomal Ca^{2+} leak channel.

The purification assay has the potential to lead to major breakthroughs in the field of lysosomal research.

Acknowledgements

This project was funded by KESS.

I would like to give a big thank you to Dr Emyr Lloyd-Evans for putting up with me as well as for all the support and guidance he has provided over the last three years. I would also like to thank the rest of the Lloyd-Evans lab for making the last three years an enjoyable experience (that includes you Luke Haslett).

I would like to thank our lab manager Dr Helen Waller-Evans for help with the use of the confocal microscope, without her help I would never have been able to do that experiment. I would also like to thank Dr Ian Williams who took the time to come over to Cardiff to teach me how to do Western Blotting. And finally I would like to thank my co-supervisor Professor Arwyn Jones for the advice he has provided during the course of this PhD.

I wouldn't be where I am now without the constant love and support of my grandparents, who I owe a huge debt of gratitude to. Also huge thanks to my Dad and the rest of my family who have helped me reach this point in my life. Also I owe a lot to Laura Francis who has been nothing but a constant wave of support this past year, thank you.

I would like to thank everyone at Liquids Research Ltd for the technical advice they have provided during the course of this PhD, as well as for making my short time working there an interesting experience.

Contents

Figures

1 Introduction

3 Effects of superparamagnetic iron oxide nanoparticles on cellular and lysosomal function

4 Developing an improved technique for magnetically purifying lysosomes

5 Characterising juvenile neuronal ceroid lipofuscinosis disease cellular phenotypes

6 Altered homeostasis in intracellular Ca^{2+} stores

List of abbreviations

AP-2	Assembly protein 2
APP	Amyloid precursor protein
ATP	Adenosine trisphosphate
BAR	Bin amphiphysin rvs
Bi1	Bax inhibitor 1
BSA	Bovine serum albumin
cADPR	Cyclic ADP ribose
CHOP	CCAAT/-enhancer binding protein homologous protein
ClC-7	Chloride channel 7
CLICs	Clathrin independent carriers
CPS	Carboxyl polystyrene particles
CtxB	Cholera toxin B subunit
DGC	Density gradient centrifugation
DPBS	Dulbecco's phosphate buffered saline
EM	Electron microscopy
ER	Endoplasmic reticulum
ERT	Enzyme replacement therapy
GlcNAc	*N*-Acetylglucosamine
GFP	Green fluorescent protein
GPN	Glycyl-phenyl-alanine 2-naphthylamide
GRAF-1	GTPase regulator associated with focal adhesion kinase 1
INCL	Infantile neuronal ceroid lipofuscinosis
IP_3	Inositol trisphosphate
JNCL	Juvenile neuronal ceroid lipofuscinosis
LAMP1/2	Lysosomal associated membrane protein 1/2
LBPA	Lyso-bisphosphatidic acid
LINCL	Late infantile neuronal ceroid lipofuscinosis
LMP	Lysosomal membrane protein
LSD	Lysosomal storage diseases
MFS	Major facilitator superfamily
MVB	Multi vesicular body
NAADP	Nicotinic acid adenine dinucleotide phosphate
NCL	Neuronal ceroid lipofuscinoses
NPC	Niemann-Pick disease type C
PFA	Paraformaldehyde

PS	Phosphatidylserine
$PI(4,5)P_2$	Phosphatidylinositol(4,5)-bisphosphate
PNS	Post nuclear supernatant
PS1	Presenilin 1
RND	Resistance nodulation division
ROS	Reactive oxygen species
SERCA	Sarco-endoplasmic reticulum Ca^{2+}-ATPase
SNARE	Soluble N-ethylmaleimide sensitive factor attachment protein receptor
SNX-9	Sorting nexin 9
SorLA	Sortilin related receptor
SPION	Superparamagnetic iron oxide nanoparticle
SRT	Substrate reduction therapy
TGN	Trans Golgi network
TMBIM	Transmembrane Bax inhibitor 1 containing motif proteins
TPC	Two pore channel
V-ATPase	Vacuolar ATPase
VAMP7	Vesicle associated membrane protein 7
VPS10	Vacuolar protein sorting 10

Looks like I picked the wrong week to quit sniffing glue
-Airplane! 1980

1.Introduction

1.1 The Endocytic pathway

Endocytosis is as an important cellular mechanism where molecules are internalized into the cell via either clathrin-dependent or independent processes (such as macropinocytosis) before being delivered to their targeted location via a complex system of organelles known as the endocytic system (Mayor and Pagano, 2007). Endocytic organelles are generally divided up into early and late compartments (Mukherjee et al., 1997). Early endosomes are often found around the periphery of the cell and they receive most types of vesicles coming from the plasma membrane. The slightly acidic pH of ~6 (Lloyd-Evans et al., 2010) inside these early endosomes causes the dissociation of cell surface receptors from their respective bound endocytosed molecules. These receptors are then recycled back to the surface of the cell (Brooks, 2009). If a molecule is directed along the endocytic pathway through the early endosome, and it is not redirected back to the plasma membrane via the recycling endosome, then it reaches the late endosome (Brooks, 2009). Currently it is unclear how material from the early endosome reaches the late endosome, but two different models have been proposed. The first is called the maturation model where the early endosome matures into a late endosome (Murphy, 1991, Stoorvogel et al., 1991), while the second model proposes that there are endocytic carrier vesicles that act as an intermediate step between the early and late endsosomes (Stoorvogel et al., 1991). Late endosomes have a pH of about ~5 when compared with the early endosomes and can traffic molecules to either the trans Golgi

Network, the plasma membrane (via the Endoplasmic Reticulum (ER)) or, if the molecule is to be degraded, the lysosome (Brooks, 2009).

1.2 Endocytic mechanisms: Clathrin mediated endocytosis

Clathrin mediated endocytosis is one of the main mechanisms for cellular internalisation of molecules through the assembly of clathrin coated vesicles that encapsulate membranes containing the molecule to be endocytosed before it is brought into the cell for processing at the designated site (Mulcahy et al., 2014). This process is highly dependent on a large range of transmembrane receptors and their respective ligands that are first involved in the nucleation of clathrin to the plasma membrane where internalisation is to occur (Boucrot and McMahon, 2011, Farsad et al., 2003) as well as being mediated by the phospholipid phosphatidylinositol (4,5)-bisphosphate, PI(4,5)P (Farsad et al., 2003). The cargo-dependent recruitment of the assembly protein 2 (AP-2) is then needed to form links with adaptor proteins and the clathrin coat to the molecule that is to be internalised (Puertollano, 2004). The plasma membrane then undergoes deformation of the cellular membrane that results in the formation of the clathrin coated bud that surrounds the molecule, with the bud then undergoing maturation before it is pinched off from the membrane (Mulcahy et al., 2014). The large GTPase membrane scission protein dynamin is recruited to the plasma membrane via the BAR (Bin Amphiphysin Rvs) domain containing membrane bending protein SNX-9 (Sorting nexin 9). The dynamin protein then undergoes

hydrolysis to promote the fusion of this newly formed clathrin vesicle with the plasma membrane, allowing for the release of clathrin coated vesicle into the cell.

The sorting of the internalised cargo occurs rapidly following clathrin mediated endocytosis (Szaszi et al., 2002). The internalised molecule may be destined for degradation so therefore it must be targeted towards the lysosome, while other internalised molecules may need to be recycled so they therefore need to be processed via the correct endocytic route. The trafficking of the endocytosed molecules is usually determined by the receptors bound to them.

The internalised clathrin coated vesicles are quickly fused with early endosomes where the contents of the vesicles are trafficked to further endocytic vesicles with the aid of a family of GTPase proteins known as Rabs. Endocytosed cargo that is to undergo recycling back to the plasma membrane is regulated by the Rab4 GTPase, or via Rab11 if the cargo is to be trafficked to the recycling endosome (Smit et al., 1993). Cargo that is to be trafficked further into the endocytic pathway requires Rab5 as well as Rab7 so that the cargo can be delivered to the late endosome/multi-vesicular body (MVB) for further sorting (Bucci et al., 1992). Cargo that makes it to the late endosome can then further undergo more sorting, with certain cargo being trafficked to the Trans Golgi Network (TGN), where Golgi apparatus enzymes modify the cargo depending on where it is to reside in the cell, via processes requiring Sorting Nexins or Rab9 dependent pathways (Carlton et al., 2004, Lombardi et al., 1993). Cargoes that have thus far not been trafficked out

of the endocytic pathway are then typically sorted to the end point of the endocytic pathway, the lysosome, for degradation.

1.3 Endocytic mechanisms: Clathrin independent endocytosis

One of the other major endocytic mechanisms cells use for the endocytosis of external molecules is known as clathrin independent endocytosis. The mechanisms behind this form of endocytosis are similar to that of clathrin mediated endocytosis but are defined by the lack of clathrin coated pits present during the endocytosis of molecules. One of the most commonly reported means of clathrin independent endocytosis is that which include the cholesterol and glycolipid rich plasma membrane buds known as caveolae (Parton et al., 1994). These caveolae domains consist of the 3 members of the caveolin family of proteins. Caveolin 1 and 2 are found in abundance in non-muscle cells while caveolin 3 is found predominantly in skeletal muscle and smooth muscle cells (Nassar et al., 2013, Tang et al., 1996). The endocytic mechanisms that utilise caveolae, as stated previously, are similar to that seen in clathrin mediated endocytosis as the caveolae form a bud around the molecules that are to be endocytosed, via receptors found in the caveolae, before this bud is internalised in a dynamin (a GTPase involved in the scission of newly formed vesicles) dependent manner (Oh et al., 1998, Yao et al., 2005). The internalised caveolae bud can then fuse with an endosome known as the caveosome in a Rab5 independent manner where the cargo can then be recycled back to the plasma membrane. The

internalised cargo can also be trafficked to the early endosome via the use of the Rab5 GTPase where the cargo can be further trafficked in a manner similar to molecules endocytosed via clathrin mediated endocytosis when they reach this stage of the endocytic pathway (Pelkmans and Zerial, 2005).

Recent evidence has emerged of a new major endocytic pathway involved in up to three times the volume internalised by clathrin mediated endocytosis known as Clathrin independent Carriers (CLICs) which is indicated to be involved in bulk inflow into the cell (Howes et al., 2010). CLICs have been identified as complex, multicomponent carriers which can interact in either a dynamin dependent or independent manner as it appears that dynamin is not necessary for the internalisation of molecules taken up via CLIC endocytosis (Kirkham et al., 2005, Sabharanjak et al., 2002). While dynamin is not necessarily needed for CLIC mediated endocytosis, it appears that GRAF-1 (GTPase regulator associated with focal adhesion kinase 1) is needed (Doherty and Lundmark, 2009, Howes et al., 2010). This protein has been shown to interact with cellular cytoskeletal components (Taylor et al., 1999) and thus be involved in the recruitment of the G-protein cell division control protein 42 (Cdc42) and ADP-ribosylation factor 1 (ARF1) which aids in the formation of the tubular and ring like structures that are utilised for the fluid phase uptake used in this form of endocytosis (Kirkham et al., 2005, Kumari and Mayor, 2008, Sabharanjak et al., 2002). The rapid recruitment of Rab11 and Rab5 following CLIC endocytosis helps facilitate the bulk of endocytosed

material to either early endosomes or recycling endosomes where the endocytosed material can be processed (Howes et al., 2010).

1.4 Endocytic mechanisms: Macropinocytosis (Fluid phase endocytosis)

Macropinocytosis (also known as fluid phase endocytosis) is an endocytic mechanism cells use to take in large solutes from the extracellular fluid (e.g. dextrans) (Bohdanowicz and Grinstein, 2013). This process is clathrin independent and requires the remodelling of actin as well as the activity of the phospholipid PtdInsP3K (Araki et al., 1996). The large molecules are taken into the cell as the plasma membrane forms an extension around them, causing fusion into the intracellular space. These large fluid filled vacuoles are then pinched into the cell. The vesicles formed in this manner can be from 0.2μM-2μM in size (Bohdanowicz and Grinstein, 2013). While not much is understood behind the mechanisms of how fluid phase endocytosis works, in comparison to other endocytic pathways, it is suggested that Rab5 plays an important role as loss of Rab5 function results in the inhibition of fluid phase endocytosis (Li et al., 1997).

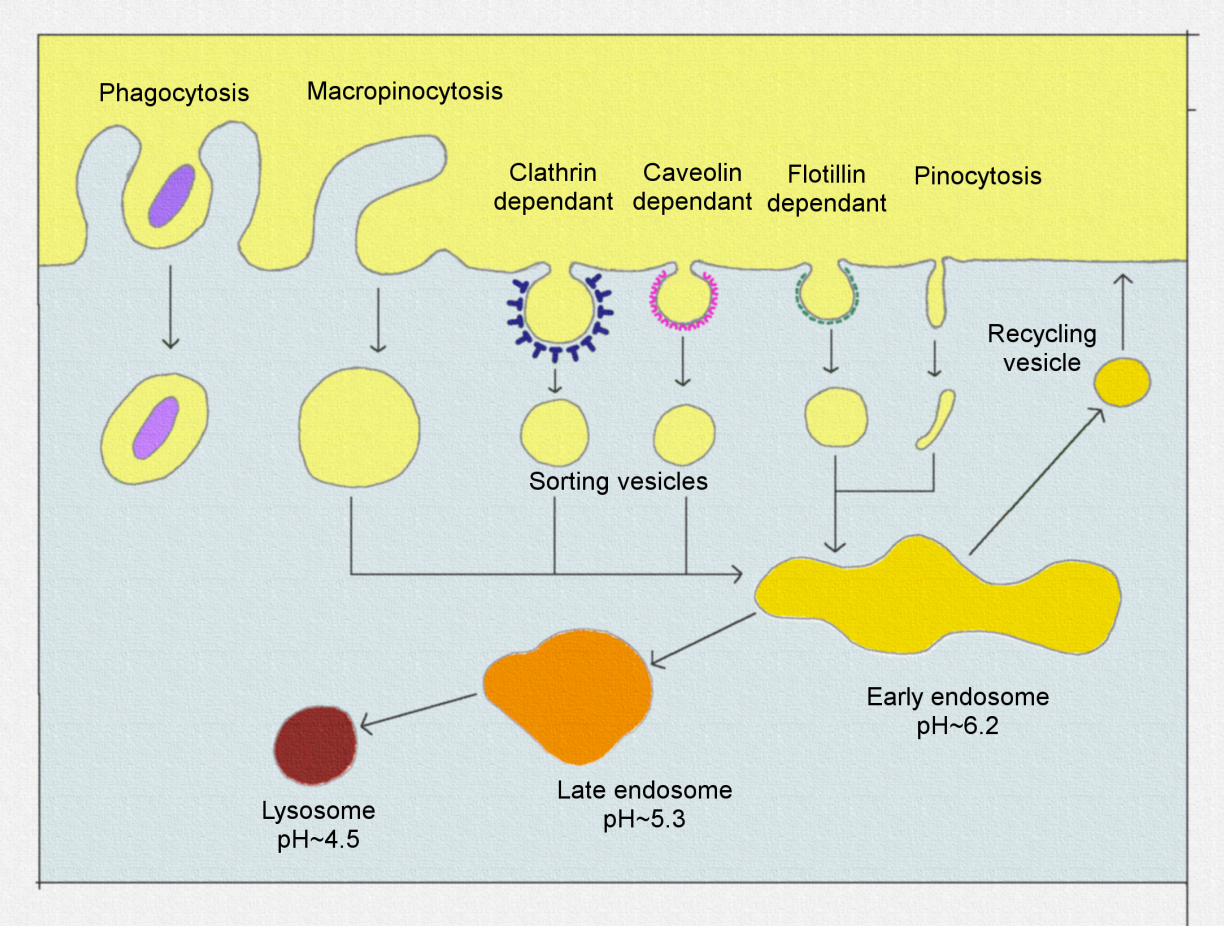

Figure 1: An overview of the different mechanisms of endocytosis the cell incorporates to bring in external cargo. Exogenous material is taken up into the cell via their respective endocytosis mechanisms into intra-cellular vesicles. The vesicles are transported to the early endosome and the material is then transported through the endocytic system. As the material passes through the different endocytic organelles they are processed and trafficked to their respective cellular destinations. Material that is not transported out of the endocytic system ends up in the in the terminal point of the endocytic system, the lysosome.

1.5 Late endosomal-lysosomal fusion

For a long time there was dispute about how macromolecules designated for transport to lysosome reached there once they were in the late endosome. Multiple different methods have been proposed such as kissing, vesicular transport, maturation and direct fusion (Luzio et al., 2000, Mullins and Bonifacino, 2001). Recent work carried out with the use

of fluorescent dextrans in normal rat kidney fibroblasts, have found that kissing and direct fusion was responsible for content mixing in late endosomes to lysosomes (Bright et al., 2005). The very first evidence of direct late endosome-lysosome fusion was found when an organelle that had a density intermediate of that of lysosomes and late endosomes also contained markers found from both organelles (Mullock et al., 1998). Following the fusion between the two organelles the hybrid organelle formed eventually undergoes a maturation process to become a lysosome again where the recycling of non-lysosomal proteins are transported back out of the maturing lysosome (Luzio et al., 2009). What has been found to be important in the fusion between late endosomes and lysosomes is the presence of soluble N-ethylmaleimide-sensitive factor attachment protein receptor (SNARE). Vesicle associated membrane protein 7 (VAMP7) is an important SNARE necessary for correct late endosome-lysosome fusion to occur (Luzio et al., 2009), as its correct localisation to the lysosomal membrane is important for other factors to be recruited to mediate fusion between the two compartments in a Ca^{2+} dependent manner (Luzio et al., 2009). Following fusion the SNARE proteins are recycled off the hybrid organelle as it slowly matures back into a lysosome until they are required for late endosome-lysosome fusion again (Luzio et al., 2009).

1.6 The Lysosome: An overview

The lysosome was first discovered by Belgium cytologist Christian de Duve in the 1960's when he was investigating carbohydrate liver metabolism and discovered that cells exposed to greater centrifugal force released more of the enzyme acid phosphatase as a direct result of the amount of damage the cell received. He theorized that there was a membrane bound organelle within the cell that encased these digestive enzymes, and this was confirmed when a technique called Density Gradient Centrifugation (DGC) was used to separate out the organelles based on their respective densities (de Duve, 1969). A lysosome is a membrane-bound organelle that is present in animal cells and has for a long time been described as the "stomach of the cell" as it has important roles in the breakdown and recycling of receptor molecules, plasma membrane repair, autophagy and the degradation of macromolecules (Luzio et al., 2007). With the advent of electron microscopy (EM) the lysosome could be described in further detail. EM showed that lysosomes make up about 5% of the total intracellular volume and are heterogeneous in morphology and size as well as being very electron dense (E, 1989).

1.7 Lysosomal pH

The inside of the lysosome itself has a very low pH of ~4.5, maintained by proton pumps (Lloyd-Evans et al., 2010). The proton pumps in question

are the Vacuolar-type $^{H+}$-ATPase (V-ATPase) proteins which are an endosomal membrane pump found through all the different endocytic organelles which utilises the free energy provided from the hydrolysis of adenosine triphosphate (ATP) to drive protons from the cytosol, against the electrochemical gradient, into the organelles lumen (Ohkuma et al., 1982). This proton channel is especially important in lysosomes as it needs to maintain its acidic pH, which it does in conjunction with pumping out K^+ ions via either a cation channel or transporter. However, the mechanisms behind this are still not fully characterised (Mindell, 2012). Other work has shown that lysosomal pH homeostasis may be maintained via a Cl^-/H^+ antiporter known as Chloride channel 7 (ClC-7) found on the lysosomal membrane (Mindell, 2012). ClC-7 belongs to a family of proteins that have been shown to have a role in the movement of two Cl^- ions against the movement of a single proton (Picollo and Pusch, 2005, Scheel et al., 2005). While it is proposed to be found on the lysosomal membrane, the true role of ClC-7 antiporters is still not fully understood on how it may help regulate lysosomal pH (Kornak et al., 2001).

While it is still not fully understood how the lysosome maintains it's pH homeostasis via the influx and efflux of cations, the function of the lysosomal V-ATPases and any potential Cl^-/H^+ antiporter is integral as it provides an optimum acidic environment for the hydrolytic enzymes the lysosome contains. This acidic optima results in the lysosomal enzymes being able to cleave the ingested macromolecules such as proteins, polysaccharides and phospholipids (Kolter and Sandhoff, 2005).

1.8 Lysosomal enzyme transport and activation

Lysosomal enzymes are synthesized in the ER and there they are glycosylated on their asparagine residues so that they can be recognised by the GlcNAc-1-phsophotransferase, thus enabling a two-step reaction where the first step involves a mannose-6-phosphate tag is attached to specific N-linked oligosaccharides. The next step involves the use of the enzyme N-acetylglucosamine-1-phosphodiester alpha-N-acetyl-glucosaminidase that removes the N-Acetylglucosamine (GlcNAc), exposing the mannose-6-receptor tag that acts as a signal (Braulke and Bonifacino, 2009). Once the newly synthesised protein reaches the TGN, it results in the binding of the mannose-6-phosphate receptor to the tag on the protein. This interaction allows the bound proteins to be transported to the endosome via adaptor proteins such as activator protein 1 (AP-1) (Doray et al., 2002). The acidic content of the late endosome causes the dissociation of the mannose phosphate receptor, which is then recycled back to the TGN (Seaman, 2004). The proteins are then further transported to lysosomes by vesicular transport or fusion. Non-soluble lysosomal membrane proteins are transported to the lysosome by either an indirect route involving the plasma membrane or by a direct intracellular route (Peden et al., 2004). Recent work has highlighted a mannose-6-phosphate in-dependent pathway for the trafficking of lysosomal enzymes via the vacuolar protein sorting 10 (VPS10) domain of family of receptors (Canuel et al., 2009). This family include the multiligand receptors sortilin as well as SorLA (Sortilin related

Receptor) (Coutinho et al., 2012), which are proposed to be responsible for the lysosomal targeting of non-enzymatic co-factors such as sphingolipid activator proteins that are necessary for the breakdown of, for example, glucosylceramide or sphingomyelin in the lysosome. It is proposed that VPS10 mediated lysosomal enzyme trafficking does not require the enzyme to be glycosylated, unlike the mannose-6-phosphate dependant pathway (Reczek et al., 2007).

Once the lysosomal enzymes reach the lysosome they become active. An example of this is how the lysosomal cathepsin enzymes become active due to the proteolytic removal of their respective propeptides in the acidic lysosomal environment (Lutgens et al., 2007).

A more direct pathway of proteins being trafficked to lysosomes is through two dileucine motifs found on the C-terminus of some lysosomal proteins (Mattera et al., 2011).

1.9 Lysosomal Membrane

The inner lumen of the lysosome is coated with a heavily glycosylated glycocalyx to prevent self-digestion of the lysosome. This modification is primarily composed of integral lysosomal membrane proteins (LMPs) all of which have multiple glycosylation sites (Saftig and Klumperman, 2009). While the exact number of LMPs has still not been revealed, currently ~25 have been identified, with most of those identified reside in the lysosomal limiting membrane (Lubke et al., 2009), The most abundant of these LMPs are the lysosomal-associated membrane proteins 1 and 2

(LAMP1/2), which comprise of the majority of the lysosomal glycocalyx membrane. Recent studies have highlighted the important contribution of LAMPs to lysosomal integrity as decreased levels of LAMP1/2 have been found to result in a higher sensitivity to anti-cancer drugs in tumour cells due to an increase in lysosomal mediated cell death (Fehrenbacher et al., 2008).

1.10 Phagocytosis

Phagocytosis is a highly conserved important cellular mechanism which is involved in engulfing invading pathogens as well as apoptotic cells >0.5mm in diameter (Luzio et al., 2007). Autophagasomes are activated when the cell undergoes highly stressful conditions such as amino acid depletion and unfolded protein response (Saftig and Klumperman, 2009). The phagosome that has engulfed this material then fuses with the lysosome, maturing into a hybrid organelle called the phagolysosome. This fusion enables the phagolysosome to degrade the engulfed material. Work carried out has found that the lysosomal membrane proteins LAMP1/2 also play an important role in phagosome-lysosomal fusion as depleted levels of LAMP result in the retardation of Rab7 recruitment to phagosomes and their subsequent fusion with lysosome (Huynh et al., 2007, Tanaka et al., 2000).

1.11 Autophagy

Autophagy, derived from the Greek to eat oneself, is the process by which cells will degrade their long-lived cellular components, including organelles, in order to maintain cellular energy levels (Luzio et al., 2007, Levine et al., 2004). Autophagy is involved in cellular processes such as starvation, cell growth, innate immunity, cellular and tissue remodelling and cell death (Luzio et al., 2007, Levine et al., 2004). There are three types of autophagy in mammalian cells, macroautophagy (associated with the degradation of large cytosolic components such as mitochondrion), chaperone mediated autophagy (associated with the direct transport of unfolded proteins into the lysosome through LAMP2A), and microautophagy (associated with the direct lysosomal uptake of material by invaginations and internalisation of the lysosome's limiting membrane) (Parzych et al., 2014). Macrophagy, is the main pathway during which autophagic material will be isolated by a double membrane to form an autophagosome (which can reach ~1μm in diameter), and subsequently fuse with lysosomes where the autophagic material can be degraded (Luzio et al., 2007, Hamasaki et al., 2013). The macroautophagy of mitochondria, or mitophagy as it is also known, is a continuous process that is vital for cell survival, and perhaps one of the most important roles for autophagy. Mitochondria are the energy source of the cell and thus maintaining functional mitochondria is vital for maintaining cellular energy (Campello et al., 2014). Furthermore, the longer lived the mitochondrion, the more reactive oxygen species (ROS)

it produces, which are capable of detrimental damage to other cellular components, and thus the catabolism of mitochondria via autophagy plays a vital role in maintaining cell function (Campello et al., 2014).

1.12 The lysosome: Emerging roles

For a long time it was believed that the lysosome acted primarily as a site of digestion in the cell, but recent research has shown that the lysosome is much more than just the stomach of the cell. It has been shown in many cell types that lysosomes might fuse with the cellular plasma membrane for wound repair. This occurs when the lysosome reacts to an increase in cytosolic Ca^{2+}, causing lysosomal exocytosis (Rodriguez et al., 1997). It has also recently emerged in the last ten years that the lysosome has a role in intracellular signalling, as it is the second largest Ca^{2+} store in the cell after the ER, containing ~500μM Ca^{2+} (Lloyd-Evans and Platt, 2011). This evidence shows that the lysosome possesses many different, dynamic interactions with other cellular compartments that are key for correct cellular function and viability.

1.13 The lysosome as an important Ca^{2+} store

Ca^{2+} is an important ion for cells as it is a major component for intracellular signalling that is needed for key functions such as fertilisation, enzyme activity, gene expression, membrane fusion, cellular motility and apoptosis (Berridge et al., 2003). As Ca^{2+} is such a potent

signalling ion it is important that its levels are tightly regulated inside the cell. This is done via a number of different mechanisms such as the use of cation exchangers and transporters and the intracellular buffering of Ca^{2+} via its storage inside organelles (Pozzan et al., 1994).

Three major intracellular messengers have been discovered to act on the mobilisation of Ca^{2+} inside the cell by acting upon specific Ca^{2+} release channels located on organelle membranes. The three messengers are inositol trisphosphate (IP_3), cyclic adenosine disphosphate ribose (cADPR) and nicotinic acid adenine di-nucleotide disphosphate (NAADP) (Bootman et al., 2002, Clapham, 1995). These secondary messengers are important for key Ca^{2+} signalling events as they receive signals at receptors located on the cell surface and then serve to greatly amplify the strength of that signal to induce major biological changes in the cell.

Work done on sea urchin egg homogenates showed that while IP_3 and cADPR were potent Ca^{2+} releasing messengers from the ER/microsome stores, NAADP was found to still release high Ca^{2+} levels in the sea urchin eggs after treatment with thapsigargin (a sarco-endoplasmic reticulum Ca^{2+} aTPase (SERCA) inhibitor) when compared with the other Ca^{2+} messengers indicating that its primary target was on another Ca^{2+} store (Churchill and Galione, 2001, Clapper et al., 1987, Genazzani and Galione, 1996). Resulting work using subcellular fractionation found that NAADP was involved in Ca^{2+} release from lysosomal-related organelles inside the sea urchin eggs, and it was thus implicated that NAADP works primarily as a lysosomal Ca^{2+} release messenger (Churchill et al., 2002). Again, additional work using the lysosomtropic agent glycyl-phenyl-

alanine 2-naphthylamide (GPN) caused disruption of the lysosomal membrane allowing for the release of the Ca^{2+} stored inside the lysosome. Subsequent treatment with NAADP displayed a diminished Ca^{2+} mediated response from lysosomal stores, further showing that NAADP is highly specific to inducing lysosomal Ca^{2+} release (Morgan and Galione, 2007).

Only recently the target for NAADP has been identified on the lysosomal membrane, this being a member of the Two Pore Channel (TPC) family. TPCs were first hypothesised to be endosomal Ca^{2+} release channels as their plant counterpart was found to be localised on the acidic vacuole Ca^{2+} store inside plant cells as well as the family of proteins having significant similarity to voltage gated Ca^{2+} and Na^{+} channels (Larisch et al., 2012, Marchant and Patel, 2013). The overexpression of green fluorescent protein (GFP) tagged TPCs in cell lines resulted in lysosomal localisation and a greater NAADP induced Ca^{2+} release in these cells, while pre-treatment with bafilomycin (an inhibitor of vATPase which de-protonates the lysosome, leading to an inability to maintain its Ca^{2+} levels) diminished the Ca^{2+} release that was seen previously, leading to the authors conclusions that NAADP acts upon TPCs to induce Ca^{2+} release from acidic stores (Marchant and Patel, 2013). Other work carried out found that TPC1 and 2 both contain dileucine motifs which are needed for correct sorting to the endo-lysosomal system (Brailoiu et al., 2010). Mutations in this targeting motif in the TPC2 protein however resulted in the mislocalisation of this channel to the plasma membrane of the cell (Brailoiu et al., 2010).

1.14 Why study lysosomal function?

It is important that we continue to study lysosomal function, particularly trafficking and degradation mechanisms of macromolecules, the process regulating their degradation and recycling and their emerging roles in Ca^{2+} signalling as defects in any of these events can potentially result in the development of lysosomal storage diseases (LSD) or loss of normal cellular function (e.g. Alzheimer's disease, talked about later).

1.15 Lipids, and their role in health and disease

Lipids are a group of molecules that are essential to cellular viability and have important roles signalling, and storing energy as integral components of cellular membranes (van Meer et al., 2008). Lipids themselves can be characterised into different groups, based on their biochemical properties, such as cholesterol, sphingolipids and phospholipids. However they have been shown to accumulate and be mistrafficked in many lysosomal storage diseases.

1.16 Lysosomal Storage diseases: An overview

LSDs are a group of >50 inherited heterogeneous disorders which are relatively rare individually, but as a group of disorders they have an incidence of 1 in 7500 births (Meikle et al., 1999, Poupetova et al., 2010). They are mainly caused by loss of activity of a soluble intra-lumenal

lysosomal enzyme leading to accumulation of its substrate, however there is a growing group of LSDs caused by loss of function of lysosomal transmembrane proteins whose functions are largely unknown and which have a broader range of consequences on lysosomal function and greater complexity of storage molecules. LSDs are the major cause of childhood neurological disease, although some forms of LSD exist that are non-neurological or manifest only during adulthood. Once these symptoms manifest, they continue to become progressively detrimental to the patients quality of life (Cox and Cachon-Gonzalez, 2012).

The term lysosomal storage disease itself is used to describe the main clinical feature observed in cells with defective lysosomal proteins. In many LSDs there is the accumulation of lipids as either a primary or secondary storage material, however this is not the case for all LSDs. While there seems to be a clear increase in the amount of intra-lysosomal storage material in a particular given disease, the causes of neurobiological defects (with or without cell death), inflammation, hypertrophy or hyperplasia, visceral fibrosis, are very difficult to understand. The recent advent of research into the development of therapies for these lysosomal disorders has resulted in a change in their clinical and pathological description for these diseases (Cox and Cachon-Gonzalez, 2012). The sheer number of different cellular mechanisms that become defected in each lysosomal storage disease means it is difficult to categorise them all under one banner (Walkley et al., 2010).

As mentioned previously, major roles of the lysosome in the cell is the autophagic clearance of other organelles and cellular components. This

process is critical for cellular survival, growth and development. The process itself is highly conserved and numerous autophagy related proteins have been found due to work on yeast models (Levine and Klionsky, 2004). Components to be digested are taken up by phagophores, which then merge with lysosomes to form autophagosomes. A good example of how this process is important for cellular viability is shown in the lysosomal disorder called Danon disease. Patients with Danon disease exhibit cardio- and skeletal myopathy as well as neurodegenerative disorders in heterozygous males (Nishino, 2006). This disorder arises from a gene mutation on the X-chromosome that encodes for the lysosomal protein LAMP 2. LAMP 2 as stated previously is important in maintaining lysosomal membrane integrity as well as it being implicated in phagosome-lysosome fusion as well as chaperone mediated autophagy (Lubke et al., 2009). In Danon disease, due to the defective LAMP-2 protein it results in an impaired fusion between lysosomes and phagophores. This results in a loss in cellular clearance of organelles and other molecules that are to be broken down, leading to a reduction in cellular viability giving rise to this fatal lysosomal disease. The disease's pathogenesis helps illustrate the importance of lysosomal mediated cellular clearance, and how the need for autophagy is necessary for life (Nishino, 2006).

As cells age they accumulate more and more damage to their organelles through factors such as oxidative stress. Because cells like neurons do not divide in adult life the cell has compensated for this by having an expansive lysosomal network for membrane recycling. Autophagic

vacuoles are trafficked along the axons of neuronal cells so to maintain an even distribution, while the lysosomes are maintained within the cell body of the axon. This is an important neural cellular function as it helps to improve autophagic clearance (Tsukita and Ishikawa, 1980). In several neurodegenerative lysosomal diseases it has been observed using electron microscopy that there is an increase in the levels of vacuoles, along with other evidence that there is disturbed autophagic clearance within the cell (Walkley et al., 2010). In some lysosomal diseases such as GM2 gangliosidosis this results in a knock on effect within the cell. This is because the cell tries to compensate for this reduced clearance by mediating the expansion of its autophagic apparatus, which further reduces the effectiveness of the autophagy process.

Defects in the regulation of intracellular Ca^{2+} have been found to give rise to neurodegeneration in some lysosomal diseases. However lysosomal diseases that share a defect in Ca^{2+} signaling each exhibit distinctly different phenotypes. An increase in the release of Ca^{2+} from the endoplasmic reticulum into the cytosol due to a defect in the ryanodine receptor (somehow caused by the storage molecule glucosylceramide) has been found in murine models of Gaucher's disease (and post-mortem patient material) due to an excess of glucosylceramide found in these lysosomal diseased cells (Pelled et al., 2005). Another LSD, GM2 gangliosidosis has increased levels of cytosolic Ca^{2+} that induces a reduced uptake of Ca^{2+} by SERCA. This is most likely due to the excess levels of the gangliosides attributed to this lysosomal disorder potentially being transported out of lysosomes to the ER (Pelled et al., 2005). Other

lysosomal disorders such as Niemann-Pick type C (NPC) show a severe effect on endosomal-lysosomal trafficking due to defects in the levels of lysosomal Ca^{2+} (Vanier, 2010).

1.17 Current methods for treating lysosomal storage diseases

Classically there are two methods to try and alleviate the onset of lysosomal storage diseases in patients by either replacing the defective enzyme with a working one or to reduce the levels of the substrate the defective enzyme breaks down, these two forms of treatment are known as enzyme replacement therapy (ERT) and substrate reduction therapy (SRT) respectively. The first US food and drug administration (FDA) approved treatment for an LSD was for Gaucher disease (an autosomal recessive disease caused by mutations on the *GBA1* gene), where the lysosomal enzyme glucocerebrosidase is defective giving rise to the accumulation of the glycolipid glucocylceramide (Platt et al., 2012). This therapy works by using purified recombinant wild type glucocerebrosidase which is then typically given to the patient intravenously every two weeks (Brady, 2010, Charrow, 2009). This initial success gave rise to similar forms of ERT for other LSDs such as Fabry disease, Pompe disease and several mucopolysaccharide storage disorders (Charrow, 2009, Kakkis, 2002, Schiffmann and Brady, 2006). However this method of treatment has its caveats. The replacement enzyme does not cross the blood brain barrier so it therefore can only be used to treat the peripheral pathology of the disease (e.g.

hepatosplenomegaly), not the central nervous system. As well as this, the procedure itself is highly invasive, as it requires the patient to receive an infusion every two weeks (with treatment taking about a few hours) for the rest of their lives (Platt et al., 2012). However patients can develop antibodies against the enzyme, reducing the efficacy of the treatment.

Another therapy developed for the treatment of lysosomal storage diseases is substrate reduction therapy. Miglustat (OGT 918, *N*-butyl-deoxynojirimycin), an oral small molecule imino sugar, has so far been approved for the treatment of type 1 Gaucher disease worldwide as well as for NPC (in most countries with the exception of the USA) (Platt et al., 2012). This form of treatment targets the Golgi ceramide specific glucosyltransferase where it prevents the synthesis of glucosylceramide, the first step in glycosphingolipids biosynthesis, therefore reducing the levels of these lipids being stored inside the lysosome (Platt et al., 2012). The benefit of this treatment compared with ERT is that it can cross the blood brain barrier so that it can be used to treat the neurological manifestations present in NPC (Patterson et al., 2007), however it does have some side effects such as inhibiting disaccharide synthesis resulting in gastrointestinal problems (Platt et al., 2012). New evidence highlights a potential inhibitory effect of miglustat on non-lysosomal glucosylceramidase, leading to elevation of glucosylceramide in all tissues.

1.18 Recent research implicates impaired lysosomal function in common major diseases

New data has shown that the lysosome has a direct role in a whole host of other major neurodegenerative diseases.

Recent work has found that mutations in the Presenilin 1 gene, *PSEN1,* that encodes for the ER associated Alzheimer's disease related protein Presenilin 1 (PS1) results in the onset of lysosomal dysfunction that may contribute to disease pathogenesis seen in Alzheimer patients (Lee et al., 2010). PS1 is an ER transmembrane protein that has a diverse role inside cells, including cell adhesion, apoptosis and Ca^{2+} homeostasis (Shen and Kelleher, 2007). It is believed that PS1 becomes active once it is cleaved to form a catalytic subunit of the γ-secretase enzyme complex which is known to be involved in the cleavage of many type 1 membrane proteins such as amyloid precursor protein (APP) (which is implicated in the accumulation of β-amyloid in Alzheimers disease) and Notch (Citron et al., 1997, De Strooper et al., 1998). Mutations in the PS1 protein have been shown to result in the mis-trafficking of the V-ATPase subunit V0a1 to the lysosomal proton pump (Lee et al., 2010). The result of this is that the V-ATPase cannot function properly, causing the lysosome to alkalinize. This results in defects in the degradation of autophagic/lysosomal substrates, giving rise to the accumulation of β-amyloid that is the main pathogenic hallmark of Alzheimer's disease (Lee et al., 2010).

The roles of lysosomes in Parkinson disease have also started to garner more attention after it was found that there was a 6-11 fold increase in the rate of developing sporadic Parkinson disease for people who were heterozygous for *GBA1* mutations (Rosenbloom et al., 2011). Currently mutations in the GBA gene are designated as the number one risk factor for the development of Parkinson disease (Sidransky et al., 2009).

Other well established diseases such as the tri-nucleotide repeat disorder Huntington's disease have been found to possess dysfunctional lysosomes, possibly resulting in a reduction in the degradation of polyglutamine residue aggregates, giving rise to the pathogenesis seen in this disease. Even prion disease such Creutzfeldt-Jakob disease have also been implicated to possess dysfunctional lysosomes (Lee et al., 2011). Due to recent research in these common neurological diseases, the role of lysosomes in cellular homeostasis, particularly clearance of defective aged cellular aggregates or organelles, has been highlighted to be important for correct cellular viability.

1.19 Niemann-Pick type C: An overview

Niemann-Pick disease type C (NPC) is a severe autosomal recessive neurodegenerative disorder. Patients with NPC often die in young infancy, but those with a severe disease progression survive until late adolescence (Maceyka et al., 2005). However some NPC patients with a much slower progression of symptoms live into adulthood. The predominant trait NPC sufferers present are cererbellar atrophy,

characterized by a selective loss of purkinje neurons, which results in ataxia (Ko et al., 2001). Other symptoms include respiratory problems, learning difficulties as well as presenting with the earliest onset of Alzheimer disease like pathology (~10 years of age) (Davies et al., 2000, Liscum, 2000). While NPC is a member of the Niemann-Pick group of LSDs, the cellular pathogenesis and patient phenotypes differ greatly from those observed in Niemann-Pick types A and B which both occur due to deficiencies in the lysosomal enzyme acid sphingomyelinase (Ikonen and Holtta-Vuori, 2004, Sturley et al., 2004). However it should be noted that acid sphingomyelinase activity is reduced in NPC disease, it is not the main cause of disease progression (Lloyd-Evans and Platt, 2010).

1.20 NPC gene mutations

NPC disease arises from autosomal recessive mutations in the genes that encode either the NPC1 (95% of cases) or NPC2 (5% of cases) proteins. A mutation in either results in a completely indistinguishable NPC phenotype. Human NPC1 gene is localised to chromosome 18q11-12 and encodes a 1278 amino acid glycoprotein that consists of 13 transmembrane domains (Park et al., 2003).

1.21 The NPC Proteins

NPC1 is a protein that is localized to the membrane of late endosomes/lysosomes and has a weak homology to mediators of cholesterol homeostasis (Patched, HMG CoA reductase), while NPC2 is a soluble protein located within the lysosome itself that acts as a cholesterol shuttle (Lloyd-Evans and Platt, 2010). Due to this it has been proposed that the NPC1 and 2 proteins must act in the same cellular pathway to deliver cholesterol out of the lysosome. So far, however, there is no direct evidence for this hypothesis and the function of the NPC1 protein function has remained largely inconclusive (Erickson et al., 2000). While the true purpose of NPC1 remains unclear, it is currently understood that NPC2 transfers cholesterol to (or away from) NPC1 via its cholesterol-binding site located on its N-terminal. This would suggest that NPC1 has a role in cholesterol regulation (Erickson et al., 2000). This would seem an appropriate hypothesis as one of the key characteristics of NPC lysosomes is the storage of multiple lipids of different classes including cholesterol, sphingomyelin and glycosphingolipid (Ginzburg et al., 2004). However, it should be noted that cholesterol transport out of lysosomes can be achieved in NPC1 null cells by a variety of cellular treatments (such as curcumin (Lloyd-Evans et al., 2008)) casting doubt on the absolute requirement for the NPC1 protein in mediating lysosomal cholesterol efflux. It has been found that the reason for the accumulation of these macromolecules in NPC cells arises from the impaired ability for lysosomal/late endosomal fusion as well as vesicular transport leading to

an accumulation of the endocytic cargo in the late endosomes (Bach et al., 1999, Christensen et al., 2002). This is believed to be because late endosome/lysosome fusion is a Ca^{2+} dependent process and that the storage of the simple sphingolipid sphingosine inside lysosomes, a specific defect of NPC disease, impairs lysosomal ability to uptake Ca^{2+}, leading to reduced lysosomal Ca^{2+} levels and release, impaired endosomal-lysosomal fusion and retarded endocytic trafficking and ultimately lipid storage in the cell (Lloyd-Evans et al., 2008). While the true role of NPC1 may remain elusive, recent homology studies have found that the NPC1 protein has strong homology with the RND (resistance-nodulation division) permease family of proteins which are a group of highly conserved proteins involved in the transport of complex lipids, antibiotics and metal ions in bacteria (Scott and Ioannou, 2004). The reduced Ca^{2+} levels in NPC lysosomes has resulted in the hypothesis that NPC1 is acting as a sphingosine transporter, however recent work has shown evidence that NPC is involved in viral efflux out of the endocytic system (Carette et al., 2011). The unknown function of NPC1 protein as well as many other lysosomal membrane proteins helps highlight the need to identify their roles so that we can fully understand how certain lysosomal storage diseases arise and how lysosomes regulate their function. However it is important to note that without LSDs we would not know about several lysosomal proteins such as TRPML1 and CLN3.

1.22 Neuronal Ceroid Lipofuscinosis

With an incidence of 1 in 12,500 live births, the Neuronal Ceroid Lipofuscinoses (NCL) are a group of autosomal recessive diseases that result in the onset of neurodegeneration in children/young adults followed by death (Bennett and Rakheja, 2013). Collectively this group of diseases is known as Batten(s) disease after Sir Frederick Batten who first characterized the disease in the early 1900's (Persaud-Sawin et al., 2007). So far 14 clinical variants have been identified (CLN1-CLN14) and the genes for all, except CLN7, have been identified (Persaud-Sawin et al., 2007). They are commonly classified into four subtypes depending on the age onset of the disease, Known as: Infantile (INCL), Late-infantile (LINCL), Juvenile (JNCL) and adult types (Kang et al., 2013).

Despite the fact that different gene mutations determine the onset of the disease, the phenotypes observed between all the NCLs are very similar which is why they are grouped together. Initial symptoms such as vision and hearing loss are first observed, followed by impaired motor function and a serious decline in the patients mental capacity as a result of neurodegeneration. By the end of the disease's progression there is widespread neuron loss followed by death. Cells present with the lysosomal accumulation of the fluorescent material called lipofuscin, specific protein accumulation such as subunit c of the mitochondrial ATPase, cell cycle dysregulation, abnormal sphingolipid/phospholipid accumulation and an increase in apoptosis in the mutant CLN cells (Palmer et al., 2013).While one of the most prominent phenotypes in

NCLs is the loss of neurons, the cellular increase in protein accumulation and lipofuscin, this is not just confined to neurons as storage bodies have been found in many different cell tissues including those outside of the central nervous system (Bennett and Rakheja, 2013).

While many of the disease causing genes have been identified it is still unclear whether there is a common link in the pathogenic mechanisms between each of the different CLN mutations.

1.23 *CLN* gene products

Multiple different genes that encode different proteins have been identified to have defects in NCL. The roles of these proteins have been found to differ from one another, as does their respective cellular localization.

The CLN proteins that are best understood are those that are expressed by the CLN1, CLN2, CLN3, CLN5, CLN6 and CLN8 genes (Persaud-Sawin et al., 2007). The protein products that are encoded by CLN1 and CLN2 are lysosomal enzymes involved in the removal of long fatty acids and tri-peptides respectively (Palmer et al., 2013). CLN6 and 8 encode membrane bound proteins while the protein that is encoded by CLN5 is a membrane glycoprotein. The protein products of CLN4,7,9 and 10 are still poorly understood and their respective proteins function is only speculated.

1.24 Theory on NCL disease mechanisms

While numerous studies have been carried out to try and further understand the pathogenic mechanisms in NCLs, it is still unclear what the major cellular defect is. A recent theory has attributed NCL pathogenesis to the accumulation of subunit c of mitochondrial ATP synthase (observed in CLN2, CLN3, CLN5, CLN6 and CLN7). Subunit c is the pore forming, membrane spanning subunit of the mitochondrial ATP synthase complex (Palmer et al., 1992). Subunit C is an important component of the ATP synthase enzyme, which is responsible for the synthesis of ATP inside the cell. The turn over of this subunit is important for correct mitochondrial function and its transport to the lysosome for degradation and its subsequent recycling as component parts back into the cell is important for cellular viability. Correct autophagy and intracellular trafficking are central to this process (Palmer et al., 2013). Problems in the trafficking and the degradation of subunit c has often been attributed to a breakdown in the catabolic pathway for this molecule resulting in a higher chance that the cell will become apoptotic due to a decrease in the cells ability to generate ATP.

The NCLs share phenotypes that are similar at the clinical level as well as the biochemical level. For this reason they are classified together as a group of storage diseases. While much research has been carried out on the different types of NCLs, most reports only concentrate on one aspect of the disease exclusively with little information on up-stream or down-

steam events or the affects on other intracellular pathways. However, one thing that a lot of researchers seem to agree on is that the NCL genes most likely belong to a common metabolic pathway (Weimer et al., 2002).

1.25 Juvenile Neuronal Ceroid Lipofuscinosis (JNCL)

JNCL (or CLN3) is the most common form of the heterogenous group of NCLs with overlapping symptoms of other NCLs. Initial symptoms of hearing loss typically present from the ages of 4-8 years old, followed by gradual loss of vision resulting in complete blindness within 2-4 years (Bennett and Rakheja, 2013). Further symptoms such as seizures, motor disorders and mental regression present themselves in the second decade of the patients' life. Patients typically live to their early 20's, however some rare cases have reported patients living into their 30's. While neuronal loss is attributed as the cause of death, some emerging evidence has suggested that other factors such as the loss defects in the patient's cardiovascular system have been reported in a growing number of cases (Kousi et al., 2012). Some evidence has shown that female patients with the same type of *CLN3* mutation as males have a milder disease progression, with many outperforming males in fine motor control (Augustine et al., 2013). While the reasons behind this are still unclear, some have speculated that this is due to hormonal differences between males and females.

1.26 The *CLN3* gene

Mutations in the *CLN3* gene results in the onset of JNCL. The gene itself has been found to be located on chromosome 16p11.2. The majority of JNCL patients (~74%) have been found to have a homozygous mutation that is the result of a 1kb genomic deletion that occurs between introns 6 and 8 (Kousi et al., 2012). A further ~22% of patients have been found to be heterozygous for this mutation. This 1kb deletion induces a frameshift mutation resulting in a premature stop codon. Exons 7 and 8, which are excised as a result of the mutation, have been predicted to encode the amphipathic helix on the luminal face of the CLN3 protein. The result of this defect in protein translation has been predicted to have an impact on the CLN3 proteins ability to form strong protein/ligand binding critical for mediating CLN3 protein function and trafficking (Golabek et al., 2001, Haskell et al., 2000).

1.27 The CLN3 protein

The CLN3 protein, encoded by the *CLN3* gene, is a 438 amino acid transmembrane protein, which is predicted to possess 6 transmembrane domains (Mao et al., 2003). The protein itself is highly conserved and ubiquitously expressed in different cell types and has an ortholog in yeast known as *CLN3p* that encodes for the Btn1p protein (also called battenin) (Jarvela et al., 1999). The *CLN3p* gene in yeast has been found to be 39% identical and 59% similar to its mammalian counterpart, however

work done on yeast models often find Golgi abnormalities which are not present in mammalian *CLN3* mutant cells. *In silico* analysis of the CLN3 protein has been used to find sequence similarity in other types of proteins. This analysis found that the CLN3 protein bears a similarity to members of the major facilitator superfamily (MFS). The MFS is a large family of transmembrane transporters that are involved in the transport of small solute uniporters, symporters and antiporters (Pao et al., 1998). These permeases play an important role in the cellular transport of simple sugars, oligosaccharides, organic and inorganic cations.

1.28 CLN3 protein trafficking and its potential role in the endo-lysosomal pathway

The CLN3 protein is synthesized in the ER and is then further processed in the Golgi apparatus where it is then transported to its cellular location. The protein has been found to have two dileucine lysosomal targeting motifs that have been hypothesized to mediate the lysosomal targeting of the CLN3 protein once it has left the Golgi apparatus (Kyttala et al., 2004, Storch et al., 2004). Another theory on CLN3 trafficking is that it is localized to the plasma membrane before being taken up by early endosomes. It is then processed along the endocytic pathway towards the lysosome (Nijssen et al., 2003, Sleat et al., 2007). *In vivo* work has been done to suggest that the Cln3 protein is expressed within the endosomes and lysosomes. Fractions taken from mouse liver found that the Cln3 protein was highly enriched in the lysosomal fraction when

compared to the ER and Golgi fractions following density gradient centrifugation (Cao et al., 2006, Ezaki et al., 2003). However the method they used does not produce pure lysosomes, so it is possibly contaminated with other organelles.

1.29 The importance for studying lysosomal proteins in an isolated system

The severe pathogenesis and poor prognosis of patients with a lysosomal storage disease helps highlight the need to understand key lysosomal regulation and function so that it may help in the development of more suitable forms of treatment in the future. While advancements have been made in recent years on our understanding of the lysosome and how it is so much more than just the stomach of the cell (which is too simplistic a terminology) many components of the lysosome are still unknown or their functions not fully characterised. This is in part due to out of date techniques used to isolate lysosomes so that they can be examined in an isolated environment, free of contamination from other organelles, and are still structurally intact and functional. The means to purify lysosomes that are functional is especially an important feature as many lysosomes in LSDs have defects in their Ca^{2+} levels or pH. Unfortunately methods such as density gradient centrifugation cannot produce functional lysosomes due to the high levels of gravitational force exerted on them during the centrifugation process.

1.30 Lysosomal purification with the use of magnetic nanoparticles

One of the main problems facing lysosomal researchers is the difficulty in purifying out lysosomes from cells without contamination from other organelles. The current method most often used is density gradient centrifugation, which is a method that separates organelles based on their respective buoyant density (Liu et al., 2012). However, the majority of lysosomal storage disorders result in primary or secondary storage of lipids in the lysosome. This accumulation results in a change in the buoyant density of the lysosome, thus leading to a heterogeneous sampling of the lysosomal population from Density Gradient Centrifugation as well as subsequent contamination by other organelles (Graham, 2001).

Previous work utilising iron based nanoparticles and a magnetic field has been done in an attempt to purify out lysosomes from cells. However, due to the instability of these nanoparticles and their poor magnetic potential led to an increase in cellular toxicity and a poor lysosomal yield obtained (Diettrich et al., 1998). The recent advancement in nanoparticle technology has resulted in the production of highly magnetic iron based nanoparticles known as Super Paramagnetic Iron Oxide Nanoparticles (SPIONs) that consist of a magnetite core functionalised with a large dextran coat (Wahajuddin and Arora, 2012). These particles offer greater potential in purifying lysosomes via magnetic separation as they have a much greater magnetic potential than the iron based nanoparticles used previously and a reduction in cellular toxicity due to stability of the dextran

coat. The importance of stable nanoparticles to purify lysosomes will be discussed further in chapter 3.

1.31 Aims

Chapter 3: To test for any increase in the levels of cellular toxicity following treatment with super paramagnetic nanoparticles. The least toxic SPIONs will be the most ideal magnetic particle to purify lysosomes.

Chapter 4: To develop an improved lysosomal magnetic purification assay, where lysosomes can be purified with high yield, low contamination from other organelles and still be functional.

Chapter 5: To observe any key phenotypic changes in *Cln3*$^{\Delta ex7/8}$ cerebellar cells to help further our understanding of the role CLN3 may have in the cell.

Chapter 6: To analyse *Cln3*$^{\Delta ex7/8}$ cerebellar Ca^{2+} levels to determine if there is a defect in Ca^{2+} homeostasis in these cells. Also to try and identify the function of CLN3.

Chapter 2:
Material and Methods

2.1 Cell culture of CHO-H1 and CHO M12 cell lines

CHO-H1 cell lines were obtained from Dr. Emyr Lloyd-Evans, Cardiff University, Cardiff. NPC1 null CHO M12 were provided as a gift from Professor Daniel Ory (St.Louis hospital). Cho-H1 and CHO M12 cells were grown in DMEM-F12 medium with supplemented 10% FCS (Sigma) and 1% L-Glutamine (Lonza) as monolayers in T75 flasks (Fisher) at 37 °C with 5% CO_2 in a humidified incubator.

2.2 Cell culture of Cln3 cerebellar cells and CLN3 mutant patient fibroblast cell lines

Precursor cerebellar cells were provided as a gift by Dr Cotman (Harvard university) and grown in DMEM (Sigma) supplemented with 24mM KCL (Sigma), 85.5μg/ml Genetecin (Gibco), 10% FCS (Sigma) and 1% L-Glutamine (Lonza) as monolayers in T75 Flasks (Fisher) at 33 °C with 5% CO_2 in a humidified incubator.

Wild type fibroblast and CLN3 mutant fibroblast cell lines were provided as a gift from Dr Sarah Mole (University College London, London). These cells were grown in DMEM medium (Sigma) supplemented with 10% FCS (Sigma) and 1% L-Glutamine (Lonza) as monolayers in T75 flasks (Fisher) at 37 °C with 5% CO_2 in a humidified incubator.

2.3 Lysosomal purification

This method was adapted from (Duvvuri and Krise, 2005).

2.3.1 SPION treatment of cells

Cells to be purified are grown in a T75 Flask (FISHER) under normal tissue culture conditions. When the cells are ~80% confluent the nanoparticle containing pulse medium is ready to be added. Cell culture media is removed from the cells and replaced with pulse media containing 1ml of Dextran stabilized 45nm magnetite particles in dH_2O (provided by Liquids Research Ltd unless stated otherwise), 9ml of cell culture medium and 100µl of 1M HEPES pH 7.2 (LONZA) before incubated under normal cell culture conditions for the designated pulse time (24 hours unless stated otherwise). A sufficient pulse time is important so to give time for the magnetic nanoparticles to reach the lysosome. Once these particles have reached the lysosome it now possesses a magnetic potential.

The pulse medium is then removed and the cells are washed once in 10ml Dulbecco's Phosphate Buffered Saline (DPBS) (SIGMA ALDRICH). Normal cell culture medium is then added to the cells where they are incubated under normal culture conditions for the appropriate chase time (24 hours unless stated otherwise). After the allotted chase time the media is removed and the cells are washed once in 10ml of DPBS and

the cells are trypsined off the flask by incubating in 1ml of 1x Trypsin (SIGMA ALDRICH) for 5 minutes at 37°C. 9ml of medium is added to the trypsinised cells to quench the Trypsin and they are then transferred to a 15ml Falcon tube (GREINER) before undergoing a low speed centrifugation (1000rpm) to pellet the cells. The medium is discarded before the pelleted cells are resuspended in 10ml of DPBS, to remove excess medium, and are again pelleted at low speed centrifugation. During this time the two buffers used are prepared and kept on ice till required.

Hypotonic buffer A consists of: 15mM Potassium Chloride (SIGMA ALDRICH), 1.5mM Magnesium Acetate (Sigma Aldrich), 1mM Dithiothreitol (FISHER), 10mM HEPES pH 7.2 and 1µl of protease inhibitor cocktail III (FISHER) and dH_2O.

Isotonic buffer B consists of: 375mM Potassium Chloride, 22.5mM Magnesium Acetate, 1mM DTT, 100µM Sucrose (SIGMA ALDRICH), 220mM HEPES pH 7.2 and 20U/mg of DNAse1 (ROCHE) and dH_2O.

2.3.2 Homogenisation of SPION treated cells

After the low speed centrifugation the DPBS is discarded and the pelleted cells are resuspended in 4ml of buffer A to rupture the cellular membrane via osmotic swelling to release the cellular organelles. The suspension is then transferred to a Dounce homogeniser (FISHER) where it is homogenised for 30 strokes to further break open the cells. The

homogenised solution is then transferred to a 50ml Falcon tube (GREINER) and passed through a 23G needle (BECTON DICKINSON) attached to a 5ml syringe to break open more cells via shear force. After this, 1ml of buffer B is added to the homogenised solution to prevent damage to the cellular organelles that had been released from the homogenised cells, and the solution is transferred to a 15ml Falcon tube. The solution is then centrifuged at 1500rpm for 10 minutes to pellet out unbroken cells.

2.3.3 Passing homogenised cell content over the LS column

After the homogenised solution has been centrifuged, the supernatant was passed over a 5ml QuadroMACS™ LS column (MILTENYI) that is attached to a 2 tesla QuadroMACS™ separation unit (MILTENYI) which has been pre-equilibrated with 1ml 0.5% Bovine Serum Albumin (SIGMA ALDRICH) in DPBS.

The supernatant is allowed to pass through the LS column where organelles (i.e. magnetite containing lysosomes) that possess a magnetic potential are retained in the column due to the magnetic field the 2-tesla magnet generates. The Supernatant that passes through the column is collected at the bottom in a 5ml tube (STAR LABS). This collected fraction is called the post nucleic supernatant (PNS) and contains material that does not possess a magnetic potential and is not retained on the column.

The pelleted, unbroken cells can be re-homogenised by repeating the homogenisation steps done in 2.3.2 to further improve the protein yield obtained from the lysosomal purification assay. Following the re-homogenisation steps the solution is then centrifuged again and the supernatant is passed through the LS column again. The supernatant that passes through the column is collected and is termed PNS2 fraction.

2.3.4 LS column Wash steps

1ml of 20U /mg DNase1 in DPBS is passed through the LS column to remove any DNA that might be causing organelles other than lysosomes to stick to the column due to DNA's sticky nature. The DNase1 solution that passes through the column is then collected in a 5ml tube. This is called the DNase1 fraction. 2ml of DPBS is then passed through the LS column to remove any remaining DNase1. The DPBS is collected in a 5ml tube and is termed the PBS fraction.

2.3.5 Elution of magnetically retained material

The LS column is then removed from the QuadroMACS™ separation unit and the magnetically retained material was eluted off the column in 0.5ml of DPBS using a plunger supplied with the columns. This eluted material is called the lysosomal fraction, due to it being enriched with lysosomes (and late-endosomes).

1µl of protease inhibitor cocktail III is then added to the lysosomal fraction to prevent degradation of the protein. For functional assays, the lysosomal fraction is kept on ice while their respective protein content is determined using a BCA protein assay. The different fractions obtained from the lysosomal purification assay that are not used straight away are kept at -20°C.

2.4 BCA protein assay

BCA Protein Assay was performed as per the manufacturer's instructions (SIGMA ALDRICH). Absorbance was read using a TECAN absorbance microplate reader at 570nm wavelength.

2.5 Preparation of Coverslips for Microscopy

Cellular suspensions were counted then seeded onto 15mm cover slips (VWR) in 24 well plates (GREINER) at ~10,000 cells per coverslip for CHO-H1 and CHO M12, Cln3 wild type and mutant cerebellar cells and human fibroblasts.

2.6 Cellular imaging via fluorescent microscopy

All images were obtained and captured with a Zeiss Axioimager inverted microscope with a Colibri LED light source, and a Zeiss Axiocam MrM

CCD camera using Axiovision software. Microscopy images were edited using Adobe Photoshop software. This software was also used to quantify the level of fluorescence present in cells after they had been stained (via thresholding). Edited cell images were arranged using Adobe Photoshop and Microsoft Powerpoint software. *n* number denotes the number of times the experiment has been repeated on separate days.

2.7 Statistical analysis

Statistical testing and graph preparation was performed using GraphPad Prism 5 (GraphPad Software, Inc). A P-Value of <0.05 was considered significant. A relative degree of significance is defined in each figure legend. Mutant CLN3 or SPION/FeO treated cells are determined to be significant against wild type/untreated controls.

2.8 Live staining

2.8.1 Dihydroethidine (DHE)

DHE (SIGMA ALDRICH) detects the presence of Super Oxide by being oxidized by it. Cell medium was removed from the cells grown on cover slips and washed with 500µl DPBS to remove excess medium, DPBS was then removed. Cells were then loaded with 50µM of DHE in DPBS and then left in the dark at ~16°C for 30 minutes. DHE solution is then removed before the cells are washed twice in 1ml DPBS. The cells are

then imaged live. Excitation 470nm, Emission 610.

2.8.2 Diphenyl-1-Pyrenylphosphine (DPPP)

DPPP (POLYSCIENCES INC) detects the presence of lipid peroxidation as it becomes fluorescent when it is oxidized by lipid hyperoxides. Cells were grown on cover slips as described in 2.5 and media was removed followed by 500µl DPBS wash, DPBS was then removed. Cells were loaded with 10µM of DPPP in DPBS and incubated at 37°C for 15 minutes. DPPP solution was removed and the cells were washed twice with 1ml DPBS and imaged live. Excitation 352nm, Emission 380nm.

2.8.3 Lysotracker green

Lysotracker green (INVITROGEN) is a probe that fluoresces when it loads into acidic compartments in the cell. Cells were grown on cover slips as described in 2.5 and media was removed followed by 500µl DPBS wash, DPBS was then removed. Cells were loaded with 200nM of Lysotracker green probe in DPBS and incubated at 37°C for 15 minutes. Lysotracker green probe was then removed and the cells were washed twice with 1ml DPBS and imaged live. Excitation: 443nm, Emission 505nm.

2.8.4 Mitotracker green

Mitotracker green (INVITROGEN) is a probe that localises to the mitochondria and fluoresces. Cells were grown on cover slips as described in 2.5 and media was removed followed by 500µl DPBS wash, DPBS was removed. Cells were then loaded with 200nM of Mitotracker green probe in DPBS and then incubated at 37°C for 15 minutes. Mitotracker green probe was then removed and the cells were washed twice with 1ml DPBS and imaged live. Excitation: 490nm, Emission 516nm.

2.8.5 Mitotracker ROS

Mitotracker ROS (INVITROGEN) is a probe that localises to the mitochondria and becomes oxidised by mitochondria produced reactive oxygen species, and fluoresces. Cells were grown on cover slips as described in 2.5 and media was removed followed by 500µl DPBS wash, DPBS was then removed. Cells were then loaded with 200nM of Mitotracker ROS probe in DPBS and then incubated at 37°C for 15 minutes. Mitotracker ROS probe was then removed and the cells were washed twice with 1ml DPBS and imaged live. Excitation: 554nm, Emission 576nm.

2.8.6 ER tracker

ER Tracker (INVITROGEN) is a probe that localises to the ER and fluoresces. Cells were grown on cover slips as described in 2.5 and media was removed followed by 500µl DPBS wash, DPBS was then removed. Cells were then loaded with 200nM of ER Tracker probe in DPBS and incubated at 37°C for 15 minutes. ER Tracker probe was then removed and the cells were washed twice with 1ml DPBS and imaged live. Excitation: 504nm, Emission 511nm.

2.8.7 LipidTOX Red

LipidTOX Red phospholipidosis (INVITROGEN) is a probe that detects phospholipidosis in the cell. Cells were grown on cover slips as described in 2.5 and media was removed followed by 500µl DPBS wash, DPBS was then removed. Cells were then loaded with 1µM of LipidTOX Red phospholipidosis probe in DPBS and then incubated at 37°C for 4 hours. LipidTOX Red phospholipidosis probe was then removed and the cells were washed twice with 1ml DPBS and imaged live. Excitation: 595nm, Emission 615nm.

2.8.8 Magic Red cathepsin B & L

Magic Red Cathepsin B & L kit (IMMUNOCHEMISTRY) was used to detect for the activity of the lysosomal enzymes Cathepsin B & L by using a substrate that releases fluorescence when it is cleaved by its respective

cathepsin enzyme. This was performed as per the manufacturers instructions. Cells were grown on cover slips as described in 2.5 and media was removed followed by 500µl DPBS wash, DPBS was then removed. Cells were then loaded with 1µM of magic red substrate in DPBS and incubated at 37°C for 30 minutes. Magic red substrate was then removed and the cells were washed twice with 1ml DPBS and imaged live. Excitation: 592nm, Emission 628nm.

2.8.9 Fura 2

Fura 2 (TEF LABS) was used to detect for the presence of Fe^{2+} in cells. Cells were grown on cover slips as described in 2.5 and media was removed followed by 500µl DPBS wash, DPBS was then removed. Cells were then loaded with 5µM of Fura 2 in complete medium containing 0.025% Pluronic F-127 (SIGMA ALDRICH) and then incubated at 37°C for 1 hour. Pluronic F-127 was used as a dispersant to prevent aggregation of the metal ion probe. Fura 2 probe was then removed and the cells were washed twice with 1ml DPBS and imaged live. Excitation: 443nm, Emission 505nm.

2.8.10 Calcein

Calcein probe (INVITROGEN) was used to detect for the presence of Fe^{3+} in cells. Cells were grown on cover slips as described in 2.5 and media was removed followed by 500µl DPBS wash, DPBS was then

removed. Cells were then loaded with 30μM of Calcein in DPBS containing and then incubated at ~16°C for 30 minutes. The Calcein probe was then removed and the cells were washed twice with 1ml DPBS and imaged live. Excitation: 485nm, Emission 530nm.

2.8.11 Phen green

Phen green (INVITROGEN) was used to detect for the presence of Zn^{2+} and Cu^{2+} in cells. Cells were grown on cover slips as described in 2.5 and media was removed followed by 500μl DPBS wash, DPBS was then removed. Cells were then loaded with 2μM of Phen green in complete medium containing 0.025% Pluronic F-127 and then incubated at 37°C for 1 hour. Pluronic F-127 was used as a dispersant to prevent aggregation of the metal ion probe. Phen green probe was then removed and the cells were washed twice with 1ml DPBS and imaged live. Excitation: 490nm, Emission 520nm.

2.8.12 Newport green

Newport green (INVITROGEN) was used to detect for the presence of Zn^{2+} and Cu^{2+} in cells. Cells were grown on cover slips as described in 2.5 and media was removed followed by 500μl DPBS wash, DPBS was then removed. Cells were then loaded with 5μM of Newport green in complete medium containing 0.025% Pluronic F-127 and then incubated at 37°C for 1 hour. Pluronic F-127 was used as a dispersant to prevent

aggregation of the metal ion probe. Newport green probe was then removed and the cells were washed twice with 1ml DPBS and imaged live. Excitation: 505nm, Emission 535nm.

2.8.13 N,N,N',N'-Tetrakis(2-pyridylmethyl)ethylenediamine (TPEN)

Phen green and Newport green experiments done with the use of the Zn^{2+} chelator, TPEN (SIGMA ALDRICH), were done the same as described above, but with 10μM TPEN added to the metal ion probe solution.

2.8.14 Lysosensor Yellow/Blue

Lysosensor Yellow/Blue (INVITROGEN) was used to measure intracellular pH levels in lysosomes. Cells were grown on cover slips as described in 2.5 and media was removed followed by 500µl DPBS wash, DPBS was then removed. Cells were washed with DPBS three times then loaded with 1μM of Lysosensor yellow/blue in DPBS for 15 minutes at 37°C. Cells were washed two times with 1ml DPBS and imaged live. Excitation: 335nm, Emission 452nm.

2.8.15 Oregon green BAPTA

Oregon green BAPTA probe (INVITROGEN) was used to measure intracellular Ca^{2+} levels in lysosomes. Cells were grown on cover slips as

described in 2.5 and media was removed followed by 500µl DPBS wash, DPBS was then removed. Cells were washed with DPBS three times then loaded with 100µM of Oregon green BAPTA in DPBS for 6 hours at 37°C. Cells were washed twice with 1ml DPBS and imaged live. 10µg/ml TRITC-Red dextran (SIGMA ALDRICH) was used as a loading control to show the Oregon green BAPTA probe was in the lysosomal compartment. Excitation: 494nm, Emission 523nm.

2.9 Western Blotting

2.9.1 Denaturing protein

100µl of lysosomal fraction/PNS fraction in H_2O to give a protein concentration of 5µg was denatured in 300µl Sample buffer (10g Glycerol (SIGMA ALDRICH), Tris-HCL (SIGMA ALDRICH), Bromophenol Blue (FISHER), SDS (FISHER) in 25ml H_2O) for 1 hour at 60°C.

2.9.2 Gel electrophoresis

The denatured proteins are loaded into wells on a 10% SDS-PAGE gel (FISHER) along with 10µl of a protein ladder (NEW ENGLAND BIO LABS). The gel is then inserted into an ATTO electrophoresis machine. The ATTO electrophoresis machine is then filled with Gel running buffer (14.4g Glycine (FISHER), 3g Tris-Base (FISHER), 1g SDS and 1 litre

H_2O). The protein loaded gel undergoes electrophoresis at 160v for 2 hours to separate proteins based on their respective molecular size.

2.9.3 Gel transfer

Immobile Transfer membrane (MILLIPORE) is washed for 1 minute in 100% Methanol (FISHER) before being washed for a few seconds in Transfer buffer (3.5g Glycine, 7g Tris-Base, 1.7g SDS and 1 litre of H_2O). The gel is then placed on top of the Immobile Transfer membrane and sandwiched between Whatman filter paper (GE HEALTHCARE) that has been soaked in transfer membrane. This is then placed in a gel transfer machine and 40mA per transfer membrane for 2 hours is applied to transfer the protein from the gel to the transfer membrane.

2.9.4 Blotting of antibodies against transfer membrane

The transfer membrane containing the proteins are then blocked overnight (to reduce non-specific binding of the antibodies) at <4°C in 50ml of 5% Marvel milk powder solution in TBS-Tween wash buffer (6g Tris-Base, 8.8g NaCl, 1ml Tween 20 (SIGMA ALDRICH) made up to 1litre with H_2O).

The milk powder solution is then washed off the transfer membrane with repeated TBS-Tween wash steps and the transfer membrane is then incubated with the primary antibody overnight at <4°C (dilutions listed

below). Unbound primary antibody is removed via repeated TBS-Tween wash steps and the transfer membrane is incubated with the secondary antibody at ~ 16°C for 1 hour. Unbound secondary antibody is removed via repeated TBS-TWEEN wash steps.

Primary antibody dilutions: GAPDH (GENETEX) 1:10,000 dilution from a 1mg/ml stock, NPC2 (SIGMA ALDRICH) 1:1000 dilution from a 0.39mg/ml stock, NPC1 (NOVUS) 1:1000 dilution from a 1.15mg/ml stock, Calnexin (ABCAM) 1:1000 dilution from a 1mg/ml stock, Cytochrome C (ABCAM) 1:5000 dilution from a 0.5mg/ml stock, Caveolin 2 (GENETEX) 1:1000 dilution from a 0.94mg/ml.

Anti mouse/Rabbit Secondary antibody dilution (THERMO SCIENTIFIC): 1:10,000 dilution from a 0.5mg/ml.

2.9.5 ECL development of antibody blotted transfer membrane

The transfer membrane is washed for 1 minute in ECL development solution from the ECL development kit (THERMO SCIENTIFIC). The membrane is then wrapped in cling film and exposed onto X-Ray film (Santa Cruz) inside a light-free case. The exposed film is then developed using an X-ray developing machine.

2.10 Enzyme assays

2.10.1 Alkaline Phosphatase

This assay was used to detect the presence of the Plasma membrane enzyme Alkaline Phosphatase in the lysosomal fraction. This assay was performed in a transparent, flat well 96 well plate (GREINER). For each well the volumes were: 20µl lysosomal fraction, 30µl DPBS and 50µl of PNP substrate mixture (SIGMA ALDRICH). Following addition of the PNP substrate mixture the plate was incubated for 1 hour at 37°C. After 1 hour 100µl of sodium hydroxide was added to stop the reaction. Absorbance was measured using a TECAN absorbance microplate reader at 405nm wavelength.

2.10.2 Alpha Mannosidase

This assay was used to detect the presence of the Golgi apparatus enzyme Alpha-Mannosidase in the lysosomal fraction. 10µl per ml of 1M HEPES (pH 7.2) was added to the PNP-α-D-mannosidase (SIGMA ALDRICH) to buffer the pH. For each well the volumes were: 20µl lysosomal fraction, 30µl DPBS and 50µl of PNP-α-D-mannosidase substrate mixture per well of a transparent, flat well Greiner 96 well plate and left for 1 hour at 37°C. 100µl of sodium hydroxide was then added to stop the reaction. Absorbance was measured using a TECAN absorbance microplate reader at 405nm wavelength.

2.10.3 MTS assay

This assay was used to detect the presence of mitochondrial activity in the lysosomal fraction. This assay was performed in a transparent, flat well 96 well plate (Greiner). This assay was performed as per the manufacturer's instructions (PROMEGA). 100µl of MTS substrate was added per well followed by 10µl of lysosomal fraction. The Plate was then left for left for 1 hour at 37°C. Absorbance was measured using a TECAN absorbance microplate reader at 405nm wavelength.

2.10.4 β-Glucuronidase Assay

This assay was used to detect the presence of the ER enzyme Beta-Glucuronidase in the lysosomal fraction. Fluorescein di-β-D-glucuronide (SIGMA ALDRICH) was used as the substrate at 0.1mM in pH 7 DPBS +1mM $MgCl_2$ and 1mM $CaCl_2$. 20µl of this was added to 20µl of the fraction sample and 60µl DPBS. This was then left for 1 hour at 37°C. Fluorescence was then examined in each well at an excitation of 355nm and an emission of 460nm.

2.10.5 Beta-Hexosaminidase assay

This assay (SIGMA ALDRICH) was used to detect the presence of the lysosomal enzyme Beta-Hexosaminidase. This assay was performed on the various assays as described in (Jeyakumar et al., 2002).

Fluorescence was then examined in each well at an excitation of 355nm and an emission of 460nm.

2.11 Functional assays on purified lysosomes

2.11.1 ACMA pH assay

9-Amino-6-Chloro-2-Methoxyacridine (ACMA) probe (MOLECULAR PROBES) was used on purified lysosomes to show their re-acidification post purification via their v-ATPase activity. The assay was performed as described in (Lichko and Okorokov, 1984).

2.11.2 Functional Ca^{2+} uptake assay

The Calcium sensitive Fluo-4 probe (INVITROGEN) was used to detect the uptake and release of Ca^{2+} from purified lysosomes. This assay was done using 25μg of protein taken from the lysosomal fraction from both CHO-H1 and CHO M12 cell lines. The Assay was performed as described in (Lloyd-Evans et al., 2003).

2.12 Fixed staining

2.12.1 Fixing cells with 4% Paraformaldyhyde (PFA)

Cells were grown on cover slips as described in 2.5 and media was

removed. Cells to be fixed are washed in 1ml DPBS followed by the addition of 300μl of 4% PFA (FISHER) in DPBS for 10 minutes at ~16°C to fix the cells. The PFA is removed and the cells undergo three 1ml 10 minute DPBS washes. The fixed cells are either stained immediately or they are stored at 4°C for later use.

2.12.2 Filipin staining

Filipin is a polyene antibiotic that fluoresces when it is bound to cholesterol. Filipin (SIGMA ALDRICH) staining was performed as described in (Lloyd-Evans et al., 2008). Cells that have been seeded and fixed on coverslips were incubated in 500µl of complete medium containing 50µg/ml of Filipin for 30 minutes in the dark at 16°C. The medium is removed and the cells are washed three times with 1ml of DPBS. The cells can then be imaged. Excitation: 380nm, emission: 405nm.

2.12.3 Lysenin staining

Lysenin toxin was used to detect the presence of sphingomyelin. Lysenin toxin (PEPTIDES INTERNATIONAL), staining was done as described in (Lloyd-Evans et al., 2008). PFA Fixed cells are incubated in Lysenin toxin at 1:1000 dilution of a 0.5µg/ml stock solution overnight at 4°C in DPBS containing 1% bovine serum albumim and 0.1% Saponin (SIGMA ALDRICH). The toxin is removed and the cells are washed three times

with 1ml DPBS. The cells are then incubated overnight at 4°C in 1:1000 dilution of the Lysenin primary antibody (PEPTIDES INTERNATIONAL) in DPBS. The primary antibody is then removed and the cells are washed three times with 1ml DPBS. The cells are then incubated with the secondary antibody Dylight 488 conjugated goat anti-mouse IgG secondary antibody (DI-2488) (VECTOR LABS) 7.5µg/ml in DPBS containing 1% bovine serum albumin and 0.1% Saponin, for 30 minutes at 16°C. This is then removed and the cells are washed three times in 1ml of DPBS. The cells are then imaged. Excitation: 493nm, emission: 518nm.

2.12.4 Bis (monoacyl) glycerophosphate/lyso-bisphosphatidic acid (p-LBPA) staining

LBPA antibody binds specifically to LBPA. PFA fixed cells were incubated overnight at 4°C in a 1 in 1000 dilution of a 0.5mg/ml stock mouse anti-pLBPA antibody (ECHELON) in blocking buffer (DPBS containing 1% BSA, 0.1% Saponin). Cells were washed three times for 5 minutes in DPBS, then incubated with Dylight 488 conjugated goat anti-mouse IgG secondary antibody (DI-2488) 7.5µg/ml in Blocking buffer for 30 minutes at room temperature. Cells were washed 3 times with 1ml DPBS and mounted and imaged. Excitation: 493nm, emission: 518nm.

2.12.5 Sarcoplasmic Endoplasmic Reticulum ATPase 2 (SERCA2) staining

SERCA2 antibody was used to detect the levels of the ER calcium influx pump SERCA2. PFA fixed cells were incubated overnight at 4°C in a 1 in 200 dilution of a 1mg/ml stock mouse anti-Serca-2 antibody (ABCAM) in blocking buffer. Cells were washed three times for 5 minutes in DPBS, then incubated with Dylight 488 conjugated goat anti-mouse IgG secondary antibody (DI-2488) 7.5µg/ml in Blocking buffer for 30 minutes at ~16 ^{o}C. Cells were washed again 3 times with 1ml DPBS and mounted and imaged. Excitation: 493nm, emission: 518nm.

2.12.6 Early Endosomal Antigen (EEA1) staining

EEA1 antibody was used to detect the levels of Early Endosomes in the cell. PFA fixed cells were incubated overnight at 4°C in a 1 in 200 dilution of 0.65mg/ml stock mouse anti-EEA1 antibody (NOVUS) in blocking buffer. Cells were washed three times for 5 minutes in DPBS, then incubated with Dylight 488 conjugated goat anti-mouse IgG secondary antibody (DI-2488) 7.5µg/ml in Blocking buffer for 30 minutes at room temperature. Cells were washed 3 times with 1ml DPBS and mounted and imaged. Excitation: 493nm, emission: 518nm.

2.12.7 GM130 staining

Gm130 antibody was used to detect the structure of the Golgi apparatus in the cell. PFA fixed cells were incubated overnight at 4°C in a 1 in 200 dilution of a 0.098mg/ml stock mouse anti-GM130 antibody (ABCAM) in blocking buffer. Cells were washed three times for 5 minutes in DPBS, then incubated with Dylight 488 conjugated goat anti-mouse IgG secondary antibody (DI-2488) 7.5µg/ml in Blocking buffer for 30 minutes at ~16 ^{o}C. Cells were washed again 3 times with 1ml DPBS and mounted and imaged. Excitation: 493nm, emission: 518nm.

2.12.8 CtxB transport assay

This assay is used to follow the endocytic transport and recycling of ganglioside GM1 using cholera toxin B subunit. 1µg/ml FITC-CtxB (SIGMA ALDRICH) working solution is made up in medium. Cells are first washed in 1ml of cold medium before 250µl of the CtxB working solution is added per well. The cells are then incubated for either a 30 minutes or 1 hour at <16°C in the dark (pulse step). After the incubation is complete the CtxB solution is removed and 1ml of pre-warmed medium is added to the cells for 1-2 hour at 37°C (chase step). After, the chase step the medium is removed and the cells are washed 3 times (5min per wash) in 1% BSA and 0.05mg/ml Heparin (TOCRIS) in cold medium (this is to remove any non-internalised plasma membrane bound CtxB). The cells are washed twice in 1ml PBS and then fixed using the PFA method as

described previously. The fixed cells are then mounted on a slide and imaged.

2.13 Ca^{2+} analysis

2.13.1 Intracellular Ca^{2+} measurements

All intracellular Ca^{2+} measurements were obtained and captured with a Zeiss Axioimager inverted microscope, which has a Colibri LED Light source. This Microscope also possesses a Zeiss Axiocam MrM CCD camera and uses the Axiovision physiology acquisition package software for Ca^{2+} analysis. Obtained Ca^{2+} measurement data were quantified and statistical tests were performed using Prism software.

2.13.2 Preparation of cells for Ca^{2+} analysis

Cellular suspensions were counted then seeded onto 8 well chamber slides (IBIDI) with ~20,000 cells per chamber well for both wild type and *Cln3*$^{\Delta ex7/8}$ cells. These were then allowed to adhere overnight under normal cell culture conditions.

2.13.3 Complete Hank's Balanced Salt solution (HBSS)

HBSS is used to keep cells viable over long experiments and is used as a substitute to cell medium as it is not fluorescent. Complete HBSS is

composed of: 1mM $CaCl_2$, 1mM $MgCl_2$, 1mM HEPES pH7.2 buffer, 1x HBSS solution (LONZA) and dH_2O.

2.13.4 Loading of Fura 2-AM Ca^{2+} probe

Cells were first washed in chilled 1% BSA complete medium. The cells were then incubated in 200μl of a 5μM Fura 2-AM (TEF LABS) working solution with 0.025% pluronic acid in complete medium for 1hr at <16°C. The cells are then washed once in Complete HBSS. The HBSS is removed. 100μl of complete HBSS is then added to the cells prior to imaging.

2.13.5 Thapsigargin mediated ER Ca^{2+} release

Thapsigargin (SIGMA ALDRICH) is a drug that blocks Ca^{2+} uptake into the ER by inhibiting its SERCA pumps. 0.1μM, 1μM or 2μM of Thapsigargin was added to Fura 2-AM loaded cells and store operated Ca^{2+} release from the ER was measured live. 2μM of Ionomycin (INVITROGEN), an Ionophore that induces Ca^{2+} release from intracellular stores with the exception of the lysososome, was added to confirm the cells were still alive.

2.13.6 GPN mediated lysosomal Ca^{2+} release

Fura 2-AM loaded cells were first treated with 2μM Thapsigargin to clamp

the ER Ca^{2+} store. 200μM of the lysosomotrophic peptide GPN (ALFA-AESAR) was then added to induce lysosomal Ca^{2+} release in the cells. 2μM of Ionomycin was then added to confirm the cells were still alive.

2.13.7 Rotenone mediated mitochondrial Ca^{2+} release

Rotenone (SIGMA ALDRICH) is a drug that induces Ca^{2+} release from the mitochondria by de-polarising its membrane. 100μl of Rotenone in complete HBSS was added to Fura 2-AM loaded cells to give a working solution of 10μM Rotenone. 100μl of Ionomycin in complete HBSS was then added to cells to give a 2μM working solution of Ionomycin. This was used to confirm the cells were viable.

2.13.8 NAADP-AM mediated lysosomal Ca^{2+} release

100μl of NAADP-AM in complete HBSS was added to Fura 2-AM loaded cells to give a working solution of 500nM NAADP-AM. NAADP-AM was used to induce Ca^{2+} release from lysosomes via their TPC2 channels.

2.13.9 Treatment with Ned19 to inhibit NAADP-AM mediated lysosomal Ca^{2+} release

Fura 2-AM loaded cells are first incubated with 5μM NED-19 (ENZO LIFE SCIENCES), a drug that blocks NAADP mediated Ca^{2+} release, in complete HBSS for 5 minutes at ~ 16°C. 100μl of NAADP-AM in

complete HBSS was then added to give a working solution of 500nM NAADP-AM to induce lysosomal Ca^{2+} release.

This protocol was also followed for the C-terminal peptide (CTP) experiment, where following Fura 2-AM staining, 100μl of CTP in complete HBSS was added to give a working solution of 50μM CTP to determine if it rescued the elevated lysosomal Ca^{2+}

2.13.10 Treatment with Nifedipine to inhibit NAADP-AM mediated lysosomal Ca^{2+} release

Fura 2-AM AM loaded cells are first incubated with 10μM Nifedipine (SIGMA ALDRICH), an L-type Ca^{2+} Channel drug inhibitor, in complete HBSS for 5 minutes at ~ 16°C. 100μl of NAADP-AM in complete HBSS was then added to give a working solution of 500nM NAADP-AM to induce lysosomal Ca^{2+} release.

2.13.11 Glutamate mediated Ca^{2+} release

Fura 2-AM loaded cells had 100μl of Glutamate (TOCRIS) in complete HBSS added to give a working solution of 10μM Glutamate to induce Ca^{2+} release.

2.13.12 Store operated Ca^{2+} entry into cells

Fura 2-AM loaded cells are contained in 100μl of low Ca^{2+} containing complete HBSS solution (20μM $CaCl_2$ instead of 1mM). 100μl of Thapsigargan in complete HBSS is added to the cells to give a working solution of 1μM Thapsigargin to empty the ER Ca^{2+} store. 1mM $CaCl_2$ is then added to induce store operated Ca^{2+} entry into the cell.

2.13.13 Design of the CLN3 C-terminal peptide

C-terminal peptides were designed by Dr Kim Wager (Cardiff University).

2.13.14 Intra-lysosomal Ca^{2+} measurements

Intra-lysosomal Ca^{2+} levels were measured using Oregon green BAPTA. Cells were treated with 100μM Oregon green BAPTA for 6 hours followed by 3 washes in 1ml PBS. 10μg/ml TRITC-dextran (SIGMA ALDRICH) was used as a loading control to show Ca^{2+} measurements were taken of the lysosome. 100μl of CTP in complete HBSS was added to the cells to give a working solution of 50μM CTP. This was to detect if there was reduced intra-lysosomal Ca^{2+} following CTP addition.

2.13.15 Measuring Ca^{2+} release via C-terminal peptides in purified lysosomes

Lysosomes from wild type and mutant cerebellar cells were purified as described previously. Purified lysosomes were incubated in 2μM Fluo-4 probe to measure Ca^{2+} release from lysosomes following 50μM addition of C-terminal peptides.

Chapter 3: Effects of superparamagnetic iron oxide nanoparticles on cellular and lysosomal function

3.1 General introduction

Lysosomal research is important to further our understanding of lysosomal proteins and how their loss of function results in the onset of lysosomal storage disease. Established techniques have attempted to purify lysosomes to aid in lysosomal research, however there are caveats to many of these techniques used (discussed further in Chapter 4). In the last 20 years the use of magnetic based iron particles has been used to some success to purify lysosomes from cells. While the methodology behind this was good, unfortunately the iron particles used proved to be unstable and toxic to cells. As technology progressed the development of a new type of highly magnetic iron particle, called superparamagnetic iron oxide nanoparticles (SPIONs), could potentially be used to purify lysosomes. But before we are able to use these particles for any kind of magnetic based lysosomal purification we must first understand if they are non-toxic to cells.

3.2 Superparamagnetic nanoparticles: An introduction

The use of magnetic nanoparticles has been garnering much interest in recent years due to their potential in revolutionizing nanomedicine and their implementation into the biomedical field (Singh et al., 2012). Superparamagnetic Iron Oxide Nanoparticles (SPIONs) are small synthetic γ-Fe_2O_3 (maghemite) or Fe_3O_4 (magnetite) particles that possess a core range that is usually <100nm in diameter (Wahajuddin

and Arora, 2012). While other metal oxides such as copper, nickel and manganese are known to exhibit superparamagnetic properties; it is either magnetite or maghemite that is the most commonly used for biomedical purposes. This is due to them being more biocompatible, as well as being more easily degradable when compared with copper, nickel and manganese. SPIONs are often coated in an organic or inorganic coating (e.g. an organic coating consisting of dextran), and the coating of these nanoparticles in a suitable polymer confers important characteristics that are needed for use in the biomedical field. By coating a SPION with an organic or inorganic polymer it helps to reduce aggregation among different SPIONs or non-specific protein binding that is often seen in uncoated particles, thus helping cellular dispersion. Another important reason for the coating is that it helps to protect the surface of the nanoparticle from oxidation. Once the SPION has been coated it has become functionalized. The important characteristic for these SPIONs is that they become magnetized when they are exposed to an external magnetic field (Petri-Fink et al., 2005). This is known as superparamagnetism. The level at which the SPIONs react and become magnetized is dependent on the size of the nanoparticle itself. A nanoparticle ranging between 10-20nm would possess a single magnetic domain independent of other nanoparticles in the vicinity of the same size and would become magnetized at a much stronger and quicker rate than that of nanoparticles of a larger size that generally become magnetized together at a slower rate due their multiple domains (Vargas et al., 2012).

Many different areas of research into using SPIONs for biomedical purposes are currently underway as researchers have found a use for them in both diagnostic and therapeutic purposes. SPIONs have been used to help improve contrast in MRI images helping to diagnose progressive diseases at a much earlier stage of development (Amstad et al., 2009). The use for SPIONs for drug delivery by using drugs conjugated to a SPION particle to improve delivery to a cancer cell for example has been an ongoing area of research to improve chemotherapeutics and radiotherapeutics (Ruoslahti et al., 2010). Another use they are recently being used for is hyperthermia treatment by heating up the SPIONs to induce cell death in tumor cells to induce cell death and to try and ablate the tumor.

3.3 Potential SPION induced cellular toxicity

Toxicity is an important factor to consider when treating cells with magnetic nanoparticles, especially Lysosomal storage disease cell lines. Oxidative stress has been reported to be elevated in many different lysosomal storage diseases, including NPC (Vazquez et al., 2012). As oxidative stress is one of the more common mediators of apoptosis (Mukherjee et al., 2005), it is important that the SPIONs used to potentially purify lysosomes do not contribute to an increase in cellular oxidative stress.

Work has been carried out to evaluate whether there are any adverse effects SPIONs might have, and their interactions at the cellular and subcellular level (Wu et al., 2010).

It is important to take into account the characteristics of the nanoparticles when it comes to discussing SPION induced toxicity in cells. The most common forms of SPIONs used for magnetic based techniques are either Magnetite (Fe_3O_4) or Maghemite (γ-Fe_2O_3) (Singh et al., 2012). As magnetite contains both Fe^{2+} and Fe^{3+} ions it can be rapidly oxidised to maghemite in the presence of air, light and also moisture (Laurent et al., 2008). Therefore the more oxidised the magnetite particle becomes the greater the ratio of maghemite to magnetite of the core is present. It is also worth noting that uncoated magnetite and maghemite particles have different toxic effects depending on the cell type, with greater levels of DNA lesions present in magnetite treated lung epithelial cells compared with maghemite treatment (Hanini et al., 2011).

One way in that the administration of magnetic nanoparticles to cells can have adverse effects is that they may act as a potential source of Reactive Oxygen Species (ROS) (Lin et al., 2010). SPIONs that are trafficked to the lysosome are then exposed to the acidic pH levels. If the SPIONs have been functionalised with a dextran coat then this will help protect the magnetite core. However once the magnetite core is exposed to the acidic conditions of the lysosomes, this provides favourable conditions for intralysosomal Fenton reactions ($H_2O_2 + Fe^{2+} \rightarrow Fe^{3+} + OH^{\cdot}$

+ OH^-), releasing H_2O_2 as a result. The production of these highly damaging free hydroxyl radicals has been shown to induce lipid peroxidation, and as the lysosomal membrane is lipid rich it may disrupt lysosomal membrane integrity (Zdolsek and Svensson, 1993).

3.4 The effects of coated and uncoated Magnetite and Maghemite particles on cell viability

A recent study examined four different SPIONs produced by the company Liquids Research Ltd: two magnetite SPIONs (one coated with a 40kDa dextran, the other one not) and two maghemite SPIONs (one coated with a 40kDa dextran, the other one not) (Singh et al., 2012). The study aimed to look at the effect these four SPIONs had on the iron redox state (the Fenton reaction mentioned previously) and whether the presence of these SPIONs resulted in an increase in genotoxicity. MCL5 (human lymphoblastoid $TK^{+/-}$) viability following treatment with four different SPIONs was analysed. However there was little to no change in the levels of MCL5 viability even in SPION concentrations reaching 100mg/ml indicating no cytotoxic potential from these SPIONs. The study then looked for an increase in the number of oxidative based lesions in 5 different genes. While it appears that there is an increase in the levels of oxidative DNA lesions when the cells are treated with maghemite, there appeared to be a great degree of variation in the levels of lesions detected (Singh et al., 2012). The study also set out to measure the amount of Fe^{3+} ions that were generated when the coated maghemite

particles were kept in 3 different pH conditions in vitro. There appears to be a huge increase in the levels of Fe^{3+} production after 48 hours when the maghemite was stored at pH 4.5 when compared with the maghemite stored at pH 5.5 and 7. As the lysosome has a pH of ~4.5 this could result in the production of large amounts of Fe^{3+} being produced inside the lysosome, possibly resulting in cytotoxic effects. However one thing that the researchers of this study did not take into account is the ionic composition of the lysosome. The large amount of protein, lipids and other macromolecules already present in the lysosome would provide a buffering effect, due to some protein/lipid ability to bind free ions (including protons) (Kobayashi et al., 1999), on the acidic conditions which could mean that the production of Fe^{3+} from ingested magnetic nanoparticles would not necessarily reach the levels observed in this study (Singh et al., 2012). An improved *in vitro* study in living cells is clearly required to better understand the potential degradation of SPIONs within lysosomes, and their potential toxic effects.

3.5 Nanoparticle loaded lysosomal structure and function

Other studies have looked at the effect of accumulation of various nanoparticles, including glass, within the lysosome and their potential effects on lysosomal morphology and function. The effects of accumulation of nanoparticles (derived from glass wool) inside the lysosome have been speculated to have an impact on the lysosomal pH, which as a result would lead to a change in the efficacy of certain types of

lysosomal enzymes (Frese et al., 2008, Garnett and Kallinteri, 2006). This in theory could mean that the accumulation of these nanoparticles could induce a lysosomal storage disease phenotype inside the cell. While it is highly unlikely that the accumulation of nanoparticles in the lysosome would induce a phenotype as severe as an LSD, it is important to take the possibility into consideration as it may have wider consequences in the medical arena where nanoparticles are currently used as a contrasting agents for MRI studies for example. One such study determined the effect of Carboxyl Polystyrene Particles (CPS) of different sizes (20-500nm) on lysosomes from endothelial cells over varying exposure times (24-96 hours) (Frohlich et al., 2012a). CPS was used as a model for the effects on nanoparticle accumulation as they are not biodegradable and the particles could be obtained in reproducible quality (Frohlich et al., 2012b). The study aimed to measure the effects on lysosomal morphology, pH and enzyme function after different exposure times to CPS (Frohlich et al., 2012a). The findings of the study showed that any damage from longer exposure to CPS was not higher than from a shorter exposure. It was speculated that this was because CPS have a high potential to bind to proteins. This could result in the formation of CPS-protein aggregates, potentially reducing the levels of the potentially toxic CPS in the cell (Mayer et al., 2009, Xia et al., 2006). These findings suggested that the exposure of CPS did not have an adverse effect on lysosomal morphology or pH. Enzyme assays were performed for the lysosomal enzymes, cathepsin B and lysosomal sulfatase to detect if there were a change in the levels of their activity when exposed to CPS

for 24 and 72 hours (Frohlich et al., 2012a). There was a small decrease in the levels of the two lysosomal enzymes detected after 24 hours of exposure with the CPS. But the levels of enzyme activity did not decrease further following 72 hours exposure to CPS. This would suggest that long term exposure from synthetic molecules does not induce an LSD phenotype, decrease lysosomal enzyme function or membrane integrity (Frohlich et al., 2012a).

3.6 Overview

By comparing commercially available dextran functionalised SPIONs, one produced by Liquids Research Ltd (LRL) and another produced by Chemicell (Chem) we aim to determine which brand of SPIONs is most stable in the cell, with the least amount of toxic effects. These two SPIONs possess a 40nm magnetic magnetite core that has been functionalised with a 40kDa dextran coat. Another type of iron based particle (sold by Sigma) called iron dextran will also be tested, as this particle is similar in properties used in past studies to magnetically purify lysosomes. This particle is composed of a dextran core encompassed with an iron oxide coat.

3.7 Results: Potential SPION induced toxicity

Unless stated otherwise, the SPIONs used for this study were the 40kDa dextran coated magnetite nanoparticles provided by LRL (these SPIONS will be referred to as LRL SPIONs from here on). Comparison of other iron based nanoparticles used are the iron oxide coated dextran particles (Sigma Iron dextran FeO) and the dextran coated magnetite SPIONs provided by Chemicell (Chem SPIONs).

3.7.1 Lysosomal levels after treatment with SPIONs and FeO particles

Lysotracker green is a probe used to detect lysosomes as it fluoresces when it loads into a highly protonated environment. CHO-H1 cells were stained with a lysotracker green probe to show for the presence of lysosomes in the cell, and reveal any possible lysosomal expansion (figure 3.1).

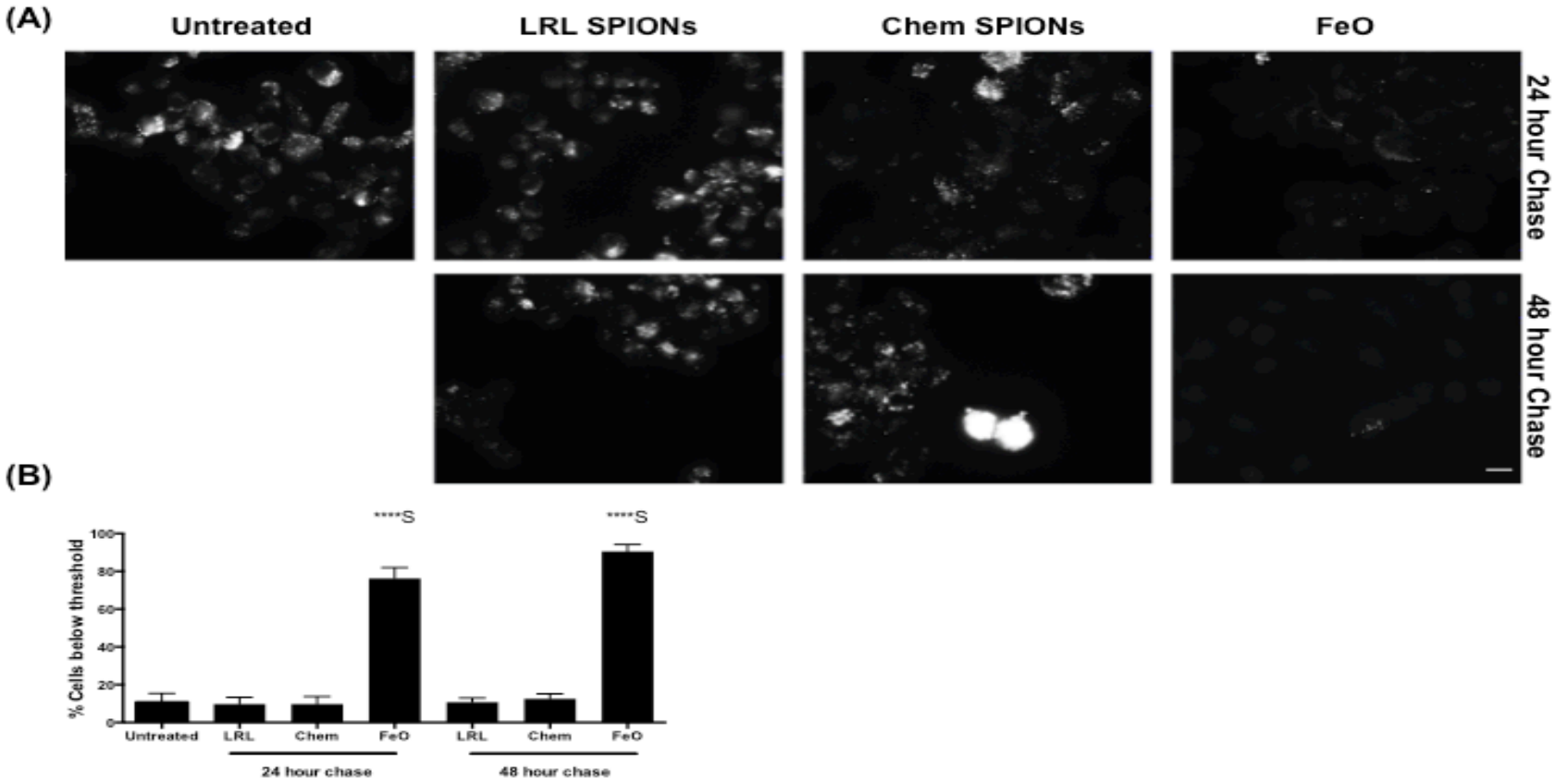

*Figure 3.1: (A) Representative images of cells stained with the Lysotracker green probe (white). Each panel is a general representation of the total population of cells observed following 24hr pulse with the different brands of SPIONs and FeO followed by a 24 hour and 48 hour chase compared to untreated cells. (B) Quantified data of (A). n=4 Values represent mean ± SD. n=3. >80 cells analysed, S denotes significance ****p< 0.0001. Scale bar =10μm.*

Untreated CHO-H1 cells stained with the lysotracker green probe showed that the majority of cells displayed normal levels of lysotracker staining (indicated by punctate fluorescence). A few untreated cells displayed higher levels of staining indicating lysosomal expansion was observed, but this was in the minority. LRL SPION treated cells after a 24 hour chase displayed similar levels of fluorescence as in untreated cells. After a 48 hour chase, there was still similar levels of punctate staining in the LRL SPIONs treated cells indicating that the lysosomes were still intact. After a 24 hour chase with Chem SPIONs there were similar levels of lysotracker staining as in the untreated cells, a small percentage of cells displayed a slightly elevated levels of lysotracker staining observed, possibly due to an expansion in the lysosomal system. Following a 48 hour chase however the levels of lysosomes detected in the cell were still similar, although some enlarged punctate staining was observed, suggesting that these lysosomes were either increasing in size or their pH had been affected due to the particles. A 24 hour chase with the FeO particles displayed a significant decrease in the levels of lysosomes detected, after a 48 hour chase little lysotracker staining was seen. This suggests that the presence of FeO particles in lysosomes is having an effect on the lysosomes ability to maintain its pH.

3.7.2 Effects on Cathepsin B activity after treatment with SPIONs or FeO particles

CHO-H1 cells were stained with the Magic Red cathepsin B probe to detect the levels of the lysosomal enzyme cathepsin B in cells following SPION or FeO treatment (figure 3.2). A reduction in staining could possibly indicate a problem with lysosomal pH, which is required for the enzyme to function. The probe works by loading a substrate into the lysosome which is then cleaved by cathepsin B causing a release of fluorescence. The greater the stain intensity then the more active cathepsin B is in the cells.

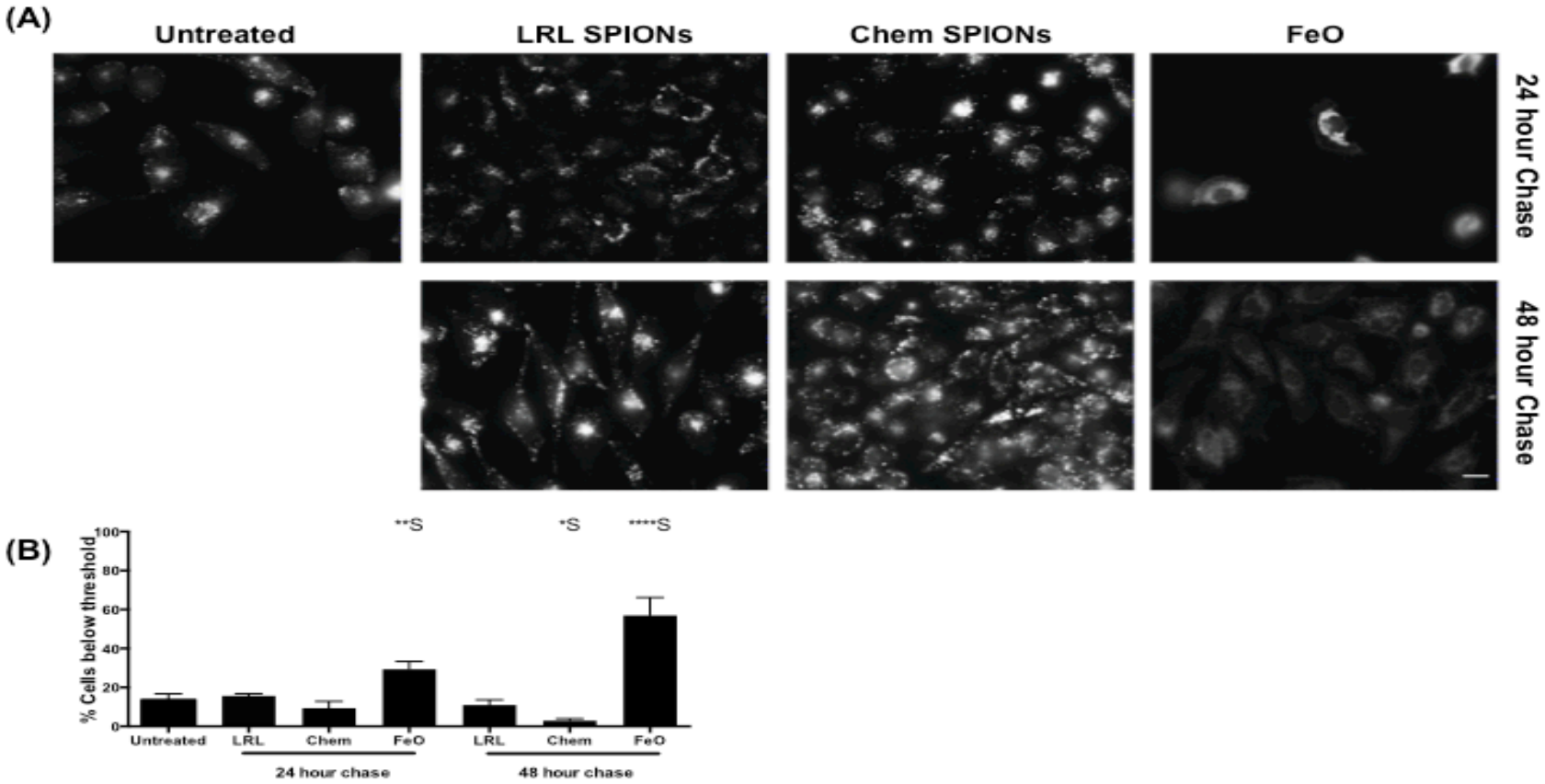

*Figure 3.2: (A) Representative images of cells stained with the Magic Red Cathepsin B probe, following treatment with the different brands of SPIONs and how this affects the activity of the lysosomal cathepsin B enzyme (white) after a 24 hour and 48 hour chase compared to untreated cells. (B) Quantified data of (A). n=3 Values represent mean ± SD. n=3. >60 cells analysed, S denotes significance *p<0.05, **p<0.01, ****p< 0.0001. Scale bar =10μm.*

LRL SPIONs treated cells following a 24 hour chase exhibited similar levels of cathepsin B activity as there was in the untreated cells. Following a 48 hour chase the cathepsin B stain was higher in the LRL SPIONs than in the untreated cells suggesting that the activity of these enzymes has increased. Interestingly, cathepsin B activity was localized more to the peri-nuclear region of the cell after this chase time, possibly suggesting the lysosomes have redistributed to this area of the cell. Elevated levels of cathepsin B activity was detected in the Chem SPIONs treated cells, implying that cathepsin B activity was elevated following the treatment of Chem SPIONs. Treatment with the FeO nanoparticles after a 24 hour chase resulted in a lower cytoplasmic cathepsin B stain in the cell. This could suggest that the lysosomes are leaking due to the unstable properties of the FeO particle and the lysosomal enzymes are now present in the cytosol. If the lysosomes are leaking out then the cytosol of the cell will now be more acidic allowing for the leaked out cathepsin B to cleave its substrates elsewhere in the cell. Following a 48 hour chase with FeO particles there was little cathepsin B activity present suggesting that lysosomal enzyme activity or integrity has dropped considerably with this treatment.

3.7.3 Effects on Cathepsin L activity following treatment with SPIONs and FeO particles

CHO-H1 cells were stained with the Magic Red cathepsin L probe to detect the levels of the lysosomal enzyme cathepsin L in cells following SPION or FeO treatment (figure 3.3). A reduction in staining could possibly indicate a problem with lysosomal pH, which is required for the enzyme to function. The probe works by loading a substrate into the lysosome which is then cleaved by cathepsin L causing a release of fluorescence. The greater the stain intensity then the more active cathepsin L in the cells is.

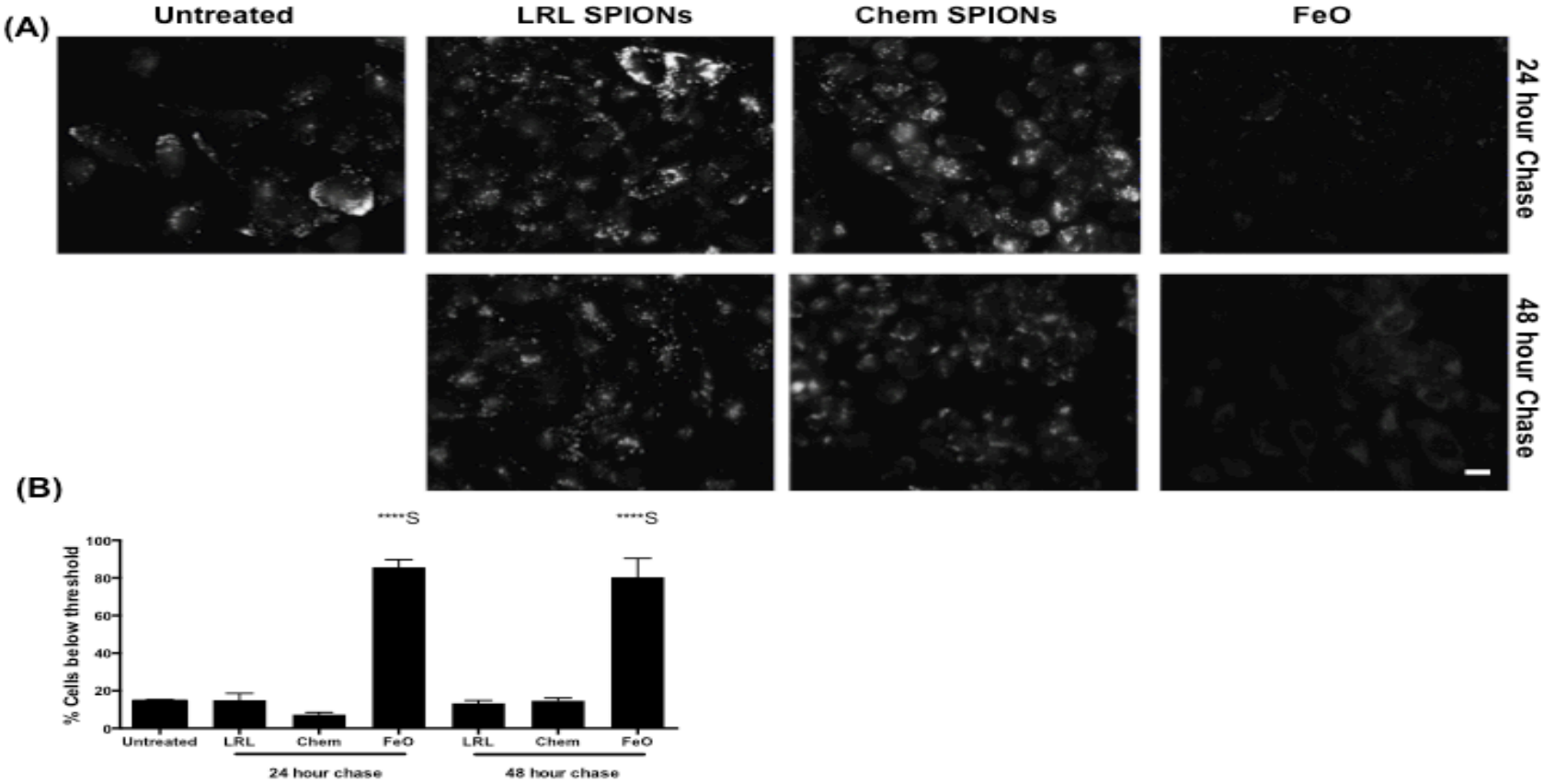

*Figure 3.3: (A) Images of cells stained with the Magic Red Cathepsin L probe. Each panel is a general representation of the total population of cells observed following treatment with the different brands of SPIONs and how this affects the activity of the lysosomal cathepsin L enzyme after a 24 hour and 48 hour chase compared to untreated cells. (B) Quantified data of (A). n=3 Values represent mean ± SD. n=3. >60 cells analysed, S denotes significance ****p< 0.0001. Scale bar =10mm.*

CHO-H1 cells were stained with the Magic Red Cathepsin L probe to measure the activity of cathepsin L (indicated by punctate staining). LRL SPION treated cells after a 24 hour chase displayed similar levels of cathepsin L activity as that seen in the untreated cells (figure 3.3). After a 48 hour chase there was slightly reduced levels of cathepsin L activity observed suggesting that after a longer chase time the LRL SPIONs only slightly effect the pH optima necessary for cathepsin L to work properly. After a 24 hour chase with Chem SPIONs there was a small increase in the levels of cathepsin L activity detected. The cathepsin L activity appears to be present in the per-nuclear region of the cell. After a 48 hour chase the cathepsin L activity decreased slightly in the Chem SPION treated cells but the staining observed was less punctate as seen previously and was now more cytoplasmic. Treatment with FeO particles resulted in greatly reduced levels of cathepsin L activity over both chase times suggesting that the presence of this particle has affected the ability of this enzyme to function correctly.

3.7.4 Determining levels of phospholipidosis in SPION and FeO particle treated cells

CHO-H1 cells were treated with the LipidTOX Red probe to measure the levels of phospholipidosis (figure 3.4) in SPION and FeO treated cells. This was done to detect if the presence of these nanoparticles in lysosomes resulted in an increase in phospholipidosis in the cell.

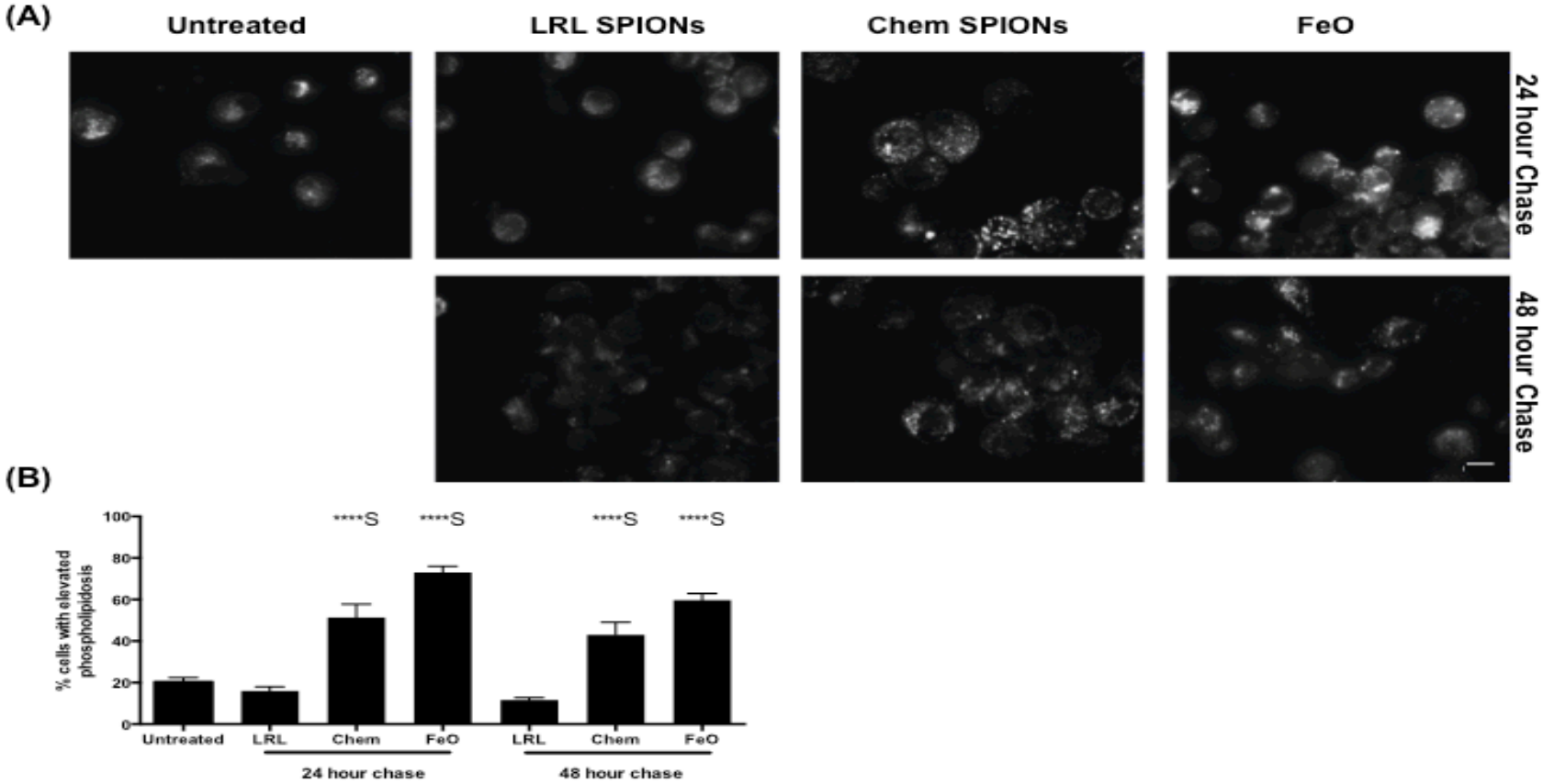

*Figure 3.4: (A) Images of cells stained with the LipidTOX Red phospholipidosis probe. Each panel is a general representation of the total population of cells observed following treatment with the SPIONs and FeO and how the levels of phospholipidosis are affected after a 24 hour and 48 hour chase compared to untreated cells. (B) Quantified data of (A). n=3 Values represent mean ± SD. n=3. >60 cells analysed, S denotes significance ****p< 0.0001. Scale bar =10μm.*

24 hour chase of LRL treated cells displayed lower levels of phospholipidosis present when compared to that of the untreated cells, while slightly reduced levels of phospholipidosis were detected after a 48 hour chase in the LRL SPION treated cells. Phospholipidosis levels detected in the Chem SPION treated cells were increased following a 24 hour chase. An increased size of puncta was seen which would suggest that greater levels of phospholipidosis were present in large endocytic vesicles such as the late endosome. Following a 48 hour chase with the Chem SPIONs fewer enlarged puncta were observed, but similar phospholipidosis levels were detected when compared with untreated cells. A 24 hour chase with FeO particles showed elevated levels of phospholipidosis in many of the cells observed. Many cells that displayed this elevated level of phospholipidosis had staining present throughout the cell. Interestingly the phospholipidosis levels decreased in the cells that underwent a 48 hour chase with the FeO particles, but this was still greater than untreated cells.

3.7.5 Effect on mitochondria numbers following SPION and FeO treatment

CHO-H1 cells were stained with the Mitotracker green probe to measure the number/distribution of Mitochondria in the cell (figure 3.5).

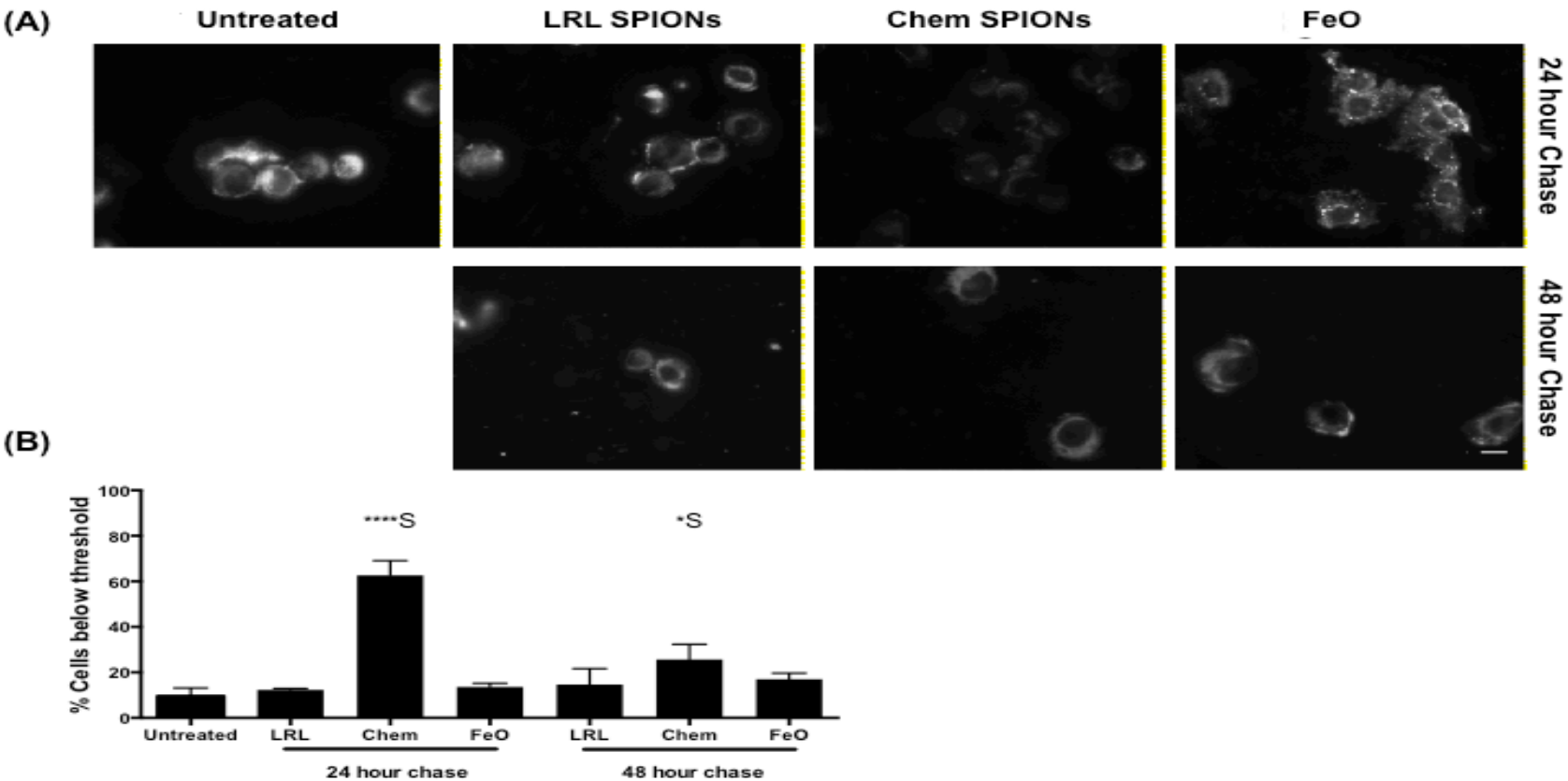

*Figure 3.5: (A) Images of cells stained with the Mitotracker green probe (mitochondria). Each panel is a general representation of the total population of cells observed following treatment with the different brands of SPIONs and how this affects the levels of mitochondria present after a 24 hour and 48 hour chase compared to untreated cells. (B) Quantified data of (A). n=3 Values represent mean ± SD. n=3. >60 cells analysed, S denotes significance *p<0.05, ****p< 0.0001. Scale bar =10μm.*

After a 24 and 48hr chase with LRL there were still similar levels of mitochondria detected to that in the untreated cells. After a 24hr chase in the Chem SPION treated cells there was a large drop in the levels of mitochondria detected. The levels detected did improve after a 48 hour chase but this was still slightly below the levels of mitochondria seen in the untreated cells. In the FeO treated cells there was an interesting phenotype observed after a 24 hour chase. Rather than a diffuse type of staining seen in the other cells, the staining was more punctate, but by a 48 hour chase the cells presented with a more diffuse staining similar to that seen in wild type.

LRL SPION treated CHO-H1 cells were stained with the mitochondrial matrix protein antibody LRP130. Using this antibody the levels of mitochondria were monitored along with those in the untreated cells. The results indicated that using another marker for mitochondria their levels do not change in LRL SPION treated cells after a 24 hour chase.

3.7.6 Levels of mitochondrial produced Reactive Oxygen Species

CHO-H1 cells were stained with the MitoROS probe to measure the levels of mitochondria ROS in the cell (figure 3.6). Elevated staining might indicate that the mitochondria are more stressed and therefore producing higher levels of ROS than normal, while lower levels of ROS would suggest that the mitochondria are not functioning at as high a capacity as mitochondrial ROS is naturally produced from correct mitochondrial function in healthy cells.

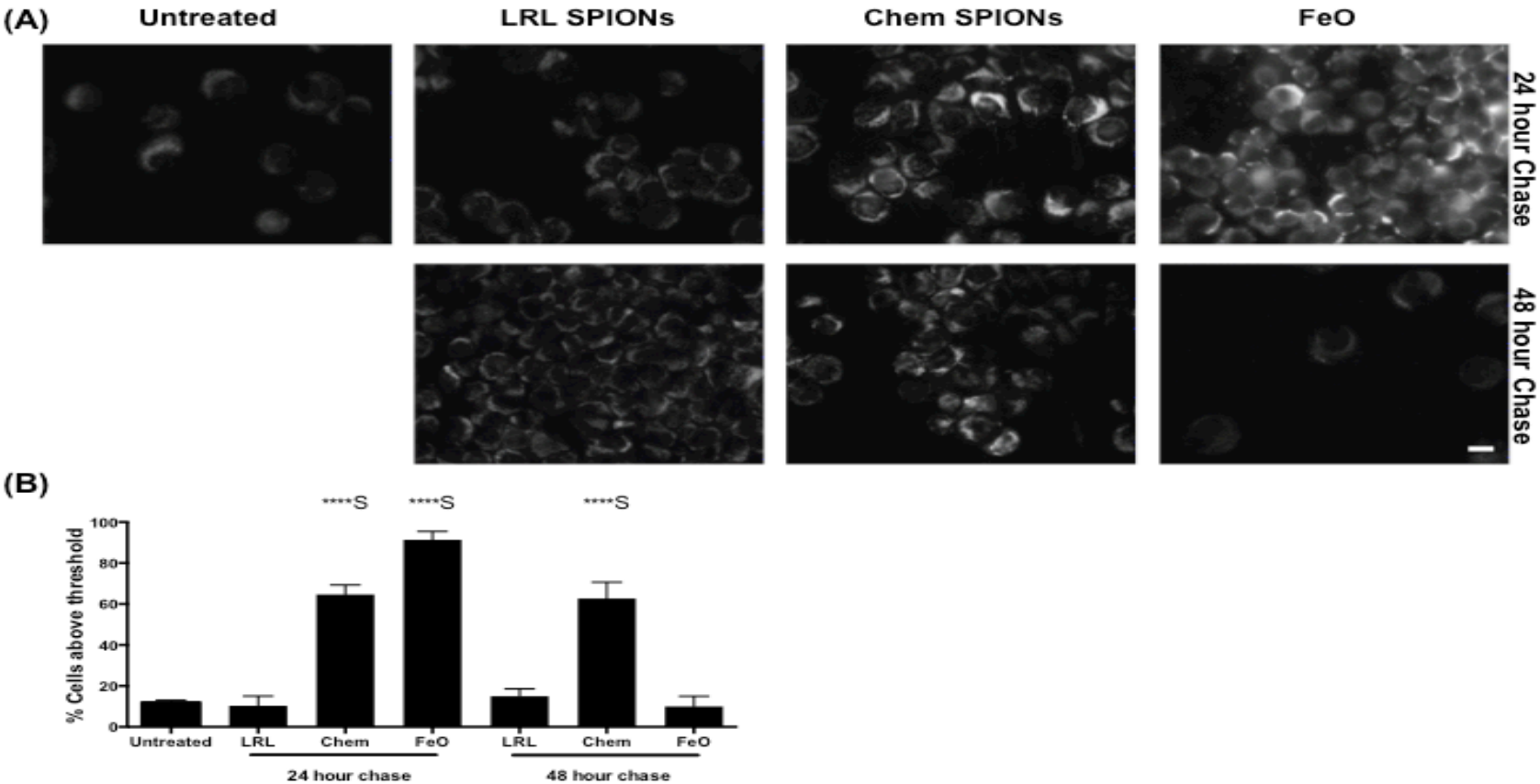

*Figure 3.6: (A) Images of cells stained with the MitoROS probe (Mitochondria produced ROS). Each panel is a general representation of the total population of cells observed following treatment with the SPION and FeO particles and how this affects the levels of mitochondria produced ROS present after a 24 hour and 48 hour chase compared to untreated cells. (B) Quantified data of (A). n=3 Values represent mean ± SD. n=3. >60 cells analysed, S denotes significance ****p< 0.0001. Scale bar =10μm.*

MitoROS staining following a 24 hour chase with LRL SPION treated cells was similar to that of the untreated cells. After a 48 hour chase with LRL SPIONs there was only a small increase (but not significantly) in the levels of MitoROS detected, indicating that the mitochondria are still working properly. After a 24 hour chase with the Chem SPION there is an elevation in the levels of MitoROS detected, suggesting that the mitochondria are producing more ROS than normal possibly due to toxic effects of increasing levels of free Fe^{2+}/Fe^{3+}. This elevated level of MitoROS staining was also observed following a 48 hour chase with Chem SPIONs. Treatment with FeO particles followed by a 24 hour chase resulted in high levels of MitoROS staining in the majority of cells observed. This indicates that the mitochondria are producing more ROS than normal due to an increase in stress, and following a 48 hour chase with FeO particles there is a large drop in ROS levels detected which could be a result of the mitochondrial function now being impaired (resulting in less ROS being produced).

3.7.7 Detecting levels of lipid Peroxidation following treatment with SPIONs and FeO particles

CHO-H1 cells were stained with the DPPP probe to detect the presence of lipid peroxidation in the cell. As little lipid peroxidation should be present in a healthy cell its presence may indicate cellular toxicity following SPION or FeO treatment.

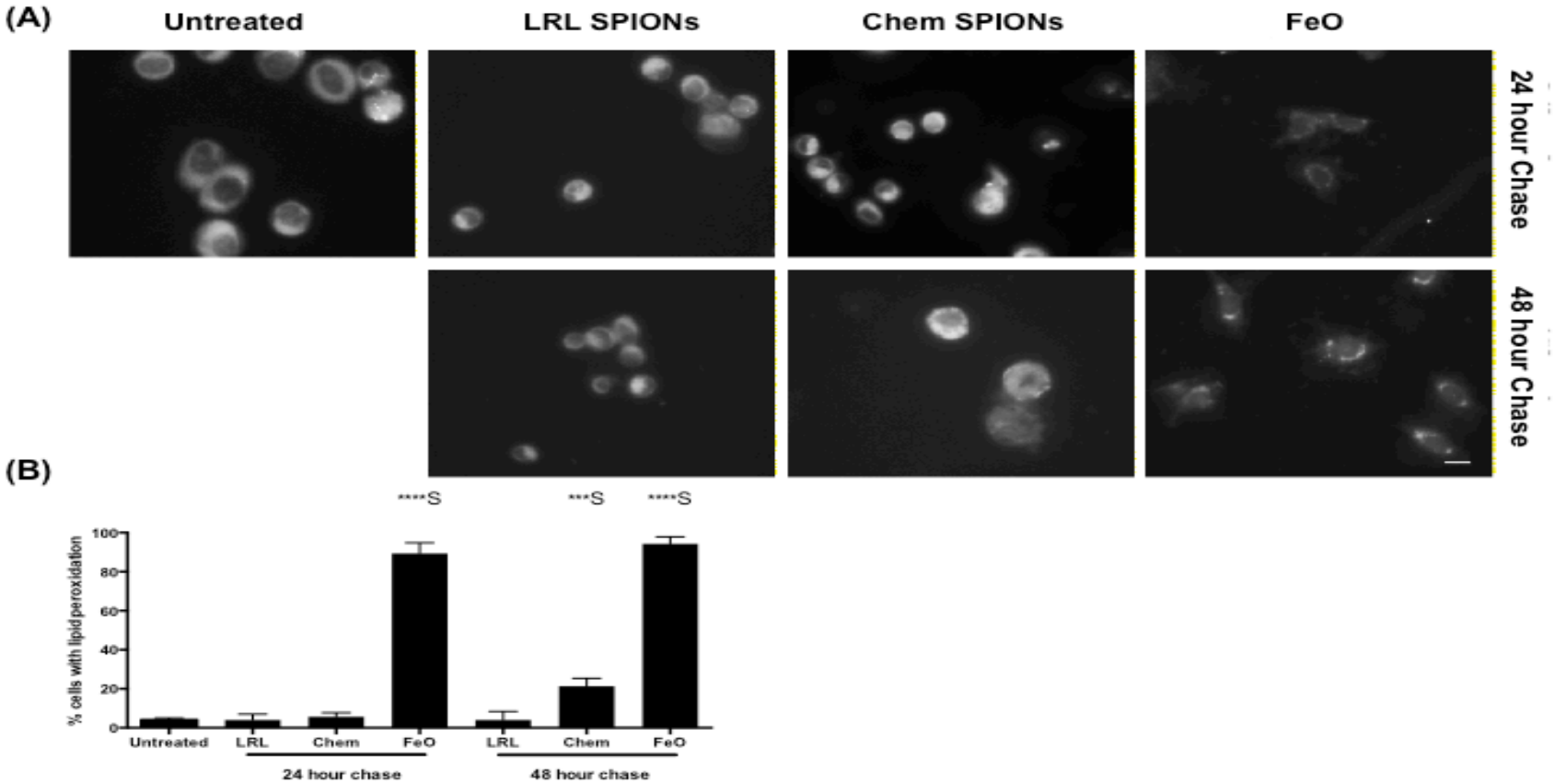

*Figure 3.7: (A) Images of cells stained with the lipid peroxidation probe DPPP. Each panel is a general representation of the total population of cells observed following treatment with SPIONs and FeO particles and how much lipid peroxidation is produced after a 24 hour and 48 hour chase compared with untreated cells. (B) Quantified data of (A). n=3 Values represent mean ± SD. N=3. >60 cells analysed, S denotes significance ***p<0.001, ****p< 0.0001. Scale bar =10μm.*

The DPPP probe produce a diffuse cellular stain when no lipid peroxidation is present, however punctate staining indicates lipid peroxidation. The majority of untreated cells displayed no lipid peroxidation when stained with DPPP, however some cells did present with small amounts of lipid peroxidation. Cells treated with LRL SPIONs after a 24 and 48 hour chase showed little to no levels of lipid peroxidation (figure 3.7). The same was seen in the Chem SPION treated cells after a 24 hour chase. But after a 48 hour chase lipid peroxidation was starting to be detected. In both the 24 hour and 48 hour chase, FeO treated cells there were high levels of lipid peroxidation detected in all the cells, evident by the distinct punctate staining around the peri-nuclear area of the cells.

3.7.8 Detecting levels of superoxide in LRL SPION and FeO particle treated cells

CHO-H1 cells were treated with the DHE probe to measure the levels of superoxide (Indicated by the punctate staining) present in the cell following a 24 and 48 hour chase with LRL SPIONs and FeO particles (figure 3.8).

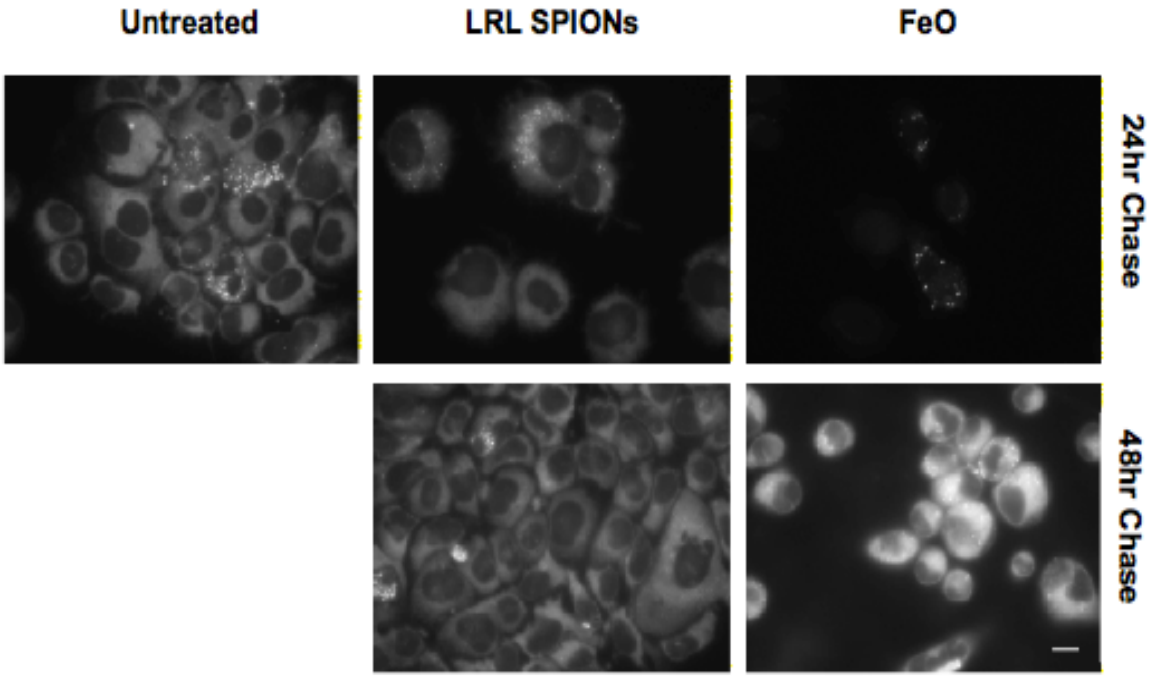

Figure 3.8: Images of cells stained with the superoxide probe DHE. Each panel is a general representation of the total population of cells observed following treatment with the different brands of SPIONs and how much superoxide is produced after a 24 hour and 48 hour chase. n=3. Scale bar =10μm.

Cells treated with LRL SPIONs after a 24 and 48 hour chase showed similar levels of super oxide present as that seen in untreated cells, suggesting that the long term presence of LRL SPIONs in lysosomes does not increase the levels of ROS in the cells. In the FeO treated cells following a 24 hour chase most cells displayed concentrated levels of super oxide around the peri-nuclear region of the cell. After a 48 hour chase a lot of the cells still displayed super oxide staining, however the diffuse stain observed in these cells appeared brighter than the untreated and LRL SPION treated cells. This could suggest that high levels of superoxide are now present throughout the cell.

3.7.9 Determining the levels of free Fe^{2+} in SPION and FeO treated cells

CHO-H1 cells were treated with the Fura 2 to measure the levels of free iron present in the cell. Fura 2 is a probe that is sensitive to free Fe^{2+}at 360nm wavelength and its fluorescence is quenched when in the presence of free Fe^{2+}.

Cells treated with LRL SPIONs for a 48 hour chase displayed slightly lower staining in the cell when compared with untreated cells, suggesting more free iron may be now present in the LRL SPION treated cells (figure 3.9). In the Chem SPION treated cells following a 48 hour chase the Fura 2 staining is even more quenched than what was seen in the LRL SPION treated cells, indicating that more free Fe^{2+} is present throughout the cell. After treatment with FeO followed by a 48 hour chase there was little Fura 2 staining present in the cell, suggesting that high amounts of free $Fe^{2+}$was present throughout the cell.

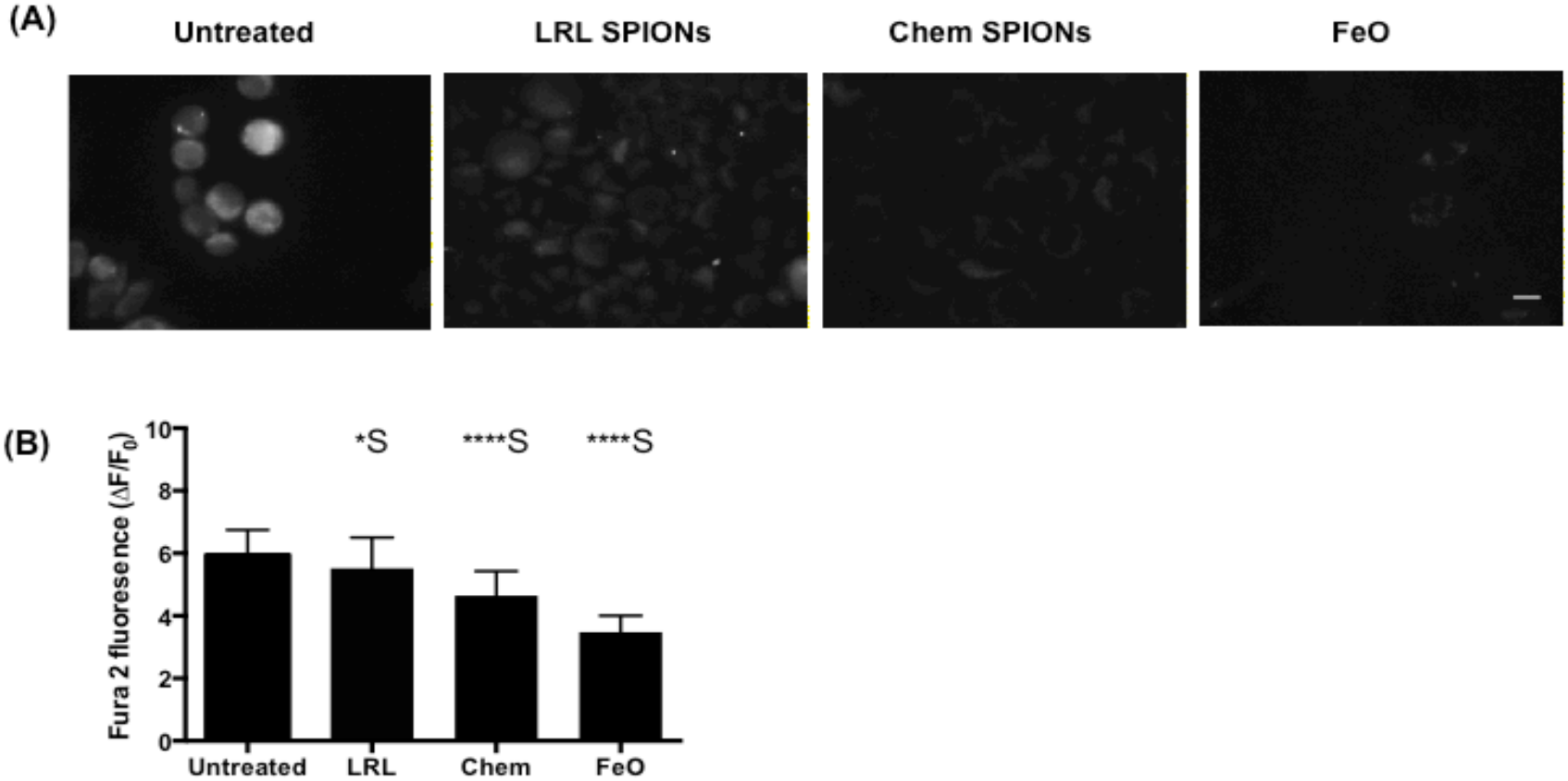

*Figure 3.9: Images of cells stained with the Fura 2 probe to detect for the presence of free iron. Each panel is a general representation of the total population of cells observed following treatment with the different brands of SPIONs and how much free iron is detected in the cell following a 48 hour chase compared with untreated cells. (B) quantified data of (A). n=3. >50 cells analysed, S denotes significance. *p<0.05, ****p<0.0001. Scale bar =10μm.*

3.7.10 Determining the levels of free Fe^{3+} in SPION and FeO treated cells

CHO-H1 cells were stained with calcein, a probe thats fluorescence is quenched in the presence of free Fe^{3+}, to determine the levels of free Fe^{3+} after a 24 hour pulse and 48 hour chase with SPIONs/FeO (figure 3.10). LRL SPION treated cells showed similar levels of calcein staining as that seen in the untreated cells, suggesting that the levels of free Fe^{3+} present in these cells are similar. Also with the levels of Fe^{2+} similar in the LRL SPION treated cells compared with untreated cells, it suggests that the dextran coat of the SPIONs is protecting the particle from the acidic environment of the lysosome. The levels of calcein stain dropped however in the Chem SPION treated cells, suggesting that the levels of Fe^{3+} are elevated in Chem SPION treated cells. The large drop in fluorescence seen in the FeO treated cells strongly suggests that there are high levels of free Fe^{3+} present in the FeO treated cells.

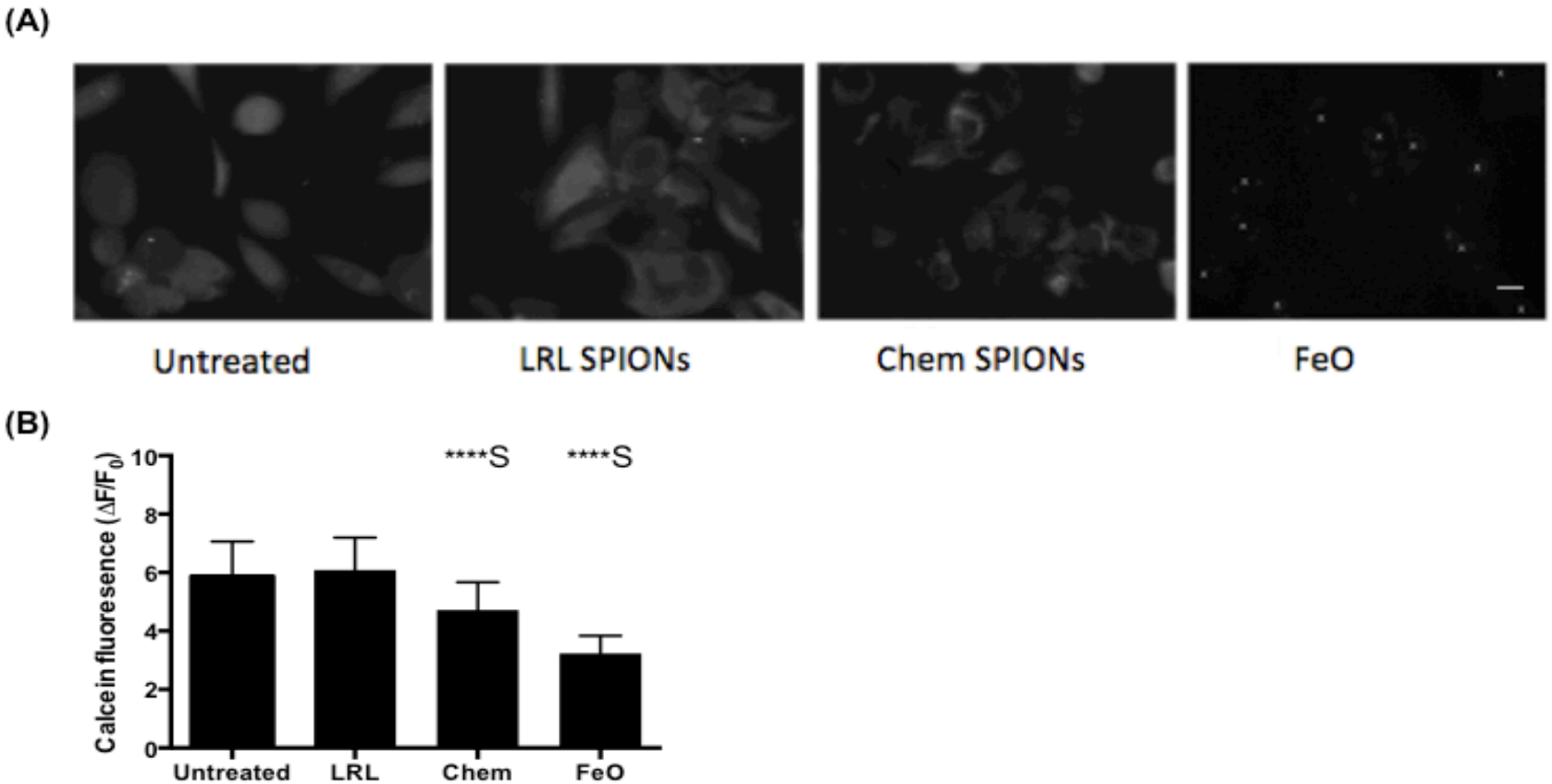

*Figure 3.10: (A) Images of cells stained with the Calcein probe to detect for the presence of free Fe^{3+}. Each panel is a general representation of the total population of cells observed following treatment with the different brands of SPIONs and how much free Fe^{3+} is detected in the cell following a 48 hour chase compared with untreated cells (B) quantified data of (A). n=2. >40 cells analysed, S denotes significance. ****p<0.0001. Scale bar =10μm.*

3.7.11 Lysosomal and phospholipidosis level comparison after treatment with 10kDa LRL SPIONs vs 40kDa LRL SPIONs

CHO-H1 cells were treated with another commercially available LRL SPION which possesses a 10kDa dextran coat as opposed to the 40kDa dextran coat that is commonly used to purify lysosomes, and lysotracker green and LipidTOX red staining was compared (figure 3.11).

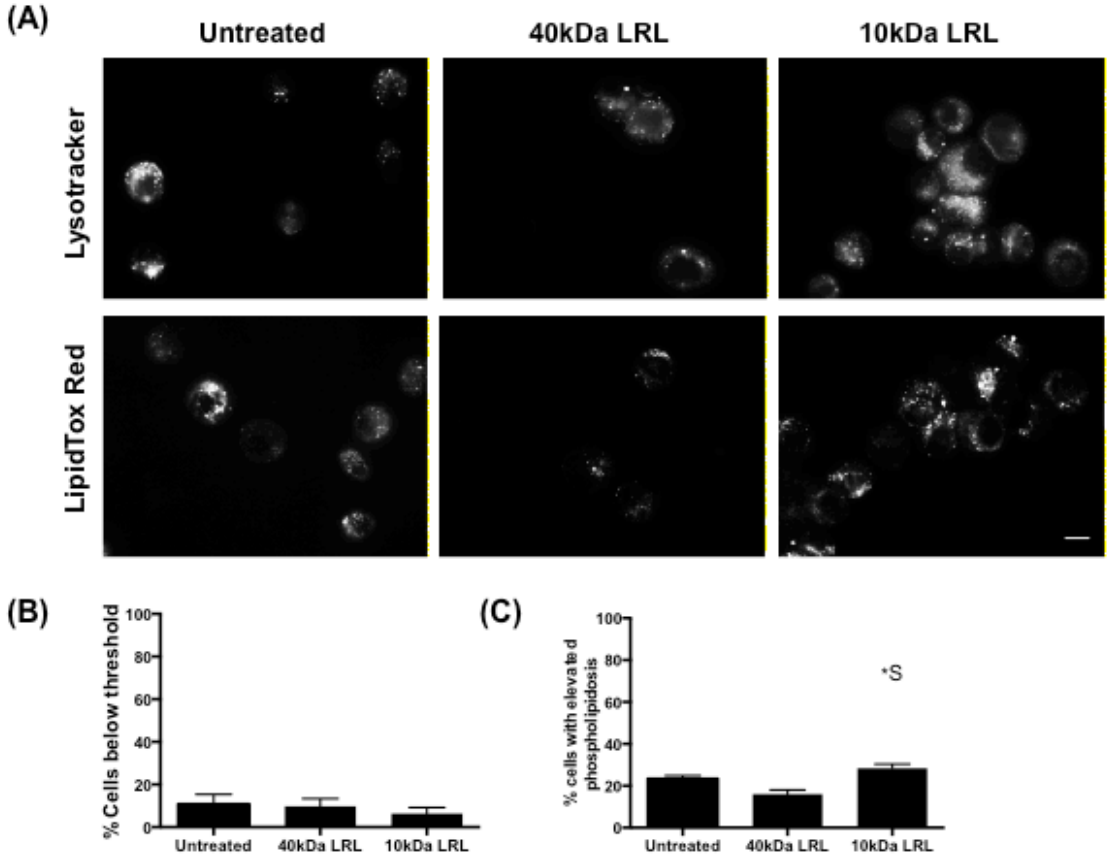

*Figure 3.11. (A) Images of cells stained with the lysotracker green and LipidTOX red probes. Each panel is a general representation of the total population of cells observed following treatment with the 40kDa and 10kDa LRL SPIONs after a 24 hour chase compared with untreated. (B) Quantified data of lysotracker data. (C) Quantified data of LipidTox red data. n=3 Values represent mean ± SD. n=3. >80 cells analysed, S denotes significance *p<0.05. Scale bar =10μm.*

Cells treated with the 10kDa LRL nanoparticle displayed similar lysotracker stain but elevated levels of LipidTOX red stain when compared to that seen in the untreated and 40kDa LRL SPION treated cells, suggesting an increase in phospholipidosis. This would suggest that the 10kDa LRL SPION is not as stable as the 40kDa LRL SPION when in the acidic environment of the lysosome, causing a small increase in toxicity present.

3.7.12 Mitochondria and their respective ROS levels after treatment with 10kDa LRL SPIONs vs 40kDa LRL SPIONs

Comparison of the mitotracker green and MitoROS stains in CHO-H1 cells treated with the other commercially available LRL SPION that possesses a 10kDa dextran coat as opposed to a 40kDa dextran coat, as well as untreated cells (figure 3.12). Cells treated with the 10kDa LRL SPION displayed mitotracker green staining similar to that seen in the 40kDa LRL SPION treated and the untreated cells. However MitoROS staining was noticeably lower in the 10kDa treated cells when compared with the untreated and 40kDa treated cells. This could indicate that 10kDa LRL SPIONs are affecting the function of the mitochondria at a much faster rate than that seen in 40kDa LRL SPION cells.

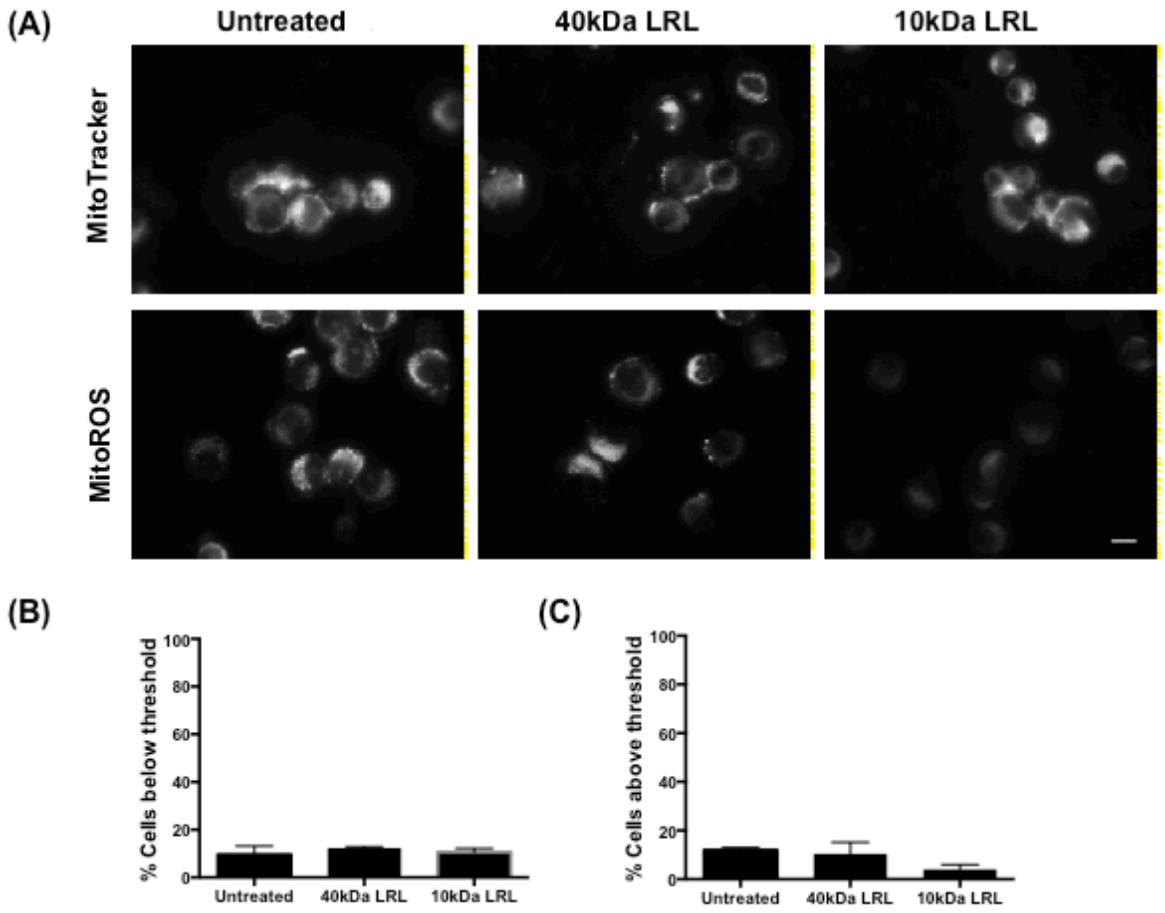

Figure 3.12: (A) Images of cells stained with the mitotracker green and MitoROS probes. Each panel is a general representation of the total population of cells observed following treatment with the 40kDa and 10kDa LRL SPIONs after a 24hr chase compared with untreated cells. (B) Quantified data of Mitotracker data. (C) Quantified data of MitoROS data. n=3 Values represent mean ± SD. n=3. >60 cells analysed. Scale bar =10μm.

3.7.13 Lipid peroxidation and superoxide levels in cells treated with 10kDa and 40kDa LRL SPIONs

Comparison of the DPPP and DHE stains in CHO-H1 cells treated with the other commercially available LRL SPION that possesses a 10kDa dextran coat as opposed to a 40kDa dextran coat, as well as untreated cells (figure 3.13).

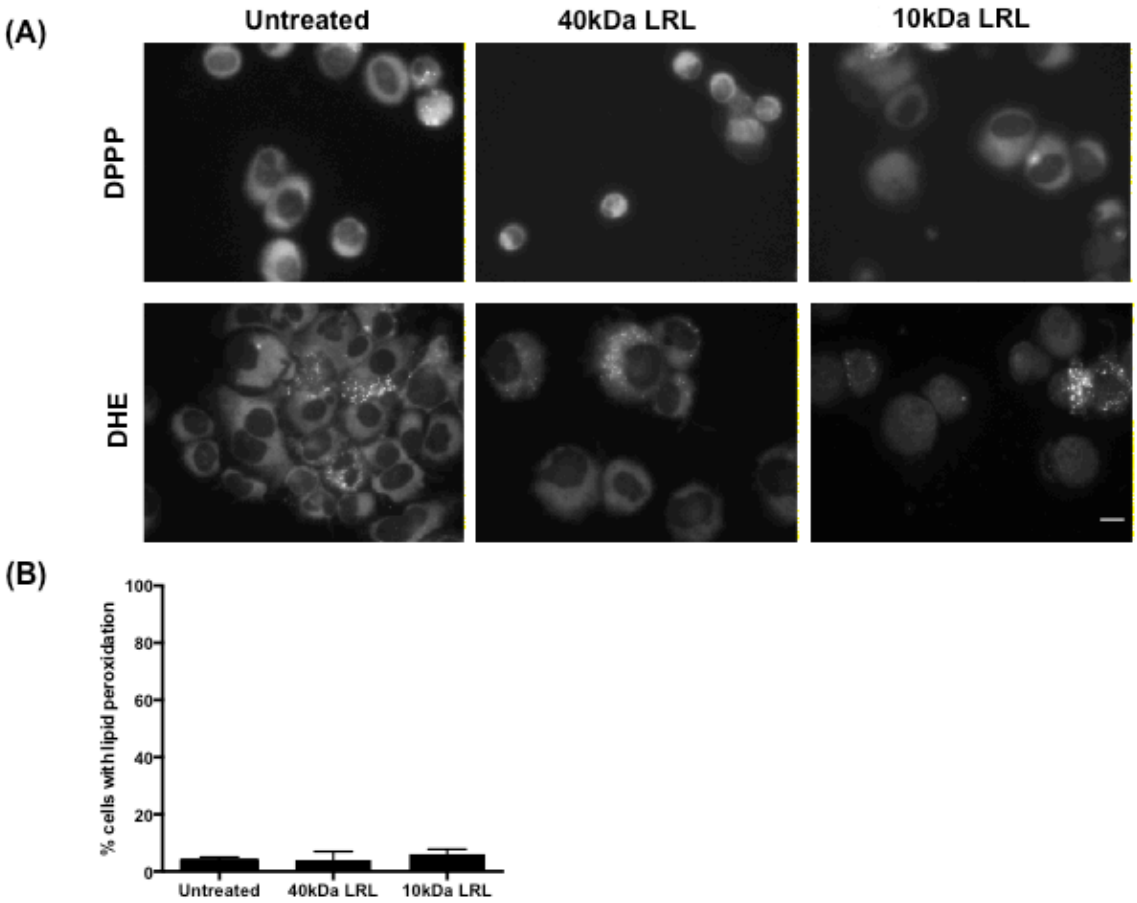

Figure 3.13: (A) Images of cells stained with the DPPP probe and DHE. Each panel is a general representation of the total population of cells observed following treatment with the 40kDa and 10kDa LRL nanoparticles after a 24hr chase compared with untreated. (B) Quantified data of DPPP data. n=3 Values represent mean ± SD. n=3. >70 cells analysed. Scale bar =10μm.

Cells treated with the 10kDa LRL SPIONs showed little to no levels of DPPP staining, indicative of lipid peroxidation, which was also seen in the untreated and 40kDa LRL nanoparticle treated cells. The DHE stain for super oxide also revealed that the majority of cells displayed little to no superoxide present which was also seen in the untreated and 40kDa LRL SPION treated cells.

3.7.14 Effect on lysosomes and their enzymes activity in CHO M12 cells following LRL SPION treatment

Lysotracker green probe and the magic kit cathepsin B and L assays were used to see if there was any lysosomal dysfunction that occurs in NPC1 null CHO M12 cells after they were treated with LRL SPIONs for a 24 hour pulse, followed by a 48 hour chase (figure 3.14).

Lysotracker green probe and the magic kit cathepsin B and L assays were used to see if there was any lysosomal dysfunction that occurs in CHO M12 cells after they were treated with LRL SPIONs for 24 hour followed by a 48 hour chase (figure 3.14). The levels of lysosomes detected via the use of lysotracker green did not change in the LRL SPION when compared with untreated CHO M12 cells. Cathepsin B activity did not change. Cathepsin L activity was marginally elevated in the SPION treated CHO M12 cells, however the important thing is that the enzyme activity doesn’t drop as that would indicate a major pH change.

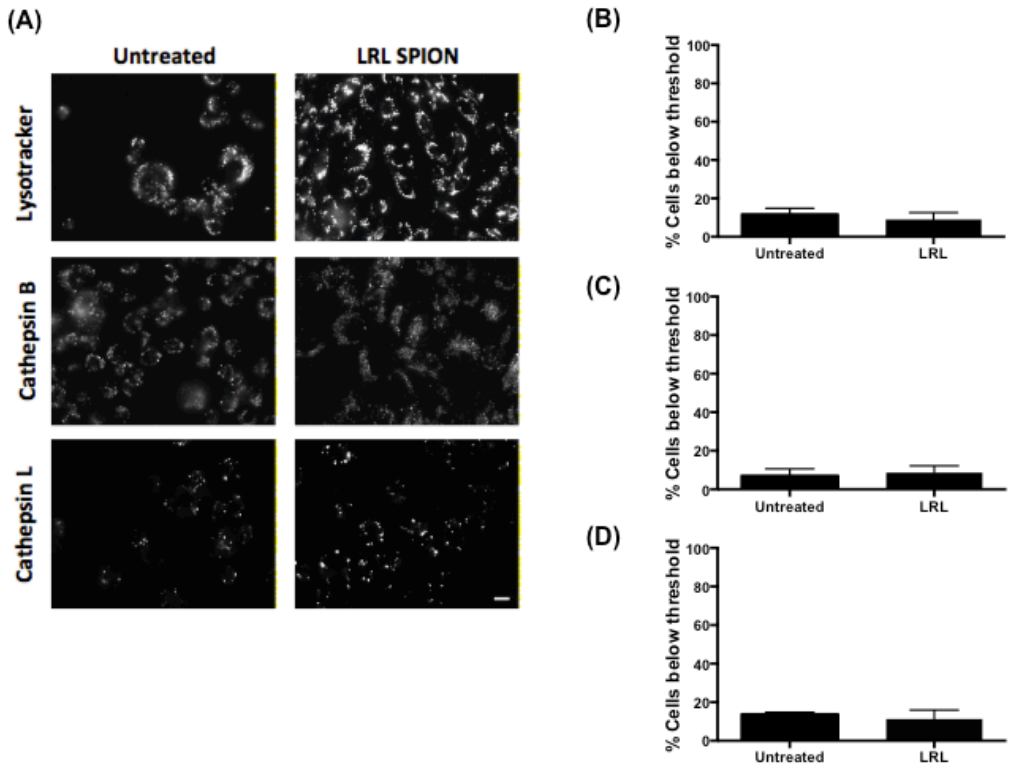

Figure 3.14: (A) Images of cells stained with Lysotracker green, magic kit Cathepsin B and L. Each panel is a general representation of the total population of cells observed following treatment with LRL SPIONs following a 24hr pulse and 48hr chase. (B) Quantified data of Lysotracker data. (C) Quantified data of cathepsin B data. (D) Quantified data of cathepsin L data. n=3 Values represent mean ± SD. n=3. >40 cells analysed. Scale bar =10μm.

3.8 Discussion

With the increasing use of SPIONs in the field of biomedicine, there is a growing interest in the toxic effects these SPIONs have once they are in the cell. Some studies have utilized the toxic effects of SPIONs to induce cells to undergo apoptosis; commonly this is used in studies for treating cancer cells (Petri-Fink et al., 2005). However for the purpose of utilizing SPIONs for the magnetic purification of lysosomes it is important to determine that the SPIONs that are loaded into the endocytic system do not induce toxicity, specifically in lysosomes. The lysosome has an acidic pH which is maintained by the V-ATPase pumps found on the lysosomal membrane. The heavily protonated intra-lysosomal lumen is tightly regulated and the acidic pH is maintained as it is necessary for many lysosomal enzymes to function (Mindell, 2012). Magnetite and maghemite based SPIONs that have been functionalized with a dextran coat have been shown to release free Fe^{2+}/Fe^{3+} when exposed for long periods in an acidic environment (Singh et al., 2012). This is a result of the dextran coat of the SPIONs being degraded inside the acidic environment of the lysosome, resulting in the magnetite core being exposed to the acidic environment. This results in degradation of the magnetite particle causing the release of free Fe^{2+}/Fe^{3+} (Singh et al., 2012). This free Fe^{2+}/Fe^{3+} then can catalyze the formation of highly reactive hydroxyl radicals which have been shown to induce an increase in cellular stress levels (Uchiyama et al., 2008). This increase in cellular stress has been found to primarily damage the mitochondrial membrane, resulting in the mitochondria losing

their membrane potential and becoming depolarised (Kim et al., 2003, Nieminen et al., 1997). This loss of mitochondrial function results in the release of pro-apoptotic proteins such as cytochrome c (Uchiyama et al., 2008).

The lysosome itself can be damaged due to the presence of free iron. The production of hydroxyl radicals has been shown to induce lipid peroxidation (Zdolsek and Svensson, 1993). As the lysosome has a lipid rich membrane the peroxidation of these lipids has been found to disrupt lysosomal membrane integrity causing the release of lysosomal enzymes and protons out of the lysosomes into the cell (Zdolsek and Svensson, 1993).

As mentioned before it is important that for the utilization of SPIONs to purify lysosomes they must not be toxic to the cells otherwise it would not be an effective means of purifying a good yield of lysosomes. Also it is important to determine that the particles do not alter the pH of the lysosome as this would induce lysosomal dysfunction and affect the function of many key lysosomal enzymes.

Cells were treated with two different types of magnetite based SPIONs (LRL SPIONs and Chemicell SPIONs) to determine any toxic effects they might induce in cells after long term exposure to the acidic environment of the lysosome. An Iron oxide coated dextran particle (FeO) was also tested, as this has similar properties to iron based nanoparticles that have been used previously to magnetically purify lysosomes (Chen et al., 2005, Diettrich et al., 1998, Duvvuri and Krise, 2005).

3.8.1 Nanoparticle effects on the lysosome and lysosomal enzymes

As the nanoparticles are taken up into the cell they are trafficked along the endocytic pathway until they reach its end point, the lysosome. As the SPIONs are primarily located inside the lysosome this is most likely where any initial toxicity would occur. Lysotracker green probe loads into high acidic compartments and fluoresces, meaning that the pH of the lysosome has an acidic pH-optima for the probe to work in it (figure 3.1). The Magic red cathepsin kits for cathepsin B and L was also used to measure the activity of these two lysosomal enzymes (figure 3.2 and 3.3). Drastic changes in the pH of the lysosome would affect the function of these two enzymes. The levels of lysosomes detected using the lysotracker green probe revealed that there was no change in the levels of lysosomes detected in the LRL SPIONs treated cells, while there appeared to be an increase in lysotracker staining in some cells treated with Chem SPIONs. No change in lysotracker staining was observed following LRL SPION treatment indicates that the long term presence of these particles in an acidic compartment appears to have no effect on lysosomal pH otherwise there would be a drastic change in lysotracker fluorescence. However the increase lysotracker staining displayed in the Chem SPION treated cells, which increased as the particles remained in the lysosome for a longer time, suggests that these particles are becoming unstable at a much faster rate than that of the LRL SPIONs. Interestingly there was a drastic reduction in lysotracker staining over the two time points monitored with cells treated with FeO particles. This

strongly suggests that these particles are highly unstable once they reach the lysosomes and are causing a reduction in the lysosomal pH, possibly by damaging the lysosomal membrane causing protons to leak out of the lysosome. The cathepsin B and L activity assays also seem to suggest this. It is only after a 48 hour chase that there is a change in cathepsin B activity in the LRL SPION treated cells, suggesting that only now they are starting to become less stable. There is a general increase in the activity of the two cathepsin enzymes observed in the Chem SPIONs treated cells at an earlier time point suggesting again that these particles are becoming unstable at a faster rate than the LRL SPIONs. Cathepsin B has been found to be a key mediator in apoptosis, so higher levels of it may be resulting in greater toxicity being present in the Chem SPION treated cells (Sandes et al., 2007). The FeO treated cells appeared to display cathepsin staining throughout the cell, not in lysosomal vesicle compartments. This may explain why lysotracker stains in FeO treated cells is so low as the lysosomal membrane has become damaged causing the leaking of protons as well as lysosomal enzymes into the cytosol. The cathepsin B enzymes are now potentially active inside the cytosol of the cell, cleaving off target proteins and other important macromolecules. After a longer chase time the level of cathepsin B activity did decrease in FeO treated cells most likely due to the cell undergoing apoptosis. Interestingly there was little change in the levels of cathepsin L activity in the SPION treated cells (figure 3.3), which suggests that any changes in the pH inside the lysosomes is still within the pH range for cathepsin L to function. Cathepsin L levels drop

drastically after FeO particle treatment though which could possibly be because it has already initiated apoptosis, and now has become inactive.

3.8.2 SPION induced Phospholipidosis

Research has been done into the fate of drugs once they enter the cell, with many drugs being cationic amphiphilic drugs (CADs) due to their respective chemical structures. It has been found that the accumulation of these CADs inside lysosomes has an effect on phospholipid metabolism resulting in the accumulation of phospholipids inside lysosomes (Anderson and Borlak, 2006). It was important to determine if the presence of SPIONs and FeO particles inside lysosomes had a similar effect as CADs do on phospholipid accumulation. LRL SPION treated cells did not exhibit an increase in the levels of phospholipidosis, which suggests that they are not exhibiting CAD like effects on phospholipid metabolism and membrane properties when they are present inside lysosomes (figure 3.4). However this was not the case with Chem SPION treated cells which did exhibit an increase in phospholipidosis which could be a result of these SPIONs not being as stable as LRL SPIONs and the free iron that is being released is having an effect on phospholipid metabolism. This also appeared to be the case with the FeO treated cells which from previous data shows they are highly unstable and greatly effect lysosomal pH and cathepsin activity, which is likely why there is an increase in phospholipidosis occurring in these cells.

3.8.3 Determining the effects on mitochondrial function

One of the areas that is most studied when It comes to the toxic effects of nanoparticles is their effect on mitochondrial viability, as mitochondria are highly susceptible to hydroxyl radicals (Zdolsek and Svensson, 1993). The mitochondria levels do not vary greatly between the treatments with the different SPION/FeO particles (figure 3.5). There does appear to be changes in the levels of mitochondrial produced reactive oxygen species (ROS) present (figure 3.6). Mitochondria naturally produce reactive oxygen species, and changes in these levels could indicate a problem in their function. LRL SPION treated cells appear to show little to no change in the levels of mitochondrial produced ROS suggesting that there is currently no effect on mitochondria function. However there does appear to be elevated levels in the FeO and Chem SPION treated cells where greater levels of mitochondria ROS is being produced. This would indicate that the mitochondria are becoming stressed and beginning to function incorrectly, causing an increase in the levels of ROS as a result. While the elevated levels are the same over the two time points measured in the Chem SPION treated cells, the levels of mitochondrial produced ROS drop dramatically between the 24 hour and 48 hour chase times in the FeO treated cells. This could be because after a 48 hour chase with FeO particles the mitochondria have become damaged to the point where they no longer function as efficiently as normal mitochondria do, releasing less mitochondria ROS as a result.

3.8.4 Lipid peroxidation and super oxide production

The DPPP probe was used to detect for the presence of lipid peroxidation occurring inside the lysosome. As the membrane of lysosome is composed heavily of lipids it is important that no lipid peroxidation was to occur when the lysosomes take up the LRL nanoparticles (figure 3.7). Any lipid peroxidation that occurs could have an effect on lysosomal membrane stability (Zdolsek and Svensson, 1993). Even after a 48 hour chase there were no signs of lipid peroxidation found in the LRL SPION treated cells. This is likely because while only a small amount of free iron may have been released from the magnetite core, it is not enough to induce lipid peroxidation. After a shorter chase time with Chem SPIONs no peroxidation was found in the cells, suggesting that at this time point the lysosomal membrane is not compromised. However this appeared to change following a 48 hour chase as lipid peroxidation was starting to appear suggesting that by this time point the lysosomal membrane is starting to become damaged. High levels of lipid peroxidation were seen in the FeO treated cells at both chase times, further highlighting the particles lack of stability as the large amount of free iron released has damaged the lysosomal membrane at a much faster rate than the two SPION particles.

The DHE stain for superoxide showed that the presence of the LRL SPIONs did not cause the levels of superoxide to increase in the cell, even after a longer chase, which like the results of the lipid peroxidation probe show how stable this nanoparticle is even after a long time in the

lysosomes acidic environment (figure 3.8). The FeO treated cells seemed to have an initial increase in the levels of super oxide which is most likely due to the FeO being converted to free iron and the release of further super oxide particles from the peroxidation of lipids. Following a longer chase time the staining for super oxides was high throughout the cell, implying that the super oxides produced from the free iron inside the lysosome has leaked out and is now present in other parts of the cell.

3.8.5 Imaging the levels of free Fe^{2+} and Fe^{3+} being released

Fura 2 is a probe that is sensitive to Fe^{2+} at 360nm wavelength, where its fluorescence is quenched when bound to free iron. The probe was used to analyse the rate of the release of iron in cells treated with the SPIONs and FeO (figure 3.9). Unsurprisingly the LRL SPION treated cells appeared to have the least amount of free Fe^{2+} release when compared with the other particles. There was a large drop in fluorescence with the probe after a longer chase time with Chem SPION treated cells which would indicate that the particles are only really stable for around a 24 hour chase. The FeO treated cells displayed large amounts of free Fe^{2+} present which explains the high levels of lipid peroxidation, lysosomal dysfunction and super oxide presence seen previously. The levels of free Fe^{3+} were also analysed and the LRL SPIONs again appeared to be the most stable as little free Fe^{2+} and Fe^{3+} was observed. The FeO particles released high levels of both forms of Fe, giving a strong indication of where the toxicity is coming from.

3.8.6 Importance of structure of dextran coat of SPIONs

As mentioned previously it is important to coat the magnetite SPION with a functionalized, biological coat to protect it from the acidic environment of the lysosome. Work done to determine if an LRL produced SPION with a 10kDa coat as opposed to a 40kDa coat resulted in a marginal increase in the levels of cellular toxicity (figures 3.11, 3.12, 3.13). With cells treated with the 10kDa SPIONs there was a slight increase in the levels of lysotracker and phospholipidosis detected, as well as a decrease in the levels of mitochondria ROS produced in the cells. However interestingly there was no major increase in the levels of super oxide or lipid peroxidation. This is most likely because the 10kDa SPIONs are reaching the lysosomes and becoming unstable at a faster rate than that seen with 40kDa SPIONs, due to the smaller dextran coat degrading faster than a 40kDa dextran coat would. This highlights the need for an adequate sized dextran coat to be functionalized to the magnetite particle, to offer suitable protection of the SPION core from the acidic environment of the lysosome.

3.8.7 Lysosomal toxicity in NPC1 null cells treated with SPIONs

CHO M12 cells are null for the protein NPC1, which results in the accumulation of lipids inside the lysosome (Lloyd-Evans and Platt, 2010). Previous work done to magnetically purify lysosomes from healthy and diseased cell resulted in toxicity in both sets of cells, but especially in the

diseased cells (Diettrich et al., 1998). As NPC1 deficiency results in the accumulation of many lipids in the lysosome, this has an effect on other important factors in the cell such as lysosomal Ca^{2+} levels as well as endocytic trafficking defects (Lloyd-Evans and Platt, 2011, te Vruchte et al., 2004). It was important to determine that while LRL SPIONs were stable in the lysosomes of healthy cells, they would also be stable in a diseased lysosome, as this would affect the ability of the SPIONs to be able to magnetically purify diseased lysosomes. The levels of lysotracker staining and the activity of cathepsin B and L were observed in CHO M12 cells which were treated for a long chase time of 48 hours, so that the SPIONs have time to reach the lysosome. There was however no changes in lysosomal levels or the activity of the two cathepsins which would indicate that these diseased lysosomes are not damaged, or their enzyme functions altered by the presence of LRL SPIONs present in them.

3.8.8 Summary

With the potential use of using highly magnetic SPIONs to purify lysosomes, it was important to determine what brand of SPIONs was the most stable inside cells. LRL produced SPIONs showed little to no toxic effects in the lysosomes following a long chase time, especially when compared with the Chem SPION and the FeO particle. Also importantly it was important that the LRL SPION did not produce any dysfunction in the lysosomes of CHO M12 cells. This means that it is a suitable nanoparticle

to utilize for the purification of lysosomes from both healthy and diseased cell lines.

Chapter 4: Developing an improved technique for magnetically purifying lysosomes

4.1 Density gradient centrifugation

As previously stated (chapter 1 general introduction), de Duve first discovered lysosomes using a technique called density gradient centrifugation. He set out to “explore the cell with a centrifuge” and was able to isolate lysosomes as well as other organelles of similar density such as peroxisomes and mitochondria (Cox and Cachon-Gonzalez, 2012). Thanks to this, de Duve and others were able to characterize the enzyme content of the isolated organelles gaining insight in the organelles function, long before they were studied under a microscope. DGC is still commonly used today in research for isolating different cell types such as cancer stem cells from a total cell population (Liu et al., 2012). The method behind using DGC for organelle isolation works by homogenising a cell to release its cellular contents. These organelles are then centrifuged at high RCF over a sucrose gradient. This results in the separation of individual organelles based on their respective density (Liu et al., 2011).

This was how de Duve isolated lysosomes for the first time and in doing so he also purified out mitochondria and peroxisomes, due to their similar densities. The main problem with DGC for organelle isolation arises when it is used to try and extract lysosomes from lysosomal storage disease cells. Lysosomes isolated from storage disease cells typically accumulate lipids either as a primary or secondary storage material (Cox and Cachon-Gonzalez, 2012). All this excess stored material leads to a

change in the buoyant density of the lysosome, due to the stored lipids making the lysosomes buoyancy lighter. When they are separated over a sucrose gradient their variable densities result in deposition of lysosomes across the gradient with predominant bands in different locations to lysosomes isolated from control cells that are often contaminated by other organelles of similar densities (Graham, 2001). This has been noted before when researchers tried extracting lysosomes from the lysosomal storage disease infantile free sialic acid storage disease (ISSD) cell lines (Mendla et al., 1988). This is a major problem that has largely stifled research into lysosomal protein function and LSDs since de Duve's groundbreaking work.

4.2 Density Gradient Electrophoresis

Density gradient electrophoresis (DGE) is a technique that not only utilizes an organelles density but also exploits its surface charge to isolate it. The idea behind this technique is that many organelles possess a similar density (e.g. lysosomes and peroxisomes) but may have a different surface charge, allowing for a second level of separation that DGC cannot provide (Tulp et al., 1993). The DGE is a specialised apparatus that isolates subcellular organelles by using a ficoll gradient that then has a current applied to it. At either end of the DGE apparatus is an anode and a cathode (top and bottom respectively) that allows the upward electrophoresis of organelles, resulting in the more negatively charged (and small) organelles being collected first (Tulp et al., 1996,

Tulp et al., 1999). A previous study attempted to purify out lysosomes from both wild type and NPC cells using DGE (work unpublished). Subcellular organelles underwent DGE and the fractions produced were collected and characterized by western blots. Each fraction contained a peak for a particular organelle indicating enrichment of this particular organelle in that fraction. While there are peaks of specific organelles in different fractions, there is a continuous high level of ER contamination detected in every fraction. This is due to the structural nature of the ER, when it is damaged (by homogenisation) it forms so called microsomes of multiple sizes and densities, resulting in high ER contamination when it comes to purification methods that utilize an organelles density. Another problem that was observed in this study was that a large amount of starting material (~20 million cells) was required to perform a single DGE purification, ultimately yielding very low quantities of pooled membranes (50-100μg). However the yield obtained from each individual fraction was only enough to perform a single western blot, which only ended up confirming that the fraction possessed ER contaminants. Thus, the technique cannot realistically be used for obtaining pure fractions of lysosomes or for performing functional assays.

4.3 The use of iron particles for purifying lysosomes

Novel techniques have been developed that utilise density gradient centrifugation to purify lysosomes by manipulating their buoyant density during the purification process. This has been done by loading the

lysosome, via the endocytic pathway, with heavy molecules such as dextrans, gold and more commonly colloidal iron (Arai et al., 1991, Arborgh et al., 1973, Henning and Plattner, 1974). The methodology behind this is that by making the lysosome as dense and heavy as possible it should be possible to isolate them from a homogenate by making it much heavier than other organelles so they would pellet under less centrifugal force when compared with other organelles (Chen and Arriaga, 2006). However this method requires multiple time-consuming centrifugation steps as well as sample clean up steps to produce a small yield of lysosomes that are often damaged by the purification process (pelleting at high speed). Another problem with this technique is that the loading of these large molecules into lysosomes can produce toxic side effects. An example of this would be the iron particle loaded into lysosomes would likely react with the high proton content inside the intralysosomal lumen, causing free iron to leach off the particle. It has been established that free iron interacts strongly with lipids to produce free radicals, which with the lysosomal membrane being lipid rich would most likely have an effect on lysosomal membrane integrity (Zdolsek and Svensson, 1993) which can have a knock on effect of causing either the dissipation of lysosomal protons (altering lysosomal pH) and Ca^{2+} content out of the lysosome (Chen and Arriaga, 2006). This could potentially lead to phospholipidosis like phenotypes or ultimately membrane damage, which is likely to induce significant cellular stress and alterations in function. To compensate for this cells would be treated for shorter amounts of time with these particles, so they are not exposed to the

acidic environment of the lysosome for to long. This was done to avoid potential toxicity issues. However this would result in less iron being loaded into the lysosome, thereby reducing the capabilities of purifying lysosomes using this method. While this method has only had limited success in purifying lysosomes from healthy cells, purifying lysosomes from lysosomal storage disease cells would be greatly more difficult. It has been well established that most lysosomal storage disease lysosomes store lipids in either a primary or secondary manner (Cox and Cachon-Gonzalez, 2012). This storage would result in the buoyancy of the lysosomes to become lighter than that of non-storing lysosomes. This would result in a greater quantity of iron/gold particles needed to be loaded into lysosomes for there to be a great enough change in their density so they are capable of being purified in this manner. Other caveats for this would also include that in many lysosomal storage diseased cells endocytic trafficking is retarded so that not enough of these particles would potentially reach the lysosome to induce a great enough change in their density (te Vruchte et al., 2004).

4.4 The initial use of magnetic nanoparticles for lysosomal purification

The first major attempt at purifying lysosomes using magnetic nanoparticles was done during the early 1990s, where dextran particles were coated in an iron oxide coat (FeO) were fed to *Dictyostelium discoideum* (Rodriguez-Paris et al., 1993). The lysosomes from the

Dictostelium discoideum were then purified with the use of a 0.8 tesla magnet. The results of this study found that ~76% of the ingested iron dextran particles were found in the lysosomal fraction they obtained, which indicated that these particles remained within the endocytic system as they are trafficked to the lysosome. This important study showed that while the iron-dextran particles may not have necessarily been the most stable particles, the use of magnetic separation to purify lysosomes was a possible alternative to purifying lysosomes from other more established techniques.

4.5 Lysosomal purification using magnetic nanoparticles

At the time in 1998 (and still in some cases today) not all defective lysosomal proteins that result in the development of a lysosomal storage disease had been characterized, or even identified. Diettrich *et al* realized the importance of proteomic research to help improve understanding of the pathogenic mechanisms that result in a lysosomal storage disease phenotype (Diettrich et al., 1998). The group knew that to effectively research and characterize these lysosomal proteins there needed to be a way to purify out the lysosome from cultured LSD cells. This problem had been ongoing since de Duve's pioneering work in efforts to isolate pure lysosomal fractions with low contamination of other organelles.

Professor Bryan Winchester's group had previously attempted to use DGC to isolate lysosomes from patients suffering from ISSD (Diettrich et al., 1998). ISSD is a rare autosomal recessive disorder where a mutation

on a gene located on chromosome 6 results in a deficiency in lysosomal sialidase, resulting in gangliosides not being broken down within the lysosome causing storage of sialic acid (Aula et al., 2002). Diettrich *et al* observed that due to the accumulation of sialic acid in the diseased cell inside the lysosomal compartment, the density is affected to the extent there is a greater level of contaminants. This obstacle led a growing need to develop a new method to purify out lysosomes, one which allowed for the purification of the compartment that is not dependent on morphology or buoyant density (as both are likely to be altered in LSDs). Diettrich *et al* took inspiration from the Rodriguez-Paris *et al* study (as described earlier) and adpated this method to exploit the endocytic trafficking of macromolecules to potentially purify lysosomes from ISSD cells. Colloidal iron dextran (FeO) was prepared as previously used by (Rodriguez-Paris et al., 1993) and then loaded into both wild type fibroblasts and ISSD fibroblasts. After an overnight chase the cells were homogenized and the released organelles were passed through a magnetic field contained in a Miltenyi MiniMACS column. The lysosomes that were now bound to the column due to the magnetic field were then eluted off using either hypotonic solution or buffers containing low concentrations of non-ionic detergents. Enzyme assays were then performed on the isolated lysosome fractions to determine the level of lysosomal enrichment achieved between the wild type and ISSD fibroblast cell lines.

An enrichment of ~50% was observed, suggesting that lysosomes were being purified. However there was still high lysosomal activity in the post

nucleic supernatant (PNS) (flow through that passed over the column). This would suggest a large amount of lysosomes are still just passing through the magnetic field. Also only a small yield of purified lysosomes was obtained, possibly due to the FeO particles possessing poor magnetic properties. An increase in cellular toxicity observed in the cells treated with the FeO particles resulted in a shorter treatment time, which would only reduce the yields further as less particles are being endocytosed into the cell due to the shorter treatment time (Diettrich et al., 1998).

A few years later a study utilized the magnetic separation method whilst researching the inter-relationship between the lysosomal proteins NPC1 and NPC2 that cause Niemann-Pick type C1 and C2 disease respectively (Chen et al., 2005). The livers of mice treated with iron dextran were harvested over a 0.5,1,2,4 hour time course following the injection of the FeO into the mouse. By doing this, they were able to isolate different fractions that contained organelles from the different parts of the endocytic pathway. This was confirmed by the use of western blotting techniques using marker proteins specific for each compartment.

By not using detergents to elute the lysosomes off the magnetic column they only obtained a low yield of protein in the lysosomal fraction (<50μg of protein). However, the benefit of not using detergents meant that the lysosomes were still structurally intact. A re-acidification assay using acridine orange was performed to show that the lysosomes were still

functional and could be re-acidified after magnetic separation, however an entire fraction was required per assay.

To fully understand the fate of drugs once they are in the cell and how they are distributed and sequestered would help researchers to design and modify the drugs so they could optimize their intracellular distribution. Duvvuri *et al* set out to improve a way to accurately measure the lysosomal accumulation of drugs as their previous attempt had taken a more indirect approach (Duvvuri and Krise, 2005). They used an adaptation of the magnetic separation method used by Diettrich *et al* to purify out lysosomes from HL-60 cells using home made FeO particles (Duvvuri and Krise, 2005). The addition of hypotonic and isotonic buffers as well as detergents used during the magnetic lysosomal purification resulted in a greater protein yield in the lysosomal elution than what was seen using this technique in previous studies (Duvvuri and Krise, 2005). However, the use of detergents means the purified lysosomes are no longer structurally intact. While the use of detergents is detrimental to the development of an assay intended to produce a lysosomal fraction that has a high yield and that functional assays can still be performed, the protocol itself is an effective way of purifying out lysosomes while using crudely made, poorly magnetic, unstable FeO particles.

One of the major developments Duvvuri and Krise made during their attempts at purifying lysosomes was the introduction of certain types of osmotic changing buffers to aid in their attempts at purifying lysosomes

(Duvvuri and Krise, 2005). The buffers they used were originally adapted from a study showing how hypotonic buffers were useful in cell homogenisation as this caused swelling and bursting of the cellular membrane, while the addition of an isotonic buffer after homogenisation helped maintain organelle structural integrity post homogenisation (Graham, 2002). The addition of these buffers to the lysosomal purification technique Duvvuri *et al* used helped increase the yield of lysosomes they obtained as more lysosomes would be passed over the magnetic field rather than be spun out with the unbroken cells during the centrifugation step of the assay (Duvvuri and Krise, 2005).

An important study was done where early endosomes were purified to study their protein content (Glebov et al., 2006). This study was important in the development of our own magnetic purification assay, as they were able to show that they could effectively purify out early endosomes. This is difficult as the pulse and chase times have to be very precise (a 10 minute pulse and a 10 minute chase), or else the magnetic nanoparticles would have already been processed out of the early endosome. While in previous studies using magnetic separation to purify out endocytic organelles has show that a reduced pulse time gives a poor yield (Diettrich et al., 1998), due to there being only a short amount of time for the cells to take up the FeO particles. However, this study was able to purify out early endosomes with a decent yield, despite there only being a 10 minute pulse time for the cells to endocytose the particles. This was due to the highly magnetic SPIONs they used, provided by

Liquids Research Ltd (LRL). The main issue to consider is that only a small amount of the LRL SPIONs would be present in the early endosome after such a short pulse time, the strong magnetic properties from the SPIONs resulted in a good amount of early endosomes to be magnetically purified out of the cell. This would indicate that LRL SPIONs had a much higher magnetic potential than the colloidal iron dextran conjugates used in the previous studies.

The pioneering work done by Professor Winchester, Professor Ioannou and Dr Krise during the last 20 years has helped pave the way for a new technique to purify lysosomes by loading them with magnetic nanoparticles via the endocytic pathway followed by their subsequent purification via a magnetic field which has resulted in a new, novel and vastly improved method for purifying lysosomes without the need for established methods such as density gradient centrifugation.

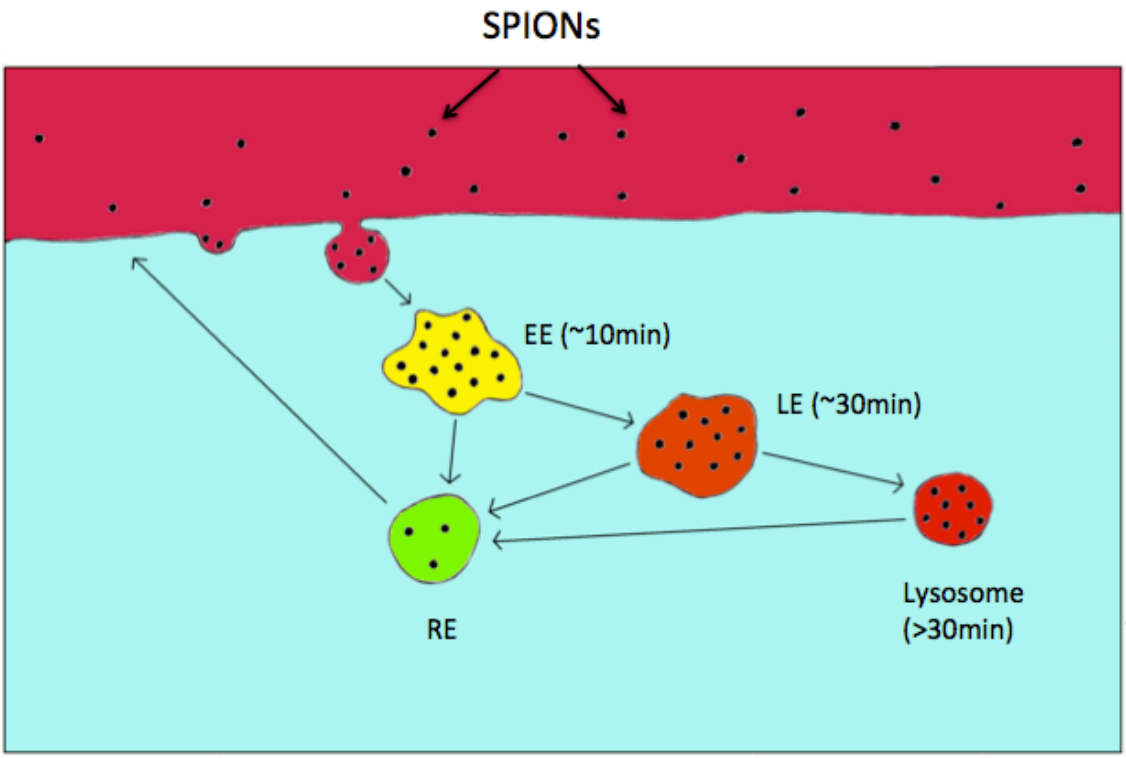

Figure 4.1: Simplified schematic on the methodology on how the dextran functionalised SPIONs are loaded into the lysosome. The SPIONs are taken up into the cell via fluid phase endocytosis, where they reach the early endosome (EE) after ~10 minutes. They are next trafficked to the late endosome (LE) after ~30 minutes. After 30 minutes of being in a healthy cell, the SPIONs should be in the late endosomal-lysososmal compartments. Some SPIONs might be recycled back out of the cell via the recycling endosome (RE).

4.6 Results

It is important to determine that the magnetic nanoparticles used to purify lysosomes are first capable of reaching lysosomes, so no other organelle is being purified. Another important factor to take to take into consideration is that endocytic uptake and the trafficking of the SPIONs will vary across different cell lines.

4.6.1 Using fluorescent LRL SPIONs to determine their subcellular localization after different chase times

LRL produced SPIONs coated with a 40kDa Dextran that contains TRITC dextran were treated to CHO-H1 and CHO M12 to measure the endocytic trafficking of these nanoparticles as they are trafficked through the endocytic system across two different chase times. These fluorescent LRL SPIONs are produced in the same way as the normal LRL SPIONs used in the lysosomal purification assay, however 1:10 of the 40kDa dextran coat is composed of TRITC dextran. The particles still possess a magnetic SPION magnetite core and 40kDa dextran coat so they should still be trafficked through the endocytic system as normal LRL SPIONs.

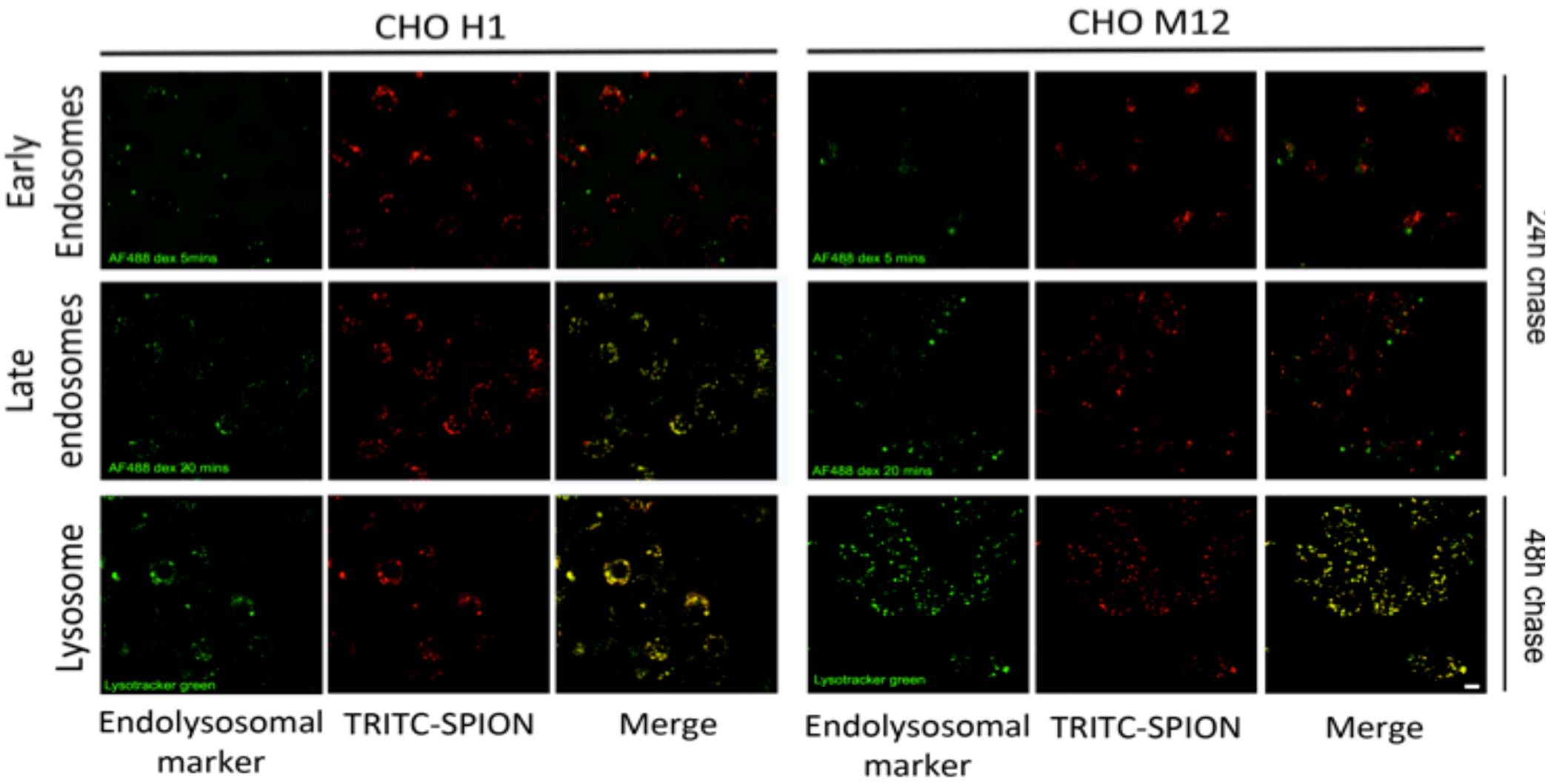
CHO H1
CHO M12
Early Endosomes
Late endosomes
Lysosome
24h chase
48h chase
AF488 dex 5mins
AF488 dex 5 mins
AF488 dex 20 mins
AF488 dex 20 mins
Lysotracker green
Lysotracker green
Endolysosomal marker
TRITC-SPION
Merge
Endolysosomal marker
TRITC-SPION
Merge

Figure 4.2: LRL SPIONs coated with TRITC dextran were treated to CHO-H1 and CHO M12 cells for a 24 hour pulse followed by a 24 or 48 hour chase. The cellular localization of the TRITC (Tetramethylrhodamine) coated SPION was then determined by the use of lysotracker green and AlexaFluo-488 dextran. A 5 minute pulse with AlexaFluo-488 was used as an early endosomal marker while a 20 minute pulse with AlexaFluo-488 will have loaded into late endosomes and can be used as a marker for them, lysotracker green was used as a lysosomal marker. The localization of the TRITC-SPIONs was then determined by measuring the levels of co-localistion with the different endocytic organelles after the two different chase times. Images displayed are representative. n=3. Scale bar =10μM.

A pulse of 5 minute and 20 minute with AlexaFluo-488 dextran was used as a marker for early and late endosomes respectively, while lysotracker green was used as a lysosomal marker. After a 24 hour pulse followed by a 24 hour chase with the LRL TRITC-SPIONs there was high co-localisation between LRL TRTIC SPIONs and AlexaFluo-488 in the late endosomal compartment, which indicates that a 24 hour pulse and 24 hour chase is enough time for LRL SPIONs to reach the late endosome-lysosomal compartments. After a 48 hour chase in the CHO-H1 cells there was high co-localisation present in the lysosomes, showing that the particles are still present in the lysosomes after an additional 24 hours. CHO M12 cells treated with a 24 hour pulse with LRL TRITC SPIONs showed no co-localisation in the early endosome or late endosome compartments (figure 4.2). This suggests that a 24 hour chase is not enough time for the nanoparticles to be trafficked to the later endocytic vesicles in CHO M12 cells, most likely due to the retarded endocytic trafficking present in NPC1 null cells (te Vruchte et al., 2004). After a 48

hour chase there is high co-localisation with lysotracker green, which shows that the SPIONs are now in the lysosomal compartment. This data shows that a longer chase time is required for the SPIONs to reach the lysosomes in CHO M12 cells so that they can then be magnetically purified.

4.6.2 Comparison of different chase times from LRL SPION treated CHO-H1 cells

The first step in developing the magnetic purification method was to determine what chase time produced the greatest amount of protein yield from the eluted lysosomal fraction after a 24 hour pulse.

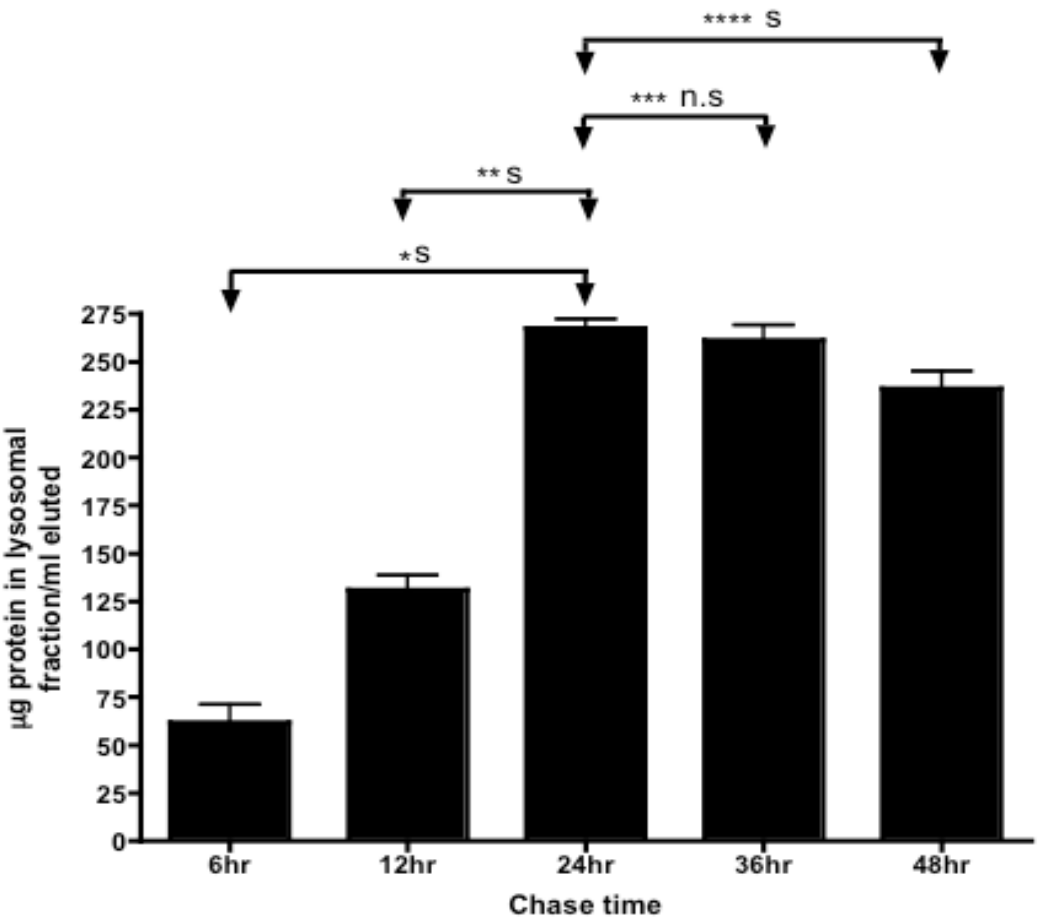

*Figure 4.3: Protein levels detected in the lysosomal fraction across different chase times following a 24 hour pulse. n=3 Values represent mean ± SD, n=3. *P <0.001; **P <0.001; ***P >0.05; ****P <0.05, S denotes significant, n.s. denotes not significant.*

CHO-H1 cells grown to confluency in a T75 flask were treated with a 24hr pulse of LRL SPIONs followed by either a 6, 12, 24, 36 or 48 hour chase. The lysosomes were then extracted using magnetic separation. BCA protein assays were performed on the lysosomal fractions obtained from each individual chase time to determine the protein content present in each fraction. The data shows that following a 24 hour pulse and a 24 hour chase is the optimum chase time to get the highest yield of

lysosomes from LRL SPION treated CHO-H1 cells (figure 4.3). Shorter chase times produce a lower yield protein in the lysosomal fraction, most likely because all the SPIONs have not been trafficked to the lysosome yet. Longer chase times result in a small decline in the protein detected in the lysosomal fraction, possibly due to the SPIONs becoming unstable and losing their magnetic capability.

4.6.3 Comparison of different Iron based nanoparticles used to purify lysosomes

Magnetic purification was performed on CHO-H1 cells that had been treated with a 24 hour pulse with FeO particles and Chem SPIONs followed by a 24 and 48 hour chase time. BCA protein assays were performed on the lysosomal fractions obtained following treating with the different iron based nanoparticles at the two different chase times and compared with the protein detected in the lysosomal fraction from the use of LRL SPIONs (figure 4.4).

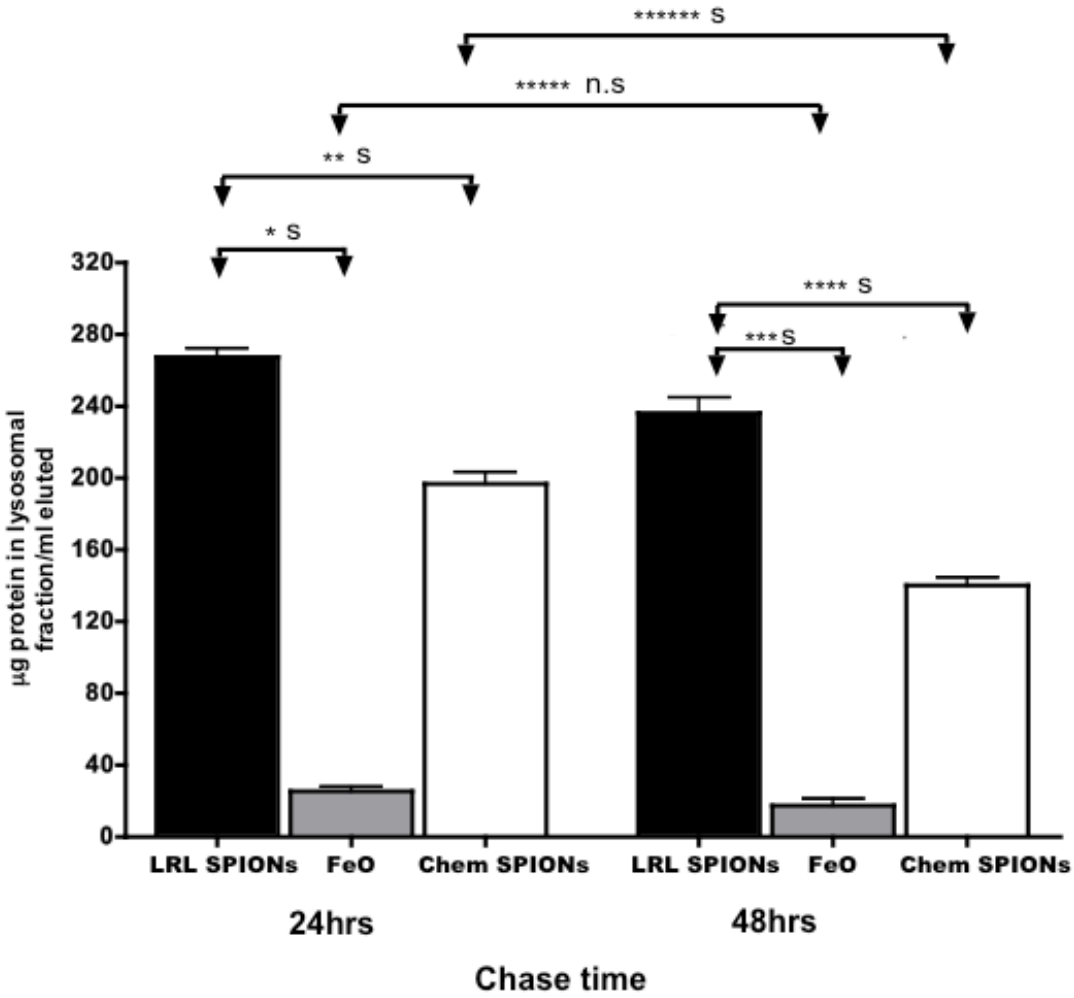

*Figure 4.4: Protein levels detected in the lysosomal fraction after purification using the three different iron based nanoparticle providers after a 24 hour pulse and a 24 and 48 hour chase. Values represent mean ± SD, n=3. S denotes significance, *P <0.001; **P <0.001; ***P <0.001;****P <0.001; *****P >0.05; ******P <0.01, s denotes Significant, n.s. denotes not significant.*

After a 24 hour chase there was significantly higher amount of protein detected in the lysosomal fraction with the use of LRL SPIONs when compared with the use of FeO and Chem SPIONs. The FeO lysosomal fraction yield following a 24 hour chase was significantly lower than both the LRL and Chem SPIONs indicating poor magnetic capabilities. After a 48hr chase, the yields detected in the lysosomal fraction dropped after

the use of FeO, LRL and Chem SPIONs. After a 48 hour chase the LRL SPIONs still resulted in the highest detected in the lysosomal fraction. Interestingly there was a greater drop in yield in the lysosomal fraction from a 24 hour chase to 48 hour chase with the use of Chem SPIONs compared with LRL SPIONs, suggesting that the Chem SPIONs are less stable over longer time periods when in lysosomes compared with LRL SPIONs. FeO lysosomal fraction yield does drop after a 48 hour chase but the drop is not significant.

4.6.4 Utilising Maghemite based SPIONs

LRL SPIONs composed of a maghemite core rather than a magnetite core was pulsed to CHO-H1 cells for 24 hour followed by a 24 hour chase. Maghemite SPIONs possess the same properties as the LRL magnetite SPIONs with the exception of the core being composed primarily of maghemite. The LRL maghemite SPIONs still have a 40kDa dextran coat so they should still be trafficked to the lysosome in the same manner as the LRL magnetite SPIONs do.

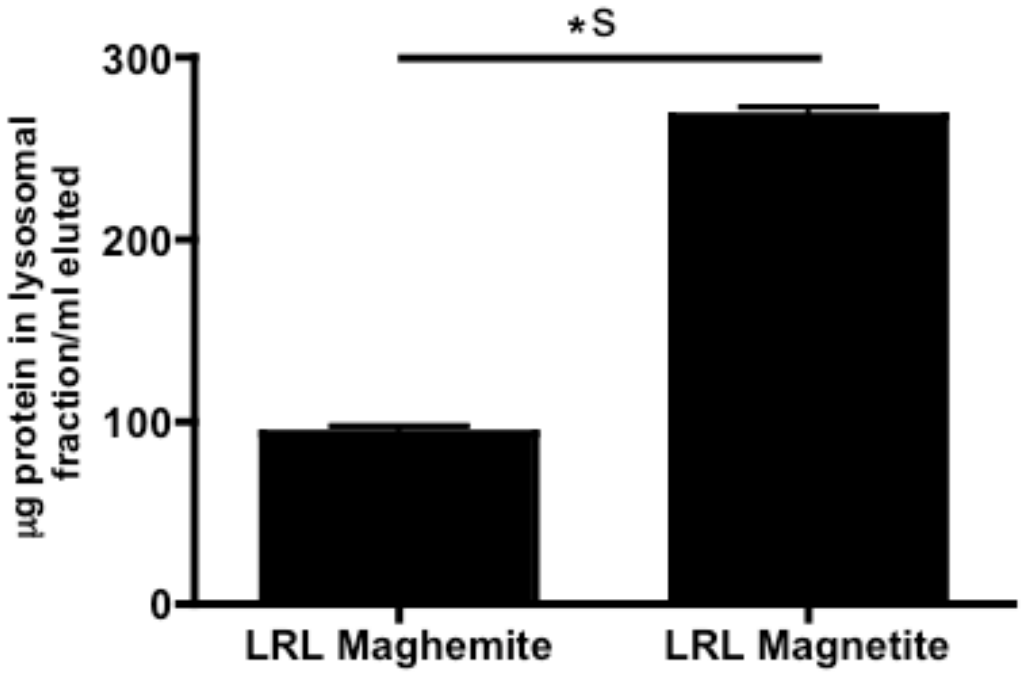

*Figure 4.5: Protein levels detected in the lysosomal fraction following purification from CHO-H1 cells with LRL Maghemite based SPIONs and a LRL Magnetite based SPIONs following a 24 hour pulse and 24 hour chase. n=3. Values represent mean ± SD. S denotes significance *P <0.001.*

The lysosomes were then purified and the yield in the lysosomal fraction was determined. There was a significantly lower yield in the lysosomal fraction when using maghemite SPIONs (figure 4.5). This is most likely due to maghemite having a lower magnetic potential than magnetite.

4.6.5 Comparison of different pulse times yields from LRL SPION purified lysosomes

CHO-H1 cells underwent a longer pulse time with LRL SPIONs to determine if giving the cells more time to take up the nanoparticles increases the yield in the lysosomal fraction.

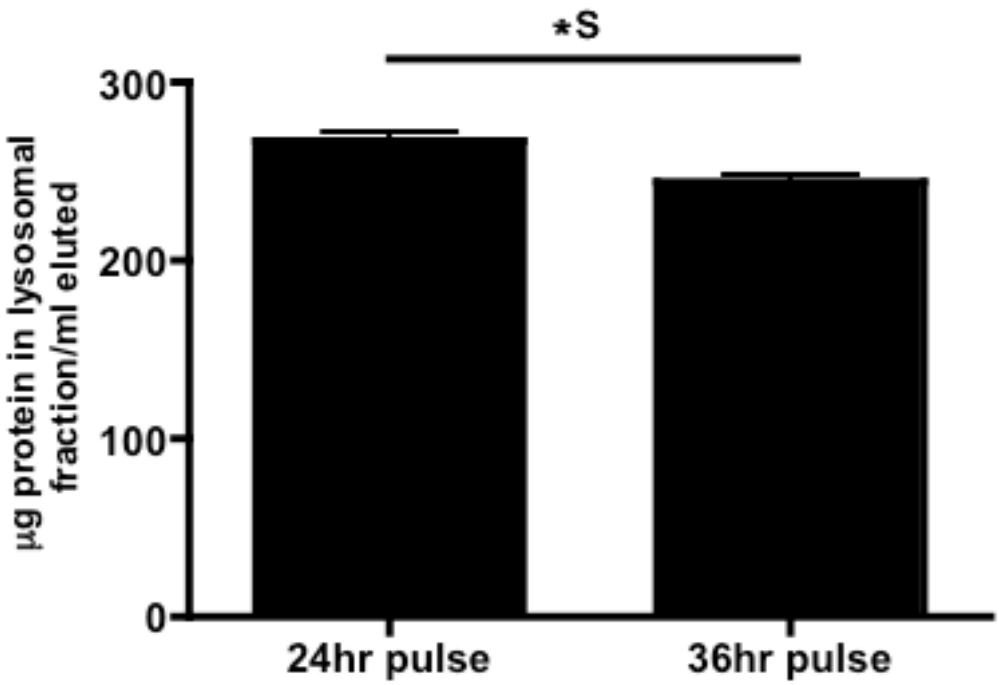

*Figure 4.6: Protein levels detected in the lysosomal fraction following purification from CHO-H1 cells from two different pulse times followed by a 24 hour chase. n=3. Values represent mean ± SD, n=3 S. denotes significant. *P<0.05.*

Graph displays the yields obtained following lysosomal purification in the lysosomal fraction from a confluent flask of T75 CHO-H1 cells that underwent a 24 or 36 hour pulse (figure 4.6), followed by a 24 hour chase using LRL SPIONs. There was a significant drop in the protein levels detected in the lysosomal fraction following a 36 hour pulse when compared with a 24hr pulse. This suggests that a 24 hour pulse is optimal for enough SPIONs to be endocytosed by the cell for the best lysosomal fraction yield.

4.6.6 Comparison of 10kDa LRL SPIONs vs 40kDa LRL SPIONs to purify lysosomes

Two types of Magnetite SPIONs are produced by Liquids Research Ltd. The Magnetite core in both are similar however they possess either a 40kDa dextran coat or a 10kDa dextran coat. The size of the dextran coat may affect the trafficking and stability of the SPIONs which may result in a lower yield in the lysosomal fraction.

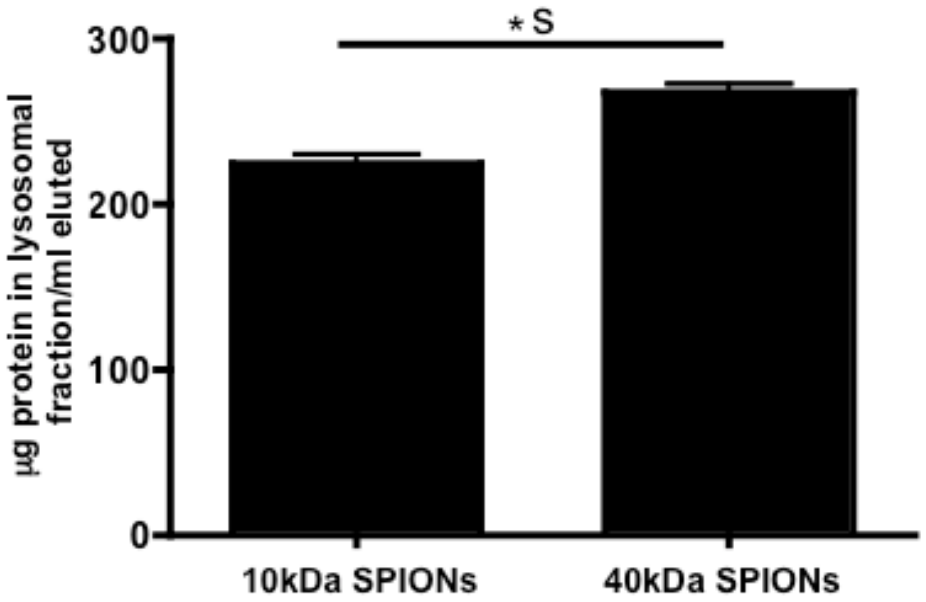

*Figure 4.7: Protein levels detected in the lysosomal fraction following purification from CHO-H1 cells using the 10kDa dextran coated LRL SPIONs compared with the normally used 40kDa dextran LRL SPIONs. Values represent mean ± SD, n=3. S denotes significant. *P<0.05.*

Figure 4.7 displays the yields obtained following lysosomal purification in the lysosomal fraction from a confluent tank of T75 CHO-H1 cells that were treated with the two different dextran sized LRL SPIONs, followed by a 24 hour pulse and a 24 hour chase. There was on average a significantly higher yield obtained using the 40kDa dextran coated LRL SPIONs when compared with the 10kDa LRL SPIONs suggesting that these particles are either not as magnetic or are more unstable (figure 4.7).

4.6.7 Comparison of utilising different centrifugation speeds during the lysosomal purification assay

Each step during the lysosomal purification assay may impact the yield obtained in the eluted lysosomal fraction. It is important to determine the optimum centrifugation speed as the lysosomes that contain the endocytosed SPIONs are now denser and may be pelleted out under faster centrifugation speeds.

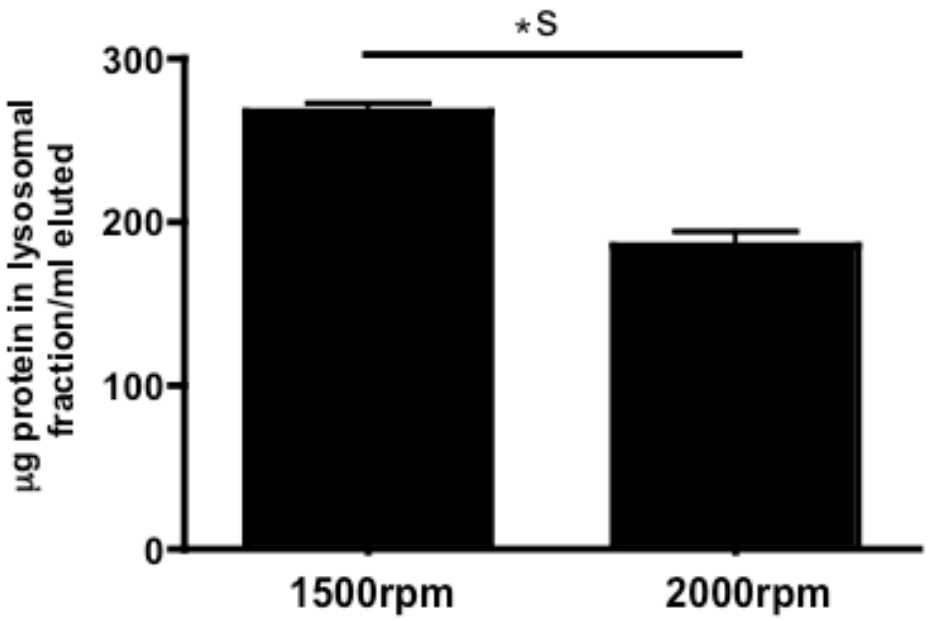

*Figure 4.8: Protein levels detected in the lysosomal fraction following purification from CHO-H1 cells following that involved two different centrifugation speeds during the assay. Values represent mean ± SD, n=3. S denotes significance *P <0.001.*

Figure 4.8 displays the yields obtained following lysosomal purification in the lysosomal fraction from a confluent tank of T75 CHO-H1 cells that underwent a 24 hour pulse followed by a 24 hour chase using LRL

SPIONs where the centrifugation speed was changed during the assay. During the lysosomal purification assay where unbroken cells and nuclei are pelleted via centrifugation, a greater centrifugation speed was administered to determine the effects on yield. There was on average a higher yield obtained when only applying 1500 rpm of centrifugal force when compared with 2000 rpm, which resulted in a significantly lower yield being obtained. This lower yield may be due to lysosomes being pelleted out during the centrifugation step, as they are now denser due to the accumulation of the SPIONs inside them.

4.6.8 Effect of varying homogenisation techniques on lysosomal purification from CHO-H1 cells

For optimum yields in the lysosomal fraction, effective homogenisation of cells during the lysosomal purification assay is essential. By utilising correct homogenisation techniques during the lysosomal purification assay should result in a greater lysosomal fraction yield.

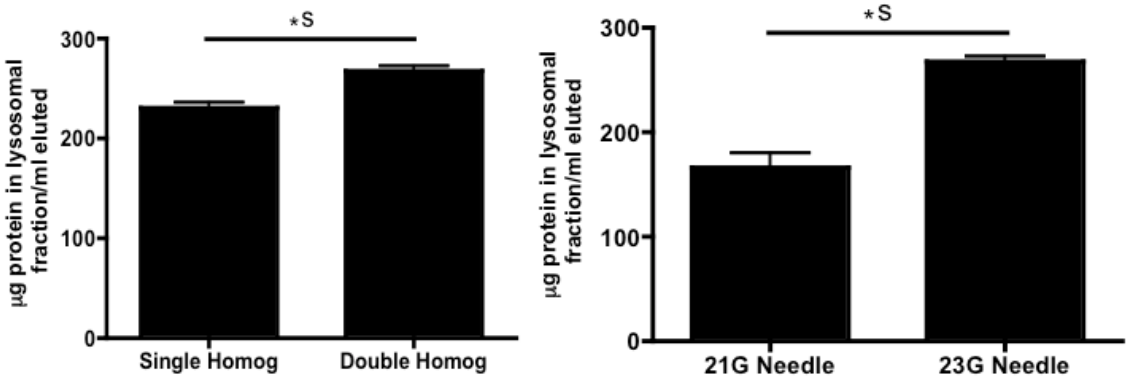

*Fig. 4.9: Graph displaying the importance on the use of suitable homogenisation techniques during the lysosomal purification assay. Values represent mean ± SD, n=3. S denotes significance *P <0.001.*

One confluent T75 tank of CHO-H1 cells were scraped into the hypotonic buffer A and subsequently homogenised. The broken cell suspension was either homogenised once (Single Homog), centrifuged and the supernatant passed over the column or the nuclear pellet from the previous step was resuspended, homogenized once more (Double Homog) centrifuged again and the second supernatant also passed over the column. Further to the Dounce homogenisation, some samples were also passed through either a 21 gauge (G) needle or a 23 G needle as indicated. Addition of the needle homogenisation step dramatically improves the yield in the lysosomal fraction by 100% (data not shown), the greatest yield is obtained following re-homogenisation of the nuclear pellet as well as constricted passage through a 23G needle (200% increase when compared to no needle) (figure 4.9).

4.6.9 The potential to re-use LS columns

The LS columns are only produced by Miltenyi and are one of the most expensive components of the lysosomal purification assay. LS columns were re-used to determine if this had an affect on the protein yield obtained in the lysosomal fraction.

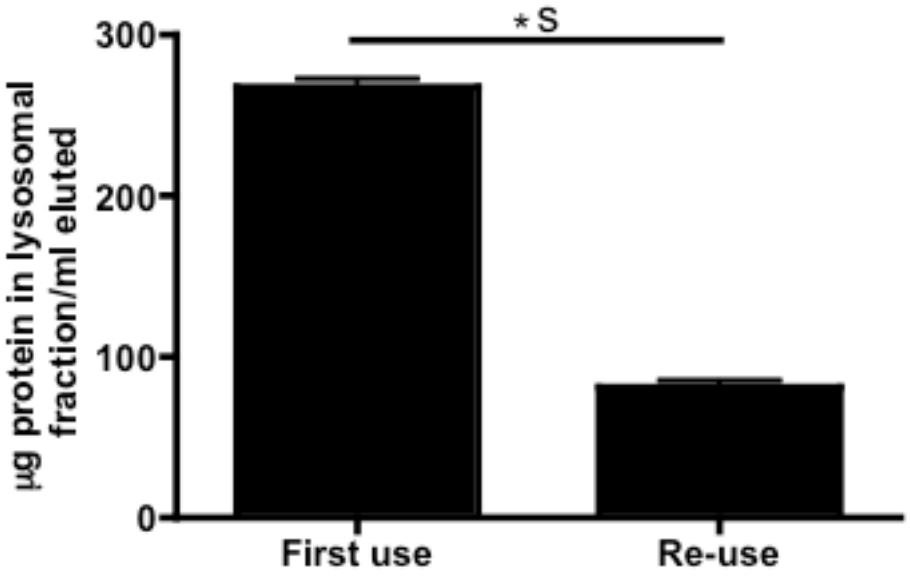

*Figure 4.10: Protein levels detected in the lysosomal fraction following purification from CHO-H1 cells with the use of a new LS column (first use) and a column that has been washed using detergents and then re-used. Values represent mean ± SD, n=3. S denotes significance *P <0.001.*

Graph displays the yields obtained following lysosomal purification in the lysosomal fraction from a confluent tank of T75 CHO-H1 cells that underwent a 24 hour pulse followed by a 24 hour chase using LRL SPIONs. As part of the assay the organelles that are not pelleted down in the centrifugation step are passed over an LS column that is attached to a two-tesla magnet. Magnetised lysosomes will stick to the column while

other organelles will pass straight through. There was a significantly higher yield in the lysosomal fraction when using a new column than what was obtained re-using an LS column that had been washed using detergents (figure 4.10). This would suggest that the LS columns are not meant to be re-used as they lose their magnetic capabilities.

4.6.10 Utilising the lysosomal purification assay in different cell types

The lysosomal purification assay was utilised on different cell lines to observe the yields obtained in the lysosomal fraction.

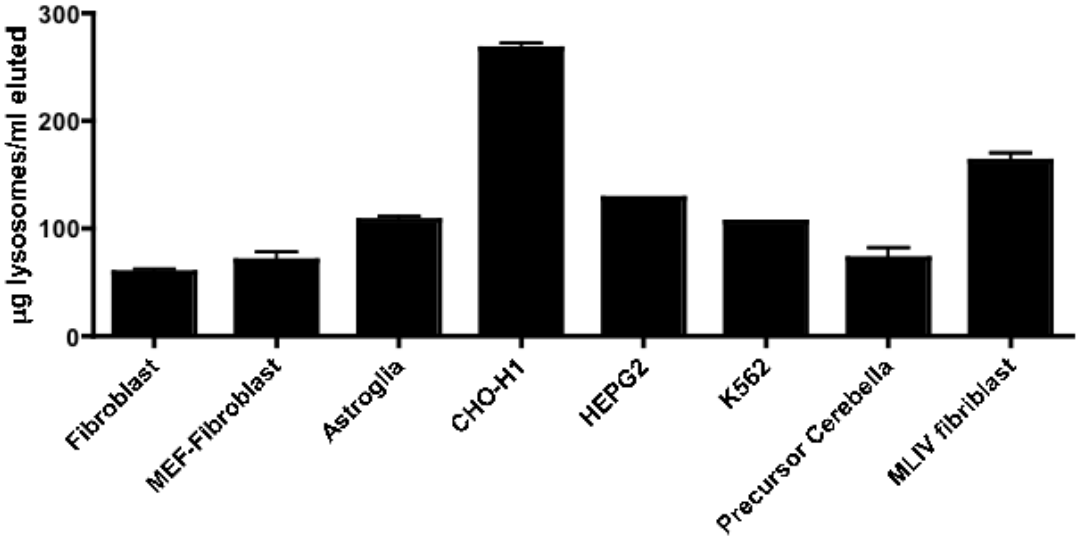

Figure 4.11: Protein levels detected in the lysosomal fraction following purification using the lysosomal purification method in different cell lines. An approximately similar number of cells were treated with LRL SPIONs for a 24 hour pulse followed by a 24 hour chase before being magnetically purified. Values represent mean ± SD.

Graph displays the yields obtained in the lysosomal fraction using different cell types following lysosomal purification on approximately the

same number of cells using LRL nanoparticles (figure 4.11). The cells were treated with a 24 hour pulse of LRL SPIONs followed by a 24 hour chase. The highest yield of protein obtained in the lysosomal fraction is from CHO-H1 cells. This would suggest that the homogenization method used during the lysosomal purification assay is tailored towards homogenizing CHO-H1 cells. A Balch homogeniser would potentially improve the lysosomal fraction yield in the other cell types as it is a much more effective means of homogenising cells.

4.6.11 Addition of sucrose to the lysosomal purification assay

The addition of sucrose to the isotonic buffer B used in the lysosomal purification assay as well as to the DPBS used to elute the material off the LS column was checked to see if this improves the protein yield obtained in the lysosomal fraction.

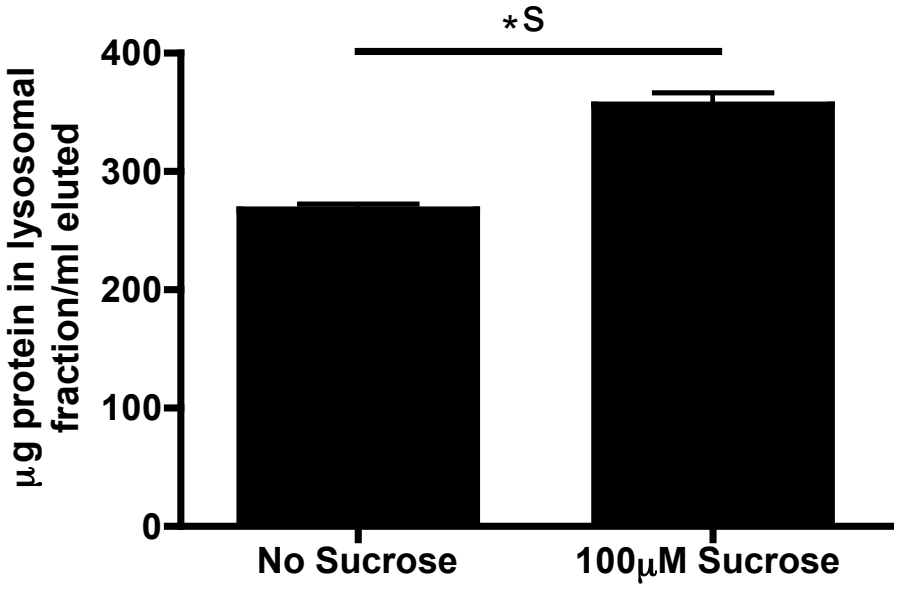

*Figure 4.12: Protein levels detected in the lysosomal fraction following purification from CHO-H1 cells when 100μM of sucrose was added to the lysosomal purification method. Values represent mean ± SD, n=3. S denotes significance *P <0.001.*

Graph displays the yields obtained following lysosomal purification in the lysosomal fraction from a confluent tank of T75 CHO-H1 cells that underwent a 24 hour pulse and a 24 hour chase using LRL SPIONs in the presence or absence of sucrose added to the isotonic buffer B used during the assay. 100μM of sucrose was added to Buffer B used in the lysosomal purification assay, as well as the lysosomes now being eluted in 100μM of sucrose in PBS. The results from adding sucrose to the method have resulted in a significant increase in the protein levels detected in the lysosomal fraction (figure 4.12), suggesting that sucrose may aid in helping maintain lysosomal integrity when they are magnetically attached to the column during the assay.

4.6.12 β-Hexosaminidase activity measured in each fraction obtained from the lysosomal purification assay

The activity of the lysosomal enzyme β-Hexosaminidase was tested in each of the fractions obtained during the different steps in the lysosomal purification assay. This was done to determine that the lysosomes were primarily retained on the LS column during the entire assay until they are eluted off.

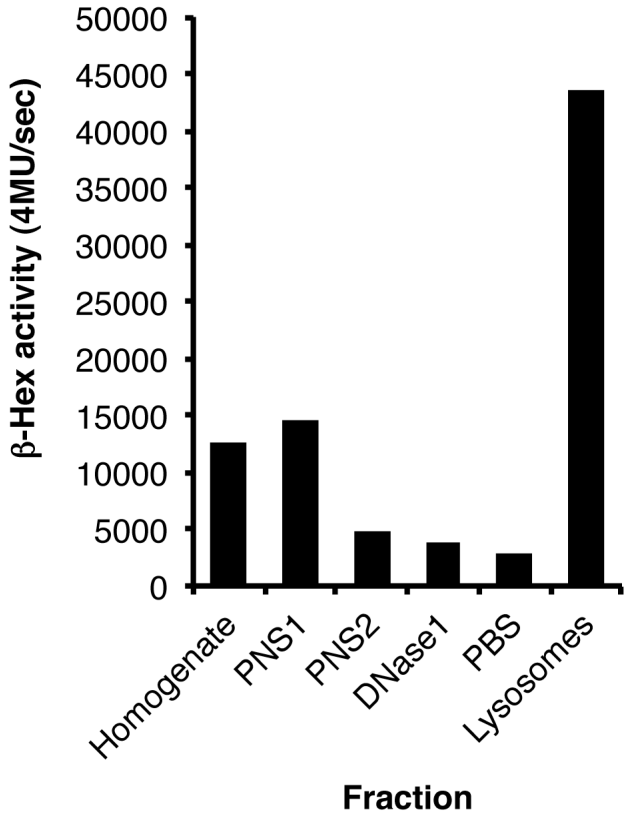

Fig. 4.13: β-hexosaminidase assay was used to detect for the presence of the lysosomal enzyme β-hexosaminidase from the different fractions obtained from the different steps in the lysosomal purification assay. n=1.

β-Hexosaminidase (β-Hex) enzyme activity in a 10μl aliquot taken from each fraction was measured using the 4-Methylumbelliferyl-N-acetyl-beta-D-glucosaminide substrate in a pH 5 sodium acetate buffer. As can be seen, some activity remains in the homogenate (this varies depending on the quality of the homogenization). The residual activity in the post-nuclear supernatant (PNS1) is reduced following re-homogenisation, centrifugation and application of the supernatant over the column (collected fraction is PNS2), indicating that some of the lysosomes do not bind to the column on first application, probably as a result of bulk flow. Lysosomes are not being sheared by the magnetic field induced by proximity to the 2 Tesla magnet as only a similar background level of β-Hexosaminidase activity can be seen in the PNS2 flow-through, the DNase wash flow through and the PBS wash flow through. If the lysosomes were succumbing to the shear forces of the magnetization protocol we would expect to see much higher β-Hexosaminidase activity in these fractions, instead we observe that most of the activity is eluted once removed from the magnet, in the lysosomal fraction (figure 4.13).

4.6.13 β–Hexosaminidase as an enzyme marker used to detect the presence of lysosomes

β- Hexosaminidase was used as an enzyme marker to determine if there is an enrichment of lysosomes in the PNS and lysosome fraction.

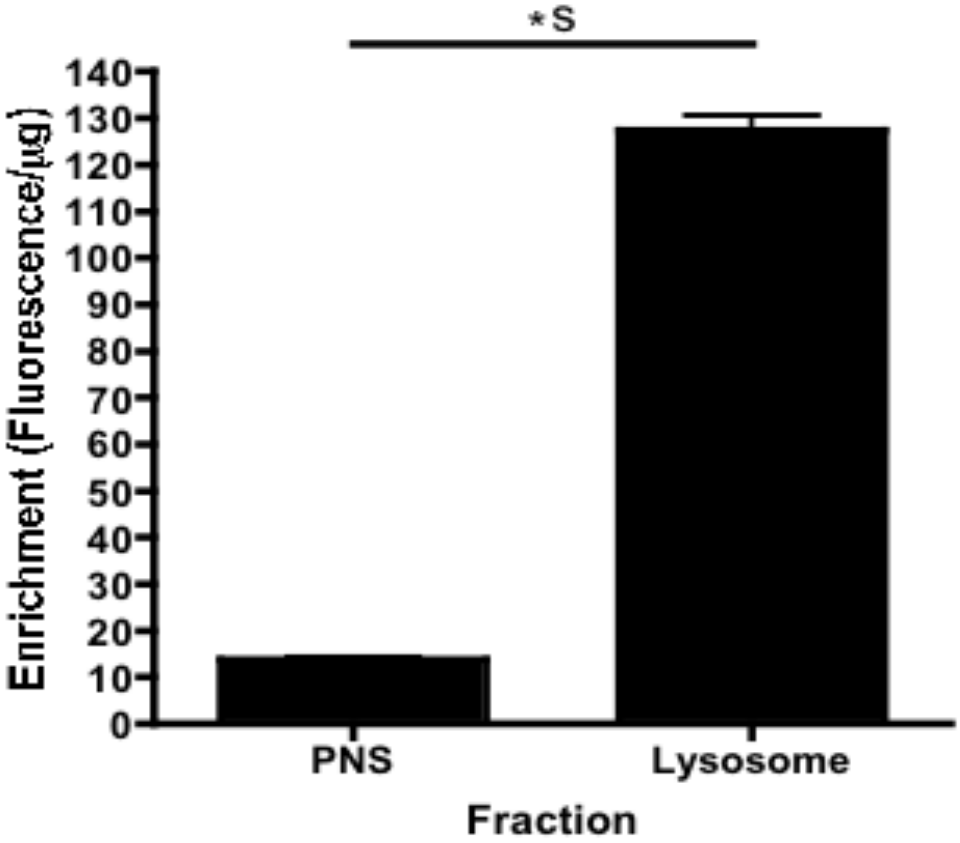

*Figure 4.14: β-Hexosaminidase enrichment (Fluorescence/mg) in the lysosomal fraction compared with the PNS fraction for use as a lysosome marker. Values represent mean ± SD, n=3. S denotes significance *P <0.001.*

The data shows that there is a significantly greater amount of beta-hexosaminidase activity present in the lysosomal fraction when compared with the PNS fraction (figure 4.14). This shows that there is a much greater enrichment of the lysosomal enzyme beta-hexosaminidase in the lysosomal fraction.

4.6.14 α-Mannosidase as a marker for the Golgi apparatus

An α- Mannosidase enzyme assay was used as a marker for the presence of the Golgi apparatus in the PNS and lysosome fraction of cells that were treated with LRL SPIONs.

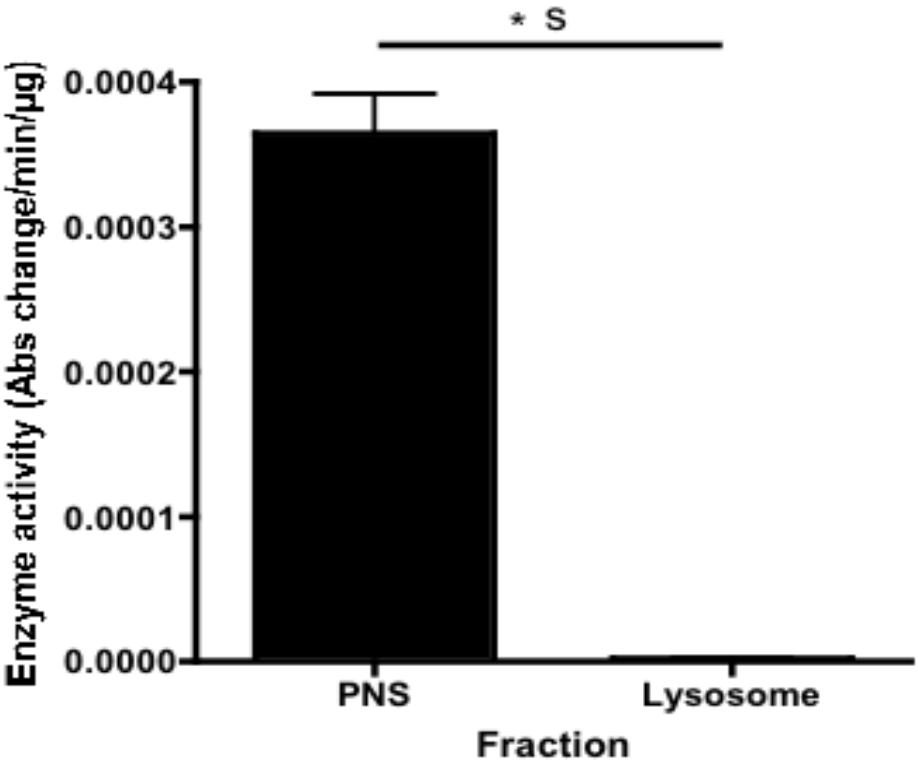

*Figure 4.15: Enzyme activity of α-Mannosidase (Abs change/min/μg) in the PNS fraction compared with the lysosomal fraction. Values represent mean ± SD, n=3. S denotes Significant *P <0.001.*

As shown in figure 4.15, α-Mannosidase activity is significantly higher in the PNS fraction compared with little to no activity detected in the lysosome fraction (figure 4.14). This would suggest that the purified lysosomal fraction was free of contamination of the Golgi apparatus.

4.6.15 Alkaline phosphatase as a marker for the presence of the plasma membrane

The Alkaline Phosphatase enzyme was used as a marker for the presence of the Plasma membrane in both the PNS and lysosome fractions of cells treated with LRL SPIONs.

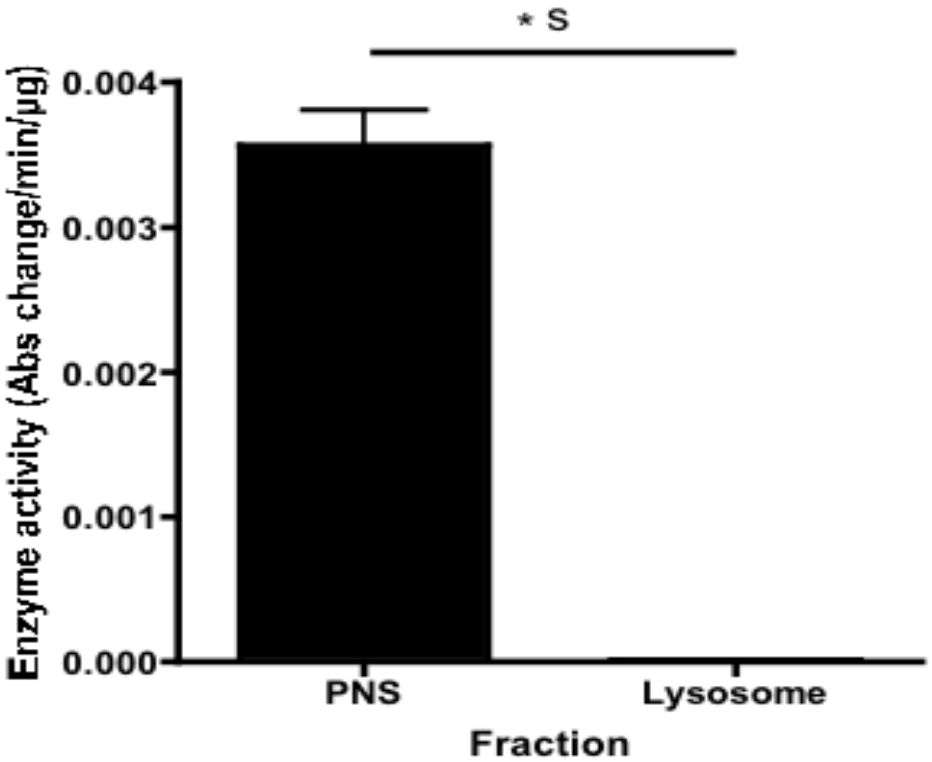

*Figure 4.16: Enzyme activity of Alkaline phosphatase (Abs change/min/μg) in the PNS fraction compared with the lysosomal fraction. Values represent mean ± SD, n=3. *P <0.001, S denotes Significant.*

As shown in figure 4.16, alkaline phosphatase enzyme activity was significantly greater in the PNS fraction and only a negligible level of activity was observed in the lysosomal fraction (figure 4.15). This would indicate that the lysosomal fraction is free from plasma membrane contamination.

4.6.16 β-Glucuronidase as a marker for the presence of the ER

β-Glucuronidase was used as a marker for the presence of the endoplasmic reticulum (ER) in the PNS and lysosomal fraction of cells treated with LRL SPIONs.

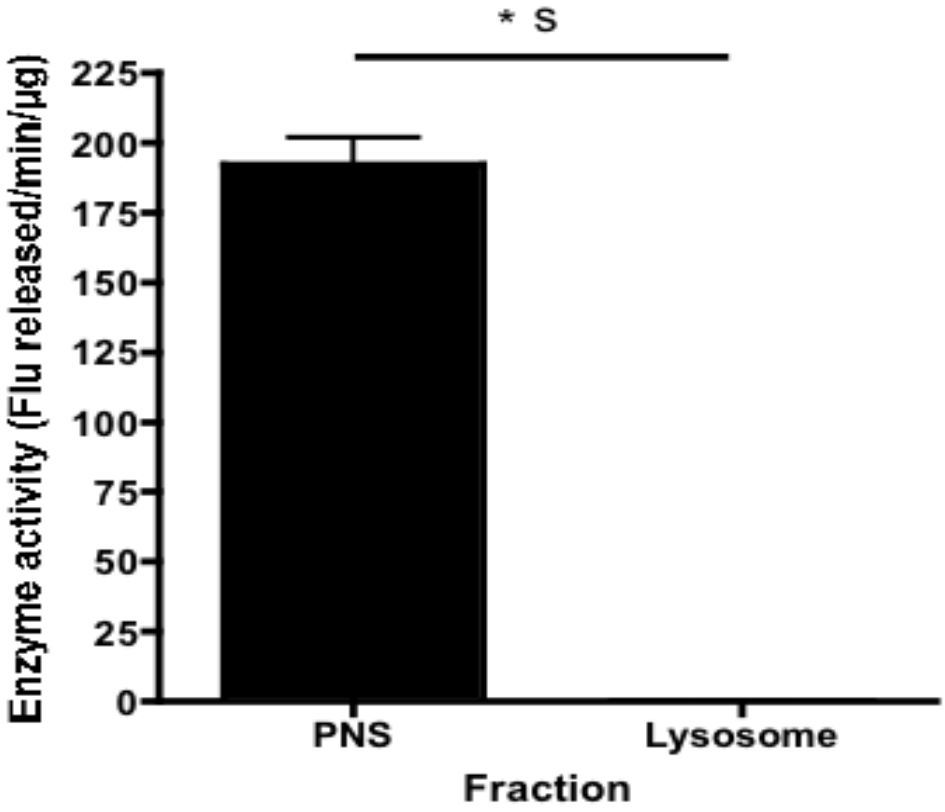

*Figure. 4.17: Enzyme activity of β-Glucuronidase (Flu released/min/µg) in the PNS fraction compared with the lysosomal fraction. Values represent mean ± SD, n=3. S denotes Significant. *P <0.001.*

There was a significantly greater amount of β-Glucuronidase activity in the PNS but no activity was detected in the lysosomal fraction (figure 4.17). This suggests that the lysosomal fraction is free from ER contamination.

4.6.17 MTS assay used to detect the presence of mitochondria

A MTS assay was used as a marker for the presence of mitochondria in cells that were treated with LRL SPIONs.

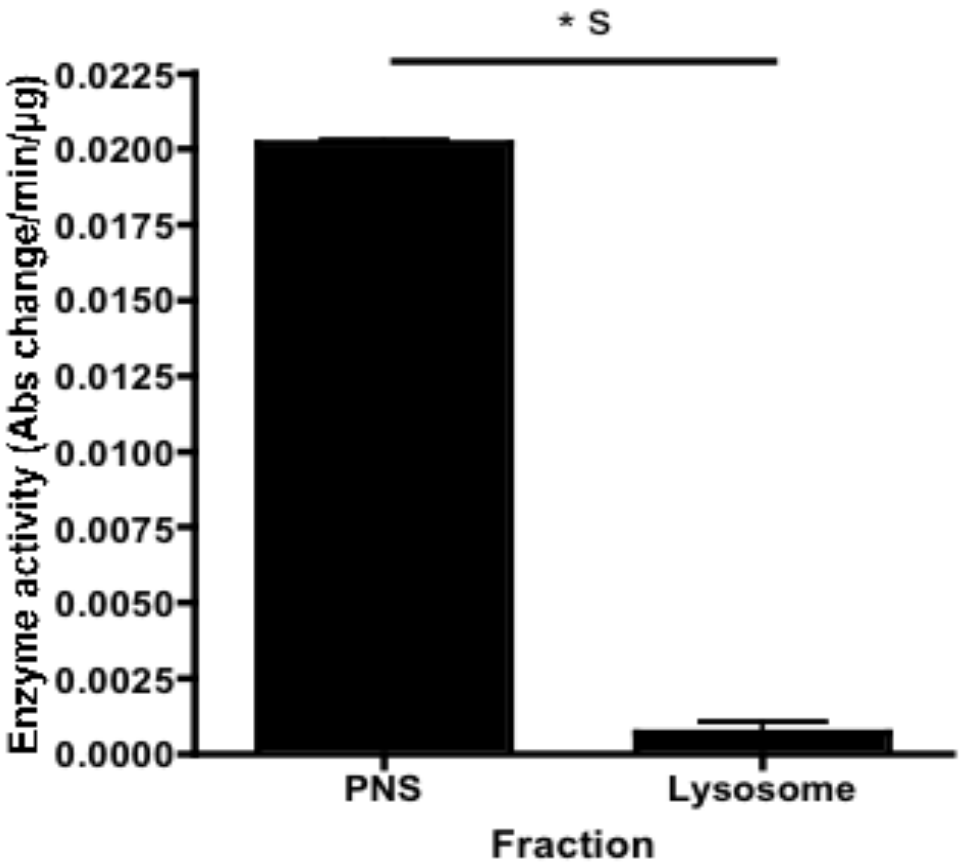

*Figure 4.18: Enzyme activity of PMS (Abs change/min/μg) in the PNS fraction compared with the lysosomal fraction for use as a mitochondria marker. Values represent mean ± SD, n=3. S denotes Significant. *P <0.001.*

As shown in figure 4.18, a significantly greater level (~20X greater) of MTS enzyme activity was detected in the PNS fraction than what was detected in the lysosomal fraction. This data suggests that there is only a small amount of mitochondrial contamination present in the lysosomal

fraction. This may be due to the mitochondria often undergoing autophagy inside the lysosome.

4.6.18 Western blots performed on the lysosomal fraction to determine purity

Lysosomal purity was determined by checking for the presence of other organelles via western blotting techniques.

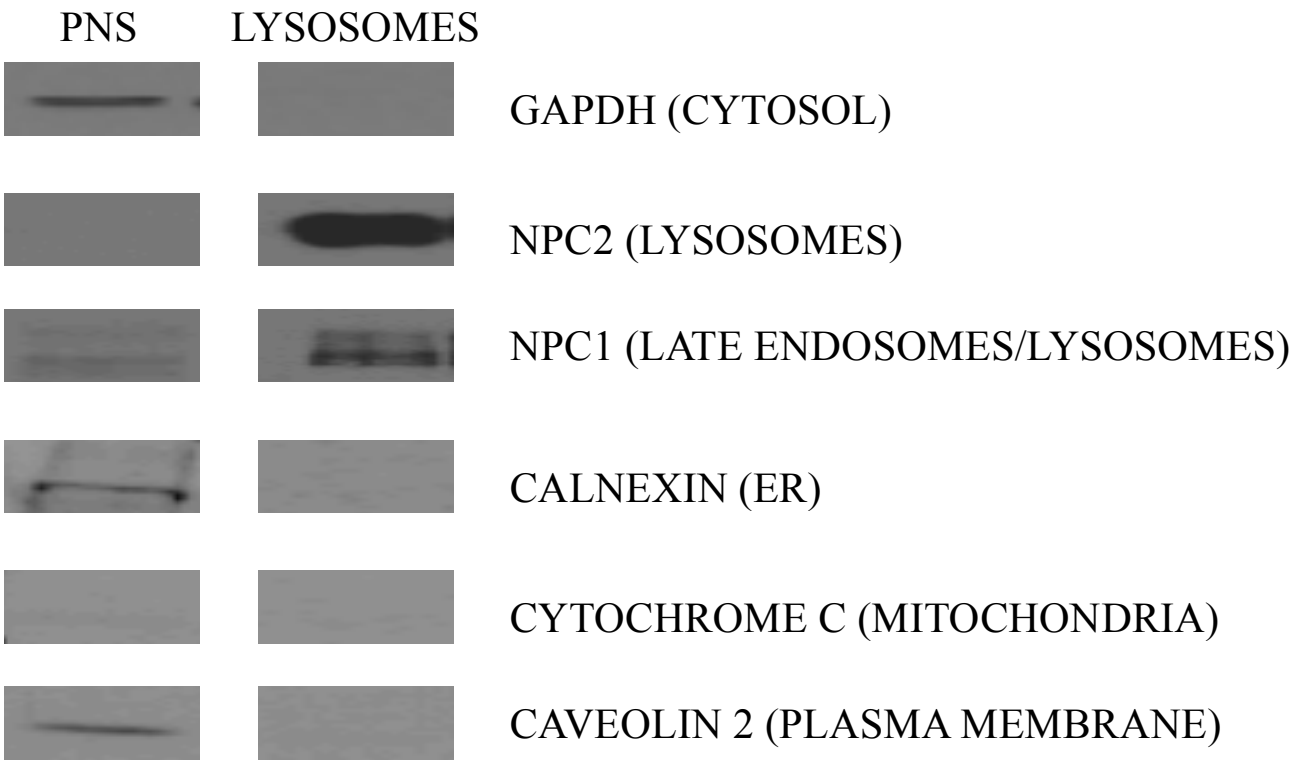

Figure 4.19: Presence of different organelles in the lysosomal fraction determined via western blotting. Different antibodies were used to determine for the presence of different organelles found in the cell. n=3.

5μg of the lysosomal fraction (from CHO-H1 cells) protein and PNS fraction protein were analysed using western blotting techniques to detect for the presence of specific organelles using corresponding antibodies (figure 4.19). The magnetically purified lysosomal fraction exhibited a large enrichment of lysosomal proteins NPC1 and NPC2, while being largely free from contamination from other organelles, with the exception of caveolin 2. There were small levels of this marker detected in the lysosomal fraction, possibly due to its presence in the late endosome during caveolin-mediated endocytosis.

4.6.19 Comparison of the lysosomal fraction yield obtained from CHO-H1 and CHO M12 cells

The lysosomal purification was utilised on NPC1 null CHO M12 cells treated with LRL SPIONs to determine it can be used in NPC1 null cells to potentially purify lysosomes.

CHO-H1 and CHO M12 cells were pulsed with LRL SPIONs for 24 hours followed by a 24 hour chase. After the lysosomes were magnetically purified and the lysosomal yield determined (figure 4.20). There is a significantly greater amount of lysosomal yield obtained from CHO-H1 cells when compared with CHO M12 cells. This is likely due to the retarded trafficking present in NPC cells so the LRL SPIONs have not reached the lysosome yet.

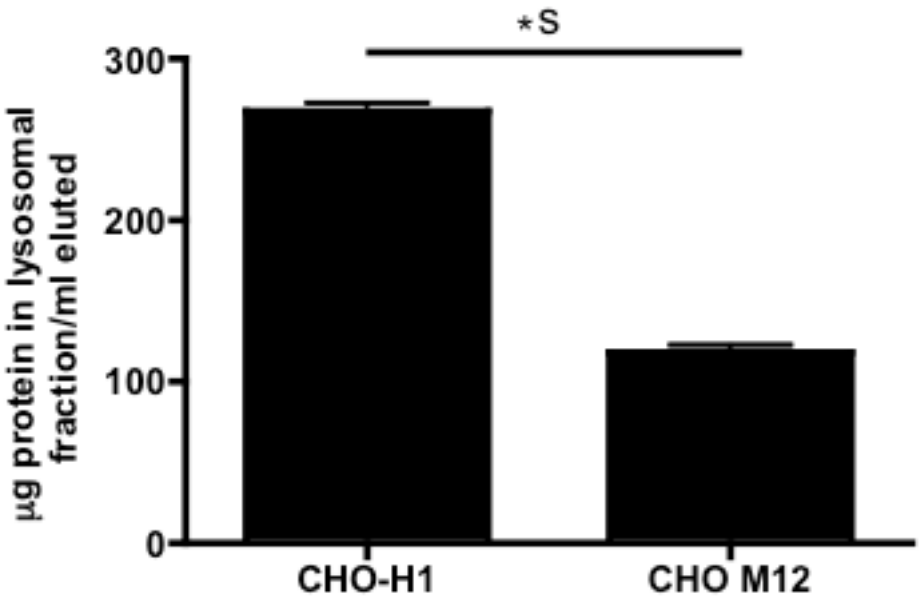

*Figure 4.20: Protein levels detected in the lysosomal fraction purified from CHO-H1 and CHO M12 treated with LRL SPIONs following a 24hr pulse and a 24hr chase. n=3. S denotes significant, *P<0.001.*

4.6.20 Comparison of the lysosomal fraction yield obtained from CHO M12 cells over two different chase times

Two different chase times were tested in CHO M12 cells to determine the optimum chase time for this cell type. As studies have shown before that NPC1 null cells have retarded endocytic trafficking so a longer chase time would result in a greater protein yield in the lysosomal fraction.

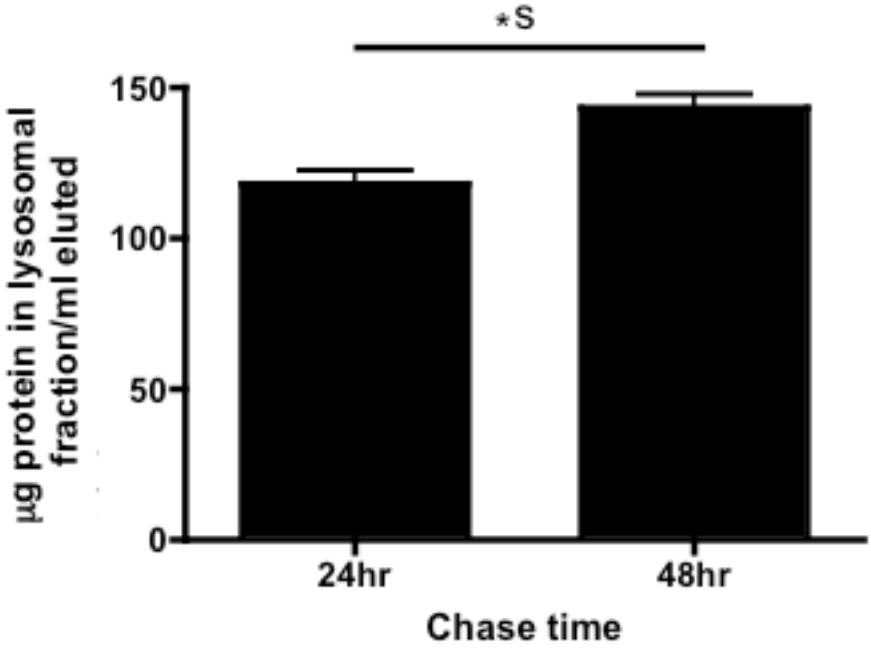

*Figure 4.21: Protein content of purified CHO M12 lysosomes treated with LRL SPIONs following a 24 hour pulse and either a 24 hour or 48 hour chase. n=3. S denotes significant, *P<0.05.*

Data shows that a yield of ~120µg per ml of lysosomes was obtained from CHO M12 cells following a 24 hour pulse and 24 hour chase. The yield of lysosomes obtained significantly increased however following a longer chase time to about ~140µg per ml (figure 4.21). This is most likely due to the SPIONs having more time to reach the lysosome after a longer chase time due to the retarded endocytic trafficking that is present in NPC null CHO M12 cells. However the yield obtained from a 48 hour chase in CHO M12 cells is still lower than what is obtained from CHO-H1 cells that had a shorter pulse. This possibly suggests that there is an uptake problem present in the CHO M12 cells where not as much of the LRL SPIONs is taken into the cell, or that a lot that is taken up is recycled back out of the cell.

4.6.21 Functional assays performed with purified CHO-H1 and CHO M12 lysosomes to measure the levels of Ca^{2+} uptake and pH re-acidification

Lysosomes were purified from CHO-H1 and CHO M12 cells (as described in chapter 2 material and methods). Fluo-4 was used as a probe to detect the levels of Ca^{2+} uptake into the purified lysosomes. This was done to show that the lysosomes in the lysosomal fraction were still intact following magnetic purification and could uptake and maintain its Ca^{2+} content. The ACMA assay was also use to show that the lysosomes could re-acidify following purification.

Once the ATP-regenerating system was added there was a higher level of Ca^{2+} uptake observed in the CHO-H1 lysosomes when compared with the CHO M12 lysosomes (figure 4.22 (A)). NAADP was added to induce Ca^{2+} release from the purified lysosomes via the TPC channels. A greater NAADP release was observed in the CHO-H1 lysosomes when compared with CHO M12 lysosomes. This strongly suggests that NAADP acts on a Ca^{2+} release channel, TPC2, on the lysosomal membrane. The further addition of the lysosomotrophic agent GPN caused further Ca^{2+} release from CHO-H1 lysosomes, but not CHO M12 lysosomes. This suggests that CHO-H1 lysosomes possess a higher Ca^{2+} content than CHO M12 lysosomes. It has been shown that NPC1 null cells possess lower lysosomal Ca^{2+} levels. The addition of C2-ceramide caused pores

to form in the lysosomal membrane, releasing the remaining Ca^{2+} content.

The rate of lysosomal re-acidification was determined (figure 4.22 (B)) using the pH sensitive ACMA probe. After the addition of the ATP regenerating system the rate of re-acidification was the same in both sets of lysosomes, indiciating there is no pH defect in CHO M12 cells. Figure 4.22 (C) shows that there was no significant difference in the rate of re-acidification in CHO-H1 and CHO M12 lysosomes.

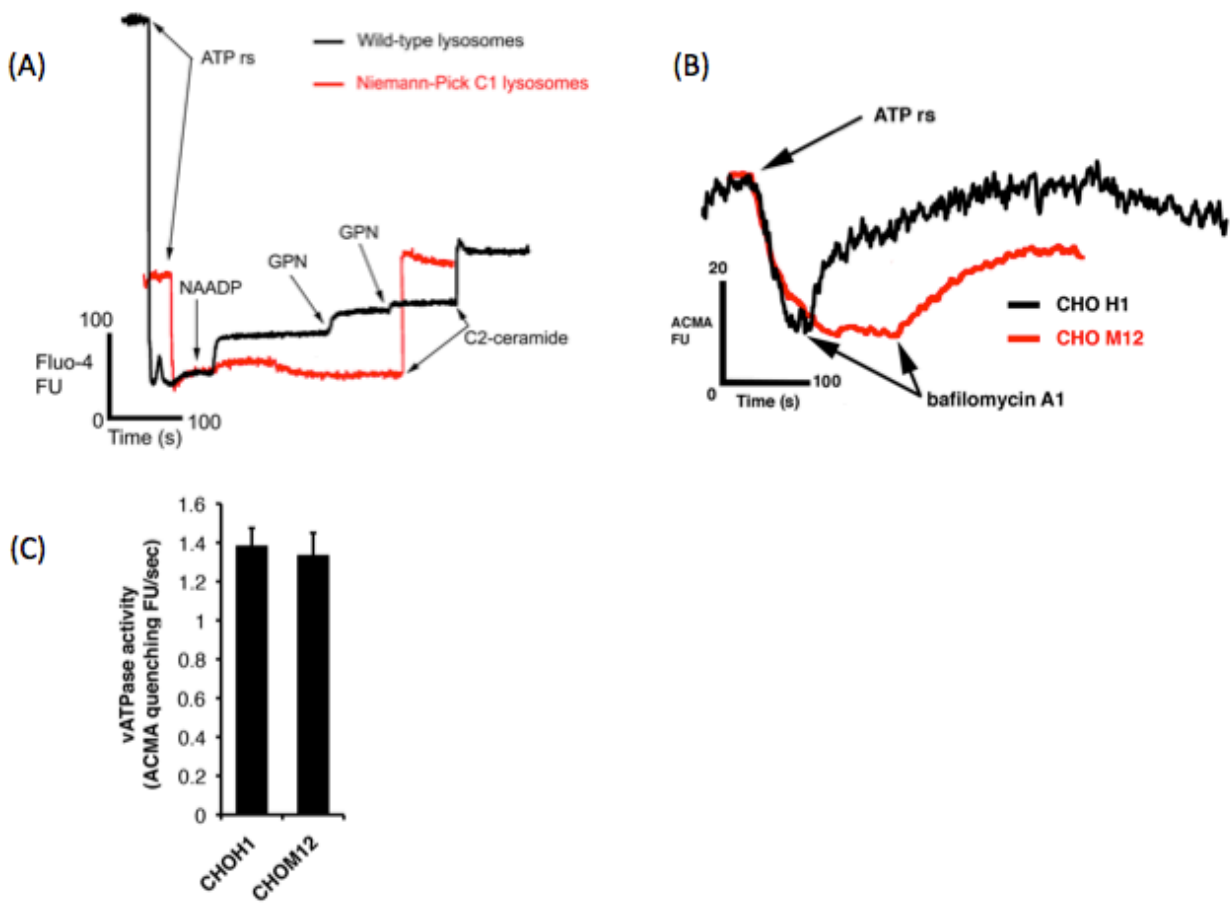

Figure 4.22 (A) *The rate of Ca^{2+} uptake was measured in both CHO-H1 and CHO M12 lysosomes to detect any Ca^{2+} uptake defects. (B) rate of re-acidification on purified lysosomes was observed. (C) quantified levels of re-acidification in CHO-H1 and CHO M12 lysosomes shows no significant difference in the rate of re-acidification. n=3*

4.7 Discussion

One of the main aims of this PhD was to develop a fast and effective way to purify lysosomes from cells where there is little contamination from other organelles as well as the lysosome still being functional. The benefit of this assay is that it is faster than more established techniques (e.g. Density gradient centrifugation) and produces a higher yield of lysosomes.

One of the key materials needed for the lysosomal purification assay is the highly magnetic superparamagnetic nanoparticles (SPIONs) that are provided by Liquids Research Ltd (LRL). The LRL SPIONs possess a greater magnetic potential than that of other magnetic nanoparticles used in previous studies that attempted to purify lysosomes via the use of magnetic purification (Chen et al., 2005, Diettrich et al., 1998, Duvvuri and Krise, 2005).

4.7.1 Importance of determining appropriate pulse/chase times

There are important factors to consider with the use of SPIONs to purify lysosomes. As mentioned before (chapter 1 introduction) the endocytic system is composed of different endocytic vesicles, with the cargoes in these vesicles present for a determinate amount of time before they are trafficked to their correct cellular location. However it is important to note that trafficking of endocytosed materials as well as the rate at which cells endocytose material from the extracellular medium, do vary between

different cell types. As a result of this it is imperative that an appropriate pulse/chase time needs to be determined when utilizing magnetic lysosomal purification in different cell types. As shown in (figure 4.2), the utilisation of magnetic fluorescent SPIONs, provided by Liquids Research Ltd, to monitor the uptake and their subsequent trafficking through the endocytic system to the lysosome. In healthy cells such as CHO-H1 we found that a 24 hour pulse and 24 hour chase was an optimal time for the SPIONs to reach the late endosomal/lysosomal vesicles (figure 4.2). This was also supported in the lysosomal fraction yields acquired as shorter chase times than 24 hour (following a 24 hour pulse) resulted in a lower lysosomal fraction yield obtained while longer chase times than 24 hour resulted in a steady decrease in yield (possibly due to the particles staring to become unstable). A longer pulse of 36 hour (followed by a 24 hour chase) also did not improve the yield and in fact resulted in a lower lysosomal fraction yield obtained (figure 4.6), which suggests that a 24 hour pulse is adequate time for CHO-H1 cells to take up a sufficient amount of SPIONs so the lysosomes can be purified. However when a 24 hour pulse and 24 hour chase is applied to NPC1 null CHO M12 cells treated with fluorescent LRL SPIONs there was little presence of these SPIONs in the late-endosome/lysosome vesicles, however the SPIONs were detected in the lysosomes following a longer chase time (figure 4.1). This explains why there is a lower lysosomal fraction yield obtained from SPION treated CHO M12 cells when there is a shorter chase time, however the yield does increase following a longer chase time (figure 4.21). The need for an increase in chase times is indicative of slower

endocytic trafficking which has been characterized before in NPC1 deficient cells. Also it has been published before that there is an endocytic uptake problem in NPC1 deficient cells, as defects in AnnexinA2 localisation result in many endocytosed molecules to be trafficked back out the cell (te Vruchte et al., 2004). This could explain why despite a longer chase time the lysosomal fraction yield obtained from CHO M12 cells is still lower than that obtained from CHO-H1 cells (figure 4.20). A longer pulse time with the SPIONs might be necessary when trying to purify lysosomes from CHO M12 cells, so as to give additional time for these cells to take up a greater amount of SPIONs.

4.7.2 Sourcing the correct magnetic nanoparticles to use for the lysosomal magnetic purification assay

Determining the correct type of iron as the SPION core is important, as it has been shown before that maghemite has lower magnetic capabilities when compared with magnetite (Chourpa et al., 2005). This was evident when lysosomes purified with maghemite based SPIONs resulted in a lower lysosomal fraction yield when compared with the lysosomal fraction yield from magnetite SPIONs (figure 4.4). Magnetite based SPIONs produced by Chemicell and LRL were utilised to purify lysosomes to highlight that even though different magnetite based SPIONs hold magnetic capabilities, they do not necessary produce similar yields. The lysosomal fraction yield over two different time points using magnetite based SPIONs resulted in a higher yield of lysosomes from the LRL

produced SPIONs when compared with the Chemicell produced ones (figure 4.4). This highlights the need to determine the most magnetic SPIONs to obtain the highest lysosomal fraction yield possible. Dextrans coated with an Iron oxide coat (FeO), which are similar in properties to what was used in previous studies to purify lysosomes (Diettrich et al., 1998), were also used to attempt to purify lysosomes. However this resulted in a poor yield in the lysosomal fraction, most likely due to the poor magnetic properties of these particles and the toxic effect it induces in the cells caused by their instability (as shown in results chapter 3). In the case with the Chemicell SPIONs it is most likely a combination of a less magnetic magnetite core and that the SPIONs become increasingly less stable the longer they are present in the lysosome that results in a lower lysosomal fraction yield obtained when compared with the LRL magnetite based SPIONs.

As mentioned previously (Results in chapter 3) the LRL SPIONs that were coated with a 10kDa dextran as opposed to a 40kDa dextran appeared to result in a marginal increase in cellular toxicity after a 24 hour pulse and 24 hour chase. This is most likely the reason why a lower lysosomal fraction yield is obtained when using the 10kDa LRL SPIONs as opposed to the 40kDa LRL SPIONs (figure 4.7), as the particles are still highly magnetic but they are potentially damaging the lysosomes resulting in less lysosomes being able to remain on the column during the magnetic purification assay.

4.7.3 Importance of the magnetic properties of LRL SPIONs once they enter a magnetic field

The hydrodynamic core of the 40kDa LRL SPION is 45nm in size, therefore they magnetize at a rapid rate as they possess fewer domains needed to reach full magnetization. However the SPIONs ability to remain in fluid phase is important as once they are in lysosomes and pass through the magnetic field during the purification assay they will be immobilized in the magnetic field. If the SPIONs were to go out of their fluid phase when they pass through a magnetic field they would solidify and form spicules, which would ultimately sheer the lysosome apart from the inside. A β-hexosaminidase assay was performed on all the fractions produced during the purification assay to measure for the presence of the lysosomal enzyme β-hexosaminidase. If the activity of this enzyme was high in the wash steps applied to the lysosomes attached to the column it would indicate that the lysosomes are structurally damaged and leaking enzymes out. The results showed that this was not the case as the majority of the enzyme activity was in the lysosomal fraction and not in the other fractions as it would be if the lysosomes were badly damaged and leaking out (figure 4.14).

4.7.4 Important homogenisation steps during the lysosomal purification assay to get the best yield

One of the biggest effects there was on the lysosomal fraction yield obtained via magnetic purification using LRL SPIONs is from the efficiency of homogenization during the purification assay. Correct homogenization is important as it is necessary for the lysosomes containing the SPIONs to be released from whole cells, other wise they would just get spun down during the centrifugation step. The addition of hypotonic and isotonic buffers used in the *Krise et al* study on magnetically purifying lysosomes helped increase the yields obtained (Duvvuri and Krise, 2005). But other homogenization steps are required for a greater yield of lysosomes to be acquired. The greatest increase in lysosomal fraction yield was via the addition of passing the cellular homogenate through a 23G needle after homogenizing with a Dounce homogenizer. The constriction force applied to the cells helps break more cells open (figure 4.9). However it was interesting to note that when a 21G needle was used instead it resulted in a lower lysosomal fraction yield (figure 4.9). This is possibly due to less constrictive force being applied to the cell homogenate to break open the cells as a 21G needle possesses a wider needle shaft. By re-suspending the nuclear pellet and unbroken cells that are pelleted down and repeating the homogenisation steps before again centrifuging and passing the supernatant through the column there is an increase in the lysosomal fraction yield (figure 4.9). This is due to more cells getting the chance to be broken up due to the

repeat homogenization steps so more lysosomes are released that can then be passed of the column.

Another variable that was found to be important during the lysosomal purification assay was the speed at which the unbroken cells and nucleic material is centrifugated down during the assay. This centrifugation step results in the organelles from the homogenized cell to be in the supernatant so that they can be passed over the LS column. By increasing the centrifugation speed during this step it results in a lower yield obtained in the lysosomal fraction (figure 4.8). This would possibly indicate that once the lysosomes have taken up the magnetic nanoparticles they are more susceptible to being pelleted out as they are now much more dense due to the accumulation of SPIONs inside them.

The results found from testing different homogenization steps and centrifugation speeds have helped highlight the need for the use of correct homogenization technique and centrifugation speeds to get the optimal lysosomal yield possible.

4.7.5 LS columns

The Miltenyi LS columns are one of the most expensive components of the lysosomal purification assay. The columns are provided exclusively from Miltenyi and are composed of tightly packed iron filings. While it states that the columns are one use only their re-usability was tested. A LS column that had just had lysosomes magnetically purified eluted off it was immediately washed multiple times with a mild detergent to remove

any lingering proteins that may still be on the column. The detergent was then removed with multiple washes with water, then left to dry following an ethanol wash. When the columns were then tested to see if they could be re-used it resulted in a significantly lower yield obtained (figure 4.10). It is still unclear why a lower lysosomal fraction yield is obtained due to the re-use of LS columns. The iron fillings may have oxidised when the column is washed multiple times, affecting the lysosomes ability to bind to it when they are passing through it during the lysosomal purification assay.

4.7.6 Determining what is the best cell type to use

As it was determined that the 40kDa LRL SPIONs were the best particles for magnetically purifying lysosomes in CHO-H1 and CHO M12 cells we wanted to show that these particles could be used for purifying lysosomes from other cell types. It was found that CHO-H1 cells produced the highest yield of lysosomes from the use of magnetic purification (figure 4.11). While the lysosomal numbers are not necessarily lower in the cell types that produced a lower yield in the lysosomal fraction (e.g. fibroblasts) it is most likely that the homogenization technique used in the assay is not sufficient in certain cell types to break open cells. The yields however could be improved by utilizing a Balch homogenizer during the homogenization steps to help break open “tougher” cells. This machine utilizes small ball bearings that passes the cell homogenate over these ball bearings in a constricted chamber to further increase yields (Manunta

et al., 2007). This additional homogenization step may be necessary for gaining higher yields of purified lysosomes in certain cell types.

4.7.7 Purity of purified lysosomes

The purified lysosomes from CHO-H1 cells were tested for the presence of other cellular organelles via the use of enzyme assays (figures 4.14-18) as well as antibodies via western blots (figure 4.19). As shown the lysosomes are highly pure from the presence of other organelle markers, and are enriched with the lysosomal protein markers NPC1 and NPC2. There was some caveolin 2 (the plasma membrane marker) present in the lysosomal elution. This however is possibly due to caveolin 2 being present in late endosomes when it is internalised with its cargo (Rodriguez et al., 2007). <5% mitochondria enzyme activity was observed in the lysosomal elution when a mitochondria enzyme assay was done on it (figure 4.18). This low level contamination most likely is due to mitochondria frequently being cleared to the lysosome via autophagy for degradation and the recycling of their components.

4.7.8 Addition of sucrose to the lysosomal purification assay

While the lysosomal purification assay is much faster than that of current established lysosomal purification techniques (~1 hour as opposed to >16 hour) the lysosomes are still magnetically bound to the LS column for a short amount of time. 100μM Sucrose was added to the isotonic buffer B

as it has been shown before that sucrose helps maintain lysosomal membrane integrity. The lysosomes are also eluted into PBS containing 100μM sucrose as this would be of benefit for functional assays to be performed on the purified lysosomes. The addition of 100μM sucrose to the lysosomal purification assay has improved the yield seen in the lysosomal fraction (figure 4.13). This would suggest that the addition of sucrose helps maintain lysosomal structure, and also stops lysosomes from bursting too soon before they are eluted off the column.

4.7.9 Functional Ca^{2+} uptake and re-acidification of purified lysosomes from CHO-H1 and CHO M12 cells

By using the magnetic lysosomal purification assay to purify lysosomes from CHO-H1 cells and NPC1 null CHO M12 cells we were able to perform functional assays on them (figure 4.22). We were able to determine there is a Ca^{2+} uptake problem in CHO M12 cells, as well as that they contained lower levels of lysosomal $Ca^{2+,}$ which has been shown before. We were able to determine that there was no pH defect in CHO M12 cells, which we could therefore suggest that Ca^{2+} defects are one of the main driving forces in NPC pathogenesis.

This shows that the lysosomes that are purified by this method can still remain structurally intact and can then be functionalized post-purification.

Chapter 5: Characterising juvenile neuronal ceroid lipofuscinosis disease cellular phenotypes

5.1 Background

CLN3 disease, also known as JNCL, is a neurological disorder that arises from mutations in the *CLN3* gene that gives rise to a progressively severe pathology starting at around 4-6 years of age leading to death, typically in the late teens/early twenties. As mentioned before, the role and function of the CLN3 protein is still widely disputed and there has been a lack of progress in mechanistic research in this field hampering not only our understanding of this disease at a cellular level but also the development of any potential treatment for CLN3 disease patients.

For us to truly be able to develop any form of therapy for JNCL we must first understand the changes in cell biology that occur following loss of CLN3 function.

5.2 Common phenotypes observed in different CLN3 mutant cells

CLN3, as well as all NCLs, are distinct in that cells present with the lysosomal accumulation of the auto-fluorescent material lipofuscin (Cao et al., 2011). This auto-fluorescent material has been found to consist of aggregates containing proteolipid which is an important component of subunit c of the mitochondria ATP synthase (Cao et al., 2011). While the storage of subunit c is common in many cell types that have mutations in *CLN3*, the molecular function is still unresolved as the loss of CLN3 function has been reported to have a broad impact on diverse cellular

processes such as vesicular trafficking, pH regulation, lipid transport and autophagy (Tecedor et al., 2013).

Many studies performed on mammalian cells have linked CLN3 with a role in endosomal organelles (Cotman and Staropoli, 2012). Several studies have shown that there are defects in lysosomal pH in different cell lines with *CLN3* mutations, with many of these studies suggesting that the lysosomal pH is more alkaline (Holopainen et al., 2001). This alkalization of the lysosomal pH has been linked with alterations in cathepsin D processing as well as the accumulation of APP (Golabek et al., 2000).

CLN3 deficiency has also been implicated to result in impaired endocytosis in mouse neurons, endothelial cells as well as patient fibroblasts (Tecedor et al., 2013). This has been speculated to be a result of alterations in the actin cytoskeleton, as CLN3 has been shown to be weakly associated with the HOOK1 protein which is important for recruitment of the cytoskeleton during endocytosis (Luiro et al., 2004). However it is still not fully understood how the absence of CLN3 impairs this network, and the knock on effect it has on endocytosis and subsequent trafficking (Schultz et al., 2014).

Autophagy has also been found to be severely affected in CLN3 mutant cells. The accumulation of subunit c has been found to be localized to autophagic vacuoles in *Cln3*$^{\Delta ex7/8}$ knock-in mouse cells, which suggests that there is a disruption in autophagosome maturation in these cells. Correct autophagy function is important for cellular viability, as it is needed for the production of key metabolites during times of stress or nutritional deprivation (Cao et al., 2006). The autophagic vacuole is

initiated by the *de novo* formation of an isolation membrane that then engulfs organelles or cytoplasmic material for degradation. This then fuses with lysosomes to become increasingly more acidic through the uptake of protons from the fused lysosomes to become an autolysosome, where the engulfed material can then be degraded and its components recycled back into the cell (Cao et al., 2006). While autophagy has been found to have an important role in other neurodegenerative diseases such as Huntingtons and Alzheimers (Palmer et al., 1995, Seehafer and Pearce, 2006), the defects in autophagosome maturation are still not fully understood in CLN3 mutant cells.

These common defects mentioned have been implied to relate closely to CLN3's function as they have been suggested to occur before the accumulation of detectable lysosomal lipid storage meaning they are possibly upstream events in CLN3 pathogenesis (Cotman and Staropoli, 2012).

5.3 Cerebellar defects seen in JNCL

The Cerebellum is a region of the brain that has an important role in motor control as well as possibly being involved in some degree of cognitive function. Within the cerebellum lies a network of different groups of tightly regulated neurons including the Purkinje cells, a group of neurons that are solely responsible for motor coordination inside the cerebellar cortex.

CLN3 has been found to be expressed in the purkinje cells of the cerebellum (Bohland et al., 2009), and research has shown that the loss of CLN3 leads to cerebellar defects. Following the loss of Cln3 in mouse studies there are a number of different phenotypes that present, such as loss of purkinje neurons and glial activation. Aberrant cell proliferation and maturation are also observed . Also a significant number of genes have been found to be altered in *Cln3* knockout mice. These gene expression changes include alterations in neurotransmission, neuronal cell structure and inflammation (Brooks et al., 2003, Weimer et al., 2009).

5.4 Purpose for phenotyping *Cln3*$^{\Delta ex7/8}$ cells

The cellular role and localization of the CLN3 protein is still not fully understood and is often the subject of controversy in the NCL field. *Cln3*$^{\Delta ex7/8}$ knock-in mice have been genetically manipulated so that they have a near identical mutation to that found in the 1kb gene deletion found in the majority of JNCL patients (Bennett and Rakheja, 2013). This mutation results in the 3-10 fold knockdown of *Cln3* mRNA levels found in the mouse tissues. While this does not completely remove all traces of Cln3 protein inside the cell, it is suitable to determine if the knockdown in *Cln3* expression results in lysosomal storage seen in other lysosomal diseases (Cotman et al., 2002).

As stated before one of the main clinical phenotypes in CLN3 patients is severe ataxia, which bears resemblance to another lysosomal storage disease, NPC. While a lot of work has been done characterizing the

pathology of the cerebellar during disease progression in NPC (particularly the loss of Purkinje neurons over time from disease onset), little work has been done to phenotype cerebellum cells that possess a mutated CLN3 protein. It is important to determine if these CLN3 mutant cerebellar cells share similarities in altered lipid content and changes in endocytic trafficking that are often altered in other types of lysosomal storage diseases.

5.5 Previous studies in *Cln3*$^{\Delta ex7/8}$ cerebellar cells

Cln3$^{\Delta ex7/8}$ knock-in mice were produced to provide a suitable neuronal cell system so that key biological processes could be observed in Cln3 mutant cells (Fossale et al., 2004).

Cln3$^{\Delta ex7/8}$ mice have been found to present with similar onset of symptoms seen in CLN3 disease patients. 10-14 week old mice start to exhibit sensory and motor coordination defects, while severe vacuolation was observed in older *Cln3*$^{\Delta ex7/8}$ mouse tissue (Staropoli et al., 2012). This would suggest that this mouse model is suitable for studying the effects of Cln3 deficiency in cells. The *Cln3*$^{\Delta ex7/8}$ cerebellar cells (cb) have been shown to accumulate subunit c of the mitochondrial ATP synthase, possess defects in autophagy, lower endocytic uptake, as well as processing defects in cathepsin D and defects in the levels of mitochondrial ATP (Fossale et al., 2004), which have been found to occur in other CLN3 mutant cell lines (Schultz et al., 2014). This would suggest

that the *Cln3*$^{\Delta ex7/8}$ cerebellar cells are a suitable Cln3 deficient model to determine key pathogenic phenotypes in the onset of CLN3 disease.

5.6 Overview

The purpose of this chapter is to attempt to characterize organelle dysfunction in *Cln3*$^{\Delta ex7/8}$ cerebellar cells to improve our understanding of where CLN3 might be working and what it may be doing in the cell. It is important to look at all organelles to potentially identify the effects Cln3 deficiency has on their respective cellular functions and how defects in this could potentially culminate in CLN3 disease. An important phenotype that will be determined is the presence of endocytic trafficking abnormalities, as this will be important to take into consideration for the potential use of magnetically purifying lysosomes from *Cln3*$^{\Delta ex7/8}$ cerebellar cells. Analysis of key phenotyping will also be done with CLN3 patient fibroblasts to help identify key phenotypic changes that are found in both *Cln3*$^{\Delta ex7/8}$ cerebellar cells as well as in patient cells. The patient cells to be analysed are one fibroblast line that is homozygous for the common 1kb mutation and one homozygous for a missense mutation found in the C-terminus of the CLN3 protein that results in CLN3 disease: the D416G mutant. Similar phenotypes observed between these different genotypes and cell lines would hopefully help elucidate CLN3's potential cellular function

5.7 Results

Despite much research being done on CLN3, the underlying cellular mechanisms that give rise to this disease are still poorly understood. Before being able to understand the mechanisms that give rise to the CLN3 phenotype we must first understand the key phenotypes present in CLN3 mutant cells, and how these phenotypes may potentially give rise to CLN3 disease.

5.7.1 Determining changes in lysosomal levels in mutant Cln3 cerebellar and CLN3 fibroblast cells

A common phenotype in many lysosomal storage diseases is an expansion in the lysosomal network. This has been hypothesised to be due to the cell up regulating the number of lysosomes to try and cope with the excess storage of lipids and other macromolecules in these diseased cells. The use of the lysotracker green probe was used to determine the number of acidic compartments present in the cell to check for any expansion of the lysosomal system.

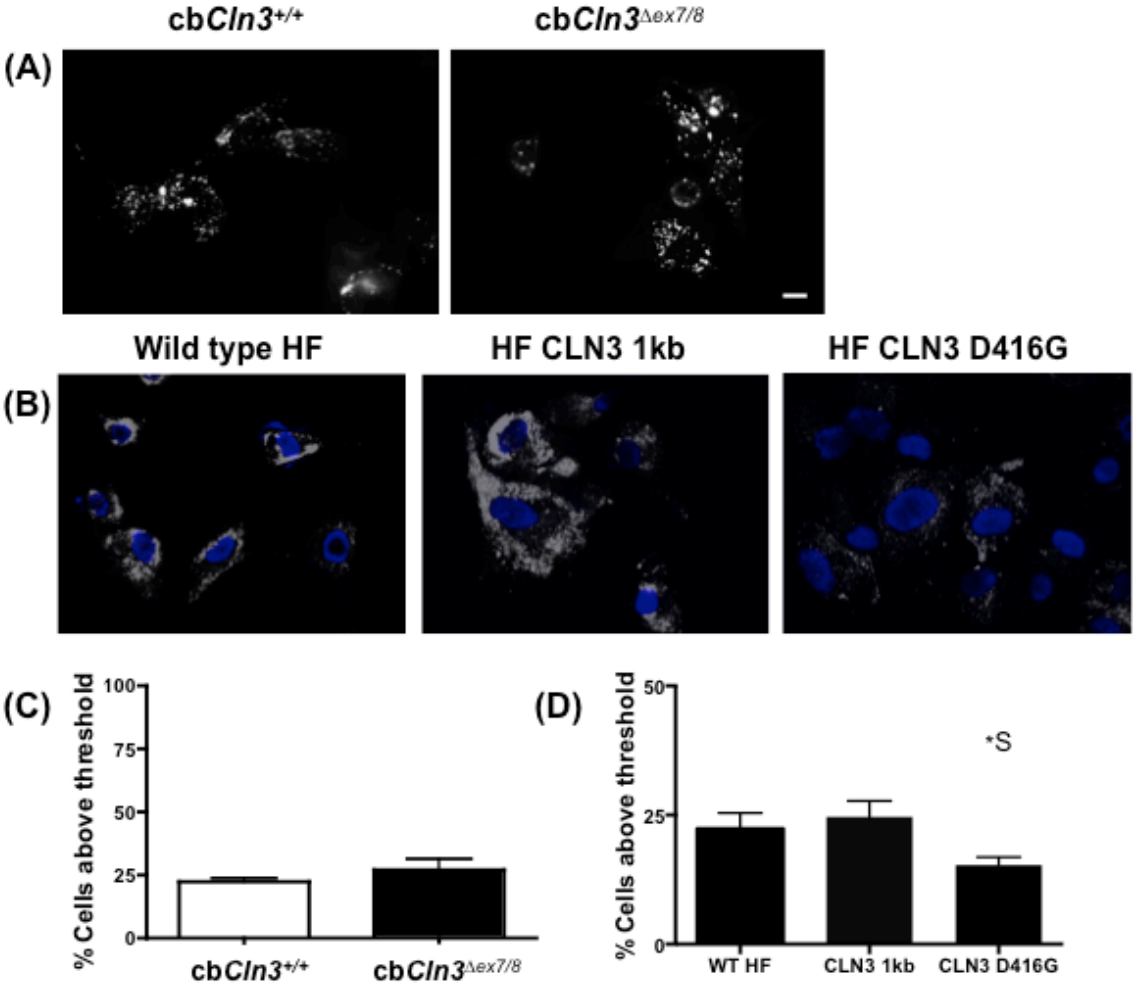

*Figure 5.1: (A) Representative Images of cbCln3$^{+/+}$ and cbCln3$^{\Delta ex7/8}$ cerebellar cells stained with lysotracker red probe (white) to detect the levels of acidic organelles (lysosomes). (B) Representative images of wild type human fibroblast (wild type HF) cells as well as human fibroblasts homozygous for the CLN3 1kb mutation (HF CLN3 1kb) and homozygous for the CLN3 D416G mutation (HF CLN3 D416G) cells stained with lysotracker red (white). Hoescht was used as a nuclear marker (blue). (C) & (D) quantified data of (A) & (B) respectively. Values represent mean ± SD. N=3. >80 cells analysed, S denotes significance *p< 0.05. Scale bars= 10μm.*

Cerebellar cells showed no change in the levels of lysosomes detected using the lysotracker red probe in either the cb*Cln3*$^{+/+}$ or cb*Cln3*$^{\Delta ex7/8}$ cells (figure 5.1). Similar levels of lysotracker red staining was observed

between wild type fibroblast and fibroblasts carrying the CLN3 1kb mutation, although a few cells showed marginally higher levels of lysotracker staining. Fibroblast cells that carry the CLN3 D416G mutation exhibited lower levels of lysotracker red staining when compared with normal and the CLN3 1kb mutation fibroblasts.

5.7.2 Cathepsin B activity in mutant Cln3 cerebellar and CLN3 fibroblast cells

Magic Red Cathepsin B kit is used to detect the activity of the lysosomal enzyme cathepsin B. The assay works by adding a cathepsin B substrate to the cells, when there is cathepsin B activity it cleaves the substrate releasing a fluorescent product. Changes in the levels of cathepsin B could potentially indicate a change in the lysosomal pH required for cathepsin B to work.

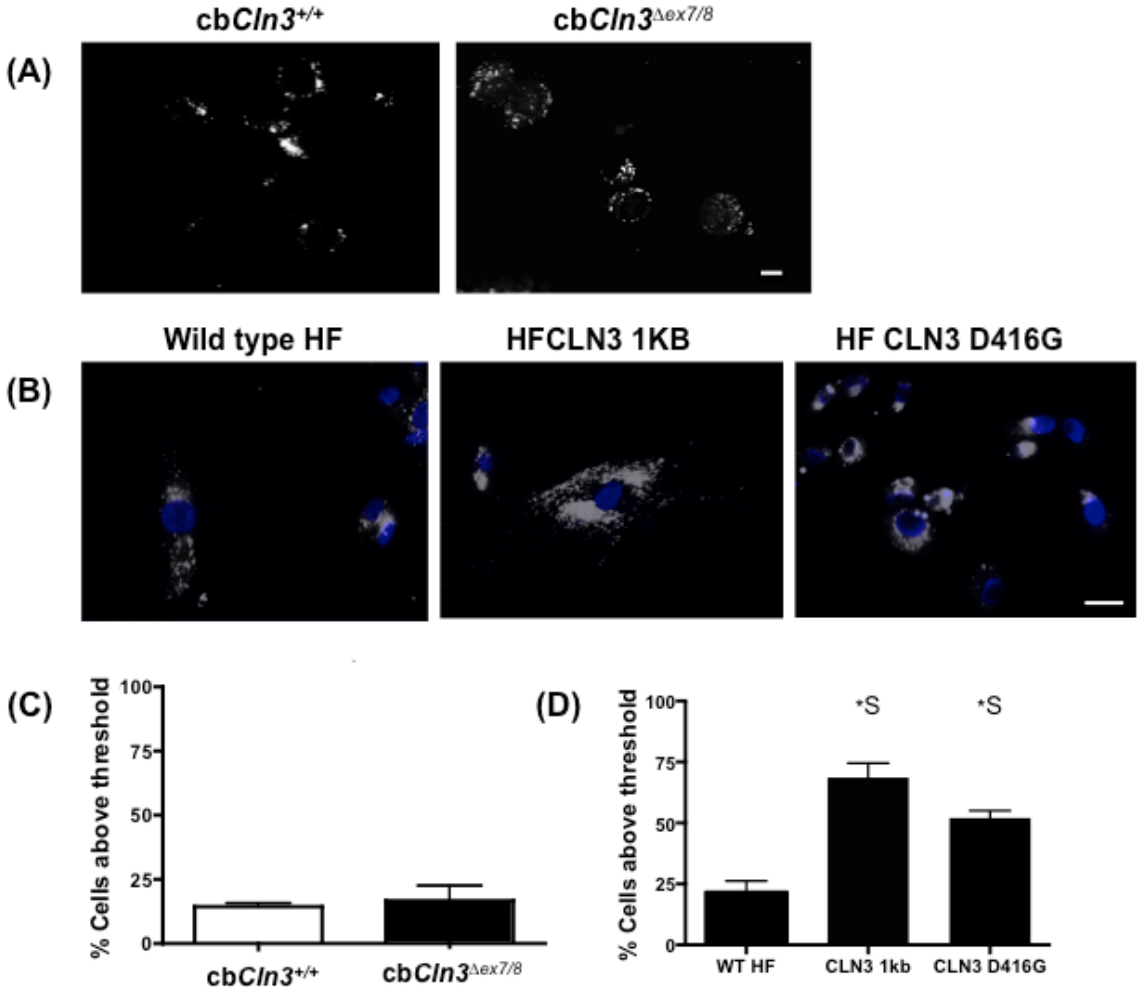

*Figure 5.2: (A) Representative Images of cbCln3$^{+/+}$ and cbCln3$^{\Delta ex7/8}$ cerebellar cells stained with Magic red cathepsin B (white) to detect the activity of the the lysosomal enzyme cathepsin B. (B) Representative images of wild type human fibroblast (wild type HF) cells as well as human fibroblasts homozygous for the CLN3 1kb mutation (HF CLN3 1kb) and homozygous for the CLN3 D416G mutation (HF CLN3 D416G) cells stained with Magic red cathepsin B (white). Hoescht was used as a nuclear marker (blue). (C) & (D) quantified data of (A) & (B) respectively. Values represent mean ± SD. N=3. >80 cells analysed, S denotes significance *p< 0.05. Scale bars= 10μm.*

No change in the levels of cathepsin B activity was observed between the two cerebellar cell types (figure 5.2). A slightly greater amount of cathepsin B activity was observed in the fibroblast cells that possess the

two CLN3 mutations when compared with the wild type fibroblast cells. This possibly indicates that lysosomal enzyme activity is elevated in CLN3 mutant lysosomes, but as cathepsin B is dependent on acidic pH optimum to work, this would suggest that CLN3 1kb mutants and D416G mutants still possess an acidic pH in the lysosome.

5.7.3 Cathepsin L activity in mutant Cln3 cerebellar and CLN3 fibroblast cells

Magic Red Cathepsin L kit is used to detect the activity of the lysosomal enzyme cathepsin L. The assay works by adding a cathepsin B substrate to the cells, when there is cathepsin L activity it cleaves the substrate releasing a fluorescent product. Changes in the levels of cathepsin L could potentially indicate a change in the lysosomal pH required for cathepsin L to work.

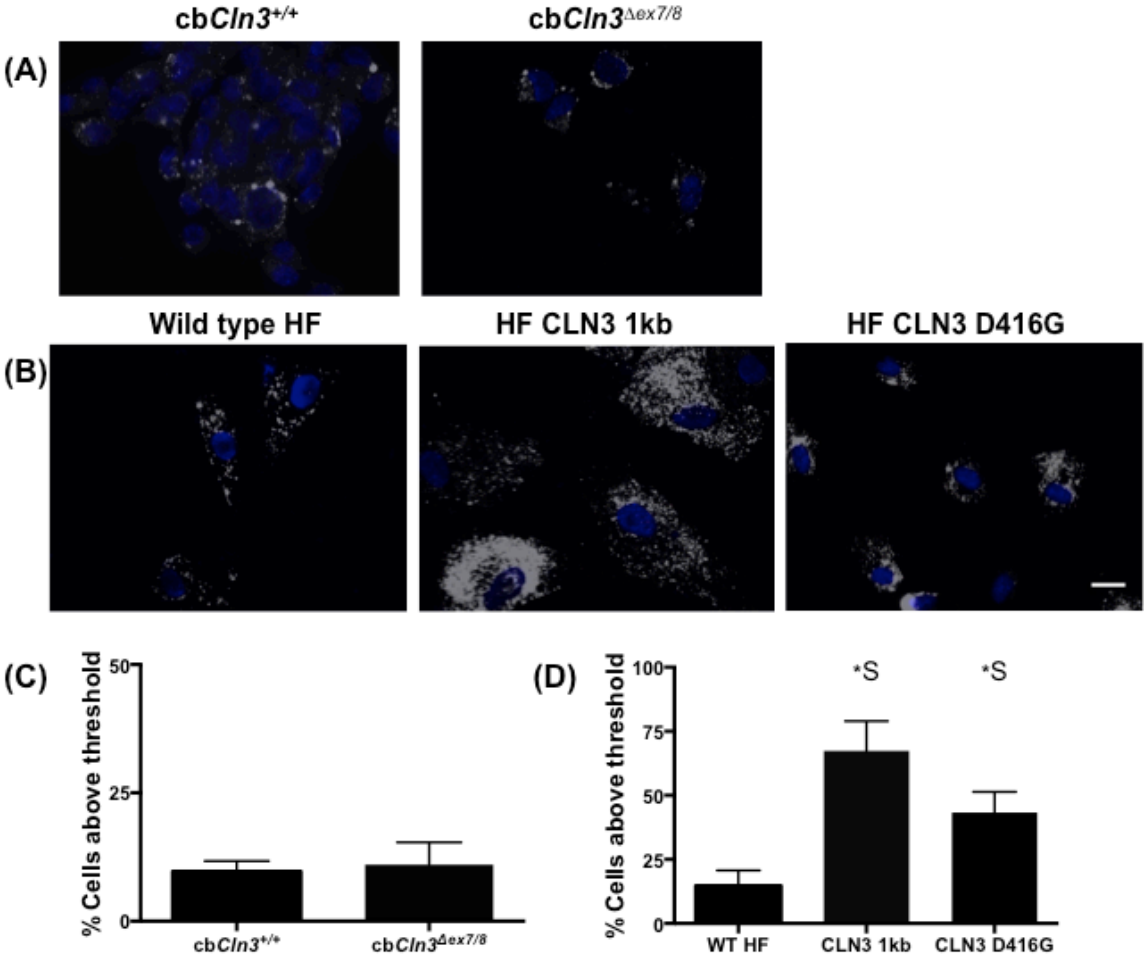

*Figure 5.3: (A) Representative Images of cbCln3$^{+/+}$ and cbCln3$^{\Delta ex7/8}$ cerebellar cells stained with Magic red cathepsin L (white) to detect the activity of the the lysosomal enzyme cathepsin L. Hoescht was used as a nuclear marker (blue). (B) Representative images of wild type human fibroblast (wild type HF) cells as well as human fibroblasts homozygous for the CLN3 1kb mutation (HF CLN3 1kb) and homozygous for the CLN3 D416G mutation (HF CLN3 D416G) cells stained with Magic red cathepsin L (white). Hoescht was used as a nuclear marker (blue). (C) & (D) quantified data of (A) & (B) respectively. Values represent mean ± SD. N=3. >80 cells analysed, S denotes significance *p< 0.05. Scale bars= 10μm.*

Magic Red Cathepsin L kit is used to detect the activity of the lysosomal enzyme cathepsin L. The assay works by adding a cathepsin L substrate

to the cells, when there is cathepsin L activity it cleaves the added substrate releasing a fluorescent product. No difference in cathepsin L activity was seen between the cb*Cln3*$^{+/+}$ and cb*Cln3*$^{\Delta ex7/8}$ cerebellar cells (figure 5.3). Interestingly greater levels of cathepsin L activity were observed in both the CLN3 mutant fibroblast cell lines when compared with the wild type fibroblast cells. Greater cathepsin L activity was detected in the CLN3 1kb mutation when compared with the CLN3 D416G mutants, suggesting greater activity of this enzyme in the 1kb mutant cells.

5.7.4 Mitochondrial numbers and function

By using Mitotracker green to detect mitochondrial levels in cells it revealed that there was no difference in the mitochondrial levels detected in both cb*Cln3*$^{+/+}$ and cb*Cln3*$^{\Delta ex7/8}$ cerebellar cells (figure 5.4). MitoROS probe is used to detect the levels of mitochondrial produced ROS, which is a natural by product of mitochondrial function (due to the formation of free electrons as a by-product of the electron transport chain) and any increase or decrease in levels can indicate mitochondrial dysfunction.

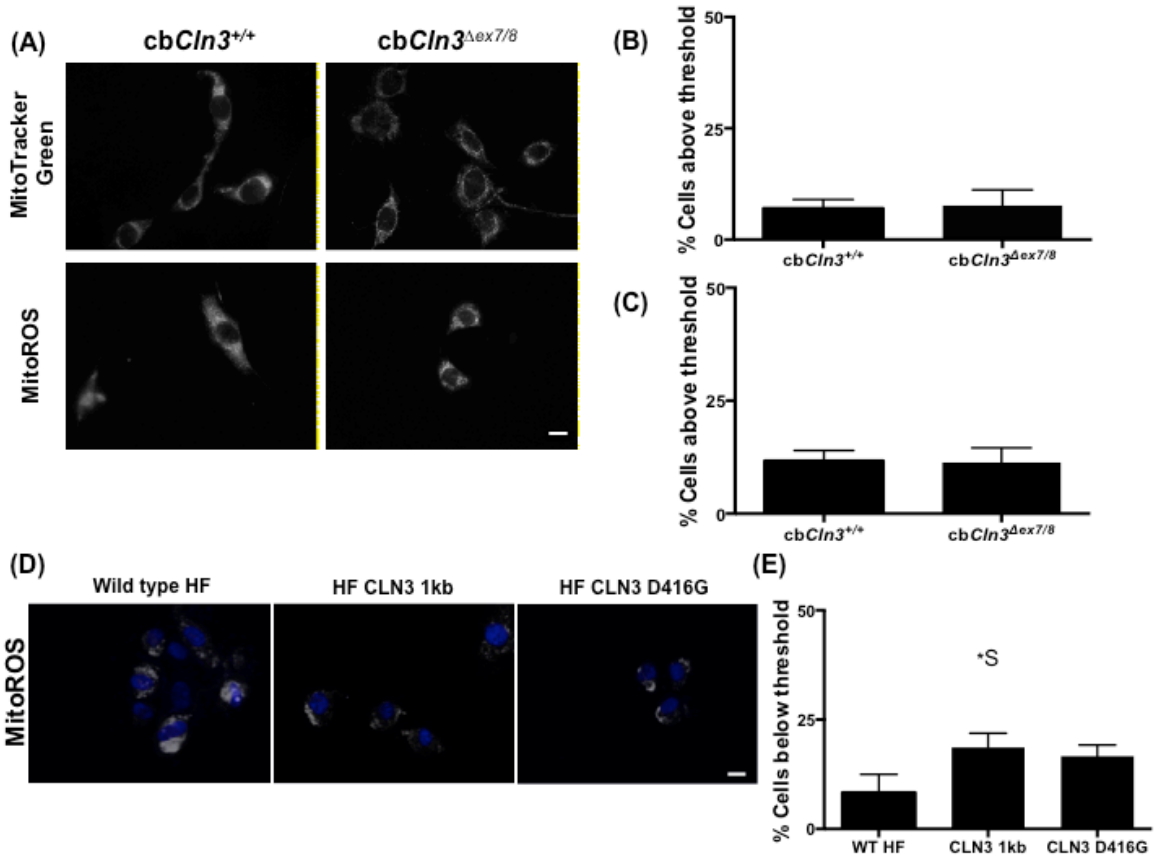

*Figure 5.4: (A) Representative Images of cbCln3$^{+/+}$ and cbCln3$^{\Delta ex7/8}$ cerebellar cells stained with Mitotracker green probe to detect mitochondrial levels and MitoROS probe to detect the levels of mitochondrial produced reactive oxygen species (ROS) (white). (D) Wild type human fibroblast cells as well as human fibroblasts homozygous for the CLN3 1kb mutation and homozygous for the CLN3 D416G mutation stained with MitoROS probe. Hoescht was used as a nuclear marker (blue). (B), (C) & (E) quantified data of (A) & (D) respectively. Values represent mean ± SD. N=3. >60 cells analysed, S denotes significance *p< 0.05. Scale bars= 10μm.*

No changes in the levels of mitochondrial produced ROS was detected in the two cerebellar cell types. By observing the stains in fibroblast cells there appears to be slightly lower levels of mitoROS staining present in both CLN3 mutant fibroblast cell lines when compared with wild type

fibroblasts. This reduction of MitoROS staining was significantly lower in the 1kb mutation cell lines. While the difference is small, it could signify that the mitochondria are starting to lose viability.

5.7.5 Levels of ER density and the ER Ca^{2+} influx pump SERCA2

SERCA 2 antibody was used to stain for the presence of the SERCA 2 Ca^{2+} channel that is responsible for the uptake of Ca^{2+} into the ER. ER tracker probe was used to stain the ER as a whole to detect for any changes in ER density in the cell, which could be a sign of ER stress.

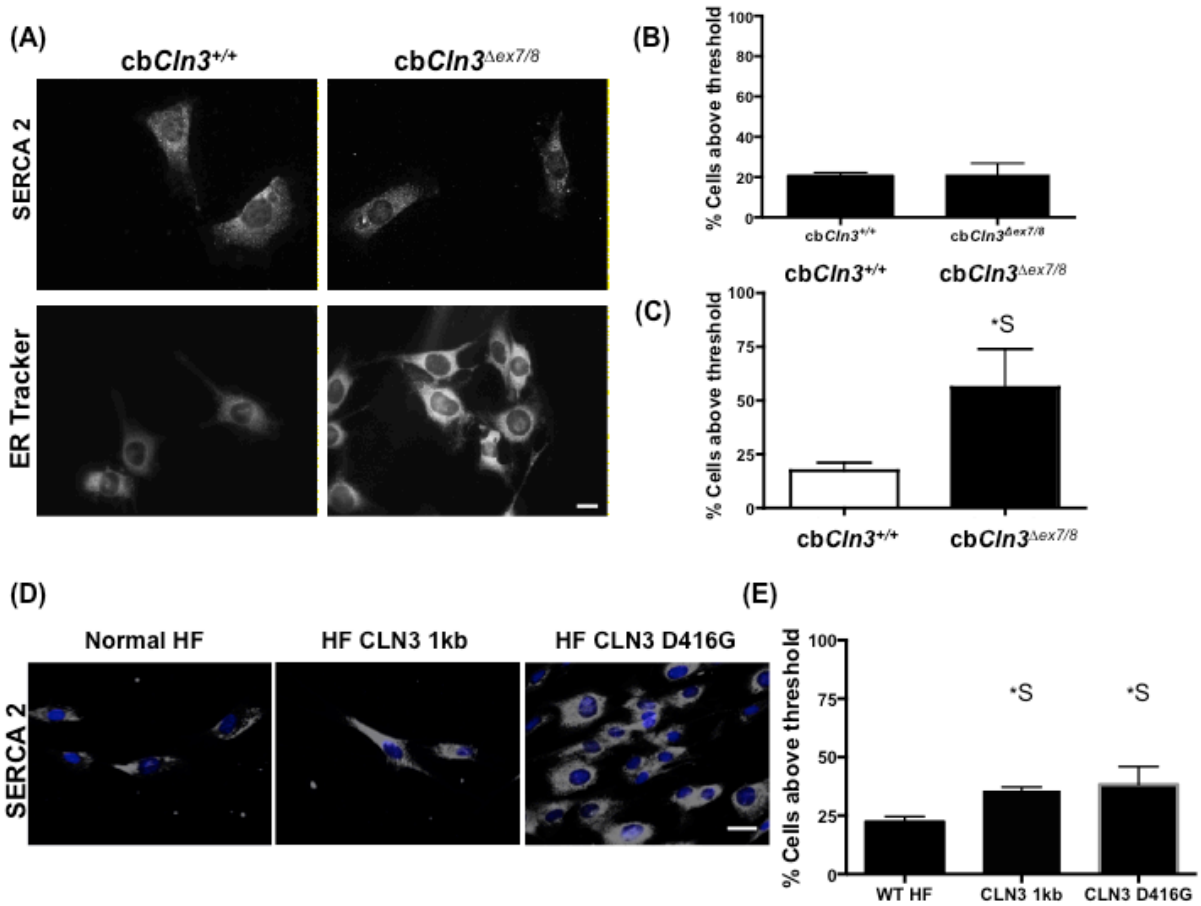

*Figure 5.5: (A) Representative Images of cbCln3$^{+/+}$ and cbCln3$^{\Delta ex7/8}$ cerebellar cells stained SERCA2 antibody and ER tracker probe to detect the levels of the SERCA2 protein and ER structure respectively (white). (D) Wild type human fibroblast cells as well as human fibroblasts homozygous for the CLN3 1kb mutation and homozygous for the CLN3 D416G mutation stained with SERCA2 antibody. Hoescht was used as a nuclear marker (blue). (B), (C) & (E) quantified data of (A) & (D) respectively. Values represent mean ± SD. N=3. >40 cells analysed, S denotes significance *p< 0.05. Scale bars= 10μm.*

There was no significant change in the levels of SERCA 2 found in the cb*Cln3*$^{\Delta ex7/8}$ cerebellar cells when compared with cb*Cln3*$^{+/+}$ cerebellar cells (figure 5.5). Staining with ER tracker revealed that there was an increase in the density of ER in the cb*Cln3*$^{\Delta ex7/8}$ cerebellar cells when compared with cerebella cb*Cln3*$^{+/+}$ cells (figure 5.5). This thickening of the ER observed in these cells would suggest that there is an increase in the levels of ER stress in the cb*Cln3*$^{\Delta ex7/8}$ cerebellar cells. Staining with

SERCA 2 antibody in the human fibroblast cells revealed a marginal increase in the levels of SERCA 2 detected in both the CLN3 mutant cell lines when compared with wild type fibroblasts. This could possibly indicate that there is an expansion of the ER membrane in both the CLN3 mutant fibroblasts, which might be a sign of the ER stress response, but additional work is required to determine this.

5.7.6 Determining changes in lipid content

One common phenotype in lysosomal storage diseases is the storage of different lipids. Three common lipids that have been found to be stored are cholesterol, sphingomyelin and LBPA. By observing the storage of these lipids may indicate a problem in the trafficking or degradation of these molecules.

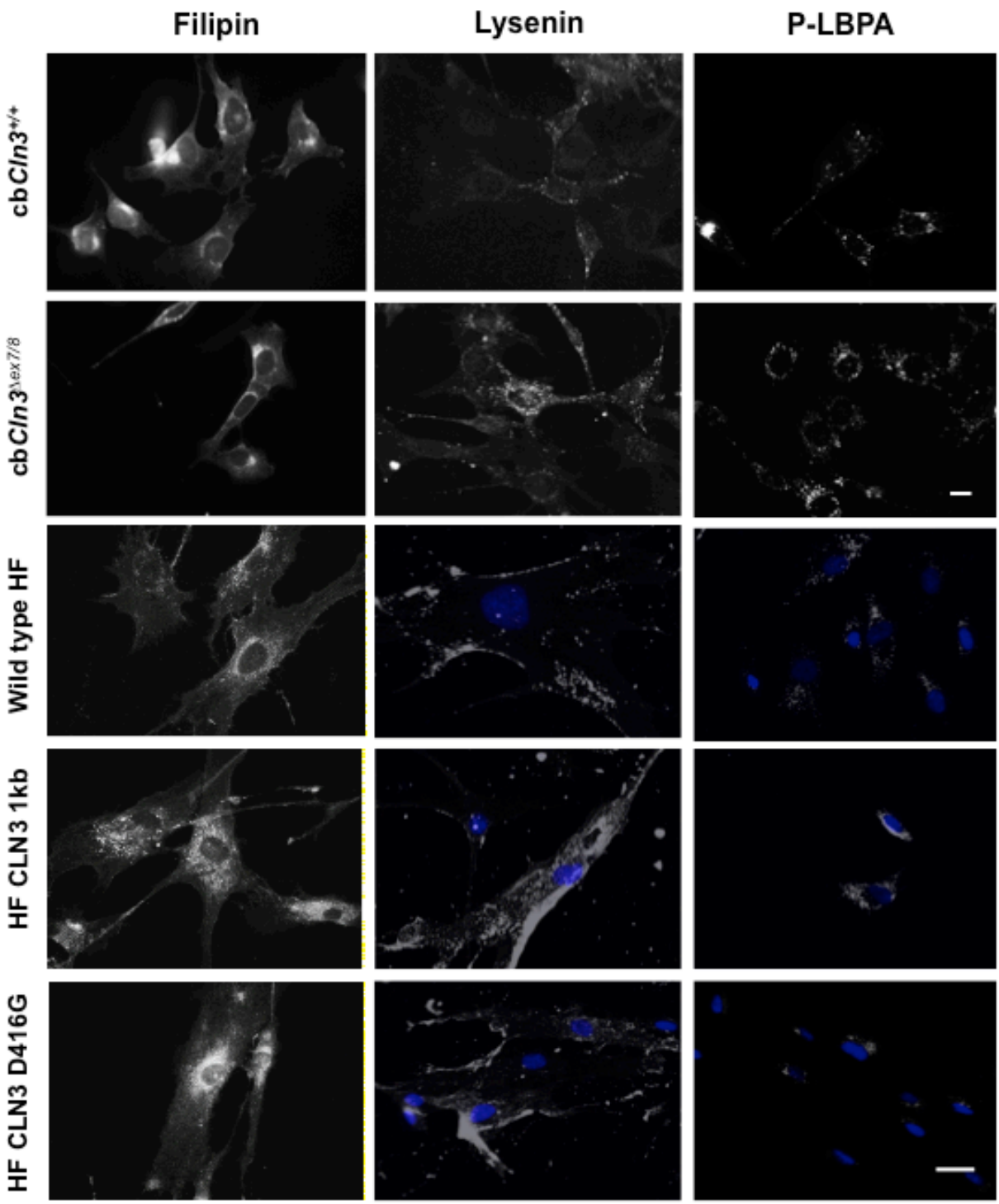

Figure 5.6: Representative Images of cbCln3$^{+/+}$ and cbCln3$^{\Delta ex7/8}$ cerebellar cells and normal human fibroblast cells as well as human fibroblasts homozygous for the CLN3 1kb mutation and homozygous for the CLN3 D416G mutation stained with Filipin, Lysenin and P-LBPA antibody to detect for the presence of Cholesterol, Sphingomyelin and LBPA respectively. Hoescht was used as a nuclear marker (blue). n=3. Scale bars= 10μm.

Filipin complex is used as a stain for free cholesterol as it specifically binds to it and fluoresces, indicated by punctate staining. By observing the filipin staining in the cells we observed that there was no change in the levels of cholesterol present between the cb*Cln3*$^{+/+}$ and cb*Cln3*$^{\Delta ex7/8}$ cerebellar cells (figure 5.6). However there was a small change in the cholesterol levels detected when comparing the CLN3 mutant fibroblast cells with normal fibroblast cells. Comparing the CLN3 1kb mutant fibroblast cells with the wild type fibroblasts revealed that the levels of cholesterol weren't significantly different between the two cell types, the distribution of cholesterol was different in the CLN3 1kb mutant cells (more peri-nuclear in normal fibroblast cells compared with general whole cell distribution seen in CLN3 1kb mutant cells). The cholesterol localization in the CLN3 D416G mutant cells is similar to that seen in wild type fibroblasts (peri-nuclear), but the overall levels of cholesterol staining observed was higher in the CLN3 D416G mutant when compared with wild type fibroblasts.

Lysenin toxin was used to detect for sphingomyelin levels (indicated by punctate staining). There was a small increase in the levels of sphingomyelin in the cerebellar cb*Cln3*$^{\Delta ex7/8}$ cells when compared to the cb*Cln3*$^{+/+}$ *cells*. The cb*Cln3*$^{\Delta ex7/8}$ cerebellar cells that exhibited higher levels of lysenin staining displayed brighter staining inside the cell, rather than the staining generally being present along the plasma membrane of the cell. Utilising lysenin toxin stain on the fibroblast cells resulted in staining of the plasma membrane in the wild type cells, however the

results seen in both CLN3 mutant fibroblast cells was more variable. In both the CLN3 mutant fibroblasts there was elevated levels of intracellular lysenin staining present in some cells, but there were also some cells that displayed similar levels of lysenin staining seen in wild type fibroblasts. However the proportion of cells that displayed intracellular lysenin staining were much higher in the CLN3 1kB mutant cells when compared with CLN3 D416G mutant cells, possibly suggesting a more severe phenotype.

P-LBPA antibody was used to detect the levels of LBPA inside the cells, indicated by punctate staining (figure 5.6). The levels of LBPA were higher in the cb*Cln3*$^{\Delta ex7/8}$ cells when compared with cb*Cln3*$^{+/+}$ cerebellar cells, suggesting an accumulation of this lipid in endosomal vesicles in cb*Cln3*$^{\Delta ex7/8}$ cerebellar cells. The levels of LBPA staining was similar in CLN3 1kb mutant fibroblast cells when compared with their respective wild type cells, implying that storage of this lipid is not present in fibroblast cells that carry the same type of mutation as the cerebellar cb*Cln3*$^{\Delta ex7/8}$ where LBPA storage seems to be up. Interestingly LBPA staining was lower in the CLN3 D416G mutant cells than what was observed in both the wild type and CLN3 1kb mutant cells, possibly suggesting defects in the synthesis of this lipid in cells that possess the CLN3 D416G mutant variant.

5.7.7 Determining changes in the Golgi apparatus

It has been implied by some research groups that CLN3 is a Golgi protein. GM130 antibody was used to detect for any changes in morphology of the Golgi apparatus in wild type and CLN mutant cells.

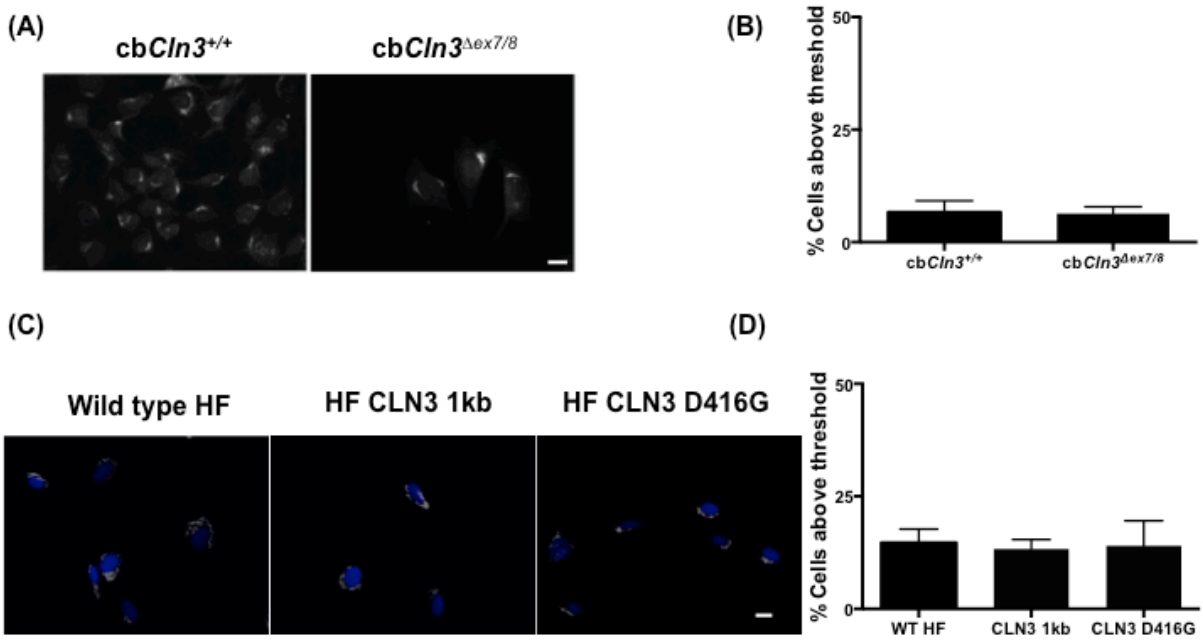

Figure 5.7: (A) Representative Images of cbCln3$^{+/+}$ and cbCln3$^{\Delta ex7/8}$ cerebellar cells stained for the Golgi protein GM130 to determine changes in Golgi structure (white). (C) Representative images of wild type human fibroblast cells as well as human fibroblasts homozygous for the CLN3 1kb mutation and homozygous for the CLN3 D416G mutation stained with the GM130 antibody (white). Hoescht was used as a nuclear marker (blue). (B) & (D) quantified data of (A) & (C) respectively. Values represent mean ± SD. n=3. >50 cells analysed. Scale bars= 10μm.

Using the GM130 antibody we observed that there were no changes in the morphology of the Golgi apparatus in both the two different cerebellar genotypes as well as the wild type and both mutant fibroblast cell lines.

(figure 5.7). This suggests that the CLN3 protein loss does not affect Golgi morphology.

5.7.8 Metal ion levels in wild type and Cln3 mutant cerebellar cells

Some studies have suggested that changes in metal ion content may lead to disease pathogenesis in lysosomal storage diseases. The use of metal ion probes was used to detect changes in tightly regulated metal ions such as Zn^{2+}, Cu^{2+} and Fe^{2+}. Loss in regulation of metal ion content may lead to disease pathogenesis.

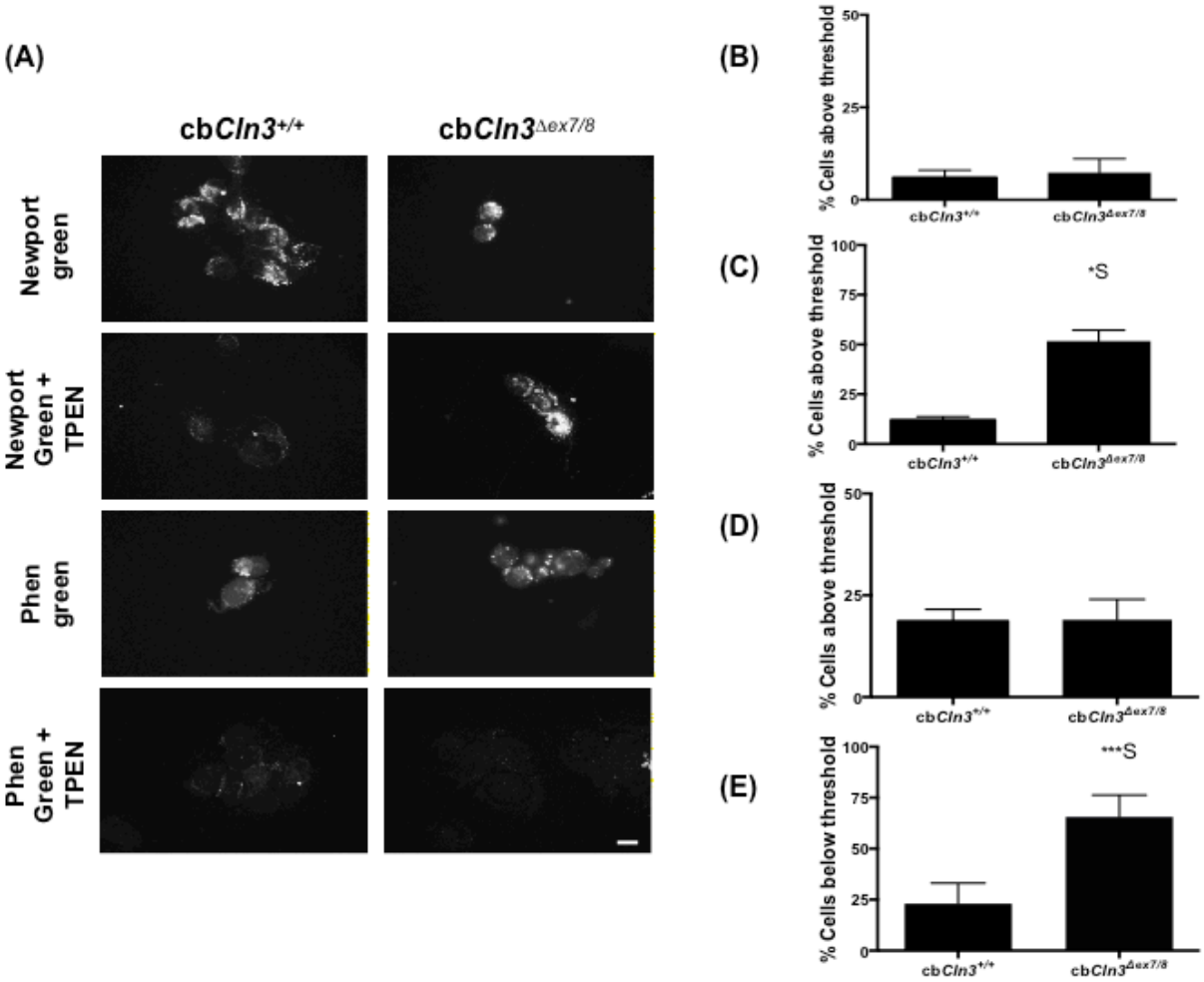

*Figure 5.8: (A) Representative images of cbCln3$^{+/+}$ and cbCln3$^{\Delta ex7/8}$ cerebellar cells stained with the Zn^{2+}, Fe^{2+} and Cu^{2+} ion probes Phen green and Newport green. Cells are also imaged using these probes in the presence of the zinc chelator TPEN. (B), (C), (D) & (E) Quantified data on Newport green, Newport green + TPEN, Phen green and Phen green + TPEN respectively. Values represent mean ± SD. N=3. >60 cells analysed for each stain. S denotes significance. *P<0.05, ***P< 0.001. Scale bars= 10μm.*

Zn^{2+} and Cu^{2+} probe Newport green showed that there was no difference in the Zn^{2+} and Cu^{2+} levels detected in the cb*Cln3*$^{+/+}$ and cb*Cln3*$^{\Delta ex7/8}$ cells (figure 5.8). The Zn^{2+} chelator TPEN is added to cells stained with newport green so that only the remaining Cu^{2+} is stained. This results in a significantly greater level of Cu^{2+} staining present in the cerebellar

cb*Cln3*$^{\Delta ex7/8}$ cells than what is seen in the cb*Cln3*$^{+/+}$. The phen green probe was also used to stain for cellular levels of Zn^{2+}. Cellular levels of Zn^{2+} was the same in the cb*Cln3*$^{+/+}$ cerebellar and cb*Cln3*$^{\Delta ex7/8}$ cells, however following the chelation of Zn^{2+} with TPEN the cb*Cln3*$^{\Delta ex7/8}$ cells exhibited significantly less fluorescence. This is possibly because phen green is quenched when it binds to Cu^{2+} and Fe^{2+} suggesting that these two metal ions are possibly elevated.

5.7.9 Early endosomal levels are elevated in cbCln3$^{\Delta ex7/8}$ and CLN3 mutant fibroblast cells

EEA1 antibody was used as a marker for the presence of early endosomes in cerebellar and fibroblast cells. An increase in the levels of early endosomes could be an indication of an increase in endocytic uptake of molecules from outside the cell as well as an increase in the endocytic trafficking of these molecules (figure 5.9).

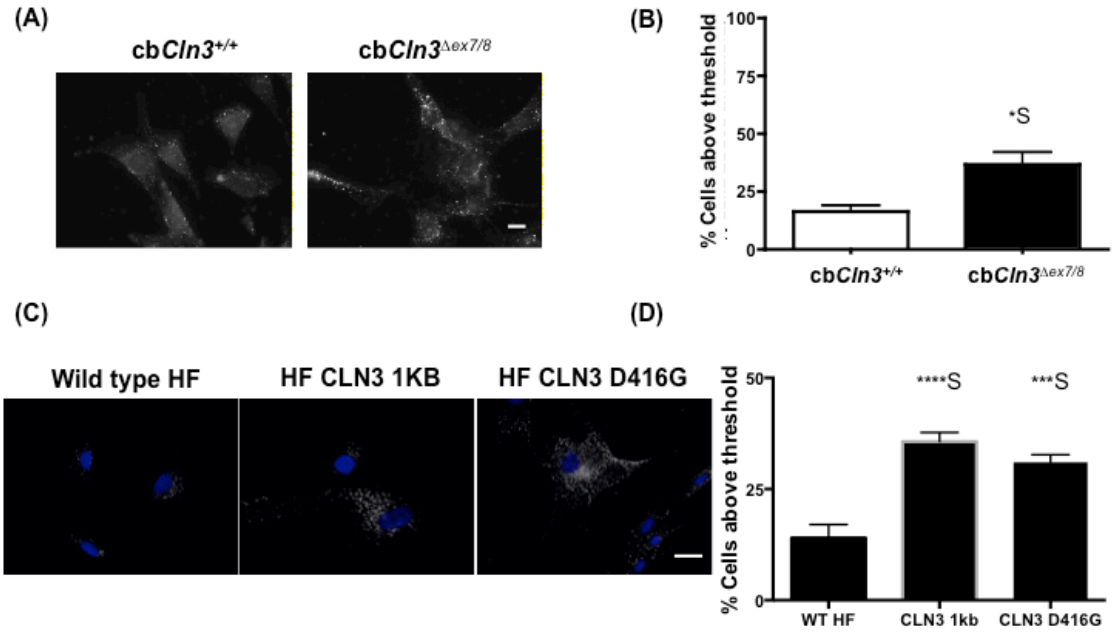

*Figure 5.9: (A) Representative Images of cbCln3$^{+/+}$ and cbCln3$^{\Delta ex7/8}$ cerebellar cells stained for the Early endosomal protein EEA1 to determine early endosomal levels (white). (C) Representative images of wild type human fibroblast cells as well as human fibroblasts homozygous for the CLN3 1kb mutation and homozygous for the CLN3 D416G mutation stained with the EEA1 antibody (white). Hoescht was used as a nuclear marker (blue). (B) & (D) quantified data of (A) & (C) respectively. Values represent mean ± SD. n=3. >70 cells analysed. S denotes significance. ***P< 0.001, ****P<0.0001. Scale bars= 10μm.*

The levels of EEA1 staining (indicated by punctate staining) was significantly higher in the cb*Cln3*$^{\Delta ex7/8}$ cerebellar cells when compared with what was seen in cb*Cln3*$^{+/+}$cells. Staining of the fibroblasts also revealed that cells carrying either the CLN3 1kb or CLN3 D416G mutation possessed elevated levels of EEA1 when compared with wild type fibroblasts.

5.7.10 Determining the rate of endocytosis by monitoring the trafficking of ganglioside GM1

CtxB transport assay was used to monitor the cellular trafficking of the GM1 ganglioside. CtxB supplied to live cells binds to GM1 ganglioside and is then internalised into the cell so that it can be used to monitor the transport of GM1 inside the cell. In healthy cells GM1 is trafficked to the Golgi (shown by bright staining round the nuclei), while in cells with retarded endocytic trafficking the GM1 stain presents itself as intra-vesicular punctate staining with little to no Golgi staining present. For counting purposes the rate of GM1 trafficking is designated into three categories: Golgi (the majority of the staining observed is in the Golgi), intermediate (there is some Golgi staining is present but there is still high amounts of GM1 (staining outside the Golgi in punctate endocytic compartments) and punctate (there is no Golgi staining present, only punctate staining). The cells were treated to both a 1 hour and 30 minute pulse to give time for the CtxB to be internalized into the cell and bind to GM1. This is then followed by either a 1 or 2 hour chase to measure GM1 trafficking.

(A)

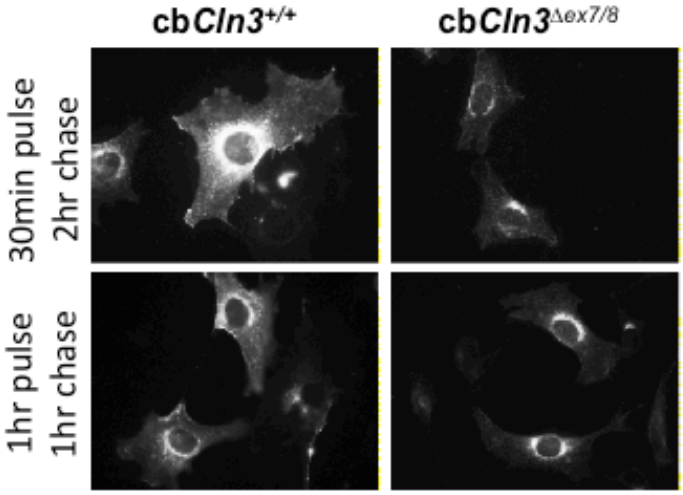
cbCln3+/+
cbCln3Δex7/8
30min pulse
2hr chase
1hr pulse
1hr chase

(B)

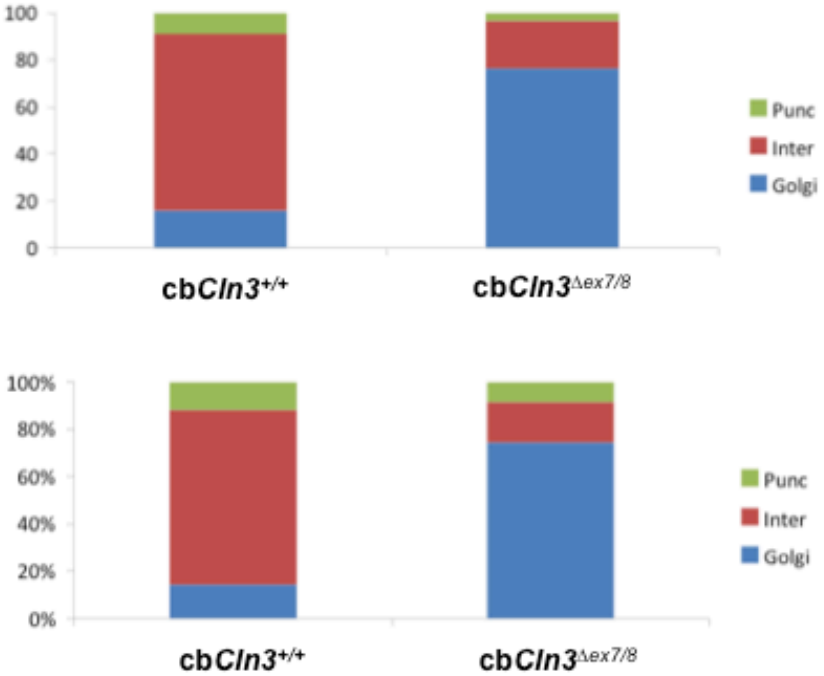
100
80
60
40
20
0
Punc
Inter
Golgi
cbCln3+/+
cbCln3Δex7/8
100%
80%
60%
40%
20%
0%
Punc
Inter
Golgi
cbCln3+/+
cbCln3Δex7/8

(C)

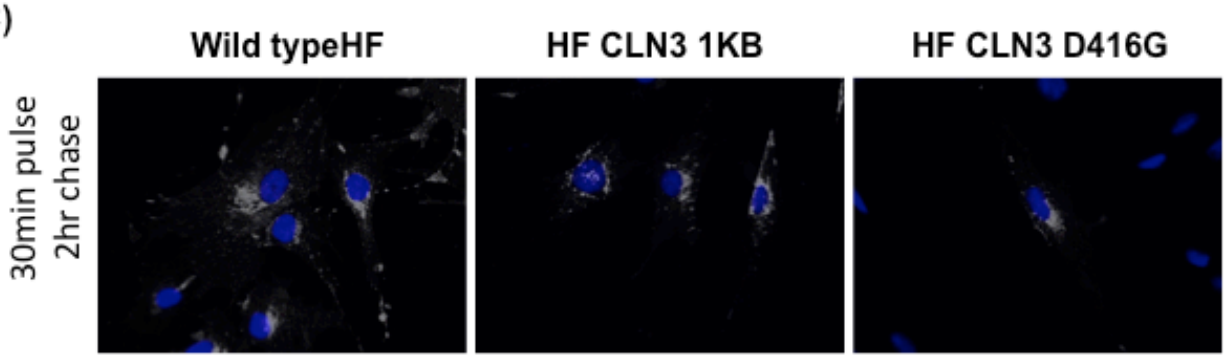
Wild typeHF
HF CLN3 1KB
HF CLN3 D416G
30min pulse
2hr chase

Figure 5.10: (A) Representative Images of cbCln3$^{+/+}$ and cbCln3$^{\Delta ex7/8}$ cerebellar cells treated with FITC-CtxB to measure the uptake and trafficking speed of ganglioside GM1 (white). (B) Respective counts of GM1 cellular location was done for both cerebellar cell types after their respective pulse/chase times. (C) Wild type human fibroblast cells as well as human fibroblasts homozygous for the CLN3 1kb mutation and homozygous for the CLN3 D416G mutation treated with FITC-CtxB to measure trafficking. Hoescht was used as a nuclear marker (blue). n=3. >100 cells counted for each pulse/chase time experiments for CtxB localization quantification.

A greater degree of Golgi staining was observed in the *cbCln3*$^{\Delta ex7/8}$ cerebellar cells when compared to cb*Cln3*$^{+/+}$cerebellar cells (figure 5.10), this would suggest that there is faster endocytic trafficking occurring in the *cbCln3*$^{\Delta ex7/8}$ cerebellar cells. By observing the cellular staining present in the fibroblast cells following a 30 minute pulse and 2 hour chase of the CtxB toxin there was a greater degree of Golgi staining evident in both the CLN3 1kb and D416G mutant genotypes when compared with the wild type fibroblast cells. This would suggest that in the CLN3 mutant cell lines there is faster endocytic trafficking occurring as was seen in the *cbCln3*$^{\Delta ex7/8}$ cerebellar cells.

5.7.11 Dextran fusion assay to determine endocytic trafficking speed.

A dextran fusion assay was performed to detect any increase in the rate of endocytic trafficking in the cerebellar cell, to confirm the phenotype we observed using the CtxB transport assay. This assay works by observing

the trafficking of fluorescent dextrans as they pass through the endocytic system.

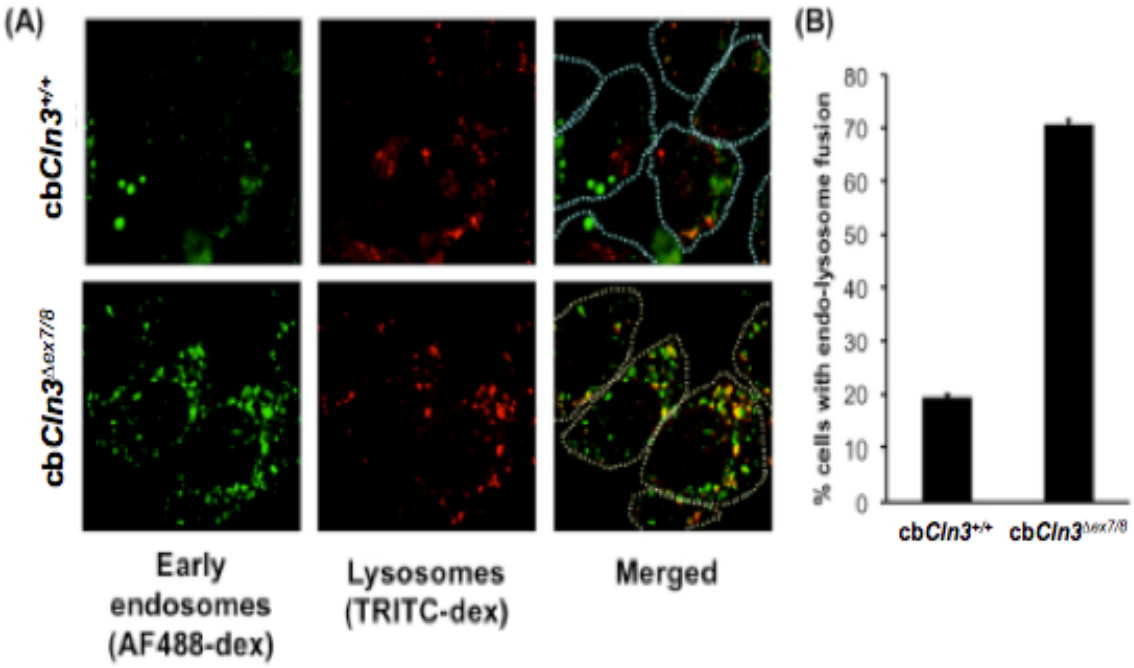

Figure 5.11: Representative images of cb*Cln3*$^{+/+}$ *and cbCln3*$^{\Delta ex7/8}$ *cerebellar cells pulsed with TRITC-dextran (red) for 24 hour and chased for 12 hour and AF488-Dextran (green) for 10 minutes so they are present in lysosomes and early endosomes respectively. (A) The treated cells are imaged for the localization of the two endocytic vesicle markers for signs of co-localisation (yellow). Lines were drawn around the cell to highlight their location (B) % of cells that exhibited overlap. Lines were drawn around the cells to highlight their location. (N=2).*

A 24 hour pulse and 12 hour chase of TRITC-dextran allows it to be trafficked to the lysosomes where it can be visualized at 570nm wavelength (Red). A pulse of 10 minutes of Alexa Fluo-488 dextran (AF488-Dex) is a suitable time for this dextran to be uptaken into the cell and the majority of the dextran to reside in the early endosomes in cells with normal trafficking rates. The early endosomes can then be visualized

at 480nm wavelength (green). Any elevated endocytic trafficking will result in a greater degree of co-localisation between the TRITC-dextran and AF488-dextrans as the AF488-dextran would have been trafficked along the endocytic pathway to the lysosome at a faster rate than normal (co-localisation visualized in yellow). A greater degree of co-localisation between the two different fluorescent dextrans was observed in the *cbCln3*$^{\Delta ex7/8}$ cerebellar cells when compared with the cb*Cln3*$^{+/+}$cells (~70% versus 20%) (figure 5.11). This data suggests that there is faster endocytic trafficking present in *cbCln3*$^{\Delta ex7/8}$ cerebellar cells compared with cb*Cln3*$^{+/+}$cerebellar cells. This result supports the CtxB transport assay data which also suggested that *cbCln3*$^{\Delta ex7/8}$ cerebellar cells have faster endocytic trafficking (figure 5.10).

5.7.12 Intra-lysosomal measurements of pH and Ca^{2+}

Ca^{2+} and pH probes were loaded into the lysosome to detect for any changes in the Cln3 mutant cerebellar cells when compared with the wild type cells. Changes in intra-lysosomal Ca^{2+} content or pH may possibly may be the reason for the elevated endocytic trafficking observed in the mutant Cln3 cells.

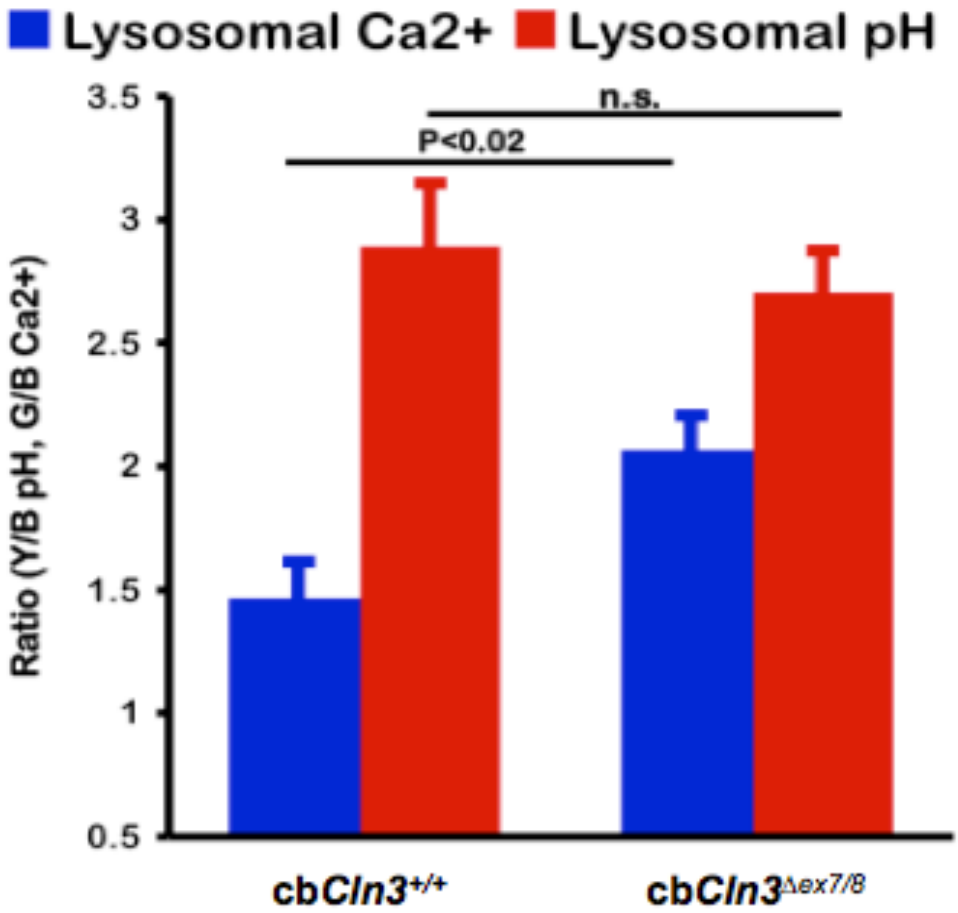

Figure 5.12: Quantified data for lysosomal Ca^{2+} and pH levels detected in cb*Cln3*$^{+/+}$ *and cbCln3*$^{\Delta ex7/8}$ *cerebellar cells. (N=2). (t-test) P<0.02, n.s. denotes not significant.*

Oregon green BAPTA was used as an intra-lysosomal Ca^{2+} probe. Quantification of the levels of lysosomal Ca^{2+} detected in cb*Cln3*$^{+/+}$and *cbCln3*$^{\Delta ex7/8}$ cerebellar cells displayed that there was a significant increase in the levels of lysosomal Ca^{2+} detected in the *cbCln3*$^{\Delta ex7/8}$ than what was seen in the cb*Cln3*$^{+/+}$cells ($p<0.02$) (figure 5.12). Lysosensor yellow/blue probe was used to detect differences in lysosomal pH. While there was a small reduction in lysosomal pH detected in the *cbCln3*$^{\Delta ex7/8}$ compared to cb*Cln3*$^{+/+}$, this was not a significant decrease ($p>0.05$).

5.8 Discussion

A majority of JNCL patients carry the 1kb deletion in the *CLN3* gene, which is predicted to result in the formation of a truncated protein product which is either rapidly degraded or non-functional (Kwon et al., 2005). Two mouse models have been produced (*Cln3*$^{\Delta ex7/8}$ *and Cln3*$^{\Delta ex7/8insneo}$) which lack exons 7-8 in the *Cln3* mouse gene to replicate the 1kb mutation commonly seen in humans, as well as a third model which has exons 1-6 missing and is considered a knockout *Cln3* mouse model (*Cln3*$^{\Delta ex1-6}$) (Cao et al., 2006, Weimer et al., 2009). While similar phenotypes have been shown across the three different mouse models there are still some phenotypic differences exhibited between the different mouse models (e.g. seizures etc). A result of the differences in phenotypes observed between the three mouse models has led some people to suggest that the Cln3 protein in these mouse models is still maintaining some functionality. The *Cln3*$^{\Delta ex7/8}$ mouse model is described as a knock-in of the common 1kb mutation (Cotman et al., 2002) which encodes a mutant CLN3 with a native C-terminus (Mao et al., 2003).

One of the most prevalent phenotypes associated with JNCL is the loss of motor coordination that can potentially be attributed to defects in the cerebellum as a result of CLN3 mutation. While cerbella cells derived from the *Cln3*$^{\Delta ex7/8}$ mouse model have been produced, little work has been done to characterise key phenotypic changes that occur in these cells due to *Cln3* mutation. Phenotyping the *Cln3*$^{\Delta ex7/8}$ was done to detect any key changes such as lipid levels, metal ion content and lysosomal pH and enzyme activities allowing us to determine the key defects resulting

in pathogenesis in the *Cln3* mutant cerebellar cells. Some work was also done on phenotyping human fibroblasts that possessed the 1kb *CLN3* mutation as well as fibroblast cells that possess the rare D416G mutation. This missense mutation is the only mutation that induces JNCL disease that is found in the C-terminus region of the CLN3 protein.

5.8.1 Lysosomal pH in CLN3 mutant cells

It has been suggested by many groups that the pH of lysosomes is altered in CLN3 mutant cells. However there are conflicting reports on whether the pH in lysosomes of CLN3 mutant cells is higher or lower, with this change in pH often attributed to defects in lysosomal enzyme activity in this disease (Golabek et al., 2000). By using the lysotracker green probe (figure 5.1) we first wanted to see if the levels of lysosomes present were increased in the different cerebellar and fibroblast genotypes. As lysotracker green requires a low pH to fluoresce it would give an indication if there was a major change in the pH of the mutant lysosomes. No difference in lysosomal levels was detected with the use of lysotracker green between cb*Cln3*$^{+/+}$ or cb*Cln3*$^{\Delta ex7/8}$ cells which appears to suggest that there is no lysosomal expansion occurring in the two different genotypes and that the pH is similar otherwise the probe would be dimmer. It was a little surprising that there was no change in lysotracker staining present between the two different cerebellar genotypes as it had previously been reported using these cells that lysotracker fluorescence decreases in the cb*Cln3*$^{\Delta ex7/8}$ cells, suggesting a elevated pH problem

(Cao et al., 2011). However a key difference in this phenotype observed between this study and the previous one was that they performed lysotracker on fixed cells. When a cell is fixed it results in pores forming in all the organelle membranes including lysosomes, causing them to no longer be able to maintain their pH gradient. This loss of pH in the fixed cells would explain why they observed decreased lysotracker staining in the same cell type compared to our findings.

Lysotracker staining was elevated in the CLN3 fibroblast cells possessing the 1kb mutation which would seem to suggest that there is an expansion in the lysosomal system in this genotype (perhaps complementary to elevated lipids), commonly observed in other lysosomal storage disease due to the accumulation of primary and secondary storage products. Interestingly the levels of lysosomes detected in the CLN3 D416G mutants were similar to that seen in wild type fibroblast cells, which would appear to indicate that there is no expansion in the lysosomal system in this genotype. Our findings on the levels of cathepsin B and L activity showed that there was no difference in the activity of either of these enzymes in the cb*Cln3*$^{+/+}$ or cb*Cln3*$^{\Delta ex7/8}$ cells suggesting that there is no drastic change in the pH levels of the lysosomes in the *Cln3* mutant cerebellar cells (figure 5.2). There was however an increase in the activity of these two cathepsin enzymes found in the CLN3 1kb and D416G mutant cells. As there is an increase in activity of these cathepsin enzymes it would suggest that the enzymes in these cells are more active, otherwise we would expect to see a drop in the enzymes activity. The use of intracellular pH probes (figure 5.12) also showed there was no

significant change in the pH levels in *Cln3* mutant lysosomes which correlates with lack of change in cathepsin activity observed in the two cerebellar cell types.

5.8.2 Mitochondrial function

One of the most predominate phenotypes observed across the majority of different cell types that possess a mutant CLN3 protein is the accumulation of subunit c of mitochondrial ATP synthase in lysosomes, which has led people to speculate that there is a problem with mitochondrial function in these mutant cells. When analysing the two cerebellar cell types there appeared to be no difference in the levels of both mitochondrial levels or the amount of mitochondrial produced ROS in the cells (figure 5.4). This was surprising as it had previously been reported using these same cells that there was an increase in the levels of subunit c in these cells, which would suggest a potential mitochondrial problem (Cao et al., 2011). The levels of mitochondria produced ROS were lower however in both the CLN3 1kb and D416G fibroblast cells. The difference observed in the CLN3 mutant fibroblast cells might be due to autophagic clearance defects, which do not seem to be present in the mutant cerebellar cells.

5.8.3 CLN3 mutations increase ER stress

Recent work performed on SH-SY5Y cells has suggested that an increase in the levels of *CLN3* expression in cells helped reduce the levels of ER stress when cells were treated with the ER stress inducing agent tunicamycin (Wu et al., 2014). A knockdown in the expression of *CLN3* resulted in an increase in the levels of ER stress, with elevated levels of the pro-apoptotic CCAAT/-enhancer-binding protein homologous protein (CHOP) (Wu et al., 2014). While there was only a marginal increase in the levels of the ER Ca^{2+} influx channel pump SERCA2 in the cb*Cln3*$^{\Delta ex7/8}$ cells there did appear to greater ER staining present in these cells compared with the cb*Cln3*$^{+/+}$ cells (figure 5.5). The increase in ER staining may be indicative of and increase in ER stress (Lindholm et al., 2006). There was an increase in the levels of SERCA2 present in the CLN3 1kb and D416G mutant cells, which could also be indicative of an increase in ER stress. Further work needs to be done to determine if down stream activators of ER stress such as CHOP are elevated in the CLN3 mutant cells.

5.8.4 Storage of lipids in CLN3 mutant cells

It has already been shown in some studies that there was lipid storage occurring in *CLN3* mutated lymphoblast cells, suggesting that the absence of CLN3 results in disruptions in lipid trafficking and metabolism (Rusyn et al., 2008). There was an increase in the levels of LPBA and

sphingomyelin in the cb*Cln3*$^{\Delta ex7/8}$ when compared with the cb*Cln3*$^{+/+}$ cells (figure 5.6). It has been found that sphingomyelin increases in *CLN3* mutated lymphoblasts possibly due to the accumulation of ceramide, reducing sphingomyelin degradation (Kang et al., 2013). This increase in sphingomyelin was present also in the CLN3 1kb and D416G mutant fibroblast cells, which would suggest that this increase in sphingomyelin is present in different mutated *CLN3* cell lines. The increase in the phospholipid LBPA has not been characterised before in mutant CLN3 cells, however it has been reported that there are lower levels of LBPA in CLN3 disease cells (Hobert and Dawson, 2007). LPBA has been found to be localised primarily in the late endosomes and has been speculated to be involved in regulating endosomal cholesterol content. Levels of endosomal cholesterol were found to decrease when LBPA was decreased due to the reduced storage capacity in the endosomal compartments (Chevallier et al., 2008). Therefore if LBPA were increased we would expect to see an increase of cholesterol in the cell. This was not the case with the cb*Cln3*$^{\Delta ex7/8}$ cells that had higher LBPA levels as the cholesterol levels detected in these cells was the same as that in the cb*Cln3*$^{+/+}$ cells. Interestingly however the levels of LBPA appeared to decrease in the CLN3 1kb and D416G mutant fibroblast cells, however the cholesterol present in these cells was elevated, particularly in the D416G mutant which had the lowest LBPA levels present. This would seem to suggest that LBPAs role in controlling the endosomal levels of cholesterol are still not fully understood.

5.8.5 CLN3 as a Golgi protein?

The localization of the CLN3 protein is still subject to debate in the NCL field. Many studies have implicated the presence of CLN3 in the late endosomal/lysosomal part of the cell as many studies into JNCL have found defects in lysosomal pH, deficiencies in bulk endocytosis as well as a defect in autophagosome maturation which requires fusion with lysosomes (Cotman and Staropoli, 2012). However some have speculated that the CLN3 protein is localized to the Golgi. Work that has implicated CLN3s role in the Golgi has primarily been done in *S.pombe* yeast. Recent studies using this yeast model have found that Btn1p deletion (Battennin the yeast orthologue of CLN3) results in disruption of the Golgi morphology as well as problems in the correct sorting of Golgi associated proteins such as the mannose-6-phosphate receptor (Codlin and Mole, 2009). Staining with a Golgi marker on the two cerebellar *Cln3* genotypes as well as in the CLN3 1kb and D416G mutant fibroblasts revealed that there appeared to be no changes in the morphology of the Golgi in these cells (figure 5.7). This would suggest that in these cell types the CLN3 protein is not acting on the Golgi. However it would be interesting to see if mannose-6-phosphate is mislocalised in these cells, to determine if there is a defect in the trafficking of some lysosomal enzymes.

5.8.6 Changes in metal ion content in cb*Cln3*$^{\Delta ex7/8}$ cells

Metal ions have many important roles in the cell such as acting as important co-factors for enzymes, however elevated levels have been found to induce cellular toxicity (Grubman et al., 2014). Levels of Cu^{2+} and Fe^{2+} were found to be elevated in cb*Cln3*$^{\Delta ex7/8}$ (figure 5.8), which supports previous work done that has found elevated levels of these metal ions in the brains of *Cln3* mutant mice (Grubman et al., 2014). This dysregulation in metal ion homeostasis could be due to CLN3s proposed role in metal ion transport as it has been found to be similar to the Major facilitator superfamily group of transmembrane metal ion transporters.

5.8.7 Elevated rate of endocytic trafficking

Correct endocytic trafficking is important for cells to process, deliver and recycle molecules to their correct cellular location. Defects in lysosomal function due to the accumulation of lipids or transport problems can result in the retardation of endocytic trafficking and the recycling of lipids.

As the early endosome is the first endocytic organelle found in the endocytic pathway we investigated structural components to determine if early endosome localisation or levels were different in the *CLN3* and *Cln3* mutant cells (figure 5.9). What was observed was an expansion of the early endosomal system in these CLN3 mutant cells which might be an indication that these organelles are capable of trafficking a greater volume of extracellular molecules along the initial part of the endocytic

pathway, or that there is a defect in transport (upregulation). Both a CtxB trafficking assay and dextran fusion assay were utilised to determine the rate of endocytic trafficking in the *CLN3* and *Cln3* mutant cells (figures 5.10 and 5.11). In the cb*Cln3*$^{\Delta ex7/8}$ cells there was faster endocytic trafficking exhibited. This contradicts some studies which have suggested that the loss of CLN3 would result in retarded endocytic trafficking due to its proposed close interaction with the Hook1 protein which is important for microtubule coordination and interactions with different Rab proteins to mediate correct endocytic trafficking (Luiro et al., 2004). Endocytic trafficking levels has previously been analysed in the cb*Cln3*$^{\Delta ex7/8}$ before where slower endocytic trafficking was observed in these cells (Cao et al., 2011). However the group used FITC-dextran to measure trafficking rates, and this dextran is pH sensitive. This pH sensitivity could mean that the FITC-dextran was trafficked to lysosomes much faster in the cb*Cln3*$^{\Delta ex7/8}$ where its fluorescence quenched due to the pH, making it appear that there was less endocytic uptake of the fluorescent dextran. Despite this there is accelerated endocytic trafficking present in the cb*Cln3*$^{\Delta ex7/8}$ cells and this has been shown using two different methods. There was elevated endocytic trafficking observed in the two CLN3 mutant cells as well, which implies that the effect of CLN3 mutant is conserved in this sense between cerebellar and fibroblast cells.

5.8.8 Lysosomal Ca^{2+} levels in cb*Cln3*$^{\Delta ex7/8}$

Ca^{2+} is an important ion in the cell, and it has an important role to play in regulating endocytic trafficking. An example of this would be in the lysosomal storage disease NPC1 where low levels of lysosomal Ca^{2+} have been measured which results in defects of late endosomal-lysosomal fusion. This defect arises due to large amounts of Ca^{2+} being required to mediate the fusion process (Lloyd-Evans and Platt, 2011). This loss of efficient fusion causes defects in the endocytic pathway leading to slower endocytic trafficking. While Ca^{2+} has been measured in NPC1 lysosomes, no work has been done to quantify the levels of Ca^{2+} in *Cln3* mutant cells. Using an intracellular Ca^{2+} probe to measure lysosomal Ca^{2+} levels there was a significant increase in the lysosomal Ca^{2+} store in cb*Cln3*$^{\Delta ex7/8}$ cells. This elevated Ca^{2+} could potentially be responsible for the accelerated trafficking being observed in these cell types.

5.8.9 Overview

Our results from this chapter show differences in the phenotypes observed between mutant CLN3 in cerebellar and fibroblast cells. This highlights the need to study different cell lines of the same disease to help further our understanding of the pathogenesis occurring in cells that are found in different parts of the body. While some lipids appeared to be elevated in in the cerebellar cells, their excess storage may still be

downstream of the initial mechanisms that result from *Cln3* mutations in cerebellar cells. The ER stress observed in the cerebellar cells could indicate that this might be a result of Ca^{2+} homeostasis problem as it is the largest Ca^{2+} store inside the cell and its close interactions with the lysosome may go some way as to explaining the increase in lysosomal Ca^{2+} levels. The work done on the fibroblast cells which possess the two different CLN3 mutations display more elevation in lipid storage when compared with what was seen in cerebellar cells. However, further work must be done on the two CLN3 mutants to accurately measure changes in lysosomal pH and Ca^{2+}. It should also be noted that the fibroblasts had more heterogenous differences, this could possibly be due to them being patient fibroblasts, which other gene variations might be present. From the initial analysis done on the two CLN3 fibroblasts it would appear that the CLN3 1kb mutation produces a more severe phenotype than that seen in that seen in the D416G cells. This could possibly be because the D416G mutant protein is still getting to its correct cellular location, but its function has been impaired by the point mutation in the C-terminus of the CLN3 protein.

Very little has been done in the CLN3 field on cellular Ca^{2+} level changes. With the evidence that suggests that intra-lysosomal Ca^{2+} is elevated in cb*Cln3*$^{\Delta ex7/8}$ it was important next to determine if this has a knock on effect on other Ca^{2+} stores found in the cell. Also it is important to determine the main cause as to why there is elevated Ca^{2+} inside lysosomes.

Chapter 6: Altered homeostasis in intracellular Ca^{2+} stores

Noticeable phenotypes observed in the *Cln3*$^{\Delta ex7/8}$ cerebellar cells were faster endocytic trafficking, thickening of the ER as well as elevated Ca^{2+} levels in the lysosome (Chapter 5 results). The elevated lysosomal Ca^{2+} might explain the other two key phenotypes observed, as there may be dysfunction in cellular Ca^{2+} homeostasis in *Cln3*$^{\Delta ex7/8}$ cerebellar cells.

6.1 Ca^{2+} homeostasis in CLN3 mutant cells

The large levels of lysosomal Ca^{2+} found in *Cln3*$^{\Delta ex7/8}$ cerebellar cells would strongly suggest that CLN3 is involved in the regulation of Ca^{2+} in this store. As Ca^{2+} is a potent cellular messenger that is involved in numerous cellular roles including apoptosis (Galione et al., 2014), it is important to determine if there are any changes in major Ca^{2+} stores in CLN3 cells.

Very few studies have looked at cellular changes in Ca^{2+} levels in *CLN3* mutant cells.

Work done in human SH-SY5Y cells (precursor neuroblastoma cells) utilized siRNA to knock down expression of *CLN3* to measure changes in total intracellular Ca^{2+} levels (An Haack et al., 2011). The use of siRNA appeared to only partially reduce the expression of the CLN3 protein however, suggesting that the siRNA used was not particularly effective. The result of siRNA induced CLN3 knock down resulted in an increase in intracellular Ca^{2+} levels observed. However the Ca^{2+} response after KCl induced depolarization was no different than that seen in the wild type cells analysed. The study then looked into the use of Ca^{2+} channel

modulators to see if these could correct the elevated intracellular Ca^{2+} levels due to CLN3 depletion. L-type Ca^{2+} channel inhibitors were chosen from the Ca^{2+} modulators screened, which were amlodipine, flunarizine, R(+) Bay K8644, nimodipine, nicardipine and nifedipine. The study proceeded to combine all these modulators together and incubated the CLN3 depleted cells to determine if this reduces intracellular Ca^{2+} levels. The treatment with multiple different L-type Ca^{2+} channel inhibitors did result in a decrease in the intracellular Ca^{2+} levels in the CLN3 depleted cells. The same group did a follow up study using siRNA to knockdown CLN3 levels in primary neurons (Warnock et al., 2013), in an effort to replicate an accurate model of the human disease. Knockdown of CLN3 by siRNA resulted in an elevation in intracellular Ca^{2+}. Cellular membrane depolarization with KCL resulted in a significant increase in intracellular Ca^{2+} levels, however this elevation was abolished with the addition of amlodipine.

This study highlights the potential use of L-type Ca^{2+} inhibitors to treat intracellular Ca^{2+} abnormalities that may occur in *Cln3*$^{\Delta ex7/8}$ cerebellar cells. But this also illustrates the difference in cell type with no KCl effect in SH-SY5Y cells, showing the importance for using suitable cells.

Another study has previously suggested that the CLN3 protein interacts with the pro-apoptotic protein calsenilin, a neuronal Ca^{2+} binding protein (Chang et al., 2007). Calsenilin binds to the C-terminus of presenilin 1 and 2 proteins and acts as a transcription repressor in the ER (Carrion et al., 1999). Calsenilin is believed to regulate diverse Ca^{2+} mediated signals, where it is involved in sensitizing neuronal cells to Ca^{2+} induced

apoptosis (Lilliehook et al., 2002). CLN3 protein was found to interact with calsenilin via a yeast two-hybrid yeast system, and it was speculated that CLN3 plays an anti-apoptotic role in the cell as a decrease in CLN3 levels and an increase in calsenilin levels resulted in increased apoptosis (Chang et al., 2007). While the mechanisms on how CLN3 interaction with calsenilin is involved in the regulation of apoptosis remains unknown, it has been suggested that mutations in *CLN3* result in the mutant CLN3 protein accumulating in the ER. The accumulation of the mis-trafficked protein may then induce ER stress, leading to dysregulation of the ER Ca^{2+} store and an increase in Ca^{2+} induced apoptosis (Chang et al., 2007).

The suggestion that CLN3 mutant proteins accumulate in the ER, inducing an increase in ER stress was further explored in a study that utilizes the ER stress inducing agent, tunicamycin (Wu et al., 2014). The ER stress response is a highly conserved function, which results in pro-apoptotic signals being released from the ER due to the unfolded protein response (Smith et al., 2011). ER stress response mediated apoptosis has previously been reported in *CLN3* mutant cells (Galizzi et al., 2011). Short hairpin RNAs were treated to SH-SY5Y cells to knockdown CLN3 expression. ER stress was then induced with tunicamycin, and this resulted in an increase in apoptotic cells. Overexpression of CLN3 resulted in a greater resistance to tunicamycin induced ER stress response, suggesting a role in suppressing Ca^{2+} induced apoptosis via the ER stress response pathway (Wu et al., 2014).

6.2 The role of CLN3: A lysosomal Ca^{2+} leak channel?

CLN3 has been found to have similarity with the major facilitator superfamily group of ion transporters (Pao et al., 1998). Because of this similarity and several studies implicating lysosomal pH irregularities in *CLN3* mutant cells it is possible that CLN3 is pH regulated or H^+ permeant. Although our data suggests that there is no difference in pH in *Cln3*$^{\Delta ex7/8}$ cerebellar cells when compared with wild type cells (results chapter 5).

The accelerated endocytic trafficking observed and the elevated lysosomal Ca^{2+} is similar to phenotypes seen in another lysosomal storage disease, mucolipidosis type IV (MLI V). TRPML1 (transient receptor potential cation channel 1) is the protein affected in MLIV and it is believed to be a Ca^{2+} leak channel located on the late endosome membrane, with the protein also believed to be pH sensitive so that it is only active in the late endosome (LaPlante et al., 2002). Other Ca^{2+} leak channels have been implicated in indirectly affecting lysosomal function, such as presenilin 1 (associated in familial Alzheimer's disease) (Lee et al., 2010).

CLN3 is strongly linked in being protective against apoptosis, similar to the function of another anti-apoptotic protein known as Bax inhibitor 1 (Bi-1).

Bi1 itself is a member of the highly conserved Transmembrane Bax Inhibitor-1 containing motif proteins (TMBIM) (Bultynck et al., 2012). BI-1 has recently been found to be an important factor in controlling ER

induced apoptosis via lowering the Ca^{2+} content of the ER. The Bi-1 protein has been found to possess a pH sensitive domain within its last 9 amino-acids, which supports the evidence that this protein acts as a H^{+}/Ca^{2+} antiporter where protons from the cytosol are pumped into the ER lumen in exchange for the release of ER Ca^{2+} to alleviate ER stress. The Ca^{2+} releasing domain was found to be on the C-terminus of the Bi-1, and the key residue was discovered to be an aspartic acid, which when changed to a glycine didn't release Ca^{2+} (Bultynck et al., 2012).

The topology of Bi-1 and CLN3 are very similar, as they both have 6 transmembrane domains, with the C-terminus of both proteins facing out into the cytosol (Bultynck et al., 2012, Mao et al., 2003). The C-terminus has also been suggested to transiently be in one of either two configurations where it is either embedded in the membrane or out into the cytosol (Mao et al., 2003). These two potential configurations may suggest that the orientation of the C-terminus of either protein changes when the protein becomes active. The similarities in the topology of Bi-1 and CLN3 as well as their suggested roles in protection against apoptosis warrants further investigation into a potential overlap of function. Recent work has found that Bi1 shares homology with a bacterial membrane transporter found in the bacteria *Bacillus Subtillis* called YetJ which has been found to be pH regulated and involved in Ca^{2+} transport across membranes (Chang et al., 2014). The YetJ protein does appear to have similarities with that of major facilitator superfamily, which could indicate, conserved functions present in YetJ, Bi-1 and the CLN3 protein.

As mentioned earlier, Bi-1 belongs to the TMBIM family of proteins which also include a Golgi protein called GAAP (Golgi anti-apoptotic protein). This may have some similarities with the CLN3 yeast orthologue Battenin.

6.3 Overview

The role of Ca^{2+} has not been characterized in CLN3 disease pathogenesis. The elevated Ca^{2+} seen in *Cln3*$^{\Delta ex7/8}$ lysosomes could suggest that CLN3 is involved in regulating Ca^{2+} in the lysosome, possibly by leak. The similarities between CLN3 and Bi1 structure could possibly reveal CLN3's true role in the cell, and these possible similarities will be explored. CLN3's role in conferring resistance to the ER stress response will also be explored as it is possible that the mutant Cln3 protein in the cerebellar cells are stuck in the ER contributing to an increase in ER stress.

6.4 Results

Our previous work measuring intra-lysosomal Ca^{2+} levels showed elevated lysosomal Ca^{2+} in the $Cln3^{\Delta ex7/8}$ cerebellar cells. Ca^{2+} dysregulartion may result in pathogenic mechanisms that give rise to CLN3 phenitypes so it is important to determine the regulation and storage of Ca^{2+} in these cells.

6.4.1 Baseline cytosolic Ca^{2+} levels

Resting baseline levels of Ca^{2+} was measured to determine if there is an elevated resting Ca^{2+} level in the $Cln3^{\Delta ex7/8}$ cerebellar cells.

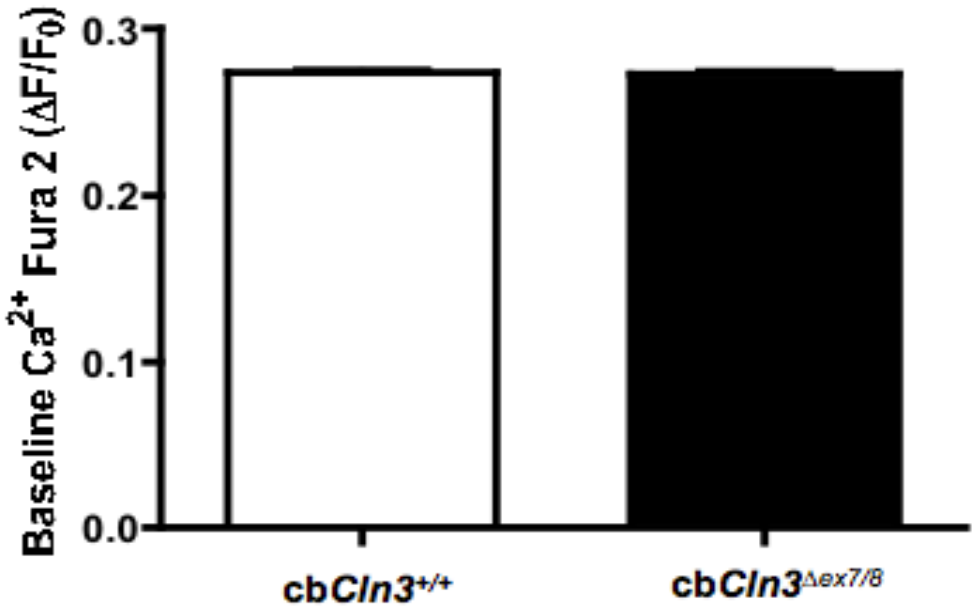

Figure 6.1: This was analysed in both cbCln3$^{+/+}$ and cbCln3$^{\Delta ex7/8}$ cells. No difference was found in the resting cytosolic Ca^{2+} levels between cbCln3$^{+/+}$ and cbCln3$^{\Delta ex7/8}$ cells. Values represent mean ± SD, n=10, P >0.05, >200 cells analysed.

Baseline, unstimulated, Ca^{2+} levels of the cytosol were analysed and the observed in the cytosolic Ca^{2+} levels between cb*Cln3*$^{+/+}$ and cb*Cln3*$^{\Delta ex7/8}$ cells over multiple different experiments. This would indicate that any changes observed in intracellular Ca^{2+} observed in cb*Cln3*$^{\Delta ex7/8}$ cells are likely to arise in defects from the major Ca^{2+} stores in the cell.

6.4.2 Ca^{2+} responses in cbCln3$^{+/+}$ and cbCln3$^{\Delta ex7/8}$ cells treated with sub-inhibitory 0.1μM Thapsigargin

As there was no difference in the resting Ca^{2+} levels in the cells, there may be a difference in the Ca^{2+} content of the different organelles. The ER is the largest Ca^{2+} store in the cell, so its Ca^{2+} content was measured using the drug Thapsigargin. Thapsigargin is a SERCA pump inhibitor that causing the release of ER Ca^{2+} by preventing Ca^{2+} uptake into the ER, thus causing a Ca^{2+} gradient difference across the ER membrane. 0.1μM thapsigargin is a sub-inhibitory concentration of thapsigargin so it should not induce a large ER Ca^{2+} release.

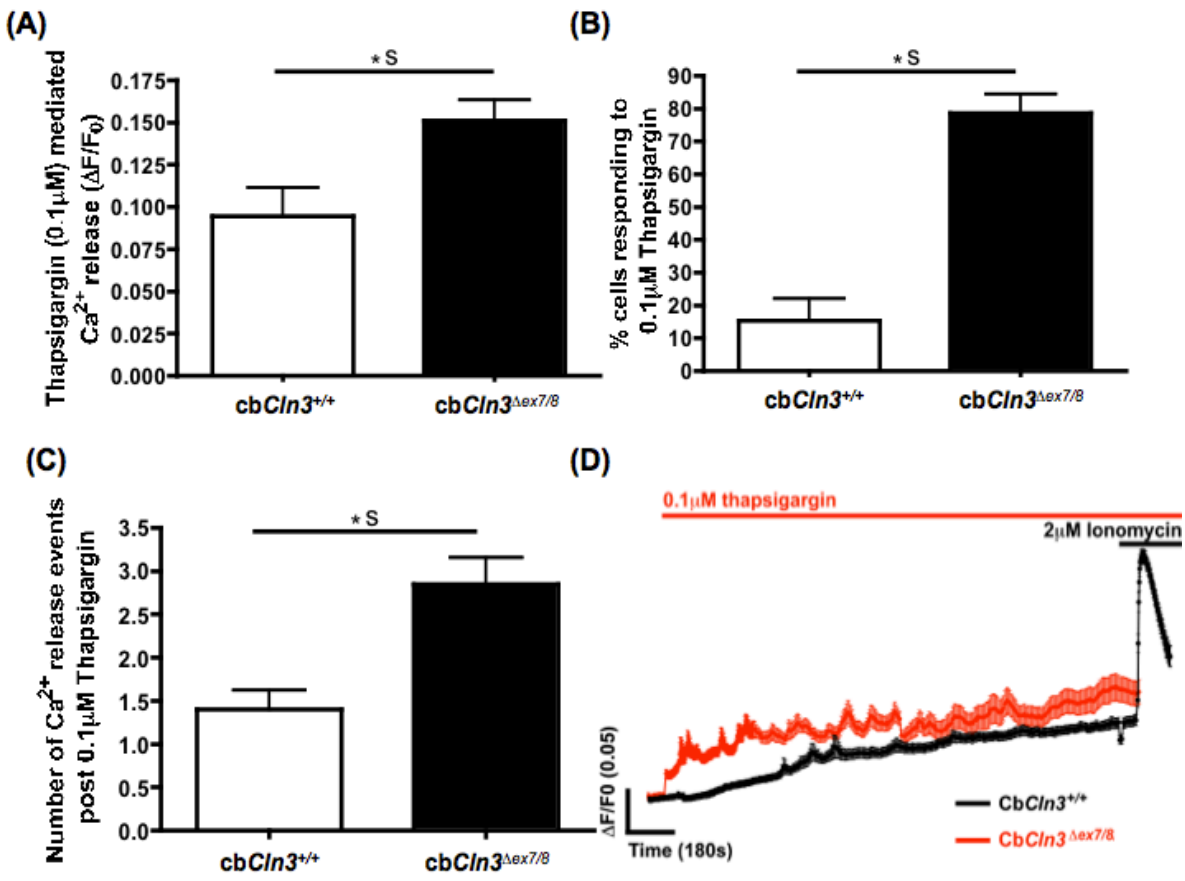

*Figure 6.2: (A) Significantly higher levels of ER Ca^{2+} release was observed in the cbCln3$^{\Delta ex7/8}$ cells when compared with cbCln3$^{+/+}$ cells. (B) Significantly more cells responded to the low levels of thapsigargin in the cbCln3$^{\Delta ex7/8}$ when compared to the cbCln3$^{+/+}$ cells. (C) cbCln3$^{\Delta ex7/8}$ cells have significantly more ER Ca^{2+} release events when compared to cbCln3$^{+/+}$ cells. (D) Averaged traces from one representative experiment from which the data from (A), (B) and (C) were analysed. 2μM Ionomycin was added at the end of the experiment to show the cells were still alive. Values represent mean ± SD n=4, >60 cells analysed. *s denotes Significant (A) P<0.05 (B) P<0.01 (C) P<0.05.*

Significantly elevated levels of Thapsigargin induced ER Ca^{2+} release were observed in cb*Cln3*$^{\Delta ex7/8}$ cells when compared with cb*Cln3*$^{+/+}$ cells (figure 6.2 (A)). Despite the cells being treated with sub-inhibitory levels of thapsigargin, there was ~50% greater release seen from the ER Ca^{2+} store in the mutant compared to the cb*Cln3*$^{+/+}$ cells (figure 6.2 (A)). Also

~80% of cb*Cln3*$^{\Delta ex7/8}$ cells responded to thapsigargin addition compared to ~10% of cb*Cln3*$^{+/+}$ cells indicating that they are more sensitive to thapsigargin at a low levels (figure 6.2 (B). The cb*Cln3*$^{\Delta ex7/8}$ cells that did release Ca^{2+} also seemed to undergo a greater number of Ca^{2+} release events from the ER (~3 events on average) when compared with the few cb*Cln3*$^{+/+}$ cells that did respond only having a single Ca^{2+} release event (figure 6.2 (C)).

6.4.3 Ca^{2+} responses in cbCln3$^{+/+}$ and cbCln3$^{\Delta ex7/8}$ cells treated with 1μM Thapsigargin

A higher concentration of thapsigargin was added to cells to detect ER Ca^{2+} release when the concentration of thapsigargin has a greater inhibitory effect.

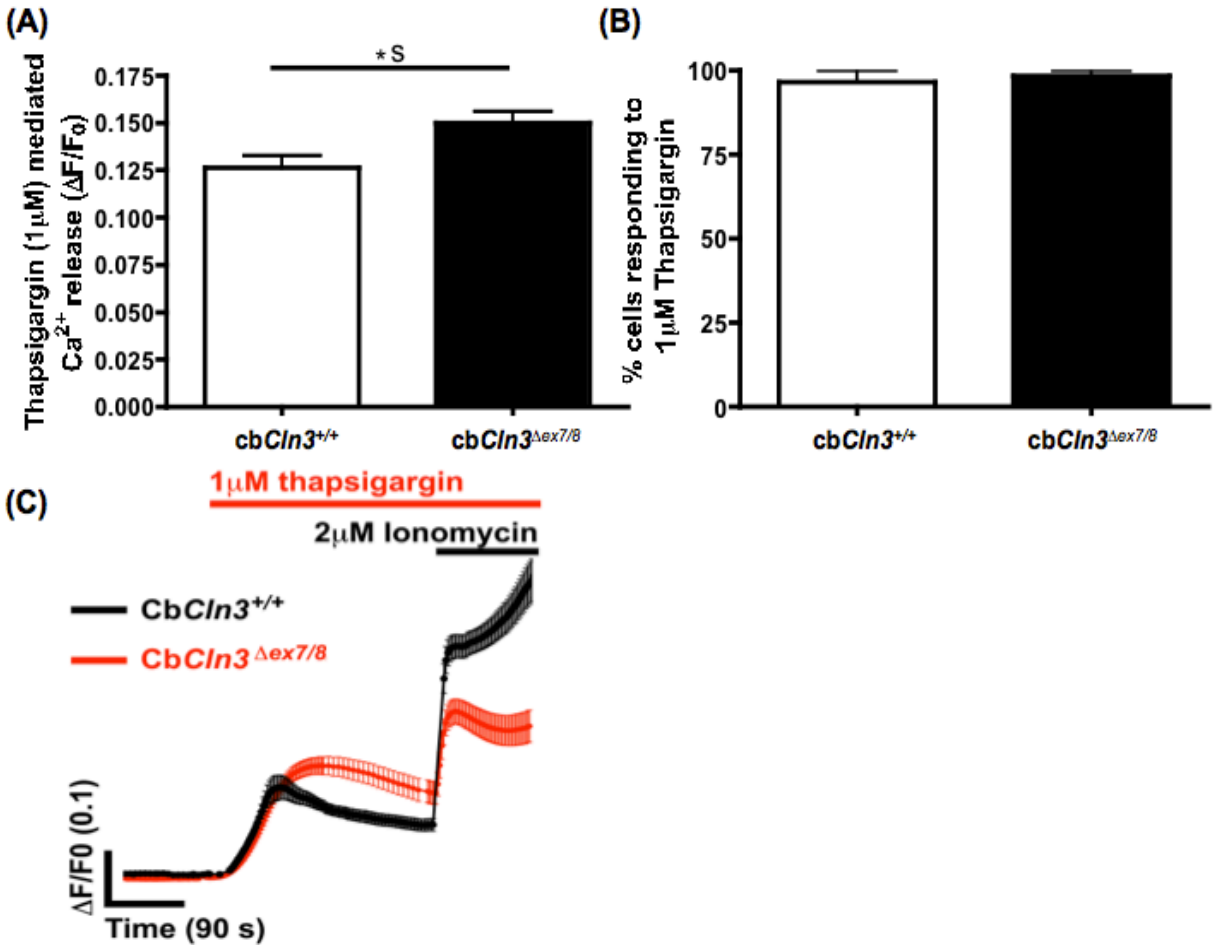

*Figure 6.3: (A) Significantly higher levels of ER Ca^{2+} release were observed in the cbCln3$^{\Delta ex7/8}$ cells when compared with cbCln3$^{+/+}$ cells. (B) The same amount of cbCln3$^{+/+}$ and cbCln3$^{\Delta ex7/8}$ cells responded to thapsigargin treatment. (C) Averaged data from one experiment to illustrate a reduction in the difference in level of Ca^{2+} released between cbCln3$^{+/+}$ and cbCln3$^{\Delta ex7/8}$ cells and that there is now only a single Ca^{2+} event observed following 1μM thapsigargin treatment in both cell types. 2μM Ionomycin was added at the end of the experiment to show the cells were still alive. Values represent mean ± SD, n=3, >50 cells analysed. *s denotes Significant (A) P<0.01 (B) P>0.05.*

Treating both cell types with 1μM thapsigargin results in ~25% more Ca^{2+} being released from the ER in the cb*Cln3*$^{\Delta ex7/8}$ when compared with the cb*Cln3*$^{+/+}$ cells (figure 6.3). The difference in the amount of Ca^{2+} being

released from the two cell types is lower than with 0.1μM thapsigargin (figure 6.2). Again, unlike the previous experiment, the same percentage of cells responded to 1μM thapsigargin in the two cell types showing that this concentration of thapsigargin is ample for eliciting a Ca^{2+} response in most cb*Cln3*$^{+/+}$ cells. Also only one Ca^{2+} release event was observed in both cell types, indicating that this concentration causes significant Ca^{2+} release from the ER Ca^{2+} store in the two cell types to the extent that no further spontaneous events are observed.

6.4.4 Ca^{2+} response in cbCln3$^{+/+}$ and cbCln3$^{\Delta ex7/8}$ cells treated with 2μM Thapsigargin

An optimum inhibitory concentration of thapsigargin was added to cells to detect ER Ca^{2+} release.

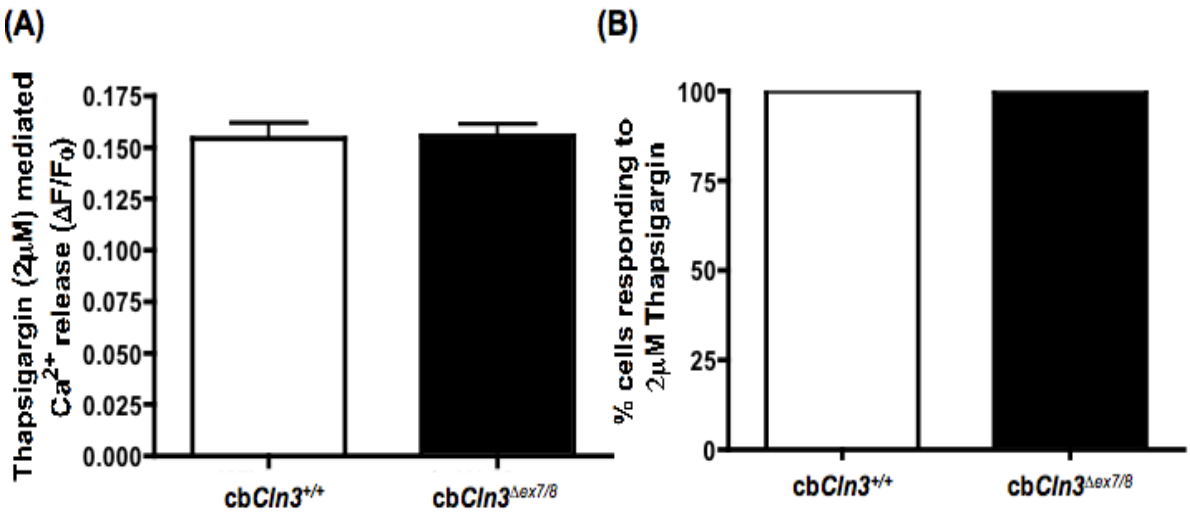

Figure 6.4: (A) Similar levels of ER Ca^{2+} release was observed in both cell types post 2μM thapsigargin treatment. (B) All cells from both cell types responded to 2μM thapsigargin treatment. Values represent mean ± SD, n=4, >60 cells analysed. (A) P>0.05 (B) P>0.05

Treating cb*Cln3*$^{+/+}$ and cb*Cln3*$^{\Delta ex7/8}$ cells with 2μM Thapsigargin resulted in all observed cells responding. The same amount of Ca^{2+} was also released from the ER store in the two cell types. This data shows that while 1μM thapsigargin is enough to completely empty the ER Ca^{2+} store in cb*Cln3*$^{\Delta ex7/8}$ cells (figure 6.3), cb*Cln3*$^{+/+}$ cells require 2μM thapsigargin to completely empty their ER Ca^{2+} store.

6.4.5 Store operated Ca^{2+} intake into the cells post ER clamping with 1μM Thapsigargin

Emptying of the ER Ca^{2+} store with thapsigargin leads to the requirement by the cell to refill the depleted store, this occurs via the action of the STIM1 and Orai channels that control store operated Ca^{2+} entry.

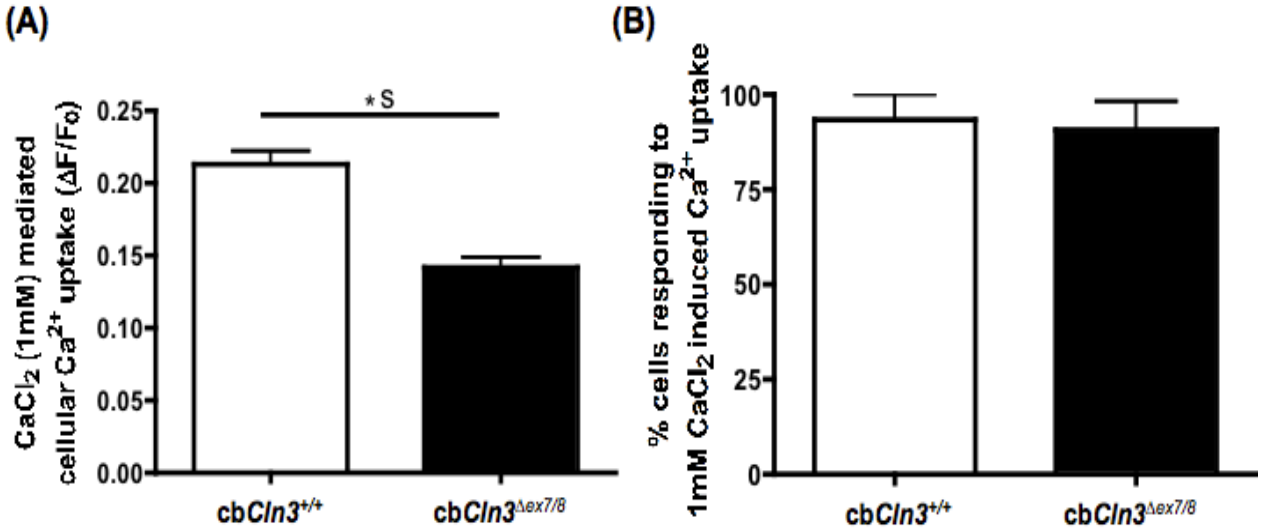

*Figure 6.5: (A) Significantly lower levels of store operated Ca^{2+} intake was observed in cbCln3$^{\Delta ex7/8}$ cells post ER clamping with 1μM thapsigargin treatment when compared with cbCln3$^{+/+}$ cells. (B) Similar levels of cells from both cell types responded to store operated uptake of Ca^{2+} into the cell. Values represent mean ± SD, n=3, >60 cells analysed. *S denotes significant (A) P<0.0001. (B) P>0.05.*

When thapsigargin is added in the absence of extracellular Ca^{2+}, store operated Ca^{2+} entry does not occur as there is no extracellular Ca^{2+} to be transported into the cell. Subsequent addition of 1mM Ca^{2+} outside the cell leads to the influx that can be measured (figure 6.5). Under these conditions we observed >50% increase in the amount of Ca^{2+} being brought back into the cell following ER Ca^{2+} store depletion in the cb*Cln3*$^{+/+}$ cells compared to cb*Cln3*$^{\Delta ex7/8}$ cells (figure 6.5). While the percentage of cells that underwent store operated Ca^{2+} re-entry was similar in both cell types, the lower amount of Ca^{2+} uptake seen in the cb*Cln3*$^{\Delta ex7/8}$ would indicate these cells either have defective store operated Ca^{2+} entry or have adjusted their response to reflect other alterations in cellular Ca^{2+} homeostasis.

6.4.6 Mitochondrial Ca^{2+} release following 10μM Rotenone treatment

Rotenone is a drug that induces Ca^{2+} release from the mitochondria by causing depolarization of the mitochondrial membrane by interfering with the mitochondria electron transport chain.

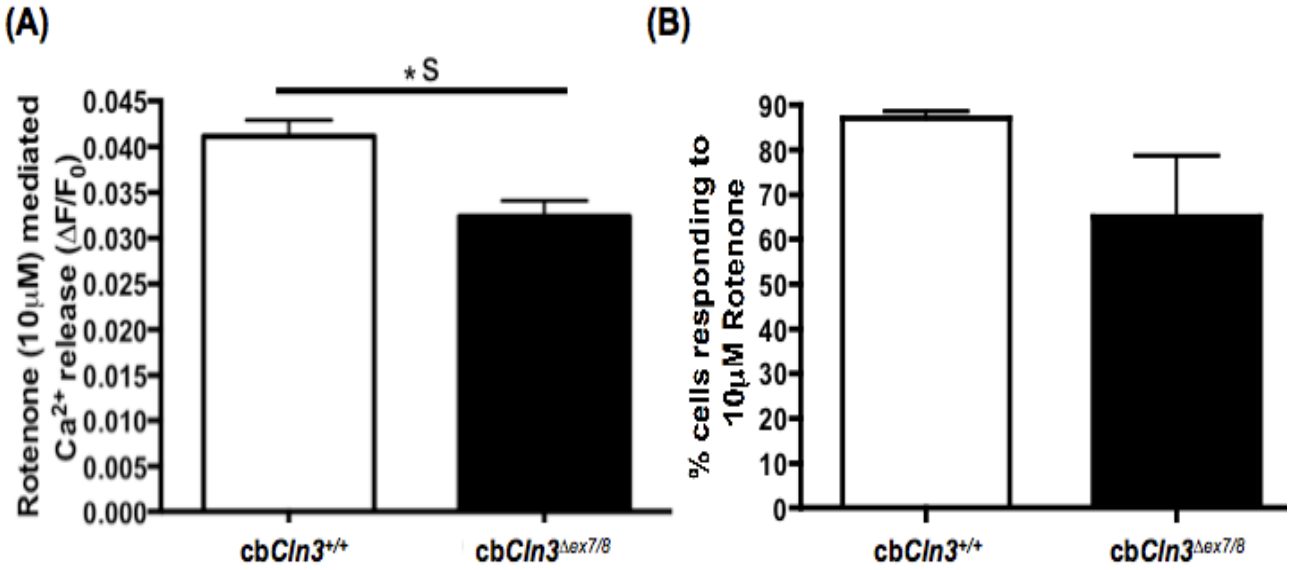

*Figure 6.6: (A) Significantly lower levels of mitochondrial Ca^{2+} release was observed in cbCln3$^{\Delta ex7/8}$ cells than in cbCln3$^{+/+}$ cells following the addition of 10μM Rotenone. (B) cbCln3$^{\Delta ex7/8}$ cells were less responsive to the addition of Rotenone as few cells responded when compared with cbCln3$^{+/+}$ cells. Values represent mean ± SD, n=3, >50 cells analysed. *S denotes significant (A) P<0.001. (B) P>0.05.*

Interestingly, cb*Cln3*$^{\Delta ex7/8}$ cells were less responsive to rotenone as a whole when compared with cb*Cln3*$^{+/+}$ cells. The cb*Cln3*$^{\Delta ex7/8}$ cells that did respond released significantly lower levels of Ca^{2+} from their mitochondria than what was observed in the cb*Cln3*$^{+/+}$ cells (figure 6.6). This would suggest that cb*Cln3*$^{\Delta ex7/8}$ mitochondria are less able to maintain their membrane potential, resulting in lower levels of Ca^{2+} being stored.

6.4.7 Lysosomal Ca^{2+} content following the addition of 200μM GPN

Using the lysosomotrophic agent GPN we were able to measure the lysosomal Ca^{2+} content in both cb*Cln3*$^{+/+}$ and cb*Cln3*$^{\Delta ex7/8}$ cells. This was done to determine if the lysosome Ca^{2+} content was elevated in the cb*Cln3*$^{\Delta ex7/8}$ cells as what was observed when using the intra-lysosomal Ca^{2+} probe Oregon Green-BAPTA.

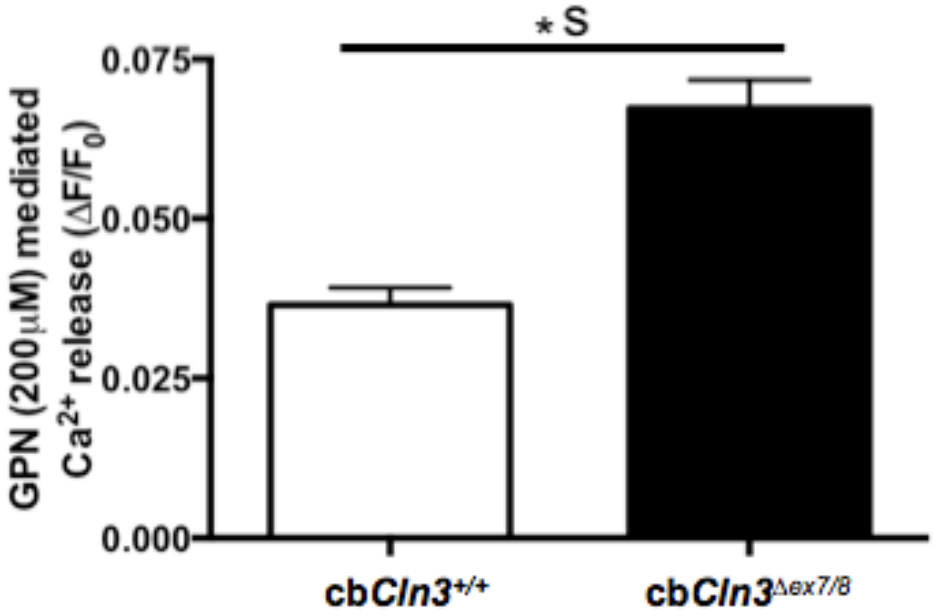

*Figure 6.7: By using the lysosomtrophic peptide GPN, greater levels of Ca^{2+} was detected in cbCln3$^{\Delta ex7/8}$ lysosomes when compared with cbCln3$^{+/+}$ lysosomes. Values represent mean ± SD, n=4, >50 cells analysed. *S denotes significant, P<0.0001.*

Using the lysosomotrophic agent GPN we were able to measure the lysosomal Ca^{2+} content in both cb*Cln3*$^{+/+}$ and cb*Cln3*$^{\Delta ex7/8}$ cells. The ER Ca^{2+} content was first clamped by the addition of 2μM thapsigargin so as to not mask the lysosomal Ca^{2+} levels post GPN addition as lysosomal Ca^{2+} release often induces Ca^{2+} release from the ER. Post clamping of

the ER, the addition of GPN revealed that the Ca^{2+} content of cb*Cln3*$^{\Delta ex7/8}$ lysosomes was significantly higher than the cb*Cln3*$^{+/+}$ lysosomes (>60%). This result recapitulates our earlier data (Chapter 5, figure 5.12) where we used intracellular Ca^{2+} probes to measure lysosomal Ca^{2+} levels which indicated there was higher Ca^{2+} levels present in cb*Cln3*$^{\Delta ex7/8}$ lysosomes than in cb*Cln3*$^{+/+}$ lysosomes.

6.4.8 : Lysosomal Ca^{2+} induced Ca^{2+} release from other cellular Ca^{2+} stores following the addition of 300μM GPN in the absence of any other Ca^{2+} agonist to clamp the intracellular stores

The release of Ca^{2+} from lysosomes has been shown to induce Ca^{2+} from other stores in the cell; primarily from the ER due to the close contact points the ER and lysosomes have inside the cell.

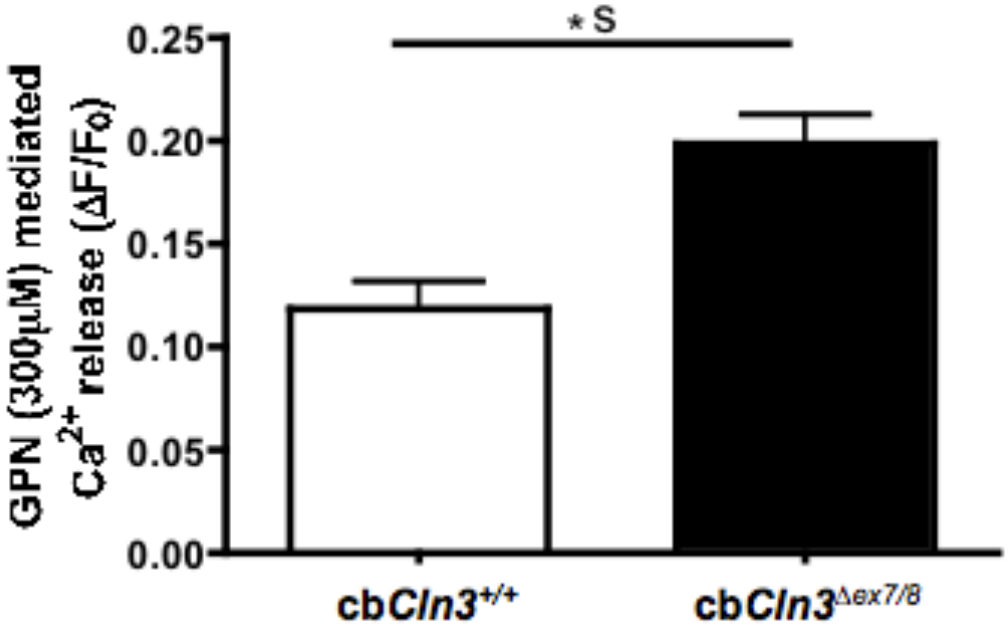

*Figure 6.8: (A) Lysosomal Ca^{2+} release induces the release of other Ca^{2+} stores, predominantely from the ER due to the close contact points between the lysosome and ER. Significantly greater levels of Ca^{2+} release were detected in the cb*Cln3*$^{\Delta ex7/8}$ cells compared with* cb*Cln3*$^{+/+}$*cells. (B) A greater amount of Ca^{2+} release events was observed in the cb*Cln3*$^{\Delta ex7/8}$ cells than in the* cb*Cln3*$^{+/+}$ *cells. Values represent mean ± SD, n=1, >20 cells analysed. *S denotes significant, (A) P<0.001.*

GPN induced lysosomal Ca^{2+} along with the release of Ca^{2+} from other stores (which were not clamped in this experiment) resulted in a significantly greater level of Ca^{2+} release in the cb*Cln3*$^{\Delta ex7/8}$ cells when compared to cb*Cln3*$^{+/+}$ cells (figure 6.8). Lysosomal Ca^{2+} release following GPN addition where the other Ca^{2+} stores are not clamped produces a greater Ca^{2+} release observed than when the other stores are clamped before the addition of GPN (figure 6.7). This is due to Ca^{2+} from other stores other than the lysosome. Interestingly, we observed multiple spontaneous Ca^{2+} release events (~2-3 on average) witnessed in the

cb*Cln3*$^{\Delta ex7/8}$ cells after an elevated Ca^{2+} release, however only a single release event was seen in the cb*Cln3*$^{+/+}$ cells.

6.4.9 Enhanced NAADP mediated Ca^{2+} release from cbCln3$^{\Delta ex7/8}$ cells can be inhibited by the TPC channel inhibitor Ned19

NAADP has been found to be a potent Ca^{2+} messenger molecule that specifically induces Ca^{2+} release from lysosomes by acting on the lysosomal membrane TPC2 channel.

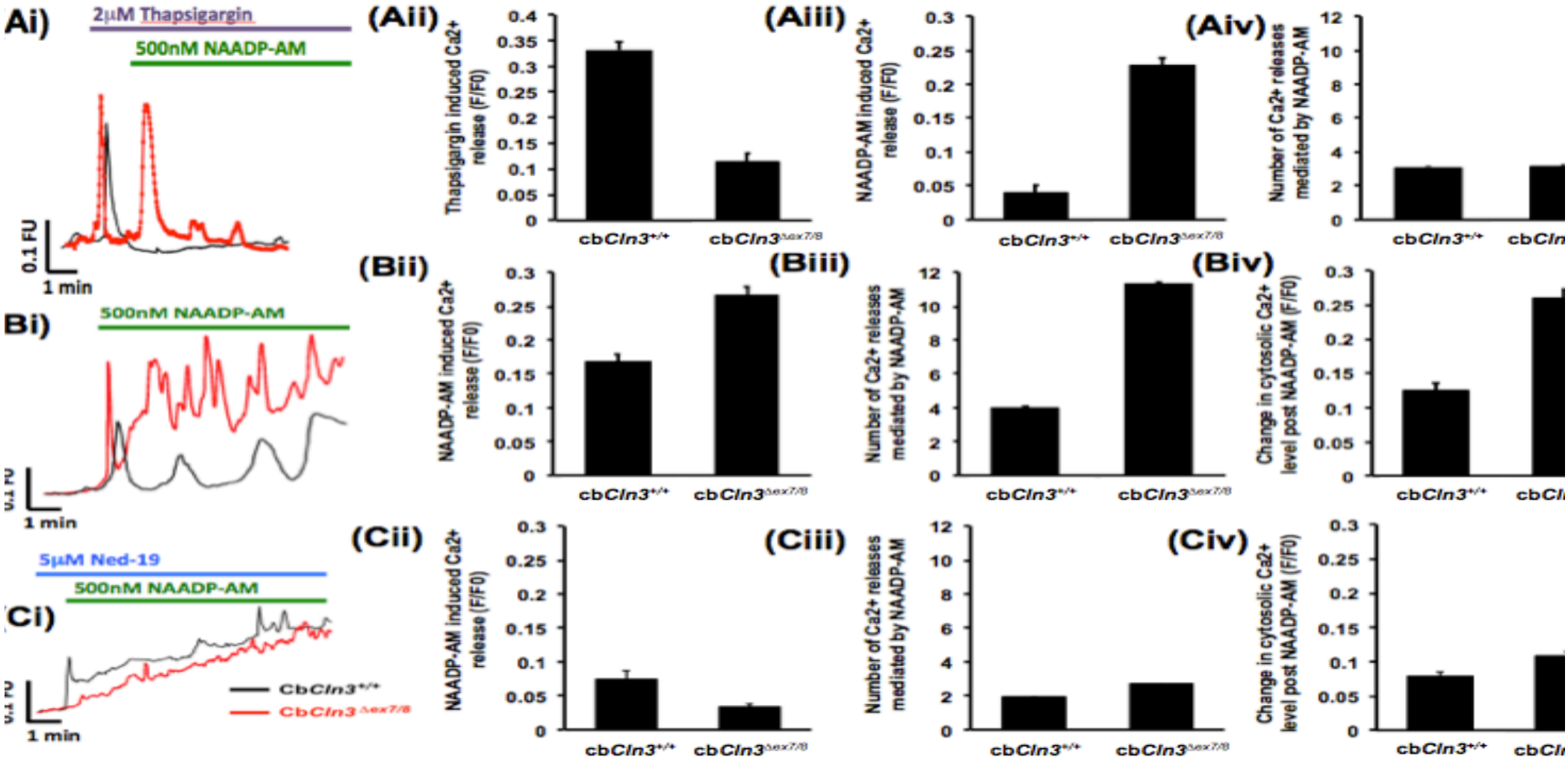
Ai)
2μM Thapsigargin
500nM NAADP-AM
0.1 FU
1 min
Bi)
500nM NAADP-AM
1 min
5μM Ned-19
500nM NAADP-AM
Ci)
1 min
Cb*Cln3*+/+
Cb*Cln3*Δex7/8
(Aii)
Thapsigargin induced Ca2+ release (F/F0)
(Aiii)
NAADP-AM induced Ca2+ release (F/F0)
(Aiv)
Number of Ca2+ releases mediated by NAADP-AM
(Bii)
NAADP-AM induced Ca2+ release (F/F0)
(Biii)
Number of Ca2+ releases mediated by NAADP-AM
(Biv)
Change in cytosolic Ca2+ level post NAADP-AM (F/F0)
(Cii)
NAADP-AM induced Ca2+ release (F/F0)
(Ciii)
Number of Ca2+ releases mediated by NAADP-AM
(Civ)
Change in cytosolic Ca2+ level post NAADP-AM (F/F0)
cb*Cln3*+/+
cb*Cln3*Δex7/8

*Figure 6.9: (Ai) Representative traces of the difference in NAADP mediated Ca^{2+} response following clamping of the ER Ca^{2+} store with 2μM Thapsigargin. (Aii) Levels of Ca^{2+} release from the ER in cb*Cln3*$^{+/+}$ and cb*Cln3*$^{\Delta ex7/8}$ cells. (Aiii) Amount of Ca^{2+} release observed between the two cell types following the addition of 500nM NAADP-AM. (AiV) Number of Ca^{2+} release events seen in cells following the addition of 500nM NAADP-AM in the two cell types. (Bi) Graph to illustrate the difference in 500nM NAADP-AM Ca^{2+} mediated response between the two cell types when the ER Ca^{2+} store has not been clamped. (Bii) Level of initial Ca^{2+} release observed in the two cell types after 500nM NAADP-AM addition without pre clamping of the ER store. (Biii) Number of Ca^{2+} release events observed in the two cell types following the addition of NAADP-AM. (BiV) Changes in the resting cytosolic Ca^{2+} level post NAADP-AM addition to the two cell types. (Ci) Ned19 blocks NAADP mediated Ca^{2+} release from the lysosomal TPC channels. Representative trace to show the dampening of the NAADP-AM Ca^{2+} release in the two cell types after the cells are pre-treated for 5minutes with 5μM Ned19. (Cii) Initial Ca^{2+} release from cells pre-treated with 5μM NED19. (Ciii) Number of Ca^{2+} release events seen in pre-treated Ned19 cells post NAADP-AM addition. (CiV) Changes in the resting cytosolic Ca^{2+} levels following the addition of NAADP-AM to pre-treated Ned19 cells. Values represent mean ± SD, n=2*

By first clamping the ER Ca^{2+} store with 2μM thapsigargin, the addition of 500nm membrane permeant NAADP-AM resulted in a much greater release (5 fold) of Ca^{2+} from the cb*Cln3*$^{\Delta ex7/8}$ cells than in the cb*Cln3*$^{+/+}$ cells (figure 6.9 (Aiii)). This would indicate that there is a greater Ca^{2+} release from the lysosome as well as other organelle Ca^{2+} stores, other than the ER in the cb*Cln3*$^{\Delta ex7/8}$ cells when compared with cb*Cln3*$^{+/+}$ cells. The number of Ca^{2+} release events exhibited in the two genotypes was the same (figure 6.9 (Aiv)) despite more Ca^{2+} release in the cb*Cln3*$^{\Delta ex7/8}$ cells. When the ER Ca^{2+} store is not first clamped prior to the addition of NAADP-AM we see a different response in the cells.

A similar amount of Ca^{2+} is released from cb*Cln3*$^{\Delta ex7/8}$ cells as was observed when the ER Ca^{2+} store had been clamped. However, a greater amount of Ca^{2+} was released in the cb*Cln3*$^{+/+}$ cells without ER clamping than with ER clamping prior to the addition of NAADP-AM (figure 6.9 (Aiv) and (Biii). This would suggest that adding NAADP-AM to the cells by itself is triggering subsequent ER Ca^{2+} release in response to lysosomal Ca^{2+} release in the cb*Cln3*$^{+/+}$ cells. Interestingly the number of Ca^{2+} events observed was greater in the cb*Cln3*$^{\Delta ex7/8}$ cells (~10) than what was seen in the cb*Cln3*$^{+/+}$ cells (~4) when only NAADP-AM is added. As well it is important to note that following the addition of NAADP-AM there is over a 100% increase in the baseline cytosolic Ca^{2+} level in cb*Cln3*$^{\Delta ex7/8}$ cells when compared with cb*Cln3*$^{+/+}$ cells, associated with a failure to return to normal baseline cytosolic Ca^{2+} levels (figure 6.9 (Biv)). This suggests the potential for higher levels of cytotoxicity occurring in the CLN3. The pre-treatment with 5μM Ned19 blocks NAADP mediated Ca^{2+} release via the lysosomal TPC channels. This inhibitory effect is evident as there is a greatly diminished Ca^{2+} release in the cb*Cln3*$^{\Delta ex7/8}$ cells to the point that they release less Ca^{2+} following NAADP-AM addition than the cb*Cln3*$^{+/+}$ cells (figure 6.9 (Cii)). The cb*Cln3*$^{+/+}$ cells also release less Ca^{2+} following pre-treatment with Ned19, but the reduction in NAADP release is not as profound as it is in cb*Cln3*$^{\Delta ex7/8}$ cells. However, while cytosolic Ca^{2+} levels only increase marginally in Ned19 treated cells following NAADP-AM addition, it does not go back to original levels (figure 6.9 (Civ)). This experiment also shows that lysosomal Ca^{2+} release via a secondary

messenger is tolerated, and is therefore not the cause of elevated lysosomal Ca^{2+}.

6.4.10 Ca^{2+} induced apoptosis in cbCln3$^{\Delta ex7/8}$ cells following NAADP-AM addition

We next looked at whether the elevated cytosolic Ca^{2+} levels was cytotoxic. Fura 2 probe was used as a vital stain to indicate the cells have not undergone necrosis as they retain the probe (not blebbing), and as a way to visualize cellular architecture.

AnnexinA5 (AnxA5) was used as a marker for cells undergoing apoptosis. This is through it binding to phosphatidylserine (PS), a lipid that usually resides on the inner leaflet of the plasma membrane. When apoptosis is triggered, it flips to the extracellular surface and is one of the earliest events in the apoptotic cascade. Annexin A5 is a Ca^{2+} dependent PS binding protein, in the presence of Ca^{2+}, and provided the cells are not necrotic, it will only bind apoptotic cells where PS has flipped.

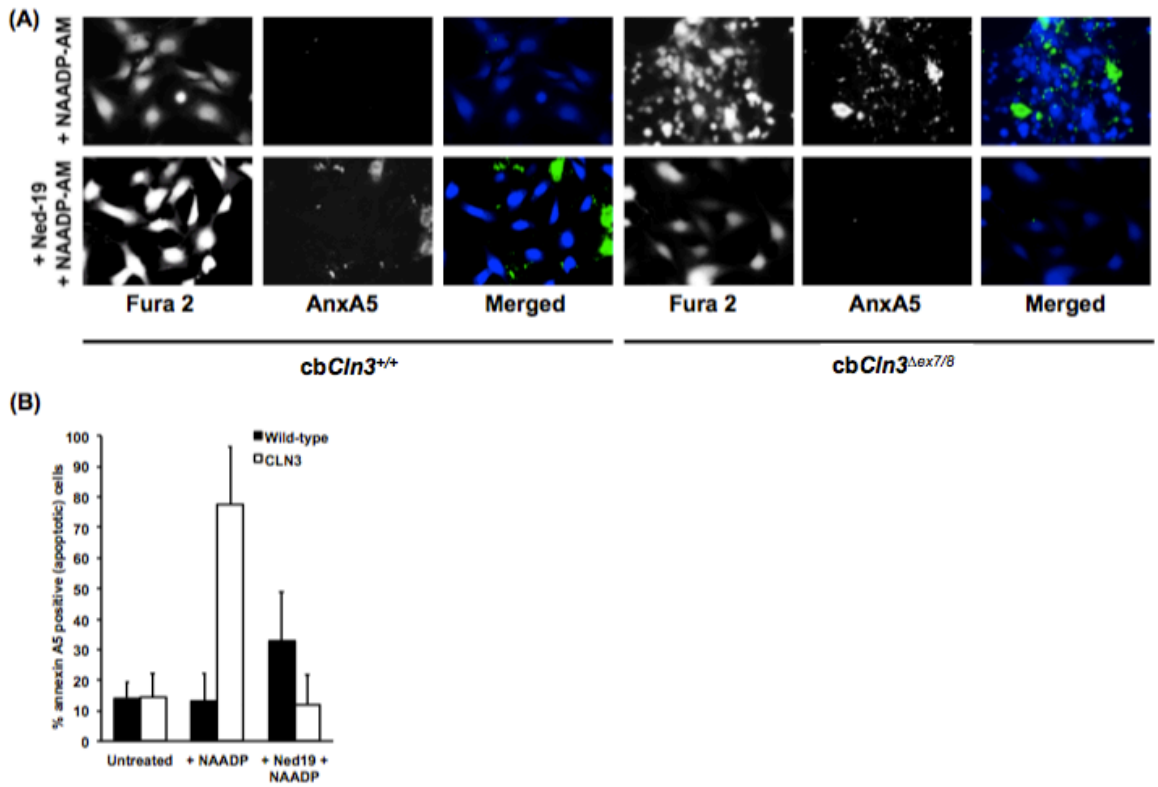

Figure 6.10: (A) Representative pictures of cbCln3$^{\Delta ex7/8}$ cells undergoing apoptosis after the addition of NAADP. This was also done on cells that were pre-treated with 5μM NED19 prior to the addition of NAADP, and the levels of apoptosis in both cell types were observed using the AnxA5 stain. (B) Counts done of the % of cells undergoing Annexin5 mediated apoptosis in both cell types following the addition of NAADP with or without NED19 pre-treatment. Values represent mean ± SD, n=2.

Following the addition of NAADP-AM to both cb*Cln3*$^{+/+}$ and cb*Cln3*$^{\Delta ex7/8}$ cells their Ca^{2+} responses were measured. The cells were then stained with the AnxA5 probe. There was a 8-fold increase in the amount of apoptosis triggered in the cb*Cln3*$^{\Delta ex7/8}$ cells when compared with when they were untreated with NAADP-AM (figure 6.10 (A) and (B)). There was a 8-fold increase in the number of observed cells undergoing apoptosis in the cb*Cln3*$^{\Delta ex7/8}$ cells post NAADP-AM addition than there was in the NAADP treated cb*Cln3*$^{+/+}$. This indicates that there is excitotoxic Ca^{2+}

induced trigger of apoptosis following release due to NAADP-AM induced lysosomal Ca^{2+} release from cb*Cln3*$^{\Delta ex7/8}$ cells. This Ca^{2+} induced apoptosis was not observed in the cb*Cln3*$^{+/+}$ cells though, indicating they are capable of maintaining Ca^{2+} homeostasis following NAADP-AM induced Ca^{2+} release (figure 6.10 (A) and (B)).

There is a drastic reduction in the levels of apoptotic cb*Cln3*$^{\Delta ex7/8}$ cells present when these cells have been pre-treated with Ned19 as the percentage of cells undergoing apoptosis are now similar levels to what is observed in cb*Cln3*$^{\Delta ex7/8}$ untreated cells (figure 6.10 (B)). The blocking of Ca^{2+} release from the lysosomal TPC2 channels via Ned19 would seem to suggest that this is an effective means of blocking NAADP-AM induced cellular toxicity, further supporting that it is Ca^{2+} induced apoptosis rather than necrosis. Surprisingly there was a three-fold increase in the number of cb*Cln3*$^{+/+}$ cells undergoing apoptosis when compared with untreated and NAADP-AM treated cb*Cln3*$^{+/+}$ cells, when the cells were pre-treated with Ned19 and the addition of NAADP-AM, indicating that the blocking of the TPC2 lysosomal Ca^{2+} release channel is detrimental to cellular viability in healthy cells.

6.4.11 5μM glutamate induced Ca^{2+} release from cbCln3$^{+/+}$ and cbCln3$^{\Delta ex7/8}$ cells

Glutamate is an important neurotransmitter that has been found to have important roles in Ca^{2+} signaling in neuronal cells, including triggering the generation of NAADP in neurons.

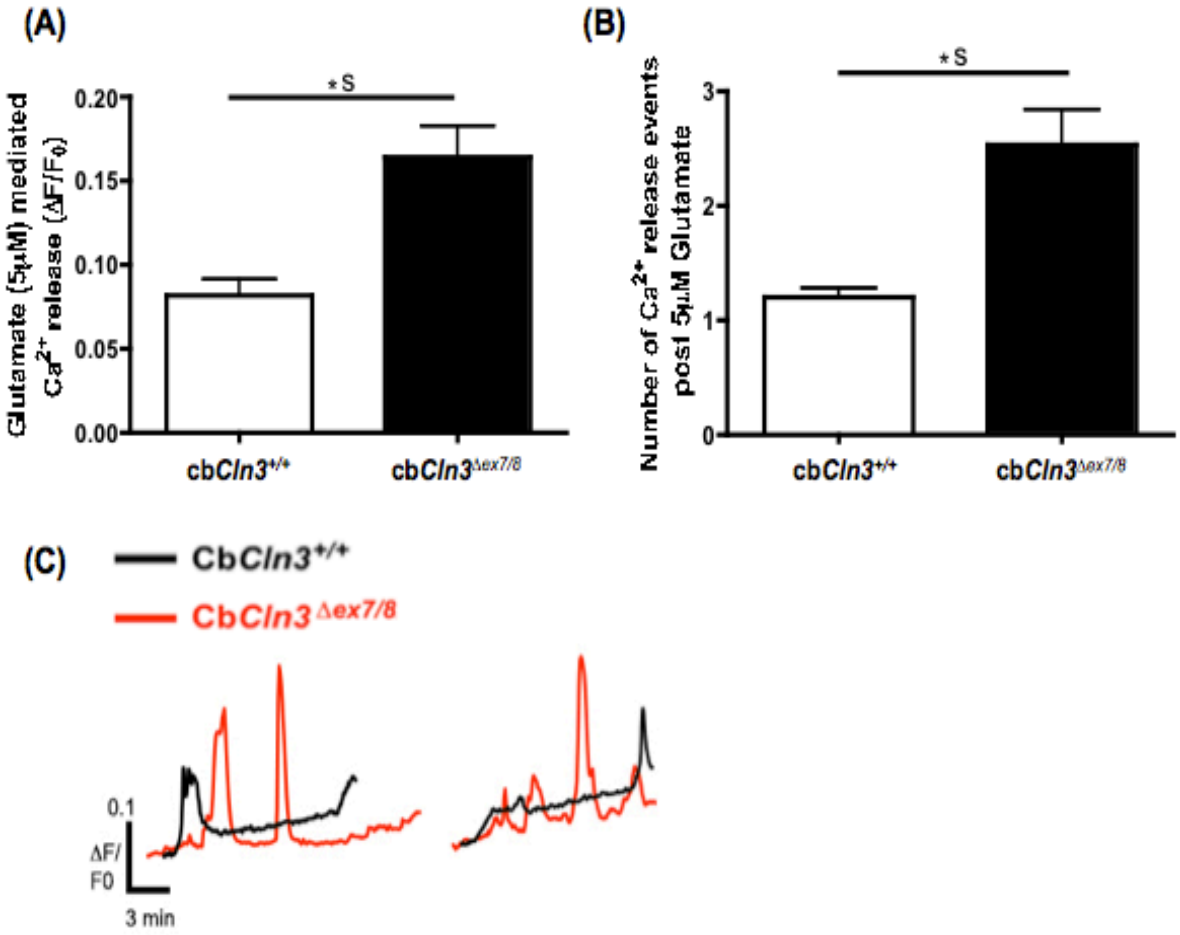

*Figure 6.11: (A) A significantly greater amount of Ca^{2+} was released after the addition of glutamate in the cbCln3$^{\Delta ex7/8}$ cells when compared with cbCln3$^{+/+}$ cells. (B) cbCln3$^{\Delta ex7/8}$ cells undergo a greater number of Ca^{2+} release events when compared with cbCln3$^{+/+}$ cells. (C) Traces of Ca^{2+} response in cbCln3$^{+/+}$ and cbCln3$^{\Delta ex7/8}$ after the addition of Glutamate. Values represent mean ± SD, n=1, >20 cells analysed. *S denotes significant, (A) P<0.0001. (B) P<0.0001.*

A greater Ca^{2+} response was seen in the cb*Cln3*$^{\Delta ex7/8}$ cells as well as multiple Ca^{2+} release events occurred when compared with cb*Cln3*$^{+/+}$ cells (figure 6.11) in a manner similar to NAADP-AM (figure 6.9). Interestingly, despite cb*Cln3*$^{\Delta ex7/8}$ cells seemingly having greater sensitivity to glutamate, exhibited by the greater Ca^{2+} release and multiple Ca^{2+} release events, few cells responded to glutamate in the mutant cells than the cb*Cln3*$^{+/+}$ cells where every cell analysed responded (Data not shown). However the data is only preliminary, as the experiment has not been repeated, therefore requires repeating before any conclusions can be made.

6.4.12 Nifedipine, an L-type Ca^{2+} channel inhibitor and weak antagonist to TPC2, partially blocks NAADP mediated Ca^{2+} release and rescues cbCln3$^{\Delta ex7/8}$ cells from excitoxic cell death

Nifedipine is an FDA approved drug that acts by blocking L-Type Ca^{2+} channels, a family to which the lysosomal TPC channel belongs to. Nifedipine may be able to inhibit the excess Ca^{2+} signalling present in cb*Cln3*$^{\Delta ex7/8}$ cells following Ca^{2+} release from the TPC2 channels after NAADP treatment.

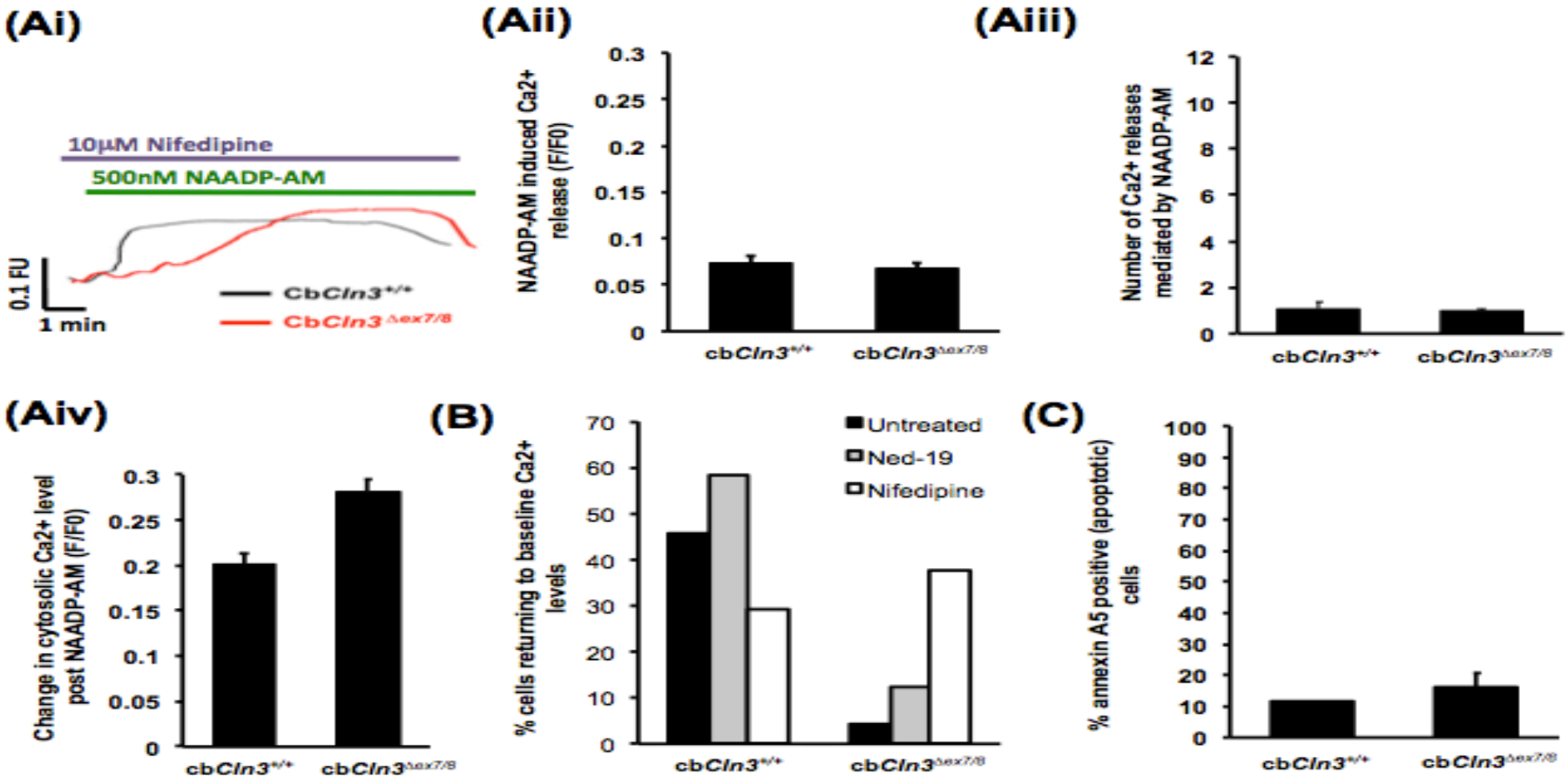
(Ai)
10µM Nifedipine
500nM NAADP-AM
0.1 FU
1 min
CbCln3+/+
CbCln3Δex7/8
(Aii)
NAADP-AM induced Ca2+ release (F/F0)
0.3
0.25
0.2
0.15
0.1
0.05
0
cbCln3+/+
cbCln3Δex7/8
(Aiii)
Number of Ca2+ releases mediated by NAADP-AM
12
10
8
6
4
2
0
cbCln3+/+
cbCln3Δex7/8
(Aiv)
Change in cytosolic Ca2+ level post NAADP-AM (F/F0)
0.3
0.25
0.2
0.15
0.1
0.05
0
cbCln3+/+
cbCln3Δex7/8
(B)
% cells returning to baseline Ca2+ levels
70
60
50
40
30
20
10
0
Untreated
Ned-19
Nifedipine
cbCln3+/+
cbCln3Δex7/8
(C)
% annexin A5 positive (apoptotic) cells
100
90
80
70
60
50
40
30
20
10
0
cbCln3+/+
cbCln3Δex7/8

Figure 6.12: (Ai) Ca^{2+} traces to illustrate the release of Ca^{2+} in pre-treated nifedipine cells following the addition of NAADP. (Aii) Levels of NAADP induced Ca^{2+} release from both cbCln3$^{+/+}$ and cbCln3$^{\Delta ex7/8}$ cells. (Aiii) The number of Ca^{2+} release events observed following the addition of NAADP in the two cell types. (B) The percentage of apoptotic cells counted in both cbCln3$^{+/+}$ and cbCln3$^{\Delta ex7/8}$ nifedipine treated cells following the addition of NAADP using the AnxA5 probe. Values represent mean ± SD, n=1.

The pre-treatment of 10μM Nifedipine before the addition of NAADP-AM resulted in a similar sustained release of Ca^{2+} in both the cb*Cln3*$^{+/+}$ and cb*Cln3*$^{\Delta ex7/8}$ cells (figure 6.12 (Ai)). There were no spontaneous Ca^{2+} release events observed in the nifedipine treated cells following NAADP-AM addition. Importantly, the cytosolic Ca^{2+} levels were also returning to baseline levels. This return to normal cytosol Ca^{2+} levels as well as no spontaneous Ca^{2+} release events may be why no Ca^{2+} induced apoptosis was triggered, as the number of apoptotic cells observed in both cell types was similarly low (~10% (figure 6.12). This is again only preliminary data, and more repeats are required before any conclusions can be made.

6.4.13 Overnight treatment with Ned19 causes increased lysosomal Ca^{2+} in cbCln3$^{\Delta ex7/8}$ cells but not cbCln3$^{+/+}$ cells

Having shown that Ned19 is capable of inhibiting NAADP mediated Ca^{2+} release from lysosomal TPCs in cb*Cln3*$^{\Delta ex7/8}$ cells (figure 6.9 (Cii)) we utilised a long term treatment with this inhibitor to determine the effects on lysosomal Ca^{2+} content.

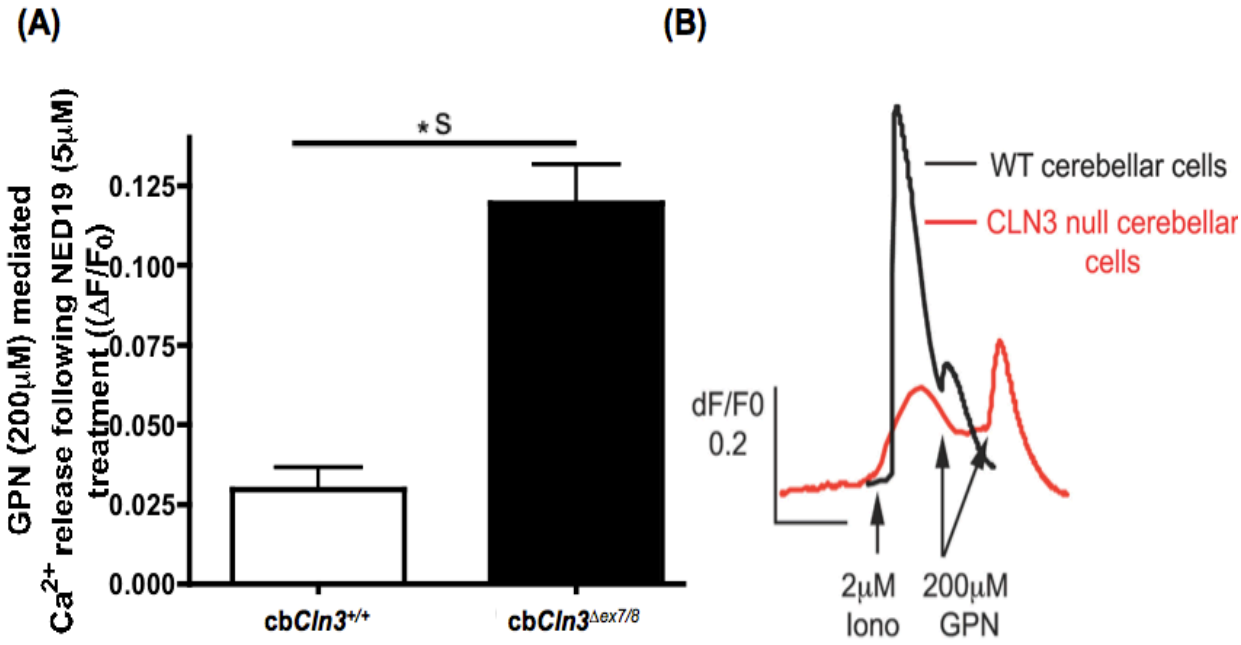

*Figure 6.13: Cells were treated with 2μM Ionomycin before the addition of GPN to clamp the other cellular Ca^{2+} stores (A) levels of lysosomal Ca^{2+} content using 200μM GPN following an overnight treatment of 5μM Ned19 in cbCln3$^{+/+}$ and cbCln3$^{\Delta ex7/8}$ cells (B) Ca^{2+} traces to highlight the difference in lysosomal Ca^{2+} in the two cell types. Values represent mean ± SD, n=2, >20 cells analysed. *S denotes significant, P<0.0001.*

By treating the cells with 5μM Ned19 overnight it should block Ca^{2+} release from the TPC channels on the lysosome. As this is blocked the lysosome would have to use a Ca^{2+} leak channel to maintain its Ca^{2+} homeostasis otherwise the Ca^{2+} content inside the lysosome would only increase as it presumably continuously pumps in more Ca^{2+}. By using GPN to measure the Ca^{2+} content of the lysosome following overnight treatment of Ned19 and the clamping of other intracellular Ca^{2+} stores using ionomycin, the lysosomal Ca^{2+} levels inside cb*Cln3*$^{\Delta ex7/8}$ lysosomes was significantly higher than what was seen in cb*Cln3*$^{+/+}$ lysosomes (figure 6.13 (A) and (B)). The lysosomal Ca^{2+} content in cb*Cln3*$^{+/+}$ cells

was similar in level to untreated Ned19 cb*Cln3*$^{+/+}$ cells (figure 6.7), suggesting that despite the major Ca^{2+} release channel of the lysosome (TPC) being blocked they are still able to maintain their lysosomal Ca^{2+} homeostasis, possibly via a leak channel. The lysosomal Ca^{2+} content of NED19 treated cb*Cln3*$^{\Delta ex7/8}$ cells increased by ~50% when compared with the Ca^{2+} content of untreated cb*Cln3*$^{\Delta ex7/8}$ lysosomes (figure 6.7). This would suggest that cb*Cln3*$^{\Delta ex7/8}$ cells are unable to leak out lysosomal Ca^{2+} unlike cb*Cln3*$^{+/+}$ lysosomes.

6.4.14 Alignment of the CLN3 C-terminus

Sequence alignment done on the C-terminus of the CLN3 protein and the Ba inhibitor 1 protein as well as the bacterial YetJ protein display high levels of similarity when the C-terminus of these proteins are aligned.

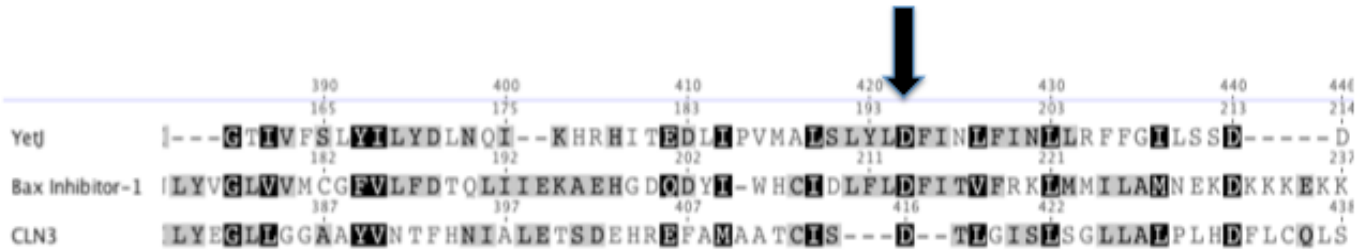

Figure 6.14: Sequence alignment of the C-terminus of the bacterial YetJ, Bax inhibitor 1 and CLN3 protein.

The arrow denotes the key aspartate residue (D) that has been found to release Ca^{2+} in the Bax inhibitor protein. Peptides were designed to match the key residues of the C-terminus of the CLN3 protein, to detect if this was capable of releasing Ca^{2+}. A mutant peptide was also designed

where the aspartate had been changed to a glycine to see if this abolishes any potential Ca^{2+} release via the use of this peptide.

6.4.15 Using CLN3 C-terminal peptides to reduce cbCln3$^{\Delta ex7/8}$ lysosomal Ca^{2+} levels following long term NED19 treatment

cb*Cln3*$^{\Delta ex7/8}$ cells were treated overnight with 5μM NED19 to induce elevated levels of lysosomal Ca^{2+} levels as seen in *figure 6.13*.

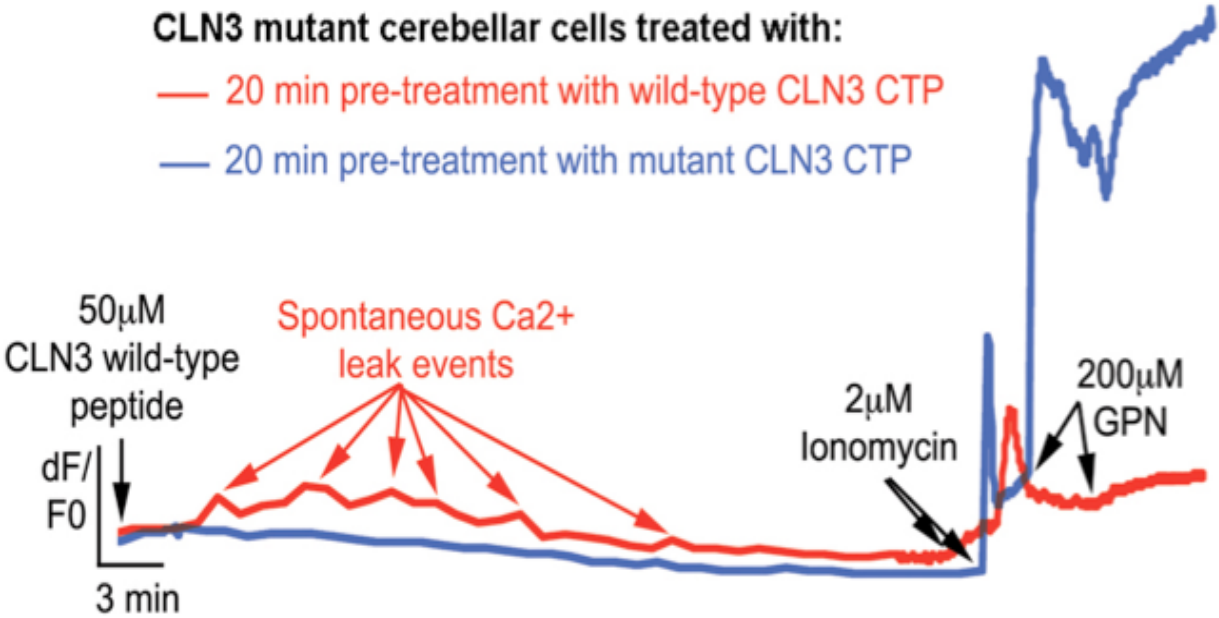

Figure 6.15: 24 hour Ned19 treated cbCln3$^{\Delta ex7/8}$ cells are loaded with fura2-AM followed by a 20 minute incubation with either the wild type or mutant CLN3 CTP. Lysosomal Ca^{2+} levels were then measured using GPN post clamping of other Ca^{2+} stores with ionomycin. Lysosomal Ca^{2+} is reduced following a 20 minute incubation with wild type CLN3 CTP, but not with the mutant CLN3 CTP. n=1

cb*Cln3*$^{\Delta ex7/8}$ cells were treated overnight with 5μM NED19 to induce elevated levels of lysosomal Ca^{2+} levels as seen in *figure 6.13*. Cells

were loaded with 50μM peptide and incubated for 20 minutes to allow time for the peptide to be taken up into the cell and be delivered to the late endosome/lysosome. The cells were then treated with 2μM ionomycin to clamp other cellular Ca^{2+} stores before the addition of 200μM GPN to measure lysosomal Ca^{2+} content. The addition of the CLN3 CTP causes multiple spontaneous Ca^{2+}, and following the addition of GPN there was a large reduction in the levels of Ca^{2+} stored inside the lysosome (figure 6.15). The D416G (mutant) CTP did not display spontaneous Ca^{2+} release events and following the addition of GPN we observed that cells treated with mutant CTP still had a large lysosomal Ca^{2+} store. This shows that the D416G CTP cannot rescue the elevated lysosomal Ca^{2+} levels, unlike the CLN3 CTP.

While this is preliminary data it suggests that the wild type CTP is capable of alleviating the elevated lysosomal Ca^{2+} levels, but the mutant peptide is not. More repeats will be needed to back up this preliminary data.

6.4.16 Measuring CTP induced leak using intra-lysosomal Ca^{2+} probes

The ability of the CLN3 CTP to induce lysosomal Ca^{2+} was measured with the use of the intra-lysosomal Ca^{2+} probe Oregon green BAPTA-1.

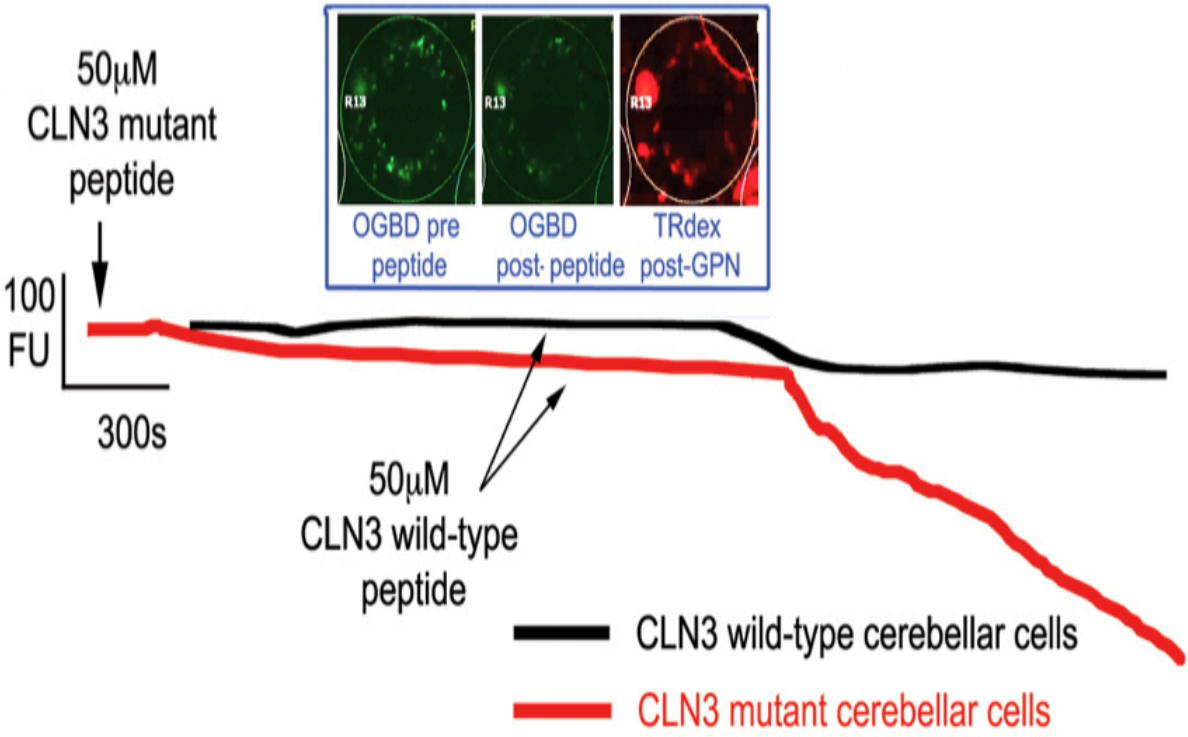

Figure 6.16: Oregon green BAPTA is used as an intracellular lysosomal Ca^{2+} probe, while TRITC-red dextran was used as a loading control. The *Addition of the CLN3 CTP, but not the CLN3 mutant CTP induces lysosomal Ca^{2+} leak in both cell types. n=1*

Both cb*Cln3*$^{+/+}$ and cb*Cln3*$^{\Delta ex7/8}$ cells are co-incubated with the Ca^{2+} probe Oregon green BAPTA-1 and Texas red dextran at 37°C for 6hrs so we are able to measure intra-vesicular lysosomal Ca^{2+} levels. cb*Cln3*$^{\Delta ex7/8}$ cells were incubated for 20 minutes with 50μM of the CLN3 mutant CTP to allow trafficking of the peptide to the lysosome. After incubation no Ca^{2+} release was observed in the cells after 20 minutes the cells were treated with 50μM of the wild type CLN3 CTP and left for the peptides to be trafficked to the lysosome. After a short time there was a reduction in the levels of intra-lysosomal Ca^{2+} detected inside the lysosomes,

indicating that Ca^{2+} was leaking out of the lysosome into the cytosol (figure 6.16). A similar response was observed in cb*Cln3*$^{+/+}$ cells after the addition of the CLN3 CTP, but the drop in intra-lysosomal Ca^{2+} was not as high as what was seen in the cb*Cln3*$^{\Delta ex7/8}$ cells. Microscopy pictures highlight high Oregon green BAPTA-1 staining in cb*Cln3*$^{\Delta ex7/8}$ lysosomes prior to the addition of the CLN3 CTP, Texas Red dextran was used as a loading control to show that Oregon green BAPTA-1 was measuring lysosomal Ca^{2+} and not that of another endocytic organelle, as well as showing the lysosomes still retain their integrity and that the probe did not just leak out of them). After the addition of the CLN3 CTP in the cb*Cln3*$^{\Delta ex7/8}$ cells there is a reduction in the fluorescence detected via the Oregon green BAPTA-1 stain, indicating that Ca^{2+} has leaked out of the lysosomes, however there was no change in Texas red dextran staining indicating the lysosomes were still intact.

While this is preliminary data, we have shown that by measuring the change in Ca^{2+} from the outside of the lysosome as well as the inside that the wild type CTP is capable of inducing lysosomal Ca^{2+} leak in living cells, and can rescue the lysosomal Ca^{2+} defect in cb*Cln3*$^{\Delta ex7/8}$ cells.

6.4.17 Utilising CLN3 CTP and CLN3 mutant CTP to measure Ca^{2+} leak from purified lysosomes.

Lysosomes from both cb*Cln3*$^{+/+}$ and cb*Cln3*$^{\Delta ex7/8}$ cells were magnetically purified (as described in chapter 2).

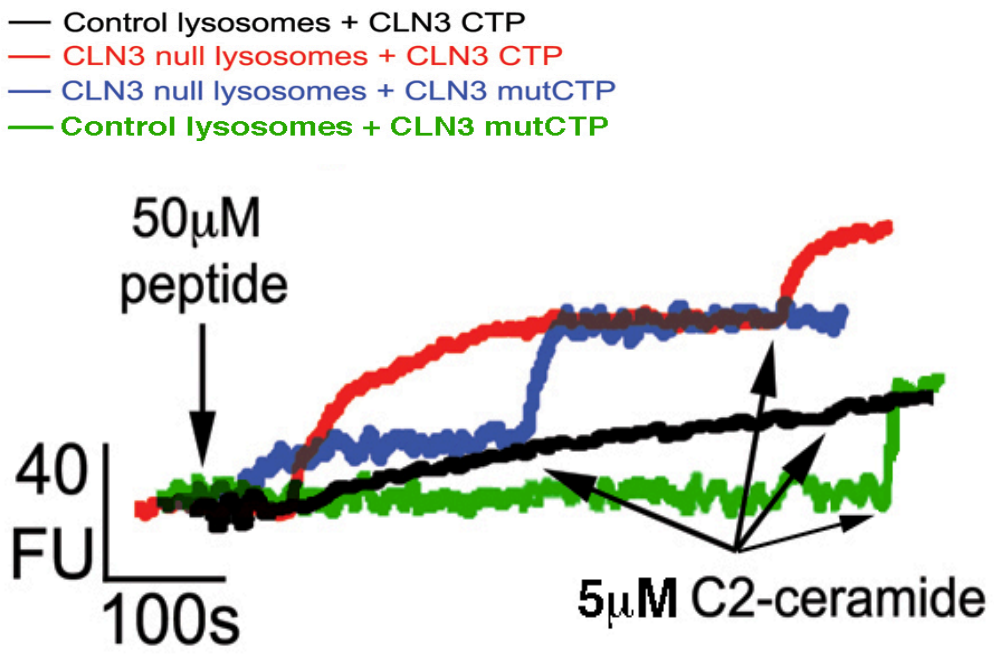

Figure 6.17: CLN3 C-terminus synthetic peptide releases Ca^{2+} from pure lysosomes, while the mutant CTP is only capable of releasing lower amounts of Ca^{2+}. C2-Ceramide was used to confirm that the lysosomes were still intact prior to addition. n=2

~40μg of purified lysosomes were incubated with 2μM of the Ca^{2+} probe Fluo-4 and physiological pH. The experiments were started via the addition of the ATP-regenerating system (data not shown). The addition of the CLN3 CTP resulted in an increase in the levels of Ca^{2+} being detected by Fluo-4 outside of the purified lysosomes, indicating Ca^{2+} leaking out of the lysosomes in both the cb*Cln3*$^{+/+}$ and cb*Cln3*$^{\Delta ex7/8}$ purified lysosomes. There was a greater degree of Ca^{2+} release detected in the cb*Cln3*$^{\Delta ex7/8}$ lysosomes when compared with the cb*Cln3*$^{+/+}$ lysosomes, indicative of the higher lysosomal Ca^{2+} content in the cb*Cln3*$^{\Delta ex7/8}$ lysosomes (figure 6.17). The addition of the CLN3 mutant CTP (CLN3 mutCTP) resulted in no Ca^{2+} being released from the purified cb*Cln3*$^{+/+}$ lysosomes but does seem to release some Ca^{2+} from the

cb*Cln3*$^{\Delta ex7/8}$ lysosomes (~66% less Ca^{2+} release when compared with the CLN3 CTP). This suggests that the D416G mutation in the C-terminus region of the CLN3 protein may hamper its ability to release Ca^{2+} but not completely block it. The results of this experiment done on purified lysosomes suggest that CLN3 CTP can induce Ca^{2+} release from lysosomes. The reduced lysosomal Ca^{2+} leak detected in the D416G mutant may be a factor in the onset of CLN3 disease. At the end of the experiment 5μM C2-Ceramide was added (indicated by arrows) to induce pores in the lysosomes membrane causing the release of their Ca^{2+} content, which is what was observed in all experiments. This data highlights that the CLN3 CTP does not induce Ca^{2+} release from lysosomes by causing the formation of pores in the lysosomal membrane.

6.4.18 Ca^{2+} uptake into purified lysosomes from cbCln3$^{+/+}$ cells and cbCln3$^{\Delta ex7/8}$ cells

Lysosomes from both cb*Cln3*$^{+/+}$ and cb*Cln3*$^{\Delta ex7/8}$ cells were magnetically purified. ~20μg of Purified lysosomes were incubated in 2μM Fluo-4 and physiological pH. An ATP-regenerating system was added so that the lysosomes could re-acidify and maintain a proton motive force necessary for Ca^{2+} uptake.

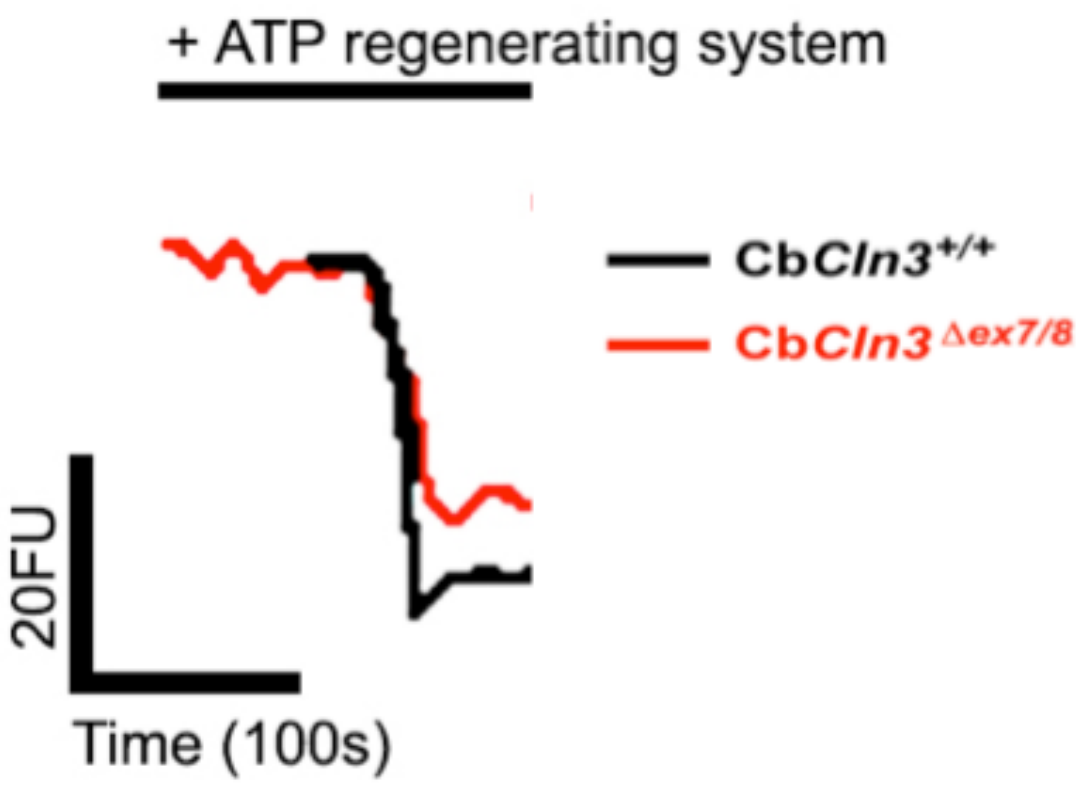

Figure 6.18: Ca^{2+} uptake is observed in both cbCln3$^{+/+}$ and cbCln3$^{\Delta ex7/8}$ cells following the addition of the ATP regenerating system. Following the addition of wild type CLN3 CTP, lysosomes from both genotypes release their Ca^{2+} content. n=1

The rate of Ca^{2+} uptake into the lysosomes was following the addition of the ATP regenerating, lysosomes from both cell types started to uptake Ca^{2+}, indicated by a drop in fluorescence as the probe no longer has Ca^{2+} to bind to as the Ca^{2+} is now in the lysosome. The rate of Ca^{2+} uptake into the purified lysosomes was the same in both the cb*Cln3*$^{+/+}$ and cb*Cln3*$^{\Delta ex7/8}$ cells, which suggests that cb*Cln3*$^{\Delta ex7/8}$ do not have an impaired Ca^{2+} uptake problem. This data is only preliminary and more repeats are needed before a conclusion can be made.

6.5 Discussion

The role of Ca^{2+} in CLN3 pathogenesis is still not fully understood, and there have been very few studies looking into the disease mechanisms that are induced by dysfunctional Ca^{2+} signaling and homeostasis. Several studies have suggested CLN3 being protective against apoptosis, and it has been found that overexpression of CLN3 helps reduce the ER stress response, although the mechanisms behind this are not well understood. The links with *CLN3* mutation and ER stress have been speculated to be due to the mutant CLN3 protein becoming trapped in the ER, inducing ER stress possibly via the unfolded protein response (Chang et al., 2007). However the elevated lysosomal Ca^{2+} could indicate that CLN3's correct role in the cell is associated with maintaining lysosomal Ca^{2+}, with the ER phenotypes observed could be a knock on effect of the *CLN3* mutant protein not being trafficked out of the ER correctly. The topological similarities CLN3 has with the pH regulated ER Ca^{2+} release channel Bi1 (Bultynck et al., 2012, Mao et al., 2003) could suggest that CLN3 maintains lysosomal Ca^{2+} homeostasis by functioning as a lysosomal Ca^{2+} leak channel and possibly regulate response to apoptosis.

6.5.1 Altered Ca^{2+} homeostasis in cb*Cln3*$^{\Delta ex7/8}$ cells

Previous studies found that there is an increase in intracellular Ca^{2+} levels in cells that have siRNA knockdown of CLN3 (An Haack et al.,

2011). While the elevation in CLN3 depleted cells was not particularly large, the study concluded that this was significant and could be a reason for neurotoxicity seen in *CLN3* mutant cells. However resting intracellular Ca^{2+} levels observed in the cb*Cln3*$^{\Delta ex7/8}$ cells were the same as that in cb*Cln3*$^{+/+}$ cells (figure 6.1) (which more closely resembles the human disease), suggesting that any Ca^{2+} defects seen in these cells will arise from their Ca^{2+} stores or is an artefact of siRNA.

6.5.2 Increased sensitivity to the ER Ca^{2+} releasing drug thapsigargin

Our data (figure 5.5) has shown that there is an increase in ER staining in the cerebellar cb*Cln3*$^{\Delta ex7/8}$ cells, which has been implicated in an increase in ER stress. Other work has shown that CLN3 depletion has resulted in SH-SY5Y cells becoming more sensitive to thapsigargin (Wu et al., 2014), possibly due to the mutant CLN3 protein becoming trapped in the ER. Our data shows that there is increased sensitivity in cb*Cln3*$^{\Delta ex7/8}$ cells when they are treated with sub-inhibitory levels of thapsigargin (figure 6.2) as cb*Cln3*$^{\Delta ex7/8}$ cells released >50% higher levels of Ca^{2+} when compared with cb*Cln3*$^{+/+}$ cells. Also 7x more cb*Cln3*$^{\Delta ex7/8}$ cells responded and there was multiple Ca^{2+} releases observed in cb*Cln3*$^{\Delta ex7/8}$ cells also. As the concentration of thapsigargin was increased however the cb*Cln3*$^{\Delta ex7/8}$ cells only had a single Ca^{2+} response. The increased sensitivity seen in the cb*Cln3*$^{\Delta ex7/8}$ cells at lower levels of thapsigargin, but similar responses to cb*Cln3*$^{+/+}$ at higher thapsigargin concentrations,

would suggest that these mutant cells are more sensitive to thapsigargin which has been previously reported (Chang et al., 2007). The multiple Ca^{2+} responses observed in the cb*Cln3*$^{\Delta ex7/8}$ cells could suggest that they have difficulty in regulating the ER Ca^{2+} store, or that the large initial release of Ca^{2+} has caused the release from other Ca^{2+} stores in the cell. If CLN3 is a Ca^{2+} leak channel it may be releasing some Ca^{2+} from the ER store, contributing to the multiple Ca^{2+} release events observed.

6.5.3 Defects in store operated Ca^{2+} re-entry in cb*Cln3*$^{\Delta ex7/8}$ cells

Store operated Ca^{2+} entry is an important mechanism that cells use to restore Ca^{2+} levels in their stores following a large Ca^{2+} release. Thapsigargin which depletes the ER Ca^{2+} store leads to a physiological requirement within the cell to refill this store. This is done via the action of the STIM1 and Orai channels that control the intake of Ca^{2+} from outside the cell. However when store operated Ca^{2+} entry was tested in the cb*Cln3*$^{\Delta ex7/8}$ and cb*Cln3*$^{+/+}$ cells there was a >50% reduction in the levels of Ca^{2+} being brought back into the cell (figure 6.5). The reason behind this is unclear, however it is strongly suggestive that there is store operated Ca^{2+} entry defects in cb*Cln3*$^{\Delta ex7/8}$ cells. However another reason might be that cb*Cln3*$^{\Delta ex7/8}$ cells have adjusted their response to reflect other alterations in cellular Ca^{2+} homeostasis.

6.5.4 Mitochondrial Ca^{2+} store levels

A lot of work done on research into CLN3 disease has found that a common phenotype that occurs in many CLN3 mutant cell types is the accumulation of subunit c of the mitochondria ATPase (Cao et al., 2011). It has been shown before that the cb*Cln3*$^{\Delta ex7/8}$ cells accumulate subunit c, and that this has been linked with a reduction in the levels of mitochondrial ATP found in the mitochondria of these cells (Cao et al., 2011). However our data seems to suggest that there is no change in the levels of mitochondria in the cell or the amount of mitochondria produced ROS (figure 5.4), suggesting that the mitochondria in the cb*Cln3*$^{\Delta ex7/8}$ cells are still capable of functioning correctly. Interestingly though the Ca^{2+} levels detected in the cb*Cln3*$^{\Delta ex7/8}$ cells was significant lower than that seen in the wild type cells (a reduction of ~25%). This would seem to suggest that the cb*Cln3*$^{\Delta ex7/8}$ cells mitochondria have an impaired function in transporting Ca^{2+}, which correlates with less ATP found in a previous study (Cao et al., 2011).

6.5.5 Lysosomal Ca^{2+} levels and its effect on lysosomal Ca^{2+} mediated release from other stores

As our previous results have shown (figure 5.12), lysosomal Ca^{2+} was elevated in cb*Cln3*$^{\Delta ex7/8}$ cells. While it has been reported before in different CLN3 mutant cells that there are defects in lysosomal pH (even though our data for the cb*Cln3*$^{\Delta ex7/8}$ cells suggests there is not in this

case), there has been no work done on measuring the levels of lysosomal Ca^{2+}. By using the lysosomtrophic agent GPN we recorded a greater elevation in lysosomal Ca^{2+} than what was seen in cb*Cln3*$^{+/+}$ cells (figure 6.7). This supports our earlier data (figure 5.12) where an intracellular Ca^{2+} probe was used to measure lysosomal Ca^{2+}. This elevation in lysosomal Ca^{2+} would strongly suggest that CLN3 has an important role to play in lysosomal Ca^{2+} homestasis, and that its absence clearly leads to accumulation of Ca^{2+} in this organelle. While it is still not known what the mechanisms are for how Ca^{2+} enters the lysosome, it is known however that it requires a proton motive force (via the vATPase proton pump) to enter (Mindell, 2012). This elevated Ca^{2+} does suggest that the cb*Cln3*$^{\Delta ex7/8}$ cells have a functional vATPase otherwise we would most likely not see this increase in lysosomal Ca^{2+}. Also our work showing cathepsin activity is normal in cb*Cln3*$^{\Delta ex7/8}$ cells further backs up our claim that there is no lysosomal pH abnormality in the cb*Cln3*$^{\Delta ex7/8}$ cells (figures 5.2 and 5.3). If lysosomal Ca^{2+} uptake is normal (as suggested by the large Ca^{2+} present in lysosomes) then it can be strongly suggested that cb*Cln3*$^{\Delta ex7/8}$ lysosomes are incapable of releasing Ca^{2+}, to maintain normal lysosomal Ca^{2+} levels. This elevated lysososmal Ca^{2+} might account for the faster endocytic trafficking observed in these cells (figures 5.10 and 5.11) as late endosome-lysosome fusion requires Ca^{2+} (Luzio et al., 2009), and with elevated Ca^{2+} already present in the lysosome it would need less time to refill its Ca^{2+} store for further fusion.

By inducing Ca^{2+} release from lysosomes with out clamping for other stores first it results in a ~60% increase in the levels of Ca^{2+} released

from the lysosome as well as other stores (figure 6.8). Lysosomal Ca^{2+} has been suggested to be required for major Ca^{2+} signaling events in the cell. The elevated lysosomal Ca^{2+} in cb*Cln3*$^{\Delta ex7/8}$ cells results in a greater amount of Ca^{2+} being released from the cells other Ca^{2+} stores, which might be one of the factors that result in cellular toxicity that is often observed in CLN3 deficient cells, and could be a new therapeutic target.

As mentioned previously (Chapter 1 intro) NAADP is a major intracellular messenger that has been found to induce Ca^{2+} release from the TPC2 release channel on the lysosome. This naturally occurring messenger would suggest that there are times when the cell needs to release large concentrations of Ca^{2+} from the lysosome to induce a major biological action (e.g. for cell division) (Galione et al., 2014). By inducing NAADP mediated Ca^{2+} release from the lysosome it resulted in a greater Ca^{2+} release in the cb*Cln3*$^{\Delta ex7/8}$ cells after the ER had been clamped (figure 6.9 Aiii) most likely due to the elevated lysosomal Ca^{2+} present. However when NAADP was added to the cells without the ER Ca^{2+} store being clamped it resulted in a greater level of Ca^{2+} release seen in the cb*Cln3*$^{\Delta ex7/8}$ cells as well as multiple Ca^{2+} release events (figure 6.9 Bii and Biii). The multiple release events observed in the cb*Cln3*$^{\Delta ex7/8}$ cells following NAADP addition would suggest that they cannot maintain correct Ca^{2+} homeostasis once a Ca^{2+} release is induced from a store. It was also observed that the cytosolic Ca^{2+} level did not return to normal in the cb*Cln3*$^{\Delta ex7/8}$ cells (figure 6.9 Bi and BiV), and that there was a greater amount of apoptosis occurring in the cb*Cln3*$^{\Delta ex7/8}$ cells than what was seen in cb*Cln3*$^{+/+}$ cells (figure 6.10). cb*Cln3*$^{\Delta ex7/8}$cells defective

capabilities in maintaining Ca^{2+} homeostasis after a large lysosomal Ca^{2+} would strongly suggest that Ca^{2+} induced apoptosis is occurring in these cells when they undergo large Ca^{2+} events. The addition of the TPC2 inhibitor NED19 reduced the level of NAADP mediated Ca^{2+} release from the lysosomes and subsequently reduced the levels of apoptosis observed in the cb*Cln3*$^{\Delta ex7/8}$ cells (figure 6.10). This data strongly indicates that elevated NAADP induced Ca^{2+} release from lysosomes, and the subsequent defects in maintaining Ca^{2+} homeostasis in the cb*Cln3*$^{\Delta ex7/8}$ cells following a large release, is a major contributor to Ca^{2+} induced apoptosis.

Also the elevated NAADP release cb*Cln3*$^{\Delta ex7/8}$ indicates that they can release Ca^{2+} in response to an agonist, so that only leaves a leak problem. Like the ER, the lysosome needs constitutively active leak channels to remove excess Ca^{2+} during the absence of a secondary messenger.

A study has found that the important neurotransmitter glutamate elevates cellular NAADP levels. When cb*Cln3*$^{\Delta ex7/8}$ cells were treated with glutamate there was a greater Ca^{2+} in these cells when compared to cb*Cln3*$^{+/+}$ cells (figure 6.11). Multiple Ca^{2+} release events were also observed. This might indicate that glutamate might be having a similar impact in inducing Ca^{2+} mediated autophagy in the brains of CLN3 disease patients. However it should be noted that these experiments require repeating before a stronger hypothesis can be postulated.

6.5.6 L-type Ca^{2+} channel inhibitor: Nifedipine

As mentioned before a study found that using different L-type Ca^{2+} channel inhibitors resulted in a reduction in the elevated intracellular Ca^{2+} levels in siRNA CLN3 knock down cells (Warnock et al., 2013). Nifedipine is a FDA approved drug that is used to treat cluster headaches, and is safe to take up to 60mg a day. By treating cells with nifedipine we were able to rescue Ca^{2+} induced apoptosis in the cb*Cln3*$^{\Delta ex7/8}$ cells following NAADP treatment, as the cytosolic Ca^{2+} levels returned to normal (figure 6.12). This return to baseline Ca^{2+} levels as well as there being no multiple Ca^{2+} releases occurring may explain why apoptosis is not being triggered. While more work needs to be done, this provides a potential treatment for CLN3 disease patients if NAADP mediated Ca^{2+} release is one of the main contributing factors behind CLN3 disease pathogenesis. As well as this, it shows that nifedipine is acting directly on the TPC channels; to alleviate the abnormal NAADP induced Ca^{2+} release from the lysosomes.

6.5.7 CLN3: potentially a Ca^{2+} leak channel

As mentioned previously (Chapter 6 introduction) the topography of CLN3 is similar to the ER Ca^{2+} leak channel Bax inhibitor 1. Bi-1 is a highly conserved protein in mammals and is found on the ER membrane, where it is suggested to take in protons into the ER lumen in exchange for Ca^{2+} to reduce ER stress (Bultynck et al., 2012). As our data suggests that

lysosomal Ca^{2+} is elevated in cb*Cln3*$^{\Delta ex7/8}$ cells, it may be possible that CLN3 is a Ca^{2+} leak channel, and that its absence in the lysosome leads to Ca^{2+} accumulation. By using a long treatment with the TPC inhibitor Ned19 to block Ca^{2+} release from these channels produced a ~60% increase in the levels of lysosomal Ca^{2+} in the cb*Cln3*$^{\Delta ex7/8}$ cells (figure 6.13). However interestingly the lysosomal Ca^{2+} levels did not increase, which suggests that with the TPC channels inhibited the lysosome is able to release Ca^{2+} from another channel on the lysosomal membrane.

Work done by our group (Personal communivation) using alignment software found that CLN3 has a 27% identity and ~50% similarity with Bi1 protein (Lloyd-Evans lab data, unpublished). Previous work done on Bi1 has found that it is the C-terminus of the protein that is responsible for Ca^{2+} release, and it was shown that by mutating aspartate (Asp-213) in the Ca^{2+} channel pore in the C-terminus resulted in the Bi1 protein to be unable to release Ca^{2+}, highlighting this residue as critical for Ca^{2+} for this channel. Interestingly this key residue is also found in the C-terminus domain in the CLN3 protein, with this residue being conserved in all upper eukaryotes (figure 6.15). As the topography of Bi1 and CLN3 are similar, especially the orientation of the C-terminus, and with CLN3 also possessing this key aspartate residue it implies that CLN3 might be a Ca^{2+} leak channel and that its absence from the lysosomal membrane results in an increase in lysosomal Ca^{2+}.

To determine if the C-terminus of the CLN3 protein was capable of inducing Ca^{2+} leak, peptides were designed where a wild type CLN3 amino acid sequence, comprising of the key aspartate residue, as well as

a mutant CLN3 peptide where the aspartate residue has been changed to a glycine (figure 6.15). Both these peptides contained the native dileucine lysosomal targeting motifs that are believed to be important in correct CLN3 processing to the lysosome. These were used to detect if the wild type peptide could induce Ca^{2+} leak and the mutant peptide could not.

Utilising the lysosomal magnetic purification assay that I have developed over the course of my PhD lysosomes were purified from cb*Cln3*$^{+/+}$ and cb*Cln3*$^{\Delta ex7/8}$ cells. By adding the wild type peptide to the cb*Cln3*$^{\Delta ex7/8}$purified lysosomes there was a release of Ca^{2+} from them (figure 6.18). However the mutant CLN3 peptide only released a small amount of Ca^{2+} from these purified lysosomes. The wild type peptide was also capable of releasing Ca^{2+} from cb*Cln3*$^{+/+}$ cells, however there was not as high a release, possibly due to the cb*Cln3*$^{+/+}$ lysosomes already possessing a functional Cln3 protein.

Intra-lysosomal Ca^{2+} measurements in whole cells also resulted in a decrease in the levels of lysosomal Ca^{2+} present in cb*Cln3*$^{\Delta ex7/8}$ lysosomes following the addition of the wild type peptide (figure 6.17). Also the wild type peptide was able to rescue the elevated lysosomal Ca^{2+} levels after long term Ned19 treatment, whilst the mutant peptide could not (6.17).

While this is only preliminary data, we have shown that the c-terminus of the CLN3 protein is capable of inducing Ca^{2+} release. The importance of utilising the lysosomal magnetic purification technique has highlighted that these peptides can anchor themselves into the lysosomal membrane

and induce Ca^{2+} release from the lysosomal Ca^{2+} store, and that that the peptide is not acting on another Ca^{2+} store that reduces lysosomal Ca^{2+}.

6.5.8 Overview

Work done on determining Ca^{2+} abnormalities in cb*Cln3*$^{\Delta ex7/8}$ cells has shown that there are numerous defects in Ca^{2+} homeostasis present in these cells. The ER Ca^{2+} defect may be due to the presence of the mutant Cln3 protein trapped there, leading to an increase in ER stress. The elevated lysosomal Ca^{2+} may be a contributing factor to NAADP induced Ca^{2+} release that results in Ca^{2+} induced apoptosis in cb*Cln3*$^{\Delta ex7/8}$ cells. However by treating the cells with the L-type Ca^{2+} channel inhibitor nifedipine the Ca^{2+} abnormalities and Ca^{2+} induced apoptosis were abolished, indicating that nifedipine may be potentially a viable therapeutic drug for treating *CLN3* mutant induced Ca^{2+} irregularities.

Also by utilising the lysosomal magnetic purification method to purify lysosomes we have been able to show that the aspartate residue located on the c-terminus of the CLN3 protein is able to mediate Ca^{2+} leak from purified lysosomes.

While this work is in its early stages, it is the first characterisation for CLN3's role in the cell and how its loss results in the formation of Ca^{2+} abnormalities that can lead to apoptosis and a loss of neurons in JNCL.

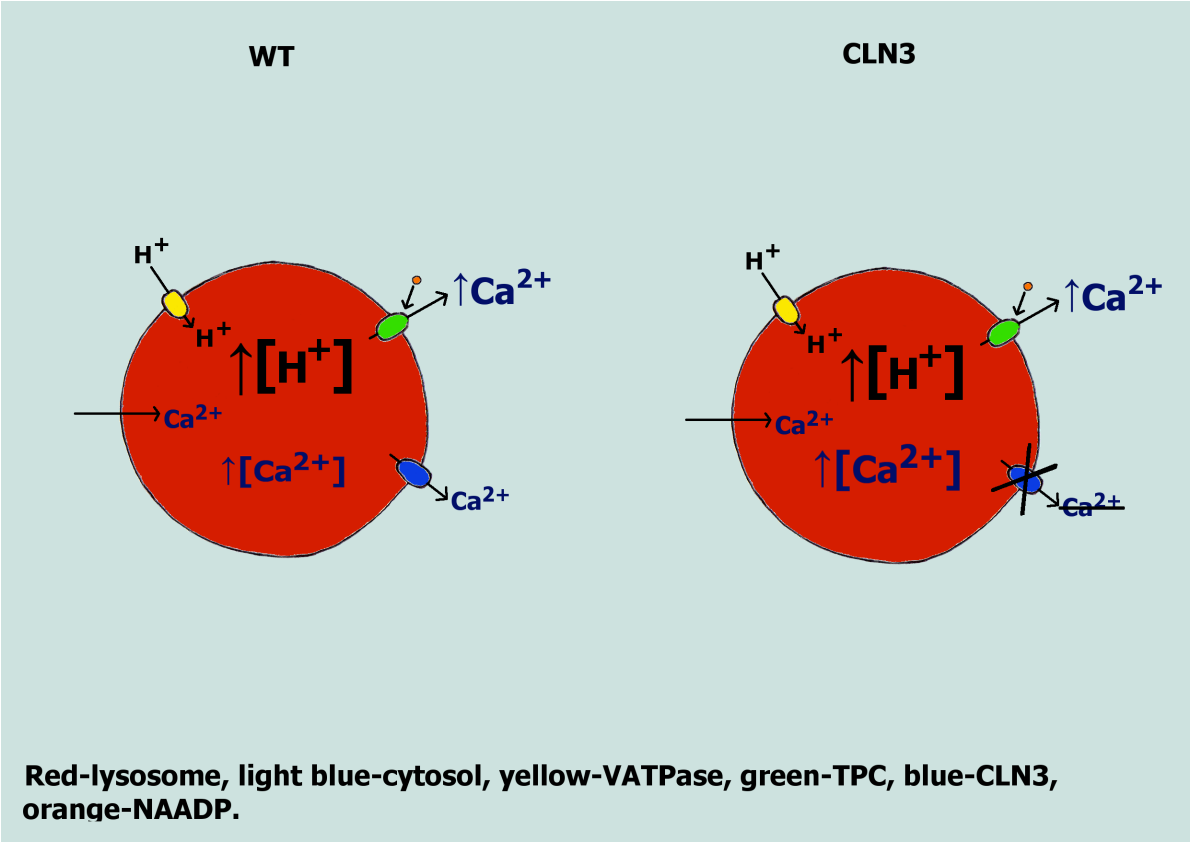

Figure 6.19: A possible mechanism for CLN3. The lysosome continuously fills with Ca^{2+} via an unknown channel and when the TPC channels aren't active the lysosome needs to maintain it's Ca^{2+} homeostasis via the use of a Ca^{2+} leak channel (CLN3). When CLN3 is mutated it is unable to get to the lysosome, so the lysosome no longer has a means of maintaining it's Ca^{2+} homeostasis via leak, therefore in CLN3 disease the lysosomal Ca^{2+} content increases.

Chapter 7: General Discussion and final conclusions

The importance of lysosomal research can be highlighted by the severity of lysosomal storage diseases, which arise when a lysosomal protein is defective. The need to understand the functions of the defective lysosomal proteins could help further our understanding in the disease mechanisms that arise during the onset of these diseases in patients. With better understanding of these diseases, it could result in the development of potential therapies for patients with lysosomal storage diseases.

The ability to study lysosomes and their components has somewhat been hampered by the difficulty in purifying lysosomes and studying them in an isolated environment. Established techniques such as density gradient centrifugation have commonly been used, but to little success as the lysosomes are often contaminated with other organelles as well as them no longer being structurally functional. The need to purify contaminant free lysosomes is obvious, however with recent discovery that the lysosomal is the second largest Ca^{2+} store in the cell, as well as how pH dysregulation in lysosomes can lead to the onset of other common neurodegenerative diseases such as Alzheimer's disease shows the requirement to purify lysosomes that are still capable of maintaining their Ca^{2+} content as well as pH levels once purified.

During the 1990s the idea that lysosomes could be purified via magnetic iron particles being loaded into them offered some hope into a new

technique that overcomes the problems of other methods of lysosomal purification (as discussed in Chapter 3). However, while the methodology behind exploiting the endocytic system to deliver these particles to lysosomes was good, unfortunately the particles themselves proved to be highly unstable once in the acidic environment of the lysosome and resulted in being toxic to cells.

By using a new type of highly magnetic iron based particle which is functionalised with a dextran coat, we wanted to see if we could improve upon previous techniques of magnetic lysosomal purification and develop our own method to produce high yields of lysosomes that are free of contamination from other organelles such as the ER, and importantly that the lysosomes are functional. First though it was important to determine that these SPIONs were not toxic to cells, as any toxicity would damage the lysosomal membrane resulting in lower yields of purified lysosomes and abnormalities in them being able to retain their Ca^{2+} and pH levels. From this study we were able to show that the SPIONs produced by the company Liquids Research Ltd were the safest particles to use and that they were stable in the lysosome for a long time when compared with another commercially available SPION. We were also able to highlight with using a similar iron based particle from previous studies, the high levels of cellular toxicity it induces.

Using our lysosomal magnetic purification method we have been able to consistently purify high yields of pure lysosomes and have been able to show that they are still functional post purification via the use of pH re-acidification assays and Ca^{2+} uptake assays (Chapter 3 results). Using

these assays on both purified wild type and NPC CHO lysosomes that there is no re-acidification problem occurring in NPC null CHO M12 cells, which supports previous data on there being no pH problem in NPC null lysosomes. With the Ca^{2+} uptake assay we have been able to show that there is a Ca^{2+} defect in NPC null lysosomes, supporting previous findings that have shown this intracellularly. While this is not new data, it highlights the benefits of being able to measure Ca^{2+} and pH defects in lysosomal storage disease lysosomes which would benefit different labs across the world.

As the lysosomal magnetic purification method has now been finalised it has been distributed to >20 labs across the world. These labs have been able to produce good yields of lysosomal protein that have low levels of contamination from other organelles using the method I developed.

The use of this method has benefited us in our research into the neuronal ceroid lipofuscinosis disease CLN3 disease. While our work on cb*Cln3*$^{\Delta ex7/8}$ cells has revealed that at storage level there is not much difference present, from a Ca^{2+} side of it there are large differences present.

Our findings that cb*Cln3*$^{\Delta ex7/8}$ cells have elevated Ca^{2+} as well as abnormal Ca^{2+} homeostasis, led us to believe that CLN3 has a role in Ca^{2+} regulation, possibly via the lysosome. Our labs further finding that CLN3 has similar homology to the Bi1 protein, and ER leak channel, where the key Ca^{2+} releasing residue in the C-terminus of the Bi-1 protein is conserved in all upper eukaryotic organisms CLN3 protein led us to hypothesis that CLN3 might be acting as a lysosomal Ca^{2+} leak channel.

By using the lysosomal magnetic purification assay, as well as designing C-terminal peptides that possess the key residue on the C-terminus of wild type CLN3 proteins, we have been able to show that the C-terminus of the CLN3 protein is capable of releasing Ca^{2+}. While this work is still in its infancy, it is the first strong suggestion of CLN3's role in the cell is. Utilising the lysosomal magnetic purification assay developed, it offers potential to further aid our understanding of not only the CLN3 protein but other important lysosomal proteins that have still not been characterised.

8 Bibliograhpy

AMSTAD, E., ZURCHER, S., MASHAGHI, A., WONG, J. Y., TEXTOR, M. & REIMHULT, E. 2009. Surface functionalization of single superparamagnetic iron oxide nanoparticles for targeted magnetic resonance imaging. *Small,* 5**,** 1334-42.

AN HAACK, K., NARAYAN, S. B., LI, H., WARNOCK, A., TAN, L. & BENNETT, M. J. 2011. Screening for calcium channel modulators in CLN3 siRNA knock down SH-SY5Y neuroblastoma cells reveals a significant decrease of intracellular calcium levels by selected L-type calcium channel blockers. *Biochim Biophys Acta,* 1810**,** 186-91.

ANDERSON, N. & BORLAK, J. 2006. Drug-induced phospholipidosis. *FEBS Lett,* 580**,** 5533-40.

ARAI, K., KANASEKI, T. & OHKUMA, S. 1991. Isolation of highly purified lysosomes from rat liver: identification of electron carrier components on lysosomal membranes. *J Biochem,* 110**,** 541-7.

ARAKI, N., JOHNSON, M. T. & SWANSON, J. A. 1996. A role for phosphoinositide 3-kinase in the completion of macropinocytosis and phagocytosis by macrophages. *J Cell Biol,* 135**,** 1249-60.

ARBORGH, B., ERICSSON, J. L. & GLAUMANN, H. 1973. Method for the isolation of iron-loaded lysosomes from rat liver. *FEBS Lett,* 32**,** 190-4.

AUGUSTINE, E. F., ADAMS, H. R. & MINK, J. W. 2013. Clinical trials in rare disease: challenges and opportunities. *J Child Neurol,* 28**,** 1142-50.

AULA, N., JALANKO, A., AULA, P. & PELTONEN, L. 2002. Unraveling the molecular pathogenesis of free sialic acid storage disorders: altered targeting of mutant sialin. *Mol Genet Metab,* 77**,** 99-107.

BACH, G., CHEN, C. S. & PAGANO, R. E. 1999. Elevated lysosomal pH in Mucolipidosis type IV cells. *Clin Chim Acta,* 280**,** 173-9.

BENNETT, M. J. & RAKHEJA, D. 2013. The neuronal ceroid-lipofuscinoses. *Dev Disabil Res Rev,* 17**,** 254-9.

BERRIDGE, M. J., BOOTMAN, M. D. & RODERICK, H. L. 2003. Calcium signalling: dynamics, homeostasis and remodelling. *Nat Rev Mol Cell Biol,* 4**,** 517-29.

BOHDANOWICZ, M. & GRINSTEIN, S. 2013. Role of phospholipids in endocytosis, phagocytosis, and macropinocytosis. *Physiol Rev,* 93**,** 69-106.

BOHLAND, J. W., BOKIL, H., ALLEN, C. B. & MITRA, P. P. 2009. The brain atlas concordance problem: quantitative comparison of anatomical parcellations. *PLoS One,* 4**,** e7200.

BOOTMAN, M. D., BERRIDGE, M. J. & RODERICK, H. L. 2002. Calcium signalling: more messengers, more channels, more complexity. *Curr Biol,* 12**,** R563-5.

BOUCROT, E. & MCMAHON, H. T. 2011. [Nucleation of clathrin-coated pits - << membrane sculptors >> at work]. *Med Sci (Paris),* 27**,** 122-5.

BRADY, R. O. 2010. Benefits from unearthing "a biochemical Rosetta Stone". *J Biol Chem,* 285**,** 41216-21.

BRAILOIU, E., RAHMAN, T., CHURAMANI, D., PROLE, D. L., BRAILOIU, G. C., HOOPER, R., TAYLOR, C. W. & PATEL, S. 2010. An NAADP-gated two-pore channel targeted to the plasma membrane uncouples triggering from amplifying Ca2+ signals. *J Biol Chem,* 285**,** 38511-6.

BRAULKE, T. & BONIFACINO, J. S. 2009. Sorting of lysosomal proteins. *Biochim Biophys Acta,* 1793**,** 605-14.

BRIGHT, N. A., GRATIAN, M. J. & LUZIO, J. P. 2005. Endocytic delivery to lysosomes mediated by concurrent fusion and kissing events in living cells. *Curr Biol,* 15**,** 360-5.

BROOKS, A. I., CHATTOPADHYAY, S., MITCHISON, H. M., NUSSBAUM, R. L. & PEARCE, D. A. 2003. Functional categorization of gene expression changes in the cerebellum of a Cln3-knockout mouse model for Batten disease. *Mol Genet Metab,* 78**,** 17-30.

BROOKS, D. A. 2009. The endosomal network. *Int J Clin Pharmacol Ther,* 47 Suppl 1**,** S9-17.

BUCCI, C., PARTON, R. G., MATHER, I. H., STUNNENBERG, H., SIMONS, K., HOFLACK, B. & ZERIAL, M. 1992. The small GTPase rab5 functions as a regulatory factor in the early endocytic pathway. *Cell,* 70**,** 715-28.

BULTYNCK, G., KIVILUOTO, S., HENKE, N., IVANOVA, H., SCHNEIDER, L., RYBALCHENKO, V., LUYTEN, T., NUYTS, K., DE BORGGRAEVE, W., BEZPROZVANNY, I., PARYS, J. B., DE SMEDT, H., MISSIAEN, L. & METHNER, A. 2012. The C terminus of Bax inhibitor-1 forms a Ca2+-permeable channel pore. *J Biol Chem,* 287**,** 2544-57.

CANUEL, M., LIBIN, Y. & MORALES, C. R. 2009. The interactomics of sortilin: an ancient lysosomal receptor evolving new functions. *Histol Histopathol,* 24**,** 481-92.

CAO, Y., ESPINOLA, J. A., FOSSALE, E., MASSEY, A. C., CUERVO, A. M., MACDONALD, M. E. & COTMAN, S. L. 2006. Autophagy is disrupted in a knock-in mouse model of juvenile neuronal ceroid lipofuscinosis. *J Biol Chem,* 281**,** 20483-93.

CAO, Y., STAROPOLI, J. F., BISWAS, S., ESPINOLA, J. A., MACDONALD, M. E., LEE, J. M. & COTMAN, S. L. 2011. Distinct early molecular responses to mutations causing vLINCL and JNCL presage ATP synthase subunit C accumulation in cerebellar cells. *PLoS One,* 6**,** e17118.

CARETTE, J. E., RAABEN, M., WONG, A. C., HERBERT, A. S., OBERNOSTERER, G., MULHERKAR, N., KUEHNE, A. I., KRANZUSCH, P. J., GRIFFIN, A. M., RUTHEL, G., DAL CIN, P., DYE, J. M., WHELAN, S. P., CHANDRAN, K. & BRUMMELKAMP, T. R. 2011. Ebola virus entry requires the cholesterol transporter Niemann-Pick C1. *Nature,* 477**,** 340-3.

CARLTON, J., BUJNY, M., PETER, B. J., OORSCHOT, V. M., RUTHERFORD, A., MELLOR, H., KLUMPERMAN, J., MCMAHON, H. T. & CULLEN, P. J. 2004. Sorting nexin-1 mediates tubular endosome-to-TGN transport through coincidence sensing of high- curvature membranes and 3-phosphoinositides. *Curr Biol,* 14**,** 1791-800.

CARRION, A. M., LINK, W. A., LEDO, F., MELLSTROM, B. & NARANJO, J. R. 1999. DREAM is a Ca2+-regulated transcriptional repressor. *Nature,* 398**,** 80-4.

CHANG, J. W., CHOI, H., KIM, H. J., JO, D. G., JEON, Y. J., NOH, J. Y., PARK, W. J. & JUNG, Y. K. 2007. Neuronal vulnerability of CLN3 deletion to calcium-

induced cytotoxicity is mediated by calsenilin. *Hum Mol Genet,* 16**,** 317-26.

CHANG, Y., BRUNI, R., KLOSS, B., ASSUR, Z., KLOPPMANN, E., ROST, B., HENDRICKSON, W. A. & LIU, Q. 2014. Structural basis for a pH-sensitive calcium leak across membranes. *Science,* 344**,** 1131-5.

CHARROW, J. 2009. Enzyme replacement therapy for Gaucher disease. *Expert Opin Biol Ther,* 9**,** 121-31.

CHEN, F. W., GORDON, R. E. & IOANNOU, Y. A. 2005. NPC1 late endosomes contain elevated levels of non-esterified ('free') fatty acids and an abnormally glycosylated form of the NPC2 protein. *Biochem J,* 390**,** 549-61.

CHEN, Y. & ARRIAGA, E. A. 2006. Individual acidic organelle pH measurements by capillary electrophoresis. *Anal Chem,* 78**,** 820-6.

CHEVALLIER, J., CHAMOUN, Z., JIANG, G., PRESTWICH, G., SAKAI, N., MATILE, S., PARTON, R. G. & GRUENBERG, J. 2008. Lysobisphosphatidic acid controls endosomal cholesterol levels. *J Biol Chem,* 283**,** 27871-80.

CHOURPA, I., DOUZIECH-EYROLLES, L., NGABONI-OKASSA, L., FOUQUENET, J. F., COHEN-JONATHAN, S., SOUCE, M., MARCHAIS, H. & DUBOIS, P. 2005. Molecular composition of iron oxide nanoparticles, precursors for magnetic drug targeting, as characterized by confocal Raman microspectroscopy. *Analyst,* 130**,** 1395-403.

CHRISTENSEN, K. A., MYERS, J. T. & SWANSON, J. A. 2002. pH-dependent regulation of lysosomal calcium in macrophages. *J Cell Sci,* 115**,** 599-607.

CHURCHILL, G. C. & GALIONE, A. 2001. NAADP induces Ca2+ oscillations via a two-pool mechanism by priming IP3- and cADPR-sensitive Ca2+ stores. *EMBO J,* 20**,** 2666-71.

CHURCHILL, G. C., OKADA, Y., THOMAS, J. M., GENAZZANI, A. A., PATEL, S. & GALIONE, A. 2002. NAADP mobilizes Ca(2+) from reserve granules, lysosome-related organelles, in sea urchin eggs. *Cell,* 111**,** 703-8.

CITRON, M., WESTAWAY, D., XIA, W., CARLSON, G., DIEHL, T., LEVESQUE, G., JOHNSON-WOOD, K., LEE, M., SEUBERT, P., DAVIS, A., KHOLODENKO, D., MOTTER, R., SHERRINGTON, R., PERRY, B., YAO, H., STROME, R., LIEBERBURG, I., ROMMENS, J., KIM, S., SCHENK, D., FRASER, P., ST GEORGE HYSLOP, P. & SELKOE, D. J. 1997. Mutant presenilins of Alzheimer's disease increase production of 42-residue amyloid beta-protein in both transfected cells and transgenic mice. *Nat Med,* 3**,** 67-72.

CLAPHAM, D. E. 1995. Calcium signaling. *Cell,* 80**,** 259-68.

CLAPPER, D. L., WALSETH, T. F., DARGIE, P. J. & LEE, H. C. 1987. Pyridine nucleotide metabolites stimulate calcium release from sea urchin egg microsomes desensitized to inositol trisphosphate. *J Biol Chem,* 262**,** 9561-8.

CODLIN, S. & MOLE, S. E. 2009. S. pombe btn1, the orthologue of the Batten disease gene CLN3, is required for vacuole protein sorting of Cpy1p and Golgi exit of Vps10p. *J Cell Sci,* 122**,** 1163-73.

COTMAN, S. L. & STAROPOLI, J. F. 2012. The juvenile Batten disease protein, CLN3, and its role in regulating anterograde and retrograde post-Golgi trafficking. *Clin Lipidol,* 7**,** 79-91.

COTMAN, S. L., VRBANAC, V., LEBEL, L. A., LEE, R. L., JOHNSON, K. A., DONAHUE, L. R., TEED, A. M., ANTONELLIS, K., BRONSON, R. T., LERNER, T. J. & MACDONALD, M. E. 2002. Cln3(Deltaex7/8) knock-in mice with the common JNCL mutation exhibit progressive neurologic disease that begins before birth. *Hum Mol Genet,* 11**,** 2709-21.

COUTINHO, M. F., PRATA, M. J. & ALVES, S. 2012. A shortcut to the lysosome: the mannose-6-phosphate-independent pathway. *Mol Genet Metab,* 107**,** 257-66.

COX, T. M. & CACHON-GONZALEZ, M. B. 2012. The cellular pathology of lysosomal diseases. *J Pathol,* 226**,** 241-54.

DAVIES, J. P., CHEN, F. W. & IOANNOU, Y. A. 2000. Transmembrane molecular pump activity of Niemann-Pick C1 protein. *Science,* 290**,** 2295-8.

DE DUVE, D. 1969. The peroxisome: a new cytoplasmic organelle. *Proc R Soc Lond B Biol Sci,* 173**,** 71-83.

DE STROOPER, B., SAFTIG, P., CRAESSAERTS, K., VANDERSTICHELE, H., GUHDE, G., ANNAERT, W., VON FIGURA, K. & VAN LEUVEN, F. 1998. Deficiency of presenilin-1 inhibits the normal cleavage of amyloid precursor protein. *Nature,* 391**,** 387-90.

DIETTRICH, O., MILLS, K., JOHNSON, A. W., HASILIK, A. & WINCHESTER, B. G. 1998. Application of magnetic chromatography to the isolation of lysosomes from fibroblasts of patients with lysosomal storage disorders. *FEBS Lett,* 441**,** 369-72.

DOHERTY, G. J. & LUNDMARK, R. 2009. GRAF1-dependent endocytosis. *Biochem Soc Trans,* 37**,** 1061-5.

DORAY, B., GHOSH, P., GRIFFITH, J., GEUZE, H. J. & KORNFELD, S. 2002. Cooperation of GGAs and AP-1 in packaging MPRs at the trans-Golgi network. *Science,* 297**,** 1700-3.

DUVVURI, M. & KRISE, J. P. 2005. A novel assay reveals that weakly basic model compounds concentrate in lysosomes to an extent greater than pH-partitioning theory would predict. *Mol Pharm,* 2**,** 440-8.

E, H. 1989. *Lysosomes,* Plenum, New York.

ERICKSON, R. P., GARVER, W. S., CAMARGO, F., HOSSAIN, G. S. & HEIDENREICH, R. A. 2000. Pharmacological and genetic modifications of somatic cholesterol do not substantially alter the course of CNS disease in Niemann-Pick C mice. *J Inherit Metab Dis,* 23**,** 54-62.

EZAKI, J., TAKEDA-EZAKI, M., KOIKE, M., OHSAWA, Y., TAKA, H., MINEKI, R., MURAYAMA, K., UCHIYAMA, Y., UENO, T. & KOMINAMI, E. 2003. Characterization of Cln3p, the gene product responsible for juvenile neuronal ceroid lipofuscinosis, as a lysosomal integral membrane glycoprotein. *J Neurochem,* 87**,** 1296-308.

FARSAD, K., SLEPNEV, V., OCHOA, G., DANIELL, L., HAUCKE, V. & DE CAMILLI, P. 2003. A putative role for intramolecular regulatory mechanisms in the adaptor function of amphiphysin in endocytosis. *Neuropharmacology,* 45**,** 787-96.

FEHRENBACHER, N., BASTHOLM, L., KIRKEGAARD-SORENSEN, T., RAFN, B., BOTTZAUW, T., NIELSEN, C., WEBER, E., SHIRASAWA, S., KALLUNKI, T. & JAATTELA, M. 2008. Sensitization to the lysosomal cell death

pathway by oncogene-induced down-regulation of lysosome-associated membrane proteins 1 and 2. *Cancer Res,* 68**,** 6623-33.

FOSSALE, E., WOLF, P., ESPINOLA, J. A., LUBICZ-NAWROCKA, T., TEED, A. M., GAO, H., RIGAMONTI, D., CATTANEO, E., MACDONALD, M. E. & COTMAN, S. L. 2004. Membrane trafficking and mitochondrial abnormalities precede subunit c deposition in a cerebellar cell model of juvenile neuronal ceroid lipofuscinosis. *BMC Neurosci,* 5**,** 57.

FRESE, M. A., SCHULZ, S. & DIERKS, T. 2008. Arylsulfatase G, a novel lysosomal sulfatase. *J Biol Chem,* 283**,** 11388-95.

FROHLICH, E., MEINDL, C., ROBLEGG, E., EBNER, B., ABSENGER, M. & PIEBER, T. R. 2012a. Action of polystyrene nanoparticles of different sizes on lysosomal function and integrity. *Part Fibre Toxicol,* 9**,** 26.

FROHLICH, E., MEINDL, C., ROBLEGG, E., GRIESBACHER, A. & PIEBER, T. R. 2012b. Cytotoxity of nanoparticles is influenced by size, proliferation and embryonic origin of the cells used for testing. *Nanotoxicology,* 6**,** 424-39.

GALIONE, A., CHUANG, K. T., FUNNELL, T. M., DAVIS, L. C., MORGAN, A. J., RUAS, M., PARRINGTON, J. & CHURCHILL, G. C. 2014. Preparation and Use of Sea Urchin Egg Homogenates for Studying NAADP-Mediated Ca2+ Release. *Cold Spring Harb Protoc,* 2014**,** pdb prot076901.

GALIZZI, G., RUSSO, D., DEIDDA, I., CASCIO, C., PASSANTINO, R., GUARNERI, R., BIGINI, P., MENNINI, T., DRAGO, G. & GUARNERI, P. 2011. Different early ER-stress responses in the CLN8(mnd) mouse model of neuronal ceroid lipofuscinosis. *Neurosci Lett,* 488**,** 258-62.

GARNETT, M. C. & KALLINTERI, P. 2006. Nanomedicines and nanotoxicology: some physiological principles. *Occup Med (Lond),* 56**,** 307-11.

GENAZZANI, A. A. & GALIONE, A. 1996. Nicotinic acid-adenine dinucleotide phosphate mobilizes Ca2+ from a thapsigargin-insensitive pool. *Biochem J,* 315 (Pt 3)**,** 721-5.

GINZBURG, L., KACHER, Y. & FUTERMAN, A. H. 2004. The pathogenesis of glycosphingolipid storage disorders. *Semin Cell Dev Biol,* 15**,** 417-31.

GLEBOV, O. O., BRIGHT, N. A. & NICHOLS, B. J. 2006. Flotillin-1 defines a clathrin-independent endocytic pathway in mammalian cells. *Nat Cell Biol,* 8**,** 46-54.

GOLABEK, A. A., KIDA, E., WALUS, M., KACZMARSKI, W., MICHALEWSKI, M. & WISNIEWSKI, K. E. 2000. CLN3 protein regulates lysosomal pH and alters intracellular processing of Alzheimer's amyloid-beta protein precursor and cathepsin D in human cells. *Mol Genet Metab,* 70**,** 203-13.

GOLABEK, A. A., KIDA, E., WALUS, M., KACZMARSKI, W., WUJEK, P. & WISNIEWSKI, K. E. 2001. CLN3 disease process: missense point mutations and protein depletion in vitro. *Eur J Paediatr Neurol,* 5 Suppl A**,** 81-8.

GRAHAM, J. M. 2001. Isolation of lysosomes from tissues and cells by differential and density gradient centrifugation. *Curr Protoc Cell Biol,* Chapter 3**,** Unit 3 6.

GRAHAM, J. M. 2002. Homogenization of mammalian cultured cells. *ScientificWorldJournal,* 2**,** 1630-3.

GRUBMAN, A., POLLARI, E., DUNCAN, C., CARAGOUNIS, A., BLOM, T., VOLITAKIS, I., WONG, A., COOPER, J., CROUCH, P. J., KOISTINAHO, J., JALANKO, A., WHITE, A. R. & KANNINEN, K. M. 2014. Deregulation of biometal homeostasis: the missing link for neuronal ceroid lipofuscinoses? *Metallomics,* 6**,** 932-43.

HANINI, A., SCHMITT, A., KACEM, K., CHAU, F., AMMAR, S. & GAVARD, J. 2011. Evaluation of iron oxide nanoparticle biocompatibility. *Int J Nanomedicine,* 6**,** 787-94.

HASKELL, R. E., CARR, C. J., PEARCE, D. A., BENNETT, M. J. & DAVIDSON, B. L. 2000. Batten disease: evaluation of CLN3 mutations on protein localization and function. *Hum Mol Genet,* 9**,** 735-44.

HENNING, R. & PLATTNER, H. 1974. Isolation of rat liver lysosomes by loading with colloidal gold. *Biochim Biophys Acta,* 354**,** 114-20.

HOBERT, J. A. & DAWSON, G. 2007. A novel role of the Batten disease gene CLN3: association with BMP synthesis. *Biochem Biophys Res Commun,* 358**,** 111-6.

HOLOPAINEN, J. M., SAARIKOSKI, J., KINNUNEN, P. K. & JARVELA, I. 2001. Elevated lysosomal pH in neuronal ceroid lipofuscinoses (NCLs). *Eur J Biochem,* 268**,** 5851-6.

HOWES, M. T., KIRKHAM, M., RICHES, J., CORTESE, K., WALSER, P. J., SIMPSON, F., HILL, M. M., JONES, A., LUNDMARK, R., LINDSAY, M. R., HERNANDEZ-DEVIEZ, D. J., HADZIC, G., MCCLUSKEY, A., BASHIR, R., LIU, L., PILCH, P., MCMAHON, H., ROBINSON, P. J., HANCOCK, J. F., MAYOR, S. & PARTON, R. G. 2010. Clathrin-independent carriers form a high capacity endocytic sorting system at the leading edge of migrating cells. *J Cell Biol,* 190**,** 675-91.

HUYNH, K. K., ESKELINEN, E. L., SCOTT, C. C., MALEVANETS, A., SAFTIG, P. & GRINSTEIN, S. 2007. LAMP proteins are required for fusion of lysosomes with phagosomes. *EMBO J,* 26**,** 313-24.

IKONEN, E. & HOLTTA-VUORI, M. 2004. Cellular pathology of Niemann-Pick type C disease. *Semin Cell Dev Biol,* 15**,** 445-54.

JARVELA, I., LEHTOVIRTA, M., TIKKANEN, R., KYTTALA, A. & JALANKO, A. 1999. Defective intracellular transport of CLN3 is the molecular basis of Batten disease (JNCL). *Hum Mol Genet,* 8**,** 1091-8.

JEYAKUMAR, M., SMITH, D., ELIOTT-SMITH, E., CORTINA-BORJA, M., REINKENSMEIER, G., BUTTERS, T. D., LEMM, T., SANDHOFF, K., PERRY, V. H., DWEK, R. A. & PLATT, F. M. 2002. An inducible mouse model of late onset Tay-Sachs disease. *Neurobiol Dis,* 10**,** 201-10.

KAKKIS, E. D. 2002. Enzyme replacement therapy for the mucopolysaccharide storage disorders. *Expert Opin Investig Drugs,* 11**,** 675-85.

KANG, S., KIM, J. B., HEO, T. H. & KIM, S. J. 2013. Cell cycle arrest in Batten disease lymphoblast cells. *Gene,* 519**,** 245-50.

KIM, J. S., HE, L., QIAN, T. & LEMASTERS, J. J. 2003. Role of the mitochondrial permeability transition in apoptotic and necrotic death after ischemia/reperfusion injury to hepatocytes. *Curr Mol Med,* 3**,** 527-35.

KIRKHAM, M., FUJITA, A., CHADDA, R., NIXON, S. J., KURZCHALIA, T. V., SHARMA, D. K., PAGANO, R. E., HANCOCK, J. F., MAYOR, S. & PARTON,

R. G. 2005. Ultrastructural identification of uncoated caveolin-independent early endocytic vehicles. *J Cell Biol,* 168**,** 465-76.

KO, D. C., GORDON, M. D., JIN, J. Y. & SCOTT, M. P. 2001. Dynamic movements of organelles containing Niemann-Pick C1 protein: NPC1 involvement in late endocytic events. *Mol Biol Cell,* 12**,** 601-14.

KOLTER, T. & SANDHOFF, K. 2005. Principles of lysosomal membrane digestion: stimulation of sphingolipid degradation by sphingolipid activator proteins and anionic lysosomal lipids. *Annu Rev Cell Dev Biol,* 21**,** 81-103.

KORNAK, U., KASPER, D., BOSL, M. R., KAISER, E., SCHWEIZER, M., SCHULZ, A., FRIEDRICH, W., DELLING, G. & JENTSCH, T. J. 2001. Loss of the ClC-7 chloride channel leads to osteopetrosis in mice and man. *Cell,* 104**,** 205-15.

KOUSI, M., LEHESJOKI, A. E. & MOLE, S. E. 2012. Update of the mutation spectrum and clinical correlations of over 360 mutations in eight genes that underlie the neuronal ceroid lipofuscinoses. *Hum Mutat,* 33**,** 42-63.

KUMARI, S. & MAYOR, S. 2008. ARF1 is directly involved in dynamin-independent endocytosis. *Nat Cell Biol,* 10**,** 30-41.

KWON, J. M., ROTHBERG, P. G., LEMAN, A. R., WEIMER, J. M., MINK, J. W. & PEARCE, D. A. 2005. Novel CLN3 mutation predicted to cause complete loss of protein function does not modify the classical JNCL phenotype. *Neurosci Lett,* 387**,** 111-4.

KYTTALA, A., IHRKE, G., VESA, J., SCHELL, M. J. & LUZIO, J. P. 2004. Two motifs target Batten disease protein CLN3 to lysosomes in transfected nonneuronal and neuronal cells. *Mol Biol Cell,* 15**,** 1313-23.

LAPLANTE, J. M., FALARDEAU, J., SUN, M., KANAZIRSKA, M., BROWN, E. M., SLAUGENHAUPT, S. A. & VASSILEV, P. M. 2002. Identification and characterization of the single channel function of human mucolipin-1 implicated in mucolipidosis type IV, a disorder affecting the lysosomal pathway. *FEBS Lett,* 532**,** 183-7.

LARISCH, N., SCHULZE, C., GALIONE, A. & DIETRICH, P. 2012. An N-terminal dileucine motif directs two-pore channels to the tonoplast of plant cells. *Traffic,* 13**,** 1012-22.

LAURENT, S., FORGE, D., PORT, M., ROCH, A., ROBIC, C., VANDER ELST, L. & MULLER, R. N. 2008. Magnetic iron oxide nanoparticles: synthesis, stabilization, vectorization, physicochemical characterizations, and biological applications. *Chem Rev,* 108**,** 2064-110.

LEE, J. H., YU, W. H., KUMAR, A., LEE, S., MOHAN, P. S., PETERHOFF, C. M., WOLFE, D. M., MARTINEZ-VICENTE, M., MASSEY, A. C., SOVAK, G., UCHIYAMA, Y., WESTAWAY, D., CUERVO, A. M. & NIXON, R. A. 2010. Lysosomal proteolysis and autophagy require presenilin 1 and are disrupted by Alzheimer-related PS1 mutations. *Cell,* 141**,** 1146-58.

LEE, S., SATO, Y. & NIXON, R. A. 2011. Lysosomal proteolysis inhibition selectively disrupts axonal transport of degradative organelles and causes an Alzheimer's-like axonal dystrophy. *J Neurosci,* 31**,** 7817-30.

LEVINE, B. & KLIONSKY, D. J. 2004. Development by self-digestion: molecular mechanisms and biological functions of autophagy. *Dev Cell,* 6**,** 463-77.

LI, G., D'SOUZA-SCHOREY, C., BARBIERI, M. A., COOPER, J. A. & STAHL, P. D. 1997. Uncoupling of membrane ruffling and pinocytosis during Ras signal transduction. *J Biol Chem,* 272**,** 10337-40.

LICHKO, L. P. & OKOROKOV, L. A. 1984. Some properties of membrane-bound, solubilized and reconstituted into liposomes H+-ATPase of vacuoles of Saccharomyces carlsbergensis. *FEBS Lett,* 174**,** 233-7.

LILLIEHOOK, C., CHAN, S., CHOI, E. K., ZAIDI, N. F., WASCO, W., MATTSON, M. P. & BUXBAUM, J. D. 2002. Calsenilin enhances apoptosis by altering endoplasmic reticulum calcium signaling. *Mol Cell Neurosci,* 19**,** 552-9.

LIN, Y., EPSTEIN, D. L. & LITON, P. B. 2010. Intralysosomal iron induces lysosomal membrane permeabilization and cathepsin D-mediated cell death in trabecular meshwork cells exposed to oxidative stress. *Invest Ophthalmol Vis Sci,* 51**,** 6483-95.

LINDHOLM, D., WOOTZ, H. & KORHONEN, L. 2006. ER stress and neurodegenerative diseases. *Cell Death Differ,* 13**,** 385-92.

LISCUM, L. 2000. Niemann-Pick type C mutations cause lipid traffic jam. *Traffic,* 1**,** 218-25.

LIU, W. H., LI, R. & DOU, K. F. 2011. Convenient and efficient enrichment of the CD133+ liver cells from rat fetal liver cells as a source of liver stem/progenitor cells. *Stem Cell Rev,* 7**,** 94-102.

LIU, W. H., WANG, X., YOU, N., TAO, K. S., WANG, T., TANG, L. J. & DOU, K. F. 2012. Efficient enrichment of hepatic cancer stem-like cells from a primary rat HCC model via a density gradient centrifugation-centered method. *PLoS One,* 7**,** e35720.

LLOYD-EVANS, E., MORGAN, A. J., HE, X., SMITH, D. A., ELLIOT-SMITH, E., SILLENCE, D. J., CHURCHILL, G. C., SCHUCHMAN, E. H., GALIONE, A. & PLATT, F. M. 2008. Niemann-Pick disease type C1 is a sphingosine storage disease that causes deregulation of lysosomal calcium. *Nat Med,* 14**,** 1247-55.

LLOYD-EVANS, E., PELLED, D., RIEBELING, C. & FUTERMAN, A. H. 2003. Lyso-glycosphingolipids mobilize calcium from brain microsomes via multiple mechanisms. *Biochem J,* 375**,** 561-5.

LLOYD-EVANS, E. & PLATT, F. M. 2010. Lipids on trial: the search for the offending metabolite in Niemann-Pick type C disease. *Traffic,* 11**,** 419-28.

LLOYD-EVANS, E. & PLATT, F. M. 2011. Lysosomal Ca(2+) homeostasis: role in pathogenesis of lysosomal storage diseases. *Cell Calcium,* 50**,** 200-5.

LLOYD-EVANS, E., WALLER-EVANS, H., PETERNEVA, K. & PLATT, F. M. 2010. Endolysosomal calcium regulation and disease. *Biochem Soc Trans,* 38**,** 1458-64.

LOMBARDI, D., SOLDATI, T., RIEDERER, M. A., GODA, Y., ZERIAL, M. & PFEFFER, S. R. 1993. Rab9 functions in transport between late endosomes and the trans Golgi network. *EMBO J,* 12**,** 677-82.

LUBKE, T., LOBEL, P. & SLEAT, D. E. 2009. Proteomics of the lysosome. *Biochim Biophys Acta,* 1793**,** 625-35.

LUIRO, K., YLIANNALA, K., AHTIAINEN, L., MAUNU, H., JARVELA, I., KYTTALA, A. & JALANKO, A. 2004. Interconnections of CLN3, Hook1 and Rab proteins link Batten disease to defects in the endocytic pathway. *Hum Mol Genet,* 13**,** 3017-27.

LUTGENS, S. P., CLEUTJENS, K. B., DAEMEN, M. J. & HEENEMAN, S. 2007. Cathepsin cysteine proteases in cardiovascular disease. *FASEB J,* 21**,** 3029-41.

LUZIO, J. P., PARKINSON, M. D., GRAY, S. R. & BRIGHT, N. A. 2009. The delivery of endocytosed cargo to lysosomes. *Biochem Soc Trans,* 37**,** 1019-21.

LUZIO, J. P., PRYOR, P. R. & BRIGHT, N. A. 2007. Lysosomes: fusion and function. *Nat Rev Mol Cell Biol,* 8**,** 622-32.

LUZIO, J. P., ROUS, B. A., BRIGHT, N. A., PRYOR, P. R., MULLOCK, B. M. & PIPER, R. C. 2000. Lysosome-endosome fusion and lysosome biogenesis. *J Cell Sci,* 113 (Pt 9)**,** 1515-24.

MACEYKA, M., SANKALA, H., HAIT, N. C., LE STUNFF, H., LIU, H., TOMAN, R., COLLIER, C., ZHANG, M., SATIN, L. S., MERRILL, A. H., JR., MILSTIEN, S. & SPIEGEL, S. 2005. SphK1 and SphK2, sphingosine kinase isoenzymes with opposing functions in sphingolipid metabolism. *J Biol Chem,* 280**,** 37118-29.

MANUNTA, M., IZZO, L., DUNCAN, R. & JONES, A. T. 2007. Establishment of subcellular fractionation techniques to monitor the intracellular fate of polymer therapeutics II. Identification of endosomal and lysosomal compartments in HepG2 cells combining single-step subcellular fractionation with fluorescent imaging. *J Drug Target,* 15**,** 37-50.

MAO, Q., FOSTER, B. J., XIA, H. & DAVIDSON, B. L. 2003. Membrane topology of CLN3, the protein underlying Batten disease. *FEBS Lett,* 541**,** 40-6.

MARCHANT, J. S. & PATEL, S. 2013. Questioning regulation of two-pore channels by NAADP. *Messenger (Los Angel),* 2**,** 113-119.

MATTERA, R., BOEHM, M., CHAUDHURI, R., PRABHU, Y. & BONIFACINO, J. S. 2011. Conservation and diversification of dileucine signal recognition by adaptor protein (AP) complex variants. *J Biol Chem,* 286**,** 2022-30.

MAYER, A., VADON, M., RINNER, B., NOVAK, A., WINTERSTEIGER, R. & FROHLICH, E. 2009. The role of nanoparticle size in hemocompatibility. *Toxicology,* 258**,** 139-47.

MAYOR, S. & PAGANO, R. E. 2007. Pathways of clathrin-independent endocytosis. *Nat Rev Mol Cell Biol,* 8**,** 603-12.

MEIKLE, P. J., HOPWOOD, J. J., CLAGUE, A. E. & CAREY, W. F. 1999. Prevalence of lysosomal storage disorders. *JAMA,* 281**,** 249-54.

MENDLA, K., BAUMKOTTER, J., ROSENAU, C., ULRICH-BOTT, B. & CANTZ, M. 1988. Defective lysosomal release of glycoprotein-derived sialic acid in fibroblasts from patients with sialic acid storage disease. *Biochem J,* 250**,** 261-7.

MINDELL, J. A. 2012. Lysosomal acidification mechanisms. *Annu Rev Physiol,* 74**,** 69-86.

MORGAN, A. J. & GALIONE, A. 2007. Fertilization and nicotinic acid adenine dinucleotide phosphate induce pH changes in acidic Ca(2+) stores in sea urchin eggs. *J Biol Chem,* 282**,** 37730-7.

MUKHERJEE, S., GHOSH, R. N. & MAXFIELD, F. R. 1997. Endocytosis. *Physiol Rev,* 77**,** 759-803.

MUKHERJEE, T. K., MUKHOPADHYAY, S. & HOIDAL, J. R. 2005. The role of reactive oxygen species in TNFalpha-dependent expression of the receptor for advanced glycation end products in human umbilical vein endothelial cells. *Biochim Biophys Acta,* 1744**,** 213-23.

MULCAHY, L. A., PINK, R. C. & CARTER, D. R. 2014. Routes and mechanisms of extracellular vesicle uptake. *J Extracell Vesicles,* 3.

MULLINS, C. & BONIFACINO, J. S. 2001. The molecular machinery for lysosome biogenesis. *Bioessays,* 23**,** 333-43.

MULLOCK, B. M., BRIGHT, N. A., FEARON, C. W., GRAY, S. R. & LUZIO, J. P. 1998. Fusion of lysosomes with late endosomes produces a hybrid organelle of intermediate density and is NSF dependent. *J Cell Biol,* 140**,** 591-601.

MURPHY, R. F. 1991. Maturation models for endosome and lysosome biogenesis. *Trends Cell Biol,* 1**,** 77-82.

NASSAR, Z. D., HILL, M. M., PARTON, R. G. & PARAT, M. O. 2013. Caveola-forming proteins caveolin-1 and PTRF in prostate cancer. *Nat Rev Urol,* 10**,** 529-36.

NIEMINEN, A. L., BYRNE, A. M., HERMAN, B. & LEMASTERS, J. J. 1997. Mitochondrial permeability transition in hepatocytes induced by t-BuOOH: NAD(P)H and reactive oxygen species. *Am J Physiol,* 272**,** C1286-94.

NIJSSEN, P. C., CEUTERICK, C., VAN DIGGELEN, O. P., ELLEDER, M., MARTIN, J. J., TEEPEN, J. L., TYYNELA, J. & ROOS, R. A. 2003. Autosomal dominant adult neuronal ceroid lipofuscinosis: a novel form of NCL with granular osmiophilic deposits without palmitoyl protein thioesterase 1 deficiency. *Brain Pathol,* 13**,** 574-81.

NISHINO, I. 2006. Autophagic vacuolar myopathy. *Semin Pediatr Neurol,* 13**,** 90-5.

OH, P., MCINTOSH, D. P. & SCHNITZER, J. E. 1998. Dynamin at the neck of caveolae mediates their budding to form transport vesicles by GTP-driven fission from the plasma membrane of endothelium. *J Cell Biol,* 141**,** 101-14.

OHKUMA, S., MORIYAMA, Y. & TAKANO, T. 1982. Identification and characterization of a proton pump on lysosomes by fluorescein-isothiocyanate-dextran fluorescence. *Proc Natl Acad Sci U S A,* 79**,** 2758-62.

PALMER, D. N., BARRY, L. A., TYYNELA, J. & COOPER, J. D. 2013. NCL disease mechanisms. *Biochim Biophys Acta,* 1832**,** 1882-93.

PALMER, D. N., BAYLISS, S. L. & WESTLAKE, V. J. 1995. Batten disease and the ATP synthase subunit c turnover pathway: raising antibodies to subunit c. *Am J Med Genet,* 57**,** 260-5.

PALMER, D. N., FEARNLEY, I. M., WALKER, J. E., HALL, N. A., LAKE, B. D., WOLFE, L. S., HALTIA, M., MARTINUS, R. D. & JOLLY, R. D. 1992.

Mitochondrial ATP synthase subunit c storage in the ceroid-lipofuscinoses (Batten disease). *Am J Med Genet,* 42**,** 561-7.
PAO, S. S., PAULSEN, I. T. & SAIER, M. H., JR. 1998. Major facilitator superfamily. *Microbiol Mol Biol Rev,* 62**,** 1-34.
PARK, W. D., O'BRIEN, J. F., LUNDQUIST, P. A., KRAFT, D. L., VOCKLEY, C. W., KARNES, P. S., PATTERSON, M. C. & SNOW, K. 2003. Identification of 58 novel mutations in Niemann-Pick disease type C: correlation with biochemical phenotype and importance of PTC1-like domains in NPC1. *Hum Mutat,* 22**,** 313-25.
PARTON, R. G., JOGGERST, B. & SIMONS, K. 1994. Regulated internalization of caveolae. *J Cell Biol,* 127**,** 1199-215.
PATTERSON, M. C., VECCHIO, D., PRADY, H., ABEL, L. & WRAITH, J. E. 2007. Miglustat for treatment of Niemann-Pick C disease: a randomised controlled study. *Lancet Neurol,* 6**,** 765-72.
PEDEN, A. A., OORSCHOT, V., HESSER, B. A., AUSTIN, C. D., SCHELLER, R. H. & KLUMPERMAN, J. 2004. Localization of the AP-3 adaptor complex defines a novel endosomal exit site for lysosomal membrane proteins. *J Cell Biol,* 164**,** 1065-76.
PELKMANS, L. & ZERIAL, M. 2005. Kinase-regulated quantal assemblies and kiss-and-run recycling of caveolae. *Nature,* 436**,** 128-33.
PELLED, D., TRAJKOVIC-BODENNEC, S., LLOYD-EVANS, E., SIDRANSKY, E., SCHIFFMANN, R. & FUTERMAN, A. H. 2005. Enhanced calcium release in the acute neuronopathic form of Gaucher disease. *Neurobiol Dis,* 18**,** 83-8.
PERSAUD-SAWIN, D. A., MOUSALLEM, T., WANG, C., ZUCKER, A., KOMINAMI, E. & BOUSTANY, R. M. 2007. Neuronal ceroid lipofuscinosis: a common pathway? *Pediatr Res,* 61**,** 146-52.
PETRI-FINK, A., CHASTELLAIN, M., JUILLERAT-JEANNERET, L., FERRARI, A. & HOFMANN, H. 2005. Development of functionalized superparamagnetic iron oxide nanoparticles for interaction with human cancer cells. *Biomaterials,* 26**,** 2685-94.
PICOLLO, A. & PUSCH, M. 2005. Chloride/proton antiporter activity of mammalian CLC proteins ClC-4 and ClC-5. *Nature,* 436**,** 420-3.
PLATT, F. M., BOLAND, B. & VAN DER SPOEL, A. C. 2012. The cell biology of disease: lysosomal storage disorders: the cellular impact of lysosomal dysfunction. *J Cell Biol,* 199**,** 723-34.
POUPETOVA, H., LEDVINOVA, J., BERNA, L., DVORAKOVA, L., KOZICH, V. & ELLEDER, M. 2010. The birth prevalence of lysosomal storage disorders in the Czech Republic: comparison with data in different populations. *J Inherit Metab Dis,* 33**,** 387-96.
POZZAN, T., RIZZUTO, R., VOLPE, P. & MELDOLESI, J. 1994. Molecular and cellular physiology of intracellular calcium stores. *Physiol Rev,* 74**,** 595-636.
PUERTOLLANO, R. 2004. Clathrin-mediated transport: assembly required. Workshop on Molecular Mechanisms of Vesicle Selectivity. *EMBO Rep,* 5**,** 942-6.
RECZEK, D., SCHWAKE, M., SCHRODER, J., HUGHES, H., BLANZ, J., JIN, X., BRONDYK, W., VAN PATTEN, S., EDMUNDS, T. & SAFTIG, P. 2007.

LIMP-2 is a receptor for lysosomal mannose-6-phosphate-independent targeting of beta-glucocerebrosidase. *Cell,* 131**,** 770-83.
RODRIGUEZ, A., WEBSTER, P., ORTEGO, J. & ANDREWS, N. W. 1997. Lysosomes behave as Ca2+-regulated exocytic vesicles in fibroblasts and epithelial cells. *J Cell Biol,* 137**,** 93-104.
RODRIGUEZ-PARIS, J. M., NOLTA, K. V. & STECK, T. L. 1993. Characterization of lysosomes isolated from Dictyostelium discoideum by magnetic fractionation. *J Biol Chem,* 268**,** 9110-6.
ROSENBLOOM, B., BALWANI, M., BRONSTEIN, J. M., KOLODNY, E., SATHE, S., GWOSDOW, A. R., TAYLOR, J. S., COLE, J. A., ZIMRAN, A. & WEINREB, N. J. 2011. The incidence of Parkinsonism in patients with type 1 Gaucher disease: data from the ICGG Gaucher Registry. *Blood Cells Mol Dis,* 46**,** 95-102.
RUOSLAHTI, E., BHATIA, S. N. & SAILOR, M. J. 2010. Targeting of drugs and nanoparticles to tumors. *J Cell Biol,* 188**,** 759-68.
RUSYN, E., MOUSALLEM, T., PERSAUD-SAWIN, D. A., MILLER, S. & BOUSTANY, R. M. 2008. CLN3p impacts galactosylceramide transport, raft morphology, and lipid content. *Pediatr Res,* 63**,** 625-31.
SABHARANJAK, S., SHARMA, P., PARTON, R. G. & MAYOR, S. 2002. GPI-anchored proteins are delivered to recycling endosomes via a distinct cdc42-regulated, clathrin-independent pinocytic pathway. *Dev Cell,* 2**,** 411-23.
SAFTIG, P. & KLUMPERMAN, J. 2009. Lysosome biogenesis and lysosomal membrane proteins: trafficking meets function. *Nat Rev Mol Cell Biol,* 10**,** 623-35.
SANDES, E., LODILLINSKY, C., CWIRENBAUM, R., ARGUELLES, C., CASABE, A. & EIJAN, A. M. 2007. Cathepsin B is involved in the apoptosis intrinsic pathway induced by Bacillus Calmette-Guerin in transitional cancer cell lines. *Int J Mol Med,* 20**,** 823-8.
SCHEEL, O., ZDEBIK, A. A., LOURDEL, S. & JENTSCH, T. J. 2005. Voltage-dependent electrogenic chloride/proton exchange by endosomal CLC proteins. *Nature,* 436**,** 424-7.
SCHIFFMANN, R. & BRADY, R. O. 2006. Development of enzyme replacement therapy for Fabry disease. *In:* MEHTA, A., BECK, M. & SUNDER-PLASSMANN, G. (eds.) *Fabry Disease: Perspectives from 5 Years of FOS.* Oxford.
SCHULTZ, M. L., TECEDOR, L., STEIN, C. S., STAMNES, M. A. & DAVIDSON, B. L. 2014. CLN3 deficient cells display defects in the ARF1-Cdc42 pathway and actin-dependent events. *PLoS One,* 9**,** e96647.
SCOTT, C. & IOANNOU, Y. A. 2004. The NPC1 protein: structure implies function. *Biochim Biophys Acta,* 1685**,** 8-13.
SEAMAN, M. N. 2004. Cargo-selective endosomal sorting for retrieval to the Golgi requires retromer. *J Cell Biol,* 165**,** 111-22.
SEEHAFER, S. S. & PEARCE, D. A. 2006. You say lipofuscin, we say ceroid: defining autofluorescent storage material. *Neurobiol Aging,* 27**,** 576-88.
SHEN, J. & KELLEHER, R. J., 3RD 2007. The presenilin hypothesis of Alzheimer's disease: evidence for a loss-of-function pathogenic mechanism. *Proc Natl Acad Sci U S A,* 104**,** 403-9.

SIDRANSKY, E., NALLS, M. A., AASLY, J. O., AHARON-PERETZ, J., ANNESI, G., BARBOSA, E. R., BAR-SHIRA, A., BERG, D., BRAS, J., BRICE, A., CHEN, C. M., CLARK, L. N., CONDROYER, C., DE MARCO, E. V., DURR, A., EBLAN, M. J., FAHN, S., FARRER, M. J., FUNG, H. C., GAN-OR, Z., GASSER, T., GERSHONI-BARUCH, R., GILADI, N., GRIFFITH, A., GUREVICH, T., JANUARIO, C., KROPP, P., LANG, A. E., LEE-CHEN, G. J., LESAGE, S., MARDER, K., MATA, I. F., MIRELMAN, A., MITSUI, J., MIZUTA, I., NICOLETTI, G., OLIVEIRA, C., OTTMAN, R., ORR-URTREGER, A., PEREIRA, L. V., QUATTRONE, A., ROGAEVA, E., ROLFS, A., ROSENBAUM, H., ROZENBERG, R., SAMII, A., SAMADDAR, T., SCHULTE, C., SHARMA, M., SINGLETON, A., SPITZ, M., TAN, E. K., TAYEBI, N., TODA, T., TROIANO, A. R., TSUJI, S., WITTSTOCK, M., WOLFSBERG, T. G., WU, Y. R., ZABETIAN, C. P., ZHAO, Y. & ZIEGLER, S. G. 2009. Multicenter analysis of glucocerebrosidase mutations in Parkinson's disease. *N Engl J Med,* 361**,** 1651-61.

SINGH, N., JENKINS, G. J., NELSON, B. C., MARQUIS, B. J., MAFFEIS, T. G., BROWN, A. P., WILLIAMS, P. M., WRIGHT, C. J. & DOAK, S. H. 2012. The role of iron redox state in the genotoxicity of ultrafine superparamagnetic iron oxide nanoparticles. *Biomaterials,* 33**,** 163-70.

SLEAT, D. E., ZHENG, H. & LOBEL, P. 2007. The human urine mannose 6-phosphate glycoproteome. *Biochim Biophys Acta,* 1774**,** 368-72.

SMIT, J. J., SCHINKEL, A. H., OUDE ELFERINK, R. P., GROEN, A. K., WAGENAAR, E., VAN DEEMTER, L., MOL, C. A., OTTENHOFF, R., VAN DER LUGT, N. M., VAN ROON, M. A. & ET AL. 1993. Homozygous disruption of the murine mdr2 P-glycoprotein gene leads to a complete absence of phospholipid from bile and to liver disease. *Cell,* 75**,** 451-62.

SMITH, M. H., PLOEGH, H. L. & WEISSMAN, J. S. 2011. Road to ruin: targeting proteins for degradation in the endoplasmic reticulum. *Science,* 334**,** 1086-90.

STAROPOLI, J. F., HALIW, L., BISWAS, S., GARRETT, L., HOLTER, S. M., BECKER, L., SKOSYRSKI, S., DA SILVA-BUTTKUS, P., CALZADA-WACK, J., NEFF, F., RATHKOLB, B., ROZMAN, J., SCHREWE, A., ADLER, T., PUK, O., SUN, M., FAVOR, J., RACZ, I., BEKEREDJIAN, R., BUSCH, D. H., GRAW, J., KLINGENSPOR, M., KLOPSTOCK, T., WOLF, E., WURST, W., ZIMMER, A., LOPEZ, E., HARATI, H., HILL, E., KRAUSE, D. S., GUIDE, J., DRAGILEVA, E., GALE, E., WHEELER, V. C., BOUSTANY, R. M., BROWN, D. E., BRETON, S., RUETHER, K., GAILUS-DURNER, V., FUCHS, H., DE ANGELIS, M. H. & COTMAN, S. L. 2012. Large-scale phenotyping of an accurate genetic mouse model of JNCL identifies novel early pathology outside the central nervous system. *PLoS One,* 7**,** e38310.

STOORVOGEL, W., STROUS, G. J., GEUZE, H. J., OORSCHOT, V. & SCHWARTZ, A. L. 1991. Late endosomes derive from early endosomes by maturation. *Cell,* 65**,** 417-27.

STORCH, S., POHL, S. & BRAULKE, T. 2004. A dileucine motif and a cluster of acidic amino acids in the second cytoplasmic domain of the batten disease-related CLN3 protein are required for efficient lysosomal targeting. *J Biol Chem,* 279**,** 53625-34.

STURLEY, S. L., PATTERSON, M. C., BALCH, W. & LISCUM, L. 2004. The pathophysiology and mechanisms of NP-C disease. *Biochim Biophys Acta,* 1685**,** 83-7.

SZASZI, K., PAULSEN, A., SZABO, E. Z., NUMATA, M., GRINSTEIN, S. & ORLOWSKI, J. 2002. Clathrin-mediated endocytosis and recycling of the neuron-specific Na+/H+ exchanger NHE5 isoform. Regulation by phosphatidylinositol 3'-kinase and the actin cytoskeleton. *J Biol Chem,* 277**,** 42623-32.

TANAKA, Y., GUHDE, G., SUTER, A., ESKELINEN, E. L., HARTMANN, D., LULLMANN-RAUCH, R., JANSSEN, P. M., BLANZ, J., VON FIGURA, K. & SAFTIG, P. 2000. Accumulation of autophagic vacuoles and cardiomyopathy in LAMP-2-deficient mice. *Nature,* 406**,** 902-6.

TANG, Z., SCHERER, P. E., OKAMOTO, T., SONG, K., CHU, C., KOHTZ, D. S., NISHIMOTO, I., LODISH, H. F. & LISANTI, M. P. 1996. Molecular cloning of caveolin-3, a novel member of the caveolin gene family expressed predominantly in muscle. *J Biol Chem,* 271**,** 2255-61.

TAYLOR, J. M., MACKLEM, M. M. & PARSONS, J. T. 1999. Cytoskeletal changes induced by GRAF, the GTPase regulator associated with focal adhesion kinase, are mediated by Rho. *J Cell Sci,* 112 (Pt 2)**,** 231-42.

TE VRUCHTE, D., LLOYD-EVANS, E., VELDMAN, R. J., NEVILLE, D. C., DWEK, R. A., PLATT, F. M., VAN BLITTERSWIJK, W. J. & SILLENCE, D. J. 2004. Accumulation of glycosphingolipids in Niemann-Pick C disease disrupts endosomal transport. *J Biol Chem,* 279**,** 26167-75.

TECEDOR, L., STEIN, C. S., SCHULTZ, M. L., FARWANAH, H., SANDHOFF, K. & DAVIDSON, B. L. 2013. CLN3 loss disturbs membrane microdomain properties and protein transport in brain endothelial cells. *J Neurosci,* 33**,** 18065-79.

TSUKITA, S. & ISHIKAWA, H. 1980. The movement of membranous organelles in axons. Electron microscopic identification of anterogradely and retrogradely transported organelles. *J Cell Biol,* 84**,** 513-30.

TULP, A., VERWOERD, D., FERNANDEZ-BORJA, M., NEEFJES, J. & HART, A. A. 1996. High resolution density gradient electrophoresis of cellular organelles. *Electrophoresis,* 17**,** 173-8.

TULP, A., VERWOERD, D. & NEEFJES, J. 1999. Lectin-induced retardation of subcellular organelles during preparative density gradient electrophoresis: selective purification of plasma membranes. *Electrophoresis,* 20**,** 438-44.

TULP, A., VERWOERD, D. & PIETERS, J. 1993. Application of an improved density gradient electrophoresis apparatus to the separation of proteins, cells and subcellular organelles. *Electrophoresis,* 14**,** 1295-301.

UCHIYAMA, A., KIM, J. S., KON, K., JAESCHKE, H., IKEJIMA, K., WATANABE, S. & LEMASTERS, J. J. 2008. Translocation of iron from lysosomes into mitochondria is a key event during oxidative stress-induced hepatocellular injury. *Hepatology,* 48**,** 1644-54.

VAN MEER, G., VOELKER, D. R. & FEIGENSON, G. W. 2008. Membrane lipids: where they are and how they behave. *Nat Rev Mol Cell Biol,* 9**,** 112-24.

VANIER, M. T. 2010. Niemann-Pick disease type C. *Orphanet J Rare Dis,* 5**,** 16.

VARGAS, H. A., AKIN, O., AFAQ, A., GOLDMAN, D., ZHENG, J., MOSKOWITZ, C. S., SHUKLA-DAVE, A., EASTHAM, J., SCARDINO, P. & HRICAK, H. 2012. Magnetic resonance imaging for predicting prostate biopsy findings in patients considered for active surveillance of clinically low risk prostate cancer. *J Urol,* 188**,** 1732-8.

VAZQUEZ, M. C., BALBOA, E., ALVAREZ, A. R. & ZANLUNGO, S. 2012. Oxidative stress: a pathogenic mechanism for Niemann-Pick type C disease. *Oxid Med Cell Longev,* 2012**,** 205713.

WAHAJUDDIN & ARORA, S. 2012. Superparamagnetic iron oxide nanoparticles: magnetic nanoplatforms as drug carriers. *Int J Nanomedicine,* 7**,** 3445-71.

WALKLEY, S. U., SIKORA, J., MICSENYI, M., DAVIDSON, C. & DOBRENIS, K. 2010. Lysosomal compromise and brain dysfunction: examining the role of neuroaxonal dystrophy. *Biochem Soc Trans,* 38**,** 1436-41.

WARNOCK, A., TAN, L., LI, C., AN HAACK, K., NARAYAN, S. B. & BENNETT, M. J. 2013. Amlodipine prevents apoptotic cell death by correction of elevated intracellular calcium in a primary neuronal model of Batten disease (CLN3 disease). *Biochem Biophys Res Commun,* 436**,** 645-9.

WEIMER, J. M., BENEDICT, J. W., GETTY, A. L., PONTIKIS, C. C., LIM, M. J., COOPER, J. D. & PEARCE, D. A. 2009. Cerebellar defects in a mouse model of juvenile neuronal ceroid lipofuscinosis. *Brain Res,* 1266**,** 93-107.

WEIMER, J. M., KRISCENSKI-PERRY, E., ELSHATORY, Y. & PEARCE, D. A. 2002. The neuronal ceroid lipofuscinoses: mutations in different proteins result in similar disease. *Neuromolecular Med,* 1**,** 111-24.

WU, D., LIU, J., WU, B., TU, B., ZHU, W. & LUO, J. 2014. The Batten disease gene CLN3 confers resistance to endoplasmic reticulum stress induced by tunicamycin. *Biochem Biophys Res Commun,* 447**,** 115-20.

WU, X., TAN, Y., MAO, H. & ZHANG, M. 2010. Toxic effects of iron oxide nanoparticles on human umbilical vein endothelial cells. *Int J Nanomedicine,* 5**,** 385-99.

XIA, T., KOVOCHICH, M., BRANT, J., HOTZE, M., SEMPF, J., OBERLEY, T., SIOUTAS, C., YEH, J. I., WIESNER, M. R. & NEL, A. E. 2006. Comparison of the abilities of ambient and manufactured nanoparticles to induce cellular toxicity according to an oxidative stress paradigm. *Nano Lett,* 6**,** 1794-807.

YAO, Q., CHEN, J., CAO, H., ORTH, J. D., MCCAFFERY, J. M., STAN, R. V. & MCNIVEN, M. A. 2005. Caveolin-1 interacts directly with dynamin-2. *J Mol Biol,* 348**,** 491-501.

ZDOLSEK, J. M. & SVENSSON, I. 1993. Effect of reactive oxygen species on lysosomal membrane integrity. A study on a lysosomal fraction. *Virchows Arch B Cell Pathol Incl Mol Pathol,* 64**,** 401-6.